Functional Characterisation of the Flax Rust AvrP/AvrP123 Avirulence Proteins

A THESIS SUBMITTED FOR THE DEGREE OF DOCTOR OF PHILOSOPHY

OF THE AUSTRALIAN NATIONAL UNIVERSITY

BY

NADYA FARAH

SEPTEMBER 2018

DECLARATION

I declare that this thesis is my own work and has not been submitted in any form for another degree or diploma at any university or other institution of higher education. Information derived from the published or unpublished work of others has been acknowledged in the text and a list of references is given. Materials obtained for use in this study that were generated by others have been acknowledged accordingly in the text.

Nadya Farah

September 2018

ACKNOWLEDGEMENTS

I would like to express my gratitude to the following people, as without them this work would not have been finished and written:

First and top most gratitude is to my supervisors: Assoc. Prof. Dr David Jones, Prof. Adrienne Hardham and Dr. Peter Dodds, who have given me the opportunity to work in an awesome research group and interact with great people. Dr. Ann-Maree Catanzariti and my former supervisor Dr. Claire Anderson, have given their creative advice and assistance throughout the course of this project. Their support is highly appreciated. As chair supervisor, David Jones has supported me from the beginning of my PhD life until the end of this journey with all his understanding, patience, knowledge, and guidance. I may have not gone through my obstacles (personal and academic) without his support.

Second of all, to all Jones lab past and present members: Dr. Yvonne Gonzalez-Cendales, Huong Do, Dr. Choon Yang (Kevin) Tee, Laura Rolston, and Dr. Jaime Simbaqueba for all those happy memorable experiences in the lab. I wish you all well and keep moving forward towards your goals and dreams in life. Also to flax rust group members at CSIRO Black Mountain: Dr. Gregory Lawrence for his assistance in providing flax seeds and rust infected flax for generating the cDNA library; Kim Newell, Dr. Maud Bernoux and Dr. Xiaoxiao Zhang for their contributions on the project. It was an honour knowing you all. Special thanks to all the plant culture service team: Christine Larsen, Jenny Rath and Steve Dempsy, who did a great job on caring for my tobacco plants and Sue Lyons who made sure everything was under control at CEF (controlled environmental facility).

Last but not least to my beloved family who alwalys be there no matter what, for being the motivation and motor of this PhD journey. Our life in Australia was the most wonderful experience that we have had as a family. I hope we can come back and visit Australia again for another adventure.

ABSTRACT

Flax rust effector proteins AvrP and AvrP123 are recognised by the flax resistance proteins, P and P1, P2, P3, respectively. Variants of these effectors with different host-recognition specificities are found in the flax rust strains 271, 339, bs25 and WA. In this study, investigation was conducted on regions in AvrP and AvrP123 that are recognised by their cognate resistance proteins. *Agrobacterium*-mediated expression of AvrP and AvrP123 variants in tobacco (*Nicotiana tabacum*) and flax (*Linum usitatissimum*) was used to observe necrosis induction as an indicator of recognition.

For AvrP, deletions were generated based on the structure of the protein, whereas domain swaps and mutations were generated based on amino acid polymorphisms present in the AvrP variant from strain 271, which is not recognised by P, P1, P2 or P3. Amino acid polymorphisms involved in AvrP recognition were found to be located near the C-terminus of the protein. From the structure of AvrP, it was known that AvrP and AvrP123 each bind three zinc atoms. Mutational disruption of zinc binding in AvrP resulted in a loss of protein stability and a loss of recognition by P.

For AvrP123, deletions and domain swaps were generated based on amino acid polymorphisms present in AvrP123 variants from strains 339, bs25 and WA. Recognition or AvrP123 by P1 was found to be determined by the mature N-terminal region of the protein just after the signal peptide, whereas P2 and P3 were found to recognise the C-terminal region of AvrP123.

In an attempt to find interactor proteins targeted by AvrP in host cells, a yeast-two hybrid assay was conducted using cDNA library derived from rust-infected flax leaves. Four candidates were identified, one candidate from the pathogen, designated SIAP (Secreted Interactor of AvrP) and three candidates from the host, phosphoglucomutase, peptidyl-prolyl cis-trans isomerase FKBP12, and DEAD-box ATP-dependent RNA helicase 56. Each of these candidates is a plausible target for AvrP effector function in the plant cells, but further analysis is required to confirm these interactions and to determine the effect of AvrP on interactor function.

ABBREVIATIONS

aa	amino acid
AD	activating domain
ARF-GAP	ADP ribosylation factor-GTPase activating protein
ATP	adenosine triphosphate
Avr	avirulence
BD	binding domain
BEC	*Blumeria* effector candidate
Bgh	*Blumeria graminis* f. sp. *hordei*
BiFC	bimolecular fluorescence complementation
bp	base pair
CC	coiled-coil
Cce1	cysteine-rich core effector 1
cDNA	copy/complementary deoxyribonucleic acid
Cf	*Cladosporium fulvum*
ChIP-seq	chromatin immunoprecipitation-sequencing
CNL	CC-NB-LRR
Co-IP	co-immunoprecipitation
CSEP	candidate secreted effector protein
CRN	crinkling and necrosis
CTP	chloroplast-targeted protein
DAMP	damage-associated molecular pattern
dCTP	deoxycytidine triphosphate
dGTP	deoxyguanosine triphosphate
dpi	days post infiltration/infection
ECD	ectodomain
ECP	extracellular protein
EGF	epidermal growth factor
EFR	elongation factor -Tu RECEPTOR
ETI	effector-triggered immunity
FLS2	FLAGELLIN SENSING2
x g	gravitational force
GPI	glycosylphosphatidylinositol
h	hour (s)
3X HA	triple hemagglutinin
HR	hypersensitive response
JAZ	JASMONATE-ZIM DOMAIN
kb	kilo base pair
kDa	kilo Dalton
LB	lysogeny broth
LIC	ligation independent cloning
LRR	leucine-rich repeat
LysM	lysine motif
MAMP	microbial-associated molecular pattern
MAPK	mitogen-activated protein kinase
MED19a	mediator subunit 19a

min	minute (s)
MLA	mildew A
MS	Murashige-Skoog
NB-LRR/NLR	nucleotide-binding leucine-rich repeat
nt	nucleotide
NTPase	nucleoside-triphosphatase
PAMP	pathogen-associated molecular pattern
PCD	plant cell death
PcF	*Phytophthora cactorum-Fragaria*
Pep1	protein essential during penetration-1
PGM	phosphoglucomutase
PHD	Plant Homeodomain
Pit2	protein involved in tumours 2
PPIase	peptidyl-prolyl isomerases
PR	pathogenesis-related
PRR	pattern recognition receptor
PSR1	*Phytophthora* suppressor of RNA silencing 1
PTI	PAMP-triggered immunity
R	resistance
REase	restriction endonuclease
RING	really interesting new gene
RK	receptor kinase
RLCK	receptor-like cytoplasmic kinase
RLP	receptor-like protein
RNA	ribonucleic acid
ROS	reactive oxygen species
RTP1p	rust transferred protein 1
s	second (s)
SD	synthetic dropout
SDM	site-directed mutagenesis
See1	seedling efficient effector 1
Sr	stem rust resistance
Tin2	Tumour inducing 2
TIR	toll-interleukin-1 receptor
TTSS	type III secretion system
Ubl	ubiquitin-like
v/v	volume per volume
w/v	weight per volume

TABLE OF CONTENTS

Chapter 1
General Introduction

1.1 Multilayered plant immunity

Plants have a multilayered immune system (Figure 1.1). When pathogenic bacteria, fungi, or oomycetes attack plant cells, pathogen-derived molecules called PAMPs (pathogen-associated molecular patterns) or MAMPs (microbial-associated molecular patterns) are released as well as host-derived molecules called DAMPs (damage-associated molecular patterns). Examples of PAMP/MAMP molecules include bacterial flagellin, peptidoglycan, lipopolysaccharides, oomycete heptaglucans, and chitin, a building block of the fungal cell wall. Examples of DAMPs include systemin, oligogalacturonides, plant elicitor peptides, extracellular ATP and extracellular DNA. If these PAMP/MAMP molecules are recognised by plant pattern recognition receptors (PPRs) that reside in the plasma membrane, they will trigger the first layer of plant immunity called PAMP-triggered immunity (PTI). However, pathogens have overcome this defence by releasing small, secreted proteins called effectors. These effectors suppress the PTI by blocking PAMP/MAMP/DAMP perception and manipulate host cells to accommodate the pathogen. Plants, on the other hand, have developed a mechanism to counter effectors via resistance proteins. Effectors that are recognised by plant resistance (R) proteins are then called avirulence (Avr) proteins. The recognition of Avr proteins by their corresponding R proteins triggers the second layer of plant immunity, called effector-triggered immunity (ETI). When R-Avr recognition occurs, several plant defence responses are induced, often including rapid host cell death at the site of infection, known as a hypersensitive response (Jones and Dangl 2006; Dodds and Rathjen 2010).

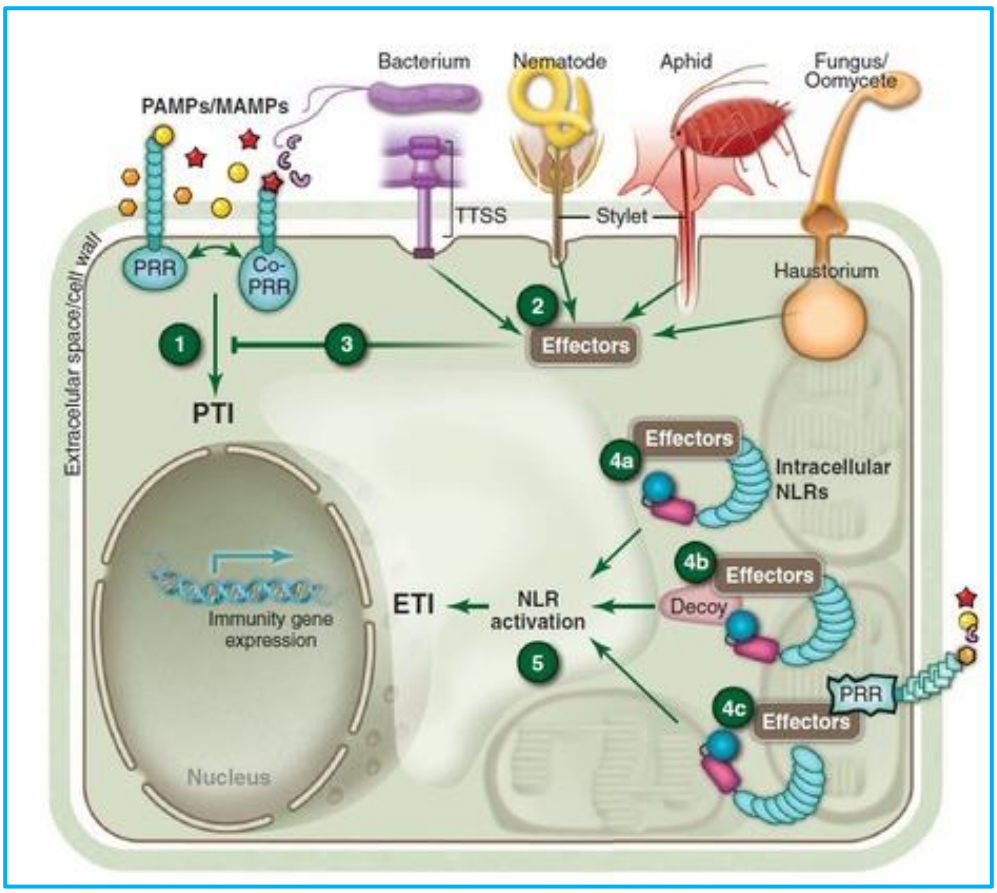

Figure 1.1 Schematic of plant multilayered immunity. Pathogens (bacteria, oomycetes, fungi, aphids and nematodes) release PAMPs/MAMPs (shapes colour-coded to their pathogens of origin) which are then recognised by plants via extracellular PRRs, which initiate PTI (step 1). Effectors are released into the plant cell apoplast and into the cytosol (step 2) to facilitate virulence by blocking PRR signalling and suppressing PTI (step 3). Intracellular NLR (nucleotide-binding leucine-rich repeat) receptors can recognise the effectors by direct interaction (step 4a), by sensing binding or modification of a decoy (Decoy Model; step 4b), or by sensing effector-mediated alteration of a host virulence target (Guard Model; step 4c). Activation of an NLR leads to ETI (step 5). Figure taken from Dangl et al. (2013).

1.1.1 Plant Resistance Proteins

Based on their protein sequences and subcellular localisation, plant resistance proteins are divided into two main categories. First, proteins from large families of receptor kinases (RKs) and receptor-like proteins (RLPs) that sense molecular patterns and effectors at the plant cell surface (Tang et al. 2017). Second, NLR proteins, which contain a nucleotide-binding (NB) domain at the center, a C-terminal leucine-rich repeat (LRR)

domain and an N-terminal interaction domain (Sukarta et al. 2016). As the first layer of plant defence, RKs and RLPs act as PRRs that recognise microbe- and host-derived elicitors (MAMP/PAMP/DAMP molecules) and trigger PTI. As the second layer of plant defence, RKs and RLPs also act as resistance proteins able to recognises apoplastic effectors and trigger ETI, whereas NLRs act as resistance proteins able to recognise cytoplasmic effectors and trigger ETI.

1.1.1.1 Plant RKs and RLPs

Analogous to receptor tyrosine kinase in animals, a plant RK consists of an ectodomain, a single transmembrane helix domain, and a cytoplasmic kinase domain (Hohmann et al. 2017). An RLP, essentially a RK without a cytoplasmic kinase domain, has a single transmembrane helix domain and may have an unstructured cytoplasmic loop. Other extracellular receptors can lack any transmembrane element, instead having a glycosylphosphatidylinositol (GPI) anchor attached to the outer face of the plasma membrane. Receptor-like cytoplasmic kinases (RLCKs), consist of a cytoplasmic kinase or pseudokinase domain but lack the extracellular domain and the transmembrane helix (Lin et al. 2015). PRRs are able to transmit extracellular signals across membranes and RLCKs regulate the activity of the resulting cytoplasmic signalling cascades. Based on differences in their ectodomains, PRRs can be classified into leucine-rich repeat (LRR) domain, lysin motif (LysM) domain, lectin domain, or epidermal growth factor (EGF)-like domain (Bohm et al. 2014; Couto and Zipfel 2016). PRRs with LRR domains preferentially bind proteins or peptides, such as the *Arabidopsis* LRR-RKs FLS2 (FLAGELLIN SENSING 2), which recognises flg22, an epitope of the bacterial flagellin (Gomez-Gomez and Boller 2000) or EFR (elongation factor -Tu RECEPTOR), which recognises the elf18 epitope of bacterial elongation factor-Tu (Zipfel et al. 2006). The LysM-containing PRRs, however, preferentially bind carbohydrate-based ligands, such as fungal chitin or bacterial peptidoglycan whereas the lectin-type PRRs and EGF-like ectodomains prefer to bind extracellular ATP or bacterial lipopolysaccharides, and plant cell-wall derived oligogalacturonides, respectively (Bohm et al. 2014; Ranf et al. 2015).

1.1.1.2 Plant NLRs

Plants recognise many pathogen effectors intracellularly via NLR proteins. The three distinct domains of plant NLR proteins are suggested to have different tasks. The NB

domain at the center functions as a hinge in a NLR switch, closed when bound to ADP and open when bound to ATP. The C-terminal LRR domain, on the other hand, determines the specificity of effector recognition. For example, the sequence of L6 and L10 proteins are identical except for the LRR region and have different specificity (Ellis et al. 1999). Domain swaps carrying the LRR region of L2 and the TIR and most of the NBS region of L6 or L10 had L2 not L6 or L10 specificity, indicating that the LRR region determines L2 specificity (Ellis et al. 1999). Similarly, six amino acid differences in the LRR region of the P and P2 resistance proteins are responsible for their different specificity (Dodds et al. 2001b). Direct interaction between effector and R protein has been shown by yeast two-hybrid analysis for AvrM:M and AvrL567:L6 pairs (Catanzariti et al. 2010; Dodds et al. 2006), but not for AvrP:P and AvrP123:P2 pairs (Zhang et al. 2018). Indirect interaction can be observed in the *Cladosporium fulvum*–tomato pathosystem between Avr2 and Cf-2, mediated by Rcr3 (Rooney et al. 2005) and in the *Arabidopsis-Pseudomonas syringae* pathosystem between RPS5 and AvrPphB*,* mediated by PBS1 (Shao et al. 2003).

Based on differences in the N-terminal domain, NLRs can be classified into TIR (Toll-Interleukin-1 receptor) domain proteins and CC (coiled-coil) domain proteins. In general, *CC-NB-LRR* genes can be found in the genomes of both monocots and dicots (Jacob et al. 2013), e.g. Sr33, Sr35 and Sr50 wheat rust R proteins, which confer resistance to stem rust caused by *Puccinia graminis* f. sp. *tritici* (Casey et al. 2016; Mago et al. 2015; Saintenac et al. 2013), whereas *TIR-NB-LRRs* are absent in monocots (Jacob et al. 2013). The TIR domain has been extensively studied in *Arabidopsis*, e.g. RPS4 and RRS1 R proteins (Gassmann et al. 1999; Deslandes et al. 2002) and several flax rust-resistance proteins (Bernoux et al. 2016; Dodds et al. 2001b). In flax, the TIR domain of L6 resistance protein is able to self-associate and this is necessary and sufficient to activate cell death even in the absence of AvrL567 (Bernoux et al. 2011).

Despite the lack of a full-length structure for a NLR protein, several studies have provided insights into NLR protein function (Cesari et al. 2014; Casey et al. 2016; Bernoux et al. 2016). The protein is considered to act as a molecular switch that shifts between two conformations: an OFF-state when closed and an ON-state when open. In the resting state (negative regulation), the protein is in the ADP-bound OFF-state.

Interaction with pathogen effectors, either directly or indirectly, will disturb the negative regulation of the NB domain, allowing the protein to change conformation into an open ATP-bound ON-state. The open, active conformation allows the exposed N-terminal domain (either TIR or CC) to dimerize and interact with signaling partners, thus activate disease resistance responses (Maekawa et al. 2011; Bernoux et al. 2011; Williams et al. 2014). How the conformational switch is triggered is still unresolved.

1.2 Plant pathogen effectors

In attempts to suppress the first layer of plant defence (PTI) and aid infection, pathogens secrete small proteins called effectors (Dodds and Rathjen 2010; Dangl et al. 2013). These effectors are translocated into plant cells where they can alter host cell structures and functions. Pathogenic bacteria release these effectors inside plant cells via a syringe-like type III secretion system (TTSS in Figure 1.1), whereas others such as oomycetes and rust fungi use a specialised structure called an haustorium (Figure 1.1), which penetrates the plant cell wall and modifies the plant plasma membrane into an extrahaustorial membrane. Effectors are then released from haustoria and transported into the plant cytoplasm through the extrahaustorial matrix. Other specialised infection structures are found within the effector-exporting biotrophic fungi, such as infection hypha and arbuscules (Rafiqi et al. 2012). Other pathogens such as nematodes and aphids use a feeding device called a stylet (Figure 1.1) to release effector-containing saliva inside plant cells to manipulate the host and promote infection (Jaouannet et al. 2014).

1.2.1 Bacterial effectors

Pathogenic bacteria have developed strategies to suppress plant defense responses and promote disease through the delivery of effectors into host cells via TTSS. These effectors target various subcellular compartments inside host cells where they may manipulate a variety of host cellular functions (Figure 1.2).

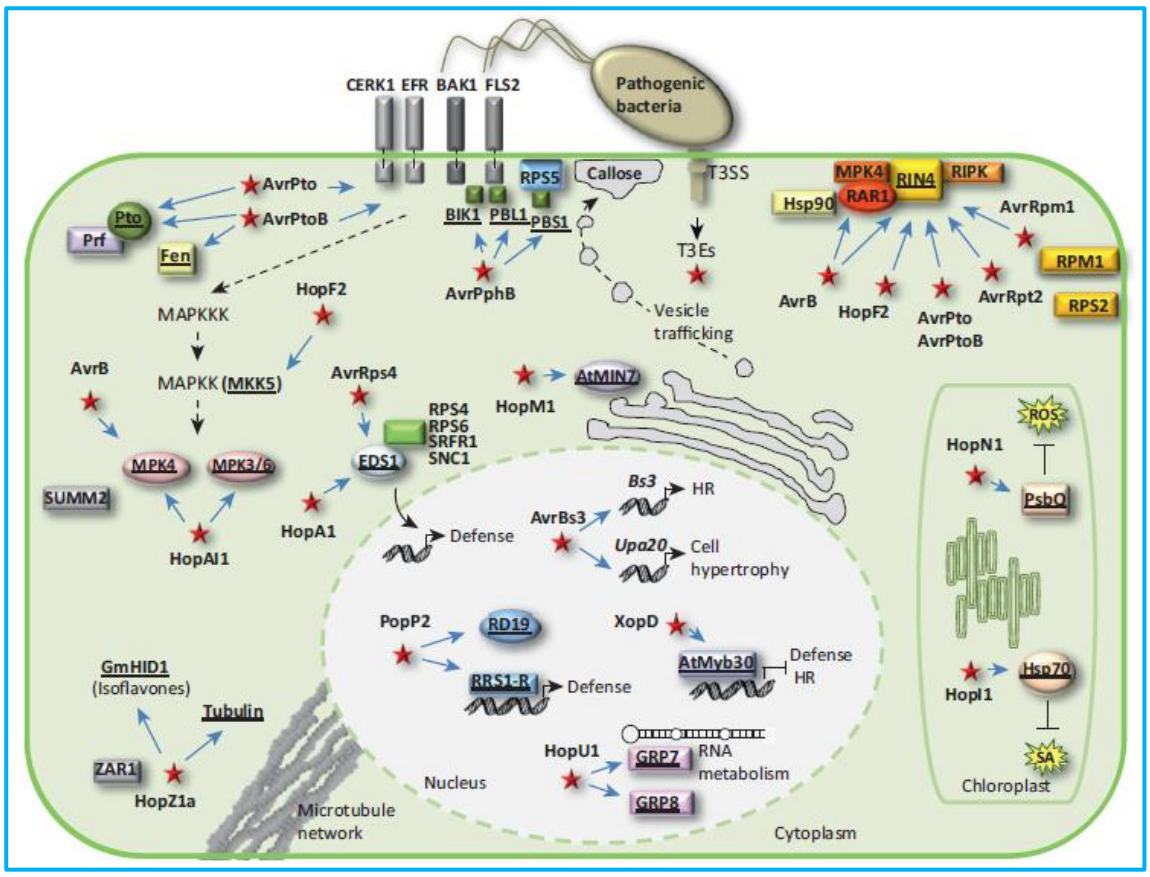

Figure 1.2 Bacterial type III effector proteins target a variety of plant proteins. Effector molecules are marked with red star whereas plant target proteins are underlined. Effectors may target multiple kinases, RIN4, chloroplast components, vesicle trafficking, MAPK signaling, or nuclear components. Image was taken from Deslandes and Rivas (2012).

Pseudomonas syringae is one of the best-studied plant-pathogenic bacteria. Some of the well-characterised *P. syringae* effectors are AvrPto and AvrPtoB targeting multiple kinases and RIN4 ; AvrB, AvrRpm1, AvrRpt2, and HopF2 targeting RIN4; HopZ1a targeting GmHID1 and tubulin; AvrPphB targeting PBS1 and related kinases; effectors targeting chloroplast components such as HopI1 which targets Hsp70 and HopN1 which targets PsbQ; effectors targeting vesicle trafficking such as HopM1 which targets AtMIN7; effectors targeting MAPK signaling such as HopF2 which targets MKK5, HopAI1 which targets MPK3, MPK4, and MPK6, and AvrB which targets RAR1 and MPK4 in addition to RIN4; effectors targeting nuclear components such as HopU1 which targets GRP7 and GRP8 and HopA1 and AvrRps4 which target EDS1 (Figure 1.2) (Deslandes and Rivas 2012). Effectors found in *Xanthomonas campestris* include TAL effectors such as AvrBs3 which target plant promoters; AvrAC which targets plant kinases and XopD which targets

the transcription factor AtMYB30; and in *R. solanacearum* PopP2 targets RD19 (Figure 1.2). These effectors have been useful in understanding NB-LRR protein-mediated resistance.

AvrPto and AvrPtoB are examples of co-evolution between plants and microbes where bacteria adapt to avoid host detection and plants develop a new recognitional ability to detect the pathogen (Deslandes and Rivas 2012). AvrPtoB is known to be larger than AvrPto and lacks the myristylation motif that is found in AvrPto (Pedley and Martin 2003). The two-unrelated effectors interact physically with Pto, an intracellular serine-threonine protein kinase (Tang et al. 1996; Kim et al. 2002; Pedley and Martin 2003) and together with the NB-LRR protein Prf activate ETI in tomato (Pedley and Martin 2003; Salmeron et al. 1996). In the absence of AvrPto, Pto is reported to interact with Prf constitutively (Mucyn et al. 2006) and negatively regulates *Prf*-mediated defences (Xing et al. 2007). Interaction of AvrPto with Pto is thought to disrupt the inhibitory effects of Pto on Prf signaling, thus allowing Pto to activate Prf (Xing et al. 2007; Dong et al. 2009). In contrast to Pto, Fen kinase, an additional member of the Pto family, does not interact with AvrPto and does not trigger resistance in tomato plants (Tang et al. 1996; Kim et al. 2002).

Initially, AvrPto was reported to bind the *Arabidopsis* receptor-like kinase BAK1, a signaling partner of FLS2 and the brassinosteroid receptor BRI1 (Shan et al. 2008). However, it was then confirmed by Xiang et al. (2011) that it was FLS2 that interacts with AvrPto and not BAK1. In addition, in *Arabidopsis* and susceptible tomato plants lacking Pto or Prf, AvrPto inhibits PTI by interacting with the FLS2 and EFR protein kinases and inhibiting their kinase activity, thereby suppressing early MAMP signalling (Xiang et al. 2008). Recently, Wu et al. (2018) reported that AvrPto interacts with *Arabidopsis* SOBIR1 and its orthologues in tomato and *Nicotiana benthamiana.*

AvrPtoB is a modular protein with an N-terminal domain (residues 1-307 that interact with Pto and elicits *Pto*-mediated plant cell death (PCD) in tomato and residues 307-387 that involved in Fen binding) and the C-terminal domain (residue 388-553) that is able to suppress PCD and carries an E3 Ub ligase activity (Abramovitch and Martin 2005; Abramovitch et al. 2006; Xiao et al. 2007). AvrPtoB is able to manipulate the host

ubiquitinylation system to suppress plant defence via the proteasomal degradation of FLS2, LysM receptor kinase CERK1, and BAK1 (Gohre et al. 2008; Gimenez-Ibanez et al. 2009; Shan et al. 2008). AvrPtoB is also able to ubiquitinylate Fen, leading to its degradation in a proteasome-dependent manner (Rosebrock et al. 2007). The Pto protein, on the other hand, has higher kinase activity than Fen which allows it to evade ubiquitination and degradation by AvrPtoB E3 ligase activity through phosphorylation of threonine-450 in AvrPtoB (Mathieu et al. 2014).

In *Arabidopsis*, the AvrB and AvrRpm1 effectors bind to the RPM1-interacting protein RIN4, which is a membrane-anchored protein required for normal development of *Arabidopsis*. AvrB and AvrRpm1 induce phosphorylation of RIN4, which is suggested to enhance its activity as a repressor of basal defences and expression of pathogenesis response genes. In a direct interaction with RPM1, RIN4 is required for activation of a RPM1-dependent hypersensitive response and RPM1-dependent inhibition of bacterial growth. RPM1 is modelled as a "guard" against pathogens effectors that manipulate RIN4 (Mackey et al. 2002).

Interestingly, the effector AvrRpt2, a cysteine protease, is also associated with RIN4 (Mackey et al. 2003). AvrRpt2 is auto-processed and activated by cyclophilin after it enters the host cell (Coaker et al. 2005). RPS2 interacts physically with RIN4 (Axtell and Staskawicz 2003) and together with RPM1 forms a complex at the plasma membrane. Instead of binding to RIN4, AvrRpt2 cleaves it at two conserved PxFGxW motifs and releases a large part of RIN4 from the plasma membrane into the cytosol (Takemoto and Jones 2005). The release of RIN4 from the membrane prevents activation of RPM1 by AvrRpm1 or AvrB (Kim et al. 2005). However, the cleavage of RIN4 releases RPS2 from the complex and triggers resistance. The interaction of RPS2 and RIN4 has allowed the plant to detect AvrRpt2 protease activity. Even though the AvrRpt2 case fits the guard model (Figure 1.1), RIN4 could also be a “decoy” since it has not been demonstrated whether RIN4 modification or elimination benefits the pathogen or not (van der Hoorn and Kamoun 2008).

Some effectors such as HopU1, an ADP-ribosyltransferase, target the plant’s response to PAMP recognition (Fu et al. 2007). *P. syringae* HopU1 is required for full virulence on

Arabidopsis thaliana and to inhibit PTI. It targets plant glycine-rich RNA-binding protein 7 (GRP7), an RNA binding protein involved in inducing early reactive oxygen species (ROS) production and late immune responses (callose deposition). Nicaise et al. (2013) discovered that besides interacting with translational components, GRP7 also binds FLS2 and EFR mRNA *in vivo* thereby promoting translation of two PRRs involved in early and late immune response. HopU1 works by preventing the binding of GRP7 to the mRNAs of FLS2 and EFR by mono-ADP-ribosylation of the GRP7 RNA-binding domain resulting in reduced FLS2 protein levels *in planta* and, as a consequence, decreased PAMP-triggered signalling.

1.2.2 Oomycete effectors

Based on 18S rRNA analysis and other characteristics, oomycetes are different from fungi which are quite distant phylogenetically (Tyler 2001). However, the destruction they cause to crops worldwide is similar to that caused by pathogenic fungi. Most of the species in the oomycete genus *Phytophthora* as well as many species in the closely related genus *Pythium* are destructive plant pathogens. The causal agent of the late-blight disease in potato, *Phytophthora infestans*, became infamous for destruction of the Irish potato crop which resulted in the Irish potato famine of 1845 and 1846. *P. infestans* and *P. sojae*, the causal agent of soybean root rot, have been well-studied and used as models for investigation of avirulence genes and their roles in plant-oomycete interaction (Tyler 2007).

Oomycetes secrete effectors that act both extracellularly and intracellularly on the plant cell. Extracellular effectors, also known as apoplastic effectors, are secreted into the host extracellular space (apoplast) where they modify the structure and function of the host (Figure 1.3) (Win et al. 2012). This type of effector is subdivided into two categories: effectors mediating protection against plant defences and effectors mediating invasion (Wawra et al. 2012). The first category includes protease-inhibitors and glucanase-inhibitors. In *P. infestans*, for example, two Kazal-like effectors, EPI1 and EPI10, have been found to specifically bind and inhibit the tomato pathogenesis-related (PR) subtilisin-like serine protease P69B, whereas EPIC1–EPIC4 are similar to cystatin-like protease inhibitors (Tian et al. 2007). Functional analysis of *P. infestans* EPIC2B revealed that it interacts with and inhibits a novel papain-like extracellular cysteine protease

termed *Phytophthora* inhibited protease 1 (PIP1), which is a PR protein closely related to Rcr3, a cysteine protease found in the tomato apoplast that functions in fungal resistance. Glucanase inhibitors released by *P. infestans* and *P. sojae* inhibit the degradation of pathogen cell wall components *in vivo* to prevent the release of oligosaccharide elicitors of host defence mechanisms (Rose et al. 2002). In the second category, pathogens release hydrolytic protein effectors such as glycosyl hydrolases found in *P. sojae* and *P. ramorum,* which are involved in plant cell wall degradation (Costanzo et al. 2006), or toxins such as those found in the PcF (*Phytophthora cactorum-Fragaria*) family, which induce necrosis (Orsomando et al. 2011).

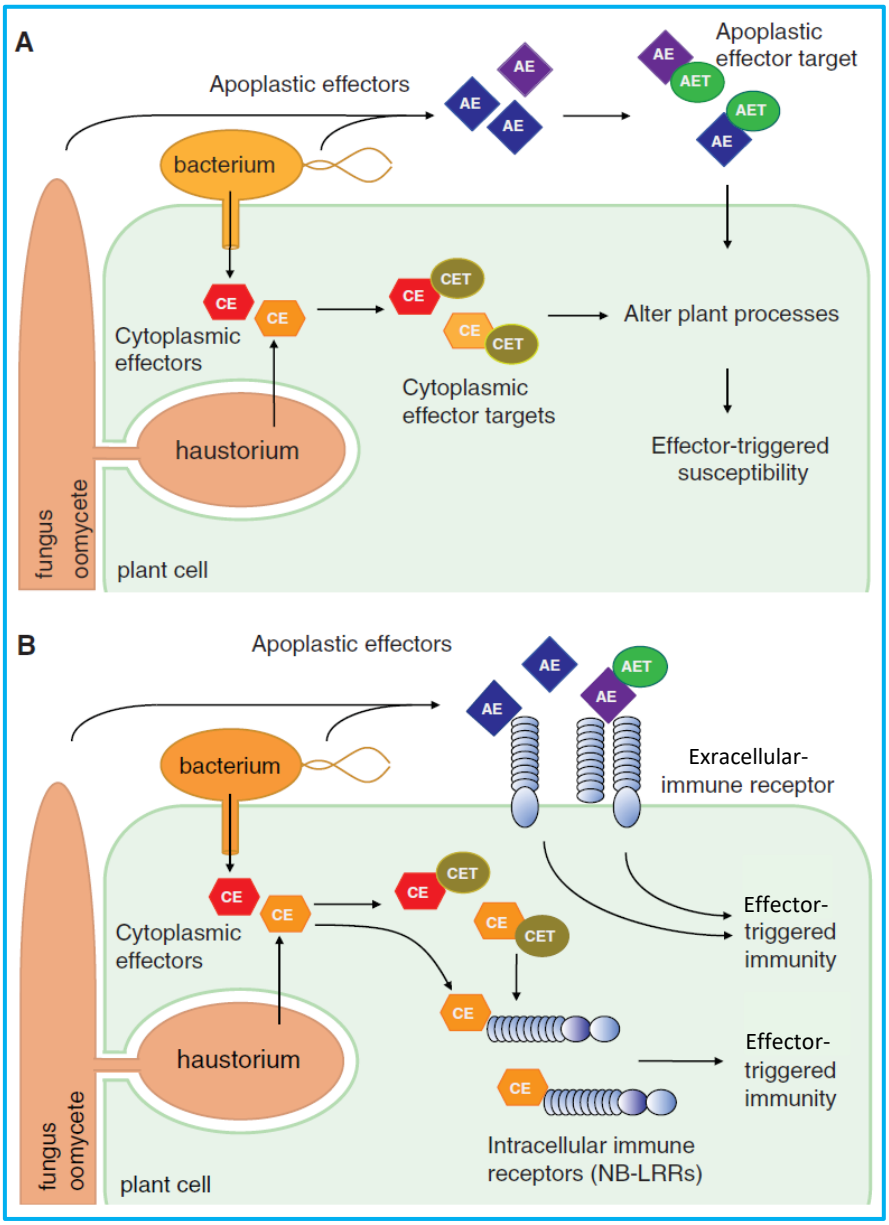

Figure 1.3 Phytopathogens such as bacteria, fungi and oomycetes secrete effectors extracellularly (apoplastic effectors, AE) and intracellularly (cytoplasmic effectors, CE), that bind or interact with extracellular and cytoplasmic targets (AET and CET). In susceptible plants (A), these interactions can alter plant cell processes and suppress immune responses, leading to effector-triggered susceptibility (ETS) and host colonisation. In resistant plants (B), these interactions are perceived by plant receptors, leading to ETI. Diagram modified from (Win et al. 2012).

Intracellular effectors are translocated into the cytoplasm of host cells and function inside host cells. In oomycetes, many of these effectors are known to contain a conserved N-terminal RXLR (arginine, any amino acid, leucine, arginine) motif followed by an EER (glutamic acid, glutamic acid, arginine) sequence which is believed to be important for effector delivery into host cells (Whisson et al. 2007; Dou et al. 2008). Recent findings by Wawra et al. (2017) have shown cleavage of the RxLR motif of native AVR3a before secretion by the pathogen, implying that the RxLR motif plays a role in secretion of the effector rather than host cell entry. The CRN (crinkling and necrosis) effectors also contain a conserved N-terminal secretion signal, more specifically a LXLFLAK (leucine, any amino acid, leucine, phenylalanine, leucine, alanine, lysine) motif that mediates translocation into plant cells (Schornack et al. 2010). Interestingly, the RXLR motif is restricted to *Phytophthora* species, such as *P. infestans* and downy mildew species such as the *Arabidopsis* downy mildew pathogen *Hyaloperonospora arabidopsidis* and few or none are found in other oomycete lineages (Adhikari et al. 2013). In contrast, CRN effectors can be found in all oomycete genomes.

At least 20 *Avr* genes have been cloned from oomycete species (*H. arabidopsidis, P. infestans* and *P. sojae*) (Anderson et al. 2015). Most of these *Avr* genes contain an RXLR motif and target various biological processes and cell compartments to suppress plant immunity. For example, the Avrblb2 effector from *P. infestans* targets the host papain-like cysteine protease C14 and inhibits its secretion into the apoplast at the haustorial interface (Bozkurt et al. 2011). Avr3b, a nudix hydrolase from *P. sojae*, with ADP-ribose/NADH pyrophosphorylase activity reduces the accumulation of ROS (Dong et al. 2011). The HaRxL44 effector from *H. arabidopsidis* interacts with Mediator subunit 19a

(MED19a), which mediates the interaction between transcriptional regulators and RNA polymerase II in the nucleus (Caillaud et al. 2013). This interaction leads to the degradation of MED19a and elevated jasmonic acid/ethylene signalling antagonistic to salicylic acid–mediated defence responses in *Arabidopsis*. The IPI-O effector targets the host legume-like lectin receptor kinase LecRK-I.9 and interferes with the cell wall-plasma membrane adhesions (Bouwmeester et al. 2011). The *Phytophthora* suppressor of RNA silencing 1 (PSR1) effector affects host RNA silencing by binding to the PSR1-interacting protein 1, a DEAH (aspartate-glutamate-alanine-histidine)-box RNA helicase protein, which likely affects the assembly of dicing complexes (Qiao et al. 2015).

In contrast to the targeting of diverse cell compartments and biological processes by RXLR effectors, the CRN effectors target nuclear compartments and induce host cell death when expressed *in planta* (Stam et al. 2013). Nuclear localisation is needed for CRN cell death activity as was shown in *P. infestans* CRN8 protein (van Damme et al. 2012), *P. sojae* PsCRN63 (Liu et al. 2011) and *P. capsici* PcCRN4 (Mafurah et al. 2015). In contrast, the PsCRN115 effector suppresses cell death and does so even when the nuclear localisation signal is mutated (Liu et al. 2011), suggesting a role for this CRN as a regulator of cell death instead of an inducer (Amaro et al. 2017).

Whilst the N-terminus of CRN effector proteins is responsible for secretion and translocation into the host cells, the C-terminus plays a role in virulence function (Zhang et al. 2016). The C-terminal (CR-toxin) domain is diverse with nucleoside-triphosphatase, restriction endonuclease, H-N-H endonuclease, protein kinase and multiple distinct peptidase domains acting as toxicity determinants. Some CRNs have been shown to interact with host DNA. For example, the *P. sojae* CRN108 contains a putative DNA-binding motif that targets conserved heat shock promoter elements to inhibit binding of the plant heat shock transcription factor AtHsfA1a, resulting in suppression of plant heat shock protein gene expression and inhibition of the plant defence response (Song et al. 2015).

1.2.3 Effectors from biotrophic and hemibiotrophic fungi

Biotrophic and hemibiotrophic fungi require living tissues in order to survive, hence maintenance of the host-feeding relationship is crucial for the pathogen, e.g. by forming specialised infection structures such as haustoria, infection hyphae and arbuscules (Figure 1.4). Some of the well-known and well-studied biotrophic and hemibiotrophic fungal-pathosystems are described below.

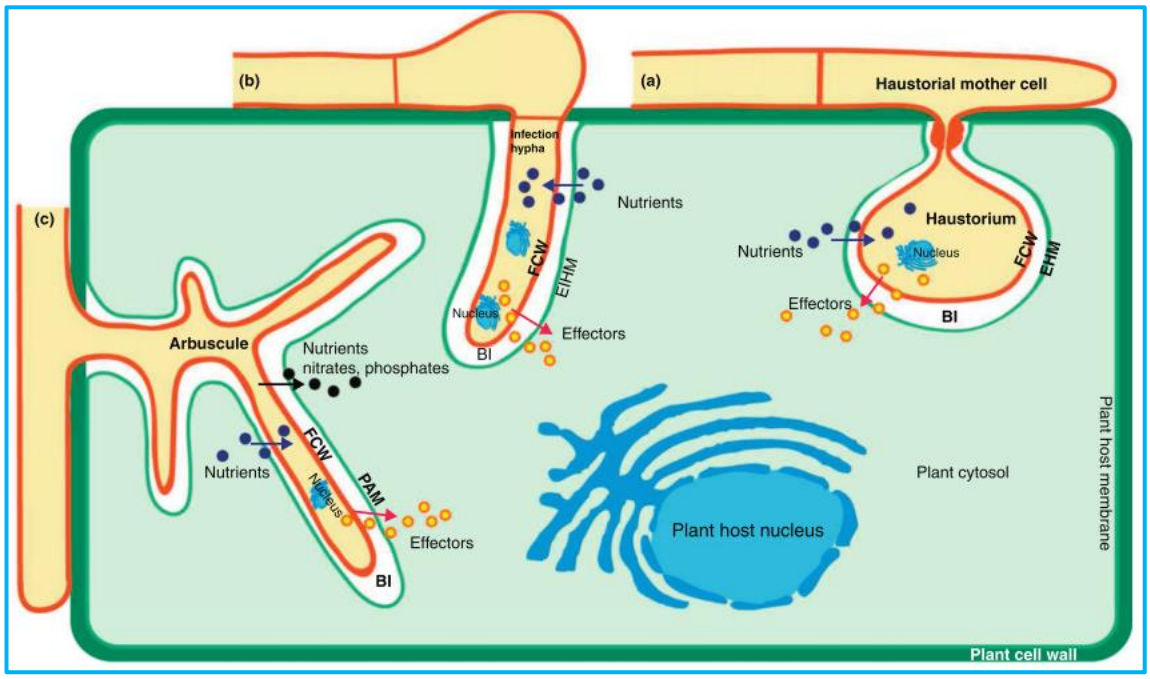

Figure 1.4 Biotrophic fungi form specialised infection structures such as haustoria (a), infection hyphae (b) and arbuscules (c), enabling them to penetrate host cells and obtain nutrients (dark blue spots). These structures are kept separated from the host cytoplasm by a modification of the plant plasma membrane into an extrahaustorial membrane (EHM) in (a), an extra-invasive hyphal membrane (EIHM) in (b) and a periarbuscular membrane (PAM) in (c). Effectors (orange spots) are secreted into the biotrophic interface (BI) between the fungal cell wall (FCW) and the modified plant plasma membrane, and translocated int o the host cytosol. Image taken from Rafiqi et al. (2012).

1.2.3.1 *Cladosporium fulvum*

The causal agent of tomato leaf mold *Cladosporium fulvum* is a biotrophic pathogen that infects leaves and grows in the apoplastic spaces without penetrating host cell walls. The tomato *Cf* genes, conferring resistance to *C. fulvum,* encode membrane-anchored extracellular proteins that contains LRRs (de Wit 1995). The *Cf-9*, *Cf-4* and *Cf-2* genes were among the first resistance genes isolated from tomato (Jones et al. 1994; Thomas

et al. 1997; Dixon et al. 1996). Similarly, the corresponding *Avr9* and *Avr4* genes were among the first avirulence genes isolated from fungal pathogens (van Kan et al. 1991; Joosten et al. 1997). Currently, 14 *Avr* and *ECP* (extracellular protein) genes have been cloned from *C. fulvum* (Mesarich et al. 2014). The eleven known Avr proteins are Avr2, Avr4, Avr4E, Avr5, Avr9, Ecp1, Ecp2-1, Ecp4, Ecp5, and Ecp6, and they trigger resistance mediated by corresponding Cf proteins in tomato. Three additional effectors, Ecp2-2, Ecp7, and CfTom1, have also been recently identified, but corresponding Cf resistance proteins from tomato have not yet been reported (Mesarich et al. 2014). All of these Avr proteins are small, cysteine-rich and contain an N-terminal signal peptide that leads to their secretion into the apoplastic spaces of infected tomato leaves (Mesarich et al. 2014).

Four Avr proteins from *C. fulvum* have been functionally characterised, namely Avr2, Avr4, Ecp6, and CfTom1. Avr2 protects the pathogen from proteases released by the host as a form of basal defence. Avr2 binds and inhibits the extracellular tomato cysteine proteases RCR3 and PIP1 (Shabab et al. 2008; Rooney et al. 2005). The RCR3-Avr2 complex is recognised by the Cf-2 protein, resulting in resistance (Rooney et al. 2005). It has been suggested that RCR3 may act as a decoy for Avr2, whereas PIP1 is likely to be the real virulence target of Avr2 (Shabab et al. 2008). Avr4, however, is a chitin-binding lectin containing an invertebrate chitin-binding domain (CBM14) (van den Burg et al. 2006). Avr4 binds to chitin present in the fungal cell wall, thus protecting the fungal cell wall against hydrolysis by host chitinases (van den Burg et al. 2006; van Esse et al. 2007). Ecp6 complements the role of Avr4. It contains LysM domains similar to chitin receptors in rice and *Arabidopsis* (de Jonge et al. 2010). Ecp6 binds to chitin fragments released from the cell walls of invading fungal hyphae by host chitinases and outcompetes host chitin receptors for the binding of chitin fragments (de Jonge et al. 2010; Sanchez-Vallet et al. 2013). The Avr4 and Ecp6 effectors thus help the pathogen to avoid detection of chitin as a PAMP by the host. Lastly, CfTom1 is a glycosyl hydrolase (GH10) that hydrolyses the antifungal glycoalkaloid α-tomatine produced by the host, into the less toxic compound tomatidine (Okmen et al. 2013). CfTom1 is reported to be required for full virulence of the fungus on tomato (Okmen et al. 2013).

1.2.3.2 *Ustilago maydis*

Ustilago maydis is a member of a large group of biotrophic basidiomycete fungi that cause smut diseases in various crops such as maize, wheat, barley, and sugar cane (Djamei and Kahmann 2012). Unlike rust fungi, smut fungi form intracellular hyphae that are encased by the host plasma membrane and the infection is characterised by the induction of anthocyanin biosynthesis and formation of tumors in aerial organs (Lanver et al. 2017).The maize *U. maydis* interaction has become a model pathosystem for studying the smut fungi (Djamei and Kahmann 2012). Smut infection involves two types of effectors, "core" effectors and organ-specific effectors (Skibbe et al. 2010). Core effectors are responsible for the suppression of plant defence responses during penetration whereas the organ-specific effectors contribute to tumour formation in maize (Djamei and Kahmann 2012). Core effectors of *U. maydis* have been identified at early stages of infection as abundant proteins in the apoplast or translocated into the plant cell. These includes Cmu1 (Djamei et al. 2011), Pep1 (protein essential during penetration-1) (Doehlemann et al. 2009), Pit2 (protein involved in tumours 2) (Mueller et al. 2013), Tin2 (tumour inducing 2) (Tanaka et al. 2014) and Cce1 (cysteine-rich core effector 1) (Seitner et al. 2018).

The apoplastic effector Pit2 inhibits a set of apoplastic maize cysteine proteases, whose activities are induced by salicylic acid in response to plant defence activation. Therefore, protease inhibition by Pit2 is essential to suppress host resistance and is required for *U. maydis* pathogenicity (Mueller et al. 2013). Pep1 also acts in the apoplast and inhibits the activity of the maize peroxidase POX12, responsible for the production of hydrogen peroxide in the apoplast (Doehlemann et al. 2009; Hemetsberger et al. 2012). Consequently, Pep1 suppresses the plant oxidative burst which is important for early plant defence. Deletion of *PEP1* allows the production of H_2O_2 and the induction of plant defence responses that prevent penetration of maize epidermal cells by the fungus. Cmu1 is an example of a translocated effector that reduces the levels of chorismate, a precursor of the salicylic acid hormone involved in plant defence (Djamei et al. 2011). Tin2 also translocates into the plant cell, where it stabilises the maize protein kinase ZmTTK1 by masking the ubiquitinylation motif in ZmTTK1. When Tin2 is present, ZmTTK1 increases anthocyanin production at the expense of lignin production, which would otherwise fortify the cell wall and provide a strong and impenetrable physical barrier to

infection (Tanaka et al. 2014). The Cce1 core effector is essential at early stages of infection and is upregulated during infection (Seitner et al. 2018). See1 (Seedling efficient effector 1) was the first organ-specific effector characterised and interferes with the MAPK-triggered phosphorylation of SGT1 (Suppressor of a G2 allele of Skp1), an important component for plant resistance and reactivation of DNA synthesis, suggesting its role in host immune responses and tumour progression (Redkar et al. 2015).

1.2.3.3 *Blumeria graminis*

The powdery mildew *Blumeria graminis* f. sp. *hordei* (*Bgh*) is an obligate biotrophic fungus that infects barley. The barley *mildew locus A* (*MLA*) encodes a number of coiled-coil (CC)-NB-LRR (CNL) receptors that each confer recognition of specific *Bgh Avr* gene products (Bai et al. 2012; Shen et al. 2003). AVR_{A10} and AVR_{k1} were the first *Avr* genes isolated from *Bgh* and both induce cell death when transiently expressed in resistant barley varieties carrying *Mla10* and *Mlk1*, respectively (Ridout et al. 2006), but, despite further investigation, the host proteins or pathways targeted by these two Avr proteins remains unknown (Amselem et al. 2015). Numerous *Blumeria* candidate secreted effector proteins (CSEPs) have been identified from *Bgh* (Spanu et al. 2010; Pedersen et al. 2012) (Schmidt et al. 2014), but little is known about their roles in pathogenicity. One of the CSEPs, CSEP0055, is reported to interact with the barley pathogenesis-related proteins PR1 and PR17 (Zhang et al. 2012). Schmidt et al. (2014) showed that the *Blumeria* effector candidates *BEC3* and *BEC4* target the host thiopurine methyltransferase, a ubiquitin-conjugating enzyme, and an ADP ribosylation factor-GTPase activating protein (ARF-GAP). They hypothesised that ARF-GAP proteins are conserved targets of powdery and downy mildew effectors and speculate that BEC4 might interfere with defence-associated host vesicle trafficking.

1.2.3.4 Rust fungi

Rust fungi (Phylum Basidiomycota, order Pucciniales) are considered major threats to global food security as they cause substantial economic damage worldwide in agriculture, horticulture and forestry. With more than 120 genera and 7000 species described, the rusts represent the largest group of phytopathogenic fungi with more than half belonging to the genus *Puccinia* (Aime 2006; Nemri et al. 2014). Some

examples of devastating, economically-important rusts are white pine blister rust, wheat stem rust, soybean rust and coffee rust. As a group, they are diverse and have a wide host range due to long co-evolution with plants, however each individual species is highly specialised and can only infect a small range of host plants. They have the most complex life cycles within the fungal kingdom, with some having up to five or six different spore stages and alternating between taxonomically unrelated host plants for completion of their life cycle (Aime 2006), while other rust fungi such as flax rust only have one host (Lawrence et al. 2007). Rust fungi are obligate biotrophs and cannot be grown *in vitro*, which limits investigation of their biology.

Rust fungi develop haustoria by penetrating the plant cell wall, invaginating the plant cell membrane and forming an extrahaustorial membrane and a discrete compartment called the extrahaustorial matrix, which is delimited by a neckband, a feature that is not present in oomycete haustoria (Catanzariti et al. 2007). Haustoria have been shown to play a major role in nutrient uptake from the host (Hahn and Mendgen 2001) as well as delivery of small secreted effectors into the extrahaustorial matrix, some of which have been shown experimentally to be further translocated into the host cell (Rafiqi et al. 2010; Kemen et al. 2005).

With 600 species in the genus, *Uromyces* represents the second largest after *Puccinia* (Voegele 2006). *Uromyces fabae* (*U. vicia-fabae*), commonly known as a bean rust, causes yield losses up to 50% in faba bean (*Vicia faba*) crops (Tissera and Ayres 1986). A recent survey of the *U. fabae* genome enabled prediction of 599 secreted proteins that could function as effectors (Link et al. 2014). Rust transferred protein 1 (RTP1p), was the first effector protein reported to translocate from pathogen extrahaustorial matrix into the host cells (Kemen et al. 2005). Homologues of RTP1 are ubiquitous among the rust fungi and shown to be specific to the order Pucciniales, suggesting it as a core conserved rust effector which could be crucial for a biotrophic lifestyle (Pretsch et al. 2013). RTP1p has been reported to contain a C-terminal domain with cysteine protease inhibitor function (Pretsch et al. 2013), but its role in pathogenicity remains to be determined.

Genomic sequencing of *Melampsora larici-populina*, the causal agent of poplar leaf rust, has enabled the prediction of 1,184 genes encoding small secreted proteins thought to

be CSEPs (Duplessis et al. 2011a). Identification of these genes was followed by high-throughput functional analyses ('effectoromics') in *N. benthamiana* to better understand their function in plant cells (Petre et al. 2015). The candidate effector MLP107772, now known as chloroplast-targeted protein 1 (CTP1), was identified and characterised by this approach and shown to target the chloroplast and mitochondria (Petre et al. 2015). Two other members of this *Melampsora*-specific gene family, CTP2 and CTP3, also targeting the chloroplast, contain N-terminal regions similar to plant chloroplast transit peptides (Petre et al. 2016). The other CSEPs tested target the nucleus, nucleolus, small cytosolic bodies, nuclear bodies, large cytosolic aggregates, nucleoplasm and the cytosol when transiently expressed in *Nicotiana benthamiana* (Petre et al. 2015) and to chloroplasts, cytosolic bodies and plasmodesmata when transiently expressed in *Arabidopsis* (Germain et al. 2018). The candidate effector MLP124017 was shown to interact *in planta* with the poplar transcriptional co-repressor TOPLESS-related 4 (PopTPR4), most likely in the nucleus (Petre et al. 2015). Interestingly, the candidate effector that localised to the plasmodesmata, MLP37347, interacts specifically with glutamate decarboxylase 1 (GAD1) (Germain et al. 2018), a protein that is normally present in the cytosol.

Puccinia graminis f. sp. *tritici* (*Pgt*), the causal agent of wheat stem rust, has become a major threat to food security worldwide due to the emergence and migration of the new highly virulent race Ug99 (Singh et al. 2011), which has overcome resistance conferred by the globally-used stem rust resistance gene *Sr31* (Pretorius et al. 2000). More than 50 race-specific *Sr* genes have been described in wheat and several have been cloned such as *Sr33* (Periyannan et al. 2013), *Sr35* (Saintenac et al. 2013), *Sr50* (Mago et al. 2015), *Sr55* (Moore et al. 2015), and *Sr57* (Krattinger et al. 2009). *Sr33*, *Sr35* and *Sr50* are homologues of the barley MLA10 resistance protein and belong to the CNL class of resistance proteins, whereas *Sr55* encodes a hexose transporter variant and *Sr57* encodes an ABC transporter.

Recently, two *Avrs* from *Pgt* have been cloned, namely *AvrSr35* (Salcedo et al. 2017) and *AvrSr50* (Chen et al. 2017). AvrSr50 binds directly to the Sr50 resistance protein and is able to trigger cell death *in planta*. Similarly, AvrSr35 is able to trigger Sr35-dependent cell death in *N. benthamiana* and wheat leaves (Salcedo et al. 2017). When expressed in

N. benthamiana, Sr35 and AvrSr35 were shown to be associated with the endoplasmic reticulum, whereas AvrSr50 has a nucleocytosolic distribution. At present, the function of these two effectors remains unknown.

1.3 The flax-flax rust system - a model system for studying plant-rust pathogen interactions

The flax (*Linum usitatissimum*)-flax rust (*Melampsora lini*) pathosystem has been used extensively to study plant-rust pathogen interaction. Flor (1942) studied the genetics of rust resistance in flax and avirulence in the fungus, which enabled him to discover and describe the gene-for-gene concept "for each gene conditioning rust reaction in the host there is a specific gene conditioning pathogenicity in the parasite". Thirty-one rust-resistance genes have been found in flax (*L. usitatissimum*) of which 20 have been cloned (Anderson et al. 1997; Ellis et al. 1999; Dodds et al. 2001a; Lawrence et al. 1995; Lawrence et al. 2010; Dodds et al. 2001b). All of the cloned resistance genes encode TIR-NB-LRR (TNL) proteins. The 31 rust-resistance genes map to five different loci (*K*, *L*, *M*, *N*, *P*) (Islam and Mayo 1990). The *L* locus contains a single gene with multiple alleles (*L*, *L1* to *L12*, and *LH*). The *M*, *N* and *P* loci, however, are more complex consisting of tandem arrays of up to 15, four and six to eight genes with a similar sequence, respectively (Ravensdale et al. 2011).

Seven avirulence genes, *AvrL567*, *AvrM*, *AvrP4*, *AvrP123*, *AvrP*, *AvrM14* and *AvrL2*, have been cloned from flax rust (Dodds et al. 2004; Catanzariti et al. 2006; Barrett et al. 2009; Anderson et al. 2016). All encode secreted proteins. Interestingly, variants of AvrL567, AvrP123, and AvrM14 are recognised by more than one resistance protein with AvrL567 variants recognised by the L5, L6 and L7 resistance proteins (Dodds et al. 2004), AvrP123 variants recognised by the P1, P2 and P3 resistance proteins (Catanzariti et al. 2006), and AvrM14 by the M1 and M4 resistance proteins (Anderson et al. 2016). Based on sequence and structural homology, AvrM14 is a member of the nudix hydrolase superfamily of hydrolytic enzymes capable of cleaving nucleoside diphosphates linked to x (any moiety) (Anderson et al., 2016). AvrP has structural similarity with plant homeodomain (PHD) zinc finger proteins (Zhang et al., 2018). The other Avr proteins, however, have no homology with any proteins of defined function in current protein databases.

Among the avirulence proteins found in flax rust, AvrL567 and AvrM have been studied more extensively. Alleles of the *AvrL567* gene are highly polymorphic, encoding 127 aa mature proteins variously recognised by the L5, L6, and L7 resistance proteins (Dodds et al. 2004). Twelve sequence variants with 35 polymorphic amino-acid sites have been identified from six rust strains, with seven variants derived from *Avr* alleles and five from *avr* alleles. However, the polymorphisms in the variant amino acid sequences resulted in differences in recognitional specificities when these alleles are expressed in *L5, L6, L7* flax and yeast. The expression of Avrs in corresponding resistant flax varieties gives a cell death response or necrosis that serves as a proxy for the hypersensitive response. AvrL567 has been shown by yeast two-hybrid analysis to interact directly with the L5 and L6 resistance proteins (Dodds et al. 2006). Site-directed mutagenesis experiments and docking models of the interaction between the structure determined for AvrL567-A and a model of the LRR region of L5 have shown that multiple contact points along the surface area of the Avr protein are required for binding of the R and Avr protein, supporting previous findings on the importance of the LRR domain for Avr recognition (Wang et al. 2007). In the cytosol, AvrL567 interacts with flax cytokinin oxidase, LuCKX1.1 (Wan et al. 2019). It is hypothesized that this interaction results in a reduced level of cytosolic cytokinin, hence benefiting the pathogen, although how this does so remains unknown.

AvrM is a member of a small gene family with at least five paralogues, *AvrM-A*, *AvrM-B*, *AvrM-C*, *AvrM-D*, and *AvrM-E* in the avirulence allele and a single gene *avrM* in the virulence allele (Catanzariti et al. 2006). The five paralogues differ in size, ranging from 212 aa (AvrM-E) to 377 aa (AvrM-B and AvrM-C). Apart from avrM and AvrM-E, the other three paralogues are recognised by the M resistance protein. AvrM-A (343 aa) triggers the strongest cell death response when expressed in *M*-containing flax and co-expressed in tobacco (Catanzariti et al. 2006). The C-terminal domain of AvrM-A is required for the M-dependent cell death, and direct interaction between this domain and M has been confirmed by yeast-two-hybrid analysis (Catanzariti et al. 2006; Catanzariti et al. 2010). Currently, the role of AvrM in pathogenicity remains unknown. Previous studies have shown that AvrM is able to enter plant cells without the presence of the pathogen (Rafiqi et al. 2010). The N-terminal regions of AvrM and AvrL567 have been shown to be

required for uptake, but, unlike the oomycete effectors, the uptake motif sequence is not conserved between different rust effectors.

AvrP4 and its virulence allele *avrP4* were identified as variants of a single gene (Catanzariti et al. 2006). All variants of *AvrP4* encode a cysteine-rich secreted protein of 67 aa, which may be processed further to a smaller mature protein. The C-terminus of AvrP4 contains six cysteine residues in a spacing consistent with a cystine knot-motif similar to that found in the *C. fulvum* Avr9 protein. When expressed transiently in *P4*-containing flax, AvrP4 is able to trigger *P4*-dependent cell death (Catanzariti et al. 2006). *AvrP123* encodes a 94 aa secreted protein recognised by the P1, P2, and P3 resistance proteins (Catanzariti et al., 2006). Barrett et al. (2009) identified several alleles of *AvrP123*, including *AvrP,* which encodes a secreted protein of 88 aa that contains 36 polymorphic amino acids relative to AvrP123 and a C-terminal truncation of 6 aa. The crystal structure of AvrP has shown that the cysteines and two of the histidines in AvrP (and most likely AvrP123) bind to three zinc atoms and are important for the structural integrity of the protein as well as recognition by the P resistance protein (Zhang et al., 2018; discussed in detail in chapter 2). The N-terminal end of the protein structure containing the first zinc-binding region displays similarities to nucleic-acid-binding and chromatin-associated proteins involved in transcriptional regulation. AvrP and AvrP123 accumulate in the plant nucleus when expressed transiently *in planta*, consistent with a possible role in manipulation of plant transcription (Zhang et al., 2018; discussed in detail in chapter 4 and 5). Mutations of several residues polymorphic between AvrP and its allelic variants resulted in a loss of recognition by P, suggesting that these residues are required for recognition (Zhang et al., 2018; discussed in detail in chapter 2).

1.4 Research project

The research presented in this thesis aimed to fill the gaps in our knowledge about recognition of the flax rust AvrP and AvrP123 effectors by the flax P, P1, P2 and P3 resistance proteins and their role as pathogenicity factors in the rust fungus-plant interaction. The first aim of this project was to find residues or domains in the AvrP/P123 avirulence proteins that are responsible for recognition by their corresponding resistance proteins. To address this aim, several approaches were used, including

deletions, and targeted mutations and domain swaps based on sequence differences between AvrP, AvrP123 and other AvrP/P123 variants found in flax rust. Mutants/domain swaps were tested using *Agrobacterium*-mediated expression assays in leaves of *P*-transgenic tobacco for AvrP recognition and leaves of flax varieties containing *P*, *P1*, *P2* or *P3* resistance genes for AvrP123 recognition. Recognition resulted in necrosis/cell death in the infiltrated leaves. Findings related to AvrP and AvrP123 recognition are presented in Chapter 2 and 3, respectively.

The second aim of this project was to identify AvrP-interacting proteins from the host. To address this aim, a yeast-two-hybrid experiment was conducted using modified AvrP (AvrP-C8) as bait and a rust-infected flax cDNA library as prey. AvrP-C8 was then chosen as bait because it showed less autoactivity in bait-only controls compared to the native forms of AvrP or AvrP123. Several putative interactor proteins were identified in the yeast-two-hybrid experiment, but these interactors still need to be confirmed and tested further. Findings related to the yeast-two-hybrid experiment are presented in Chapter 4.

Chapter 2

Recognition of AvrP*

*The contents of this chapter were published in part in: Xiaoxiao Zhang, Nadya Farah, Laura Rolston, Daniel J. Ericsson, Ann-Maree Catanzariti, Maud Bernoux, Thomas Ve, Katerina Bendak, Chunhong Chen, Joel P. Mackay, Gregory J. Lawrence, Adrienne Hardham, Jeffrey G. Ellis, Simon J. Williams, Peter N. Dodds, David A. Jones and Bostjan Kobe. (2018) Crystal structure of the *Melampsora lini* effector AvrP reveals insights into a possible nuclear function and recognition by the flax disease resistance protein P. *Molecular Plant Pathology* 19 (5): 1196-1209. (Appendix 3)

2.1 Introduction

The flax rust *AvrP* avirulence gene is allelic to the *AvrP123* gene, which was originally predicted to encode a Kazal serine protease inhibitor (Catanzariti et al. 2006; Barrett et al. 2009). *AvrP* encodes a small secreted protein of 88 amino acid residues excluding the signal peptide. AvrP is also a cysteine-rich protein with ten cysteines excluding the signal peptide (Figure 2.1D). Analysis of purified AvrP protein has shown that these cysteine residues bind to Zn^{2+} ions rather than form disulphide bonds (Figure 2.1; (Zhang et al. 2018)). Based on the structure of AvrP, there are three Zn^{2+} binding sites found in AvrP (Figure 2.1A), comprising four cysteines (C36, C38, C78, C81) designated Zn1, three cysteines and one histidine (C53, C67, C89, H93) designated Zn2 and three cysteines and one histidine (C59, C61, C97, H101) designated Zn3 (Figure 2.1B-D). The C4–C3H (four cysteines and three cysteines one histidine) signature resembles the plant homeodomain (PHD) finger (Schindler et al. 1993) and RING (really interesting new gene) finger (Aasland et al. 1995) which each bind two Zn^{2+} ions.

AvrP is specifically recognised by the flax P resistance protein and not by the P1, P2 or P3 resistance proteins (Barrett et al. 2009). The *P* resistance gene is a member of the same complex *P* locus as *P2*, and both encode proteins with a nucleotide binding site (NBS), leucine-rich repeat (LRR) domain and an N-terminal Toll/interleukin-1 receptor (TIR) homology domain as well as a C-terminal non-LRR (CNL) domain of 153 amino acid residues (Dodds et al. 2001b). Interestingly, there are ten amino acid differences

between the P and P2 sequences, and changes in six of these residues located within the predicted β-strand/β-turn motif of four LRR units are able to change P2 specificity into P (Dodds et al. 2001b).

Several variants of *AvrP* and *AvrP123* have been found in flax rust (Table 2.1) (Dodds & Thrall, 2009). One of the variants, namely the 271 allele, which is not recognised by P, P1, P2 or P3, was used to investigate the recognition of AvrP (section 2.3.4). Other variants (339, bs25 and WA isolates) were used to study the recognition of AvrP123 (Chapter 3).

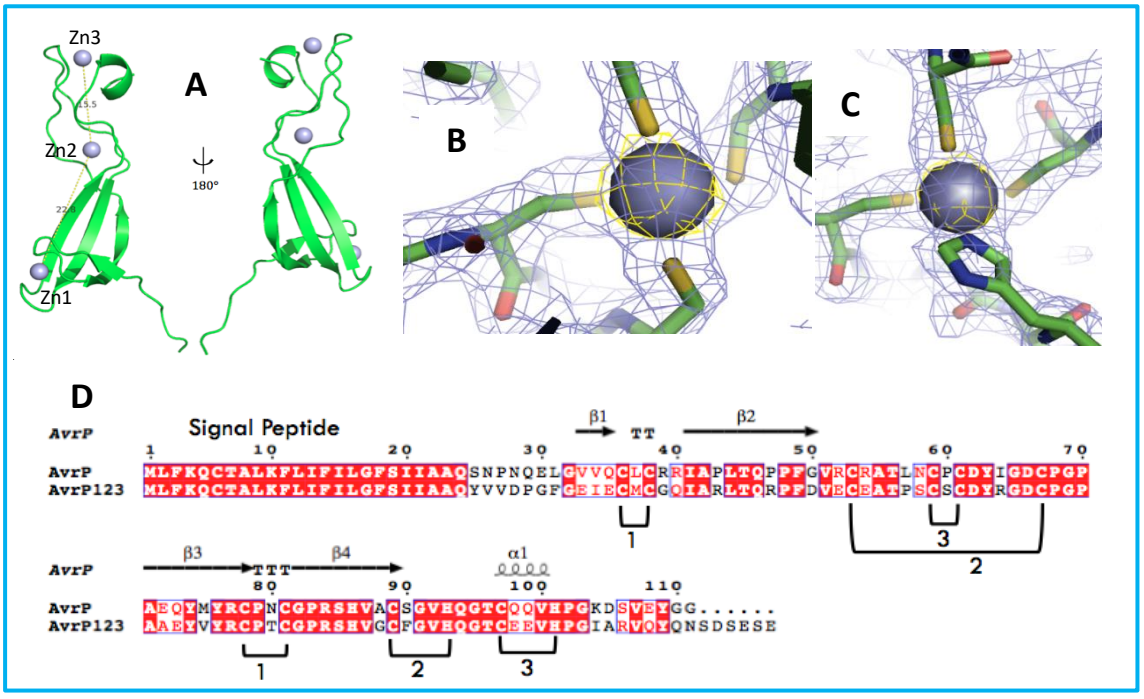

Figure 2.1 AvrP structure. (A) The overall structure of AvrP is shown as a ribbon diagram with three zinc ions bound at Zn1, Zn2 and Zn3 shown as grey spheres. (B,C) The tetrahedral coordination of zinc ions at Zn1 (B) and Zn2 (C) with cysteines (yellow sticks) and histidine (blue-green stick). (D) Sequence alignment of AvrP (Genbank accession number ACD49715) and AvrP123 (ABB96267). AvrP secondary structure is shown above the alignment. Zinc-binding residues are numbered according to their corresponding zinc ions (Zhang et al. 2018).

Table 2.1 *AvrP/P123* variants found in flax rust

	P1	P2	P3	P
AvrP123	+	+	+	-
AvrP	-	-	-	+
271	-	-	-	-
339	-	±	+	+
bs25	-	+	-	-
WA	-	+	+	-

Table taken from Dodds and Thrall (2009) showing AvrP/P123 variants and their recognition following *Agrobacterium*-mediated expression in flax varieties carrying the *P1*, *P2*, *P3* or *P* resistance genes. + indicates necrosis; - indicates no necrosis; ± indicates weak necrosis/chlorosis.

This chapter describes several approaches that were used to investigate the recognition of AvrP. These included deletions, domain swaps and site-directed mutations. Deletions were based on the AvrP structure (section 2.3.2). The importance of binding with Zn^{2+} ions for recognition by P was investigated by site-directed mutagenesis (section 2.3.3). Lastly, domain swaps were constructed to introduce polymorphic residues from the 271 variant into AvrP and vice versa (section 2.3.4). All mutants were expressed in transgenic tobacco *P* plants via *Agrobacterium*-mediated transformation and assessed for their ability to induce necrosis.

2.2 Materials and Methods

2.2.1 Bacterial cultures and antibiotics

Escherichia coli Mach1 (Invitrogen, Carlsbad, CA, USA) was used for routine cloning and generation of mutant gene constructs unless mentioned otherwise whereas *Agrobacterium tumefaciens* strain GV3101 (pMP90) was used for gene expression in tobacco. Cultures were grown in Lysogeny Broth (LB) liquid medium (10 g tryptone, 5 g yeast extract and 10 g NaCl per litre) and on LB plus 1.5% (w/v) agar (LBA) plates containing appropriate antibiotics as required. Antibiotic concentrations used were 50 µg/ml kanamycin, 50 µg/ml rifampicin, 25 µg/ml gentamycin and 10 µg/ml tetracycline. Liquid cultures of *E. coli* were grown overnight at 37 °C on a rotary shaker at 200-250 rpm whereas *E. coli* grown on agar plates was incubated overnight at 37 °C.

Agrobacterium cells were grown for 2–3 days at 28 °C in LB media with the same antibiotics concentrations as above.

2.2.2 Preparation of competent cells

For the preparation of competent *E. coli,* cells from a frozen stock were grown overnight in 10 ml of LB at 37 °C. Four ml of the culture was used to inoculate 400 ml of LB containing 10 mM $MgCl_2$ and incubated on a rotary shaker for 2–3 hours at 37 °C until the optical density at 600 nm (OD_{600}) reached 0.6 (approximately 10^8 cells per ml). The liquid culture was chilled on ice for 30 min then centrifuged at 6000 x *g* for 5 min at 4 °C. Cells were then resuspended in 200 ml of cold 50 mM $CaCl_2$ followed by incubation on ice for 20 min. Cell suspensions were re-centrifuged at 6000 x *g* for 5 min at 4 °C. The pellets were resuspended in 8 ml of 50 mM $CaCl_2$ with 10% (v/v) glycerol. The competent cells were pipetted into pre-chilled microcentrifuge tubes as 200 µl aliquots, frozen in liquid nitrogen and stored at – 80 °C.

For the preparation of electrocompetent *Agrobacterium,* cells from a frozen stock were plated on LBA + rifampicin + gentamycin and incubated for 2 days at 28 °C. A single colony was picked from the plate and resuspended in 3 ml of liquid LB + rifampicin + gentamycin and incubated overnight with shaking at 28 °C for 2 days. One ml of the overnight culture was added to 100 ml of LB without any antibiotic and incubated at 28 °C with shaking until the OD_{600} reached 0.6–0.8. After the required OD was reached, the culture was put on ice for 10 min, then centrifuged at 5000 x *g* for 10 min at 4 °C. The pellet was resuspended in 50 ml of sterile deionised water and centrifuged at 5000 x *g* for 10 min at 4 °C. The washing step with sterile deionised water was repeated 3 times. The pellet was then resuspended in 25 ml ice-cold sterile 10% (v/v) glycerol, centrifuged at 5000 x *g* for 10 min at 4 °C. The pellet was then resuspended in 1 ml ice-cold sterile 10% (v/v) glycerol and 50 µl aliquots were pipetted into pre-chilled 1.5 ml microcentrifuge tubes and frozen in liquid nitrogen. The competent cells were then stored at -80 °C.

2.2.3 Transformation of competent cells

Competent *E. coli* were transformed with 1–10 ng of plasmid DNA as follows. Frozen competent cells were thawed on ice. The plasmid or ligation to be transformed was

added to a 100 µl aliquot of cells and incubated on ice for at least 30 min. The cells were then heat shocked at 42 °C for 45 s and placed on ice again for 2 min to recover. LB media was added to a volume of 1 ml and the cells incubated with shaking at 37 °C for 45 min before spreading onto LB agar plates with appropriate antibiotics and incubating at 37 °C overnight.

Electrocompetent *Agrobacterium* cells were transformed with 100 ng of plasmid DNA as follows. Frozen competent cells were thawed on ice and 50 µl transferred to a 2 mm-gap electroporation cuvette (Bio-Rad, Hercules, CA, USA). Electroporation was performed using Bio-Rad MicroPulser electroporator using a 2.5 kV pulse, 400 Ω resistance, and 25 µF capacitance. The cells were transferred into a 1.5 ml microcentrifuge tube and revived with 1 ml of LB followed by incubation on a shaker at 28 °C for 2–3 hours. Cells (100 µl) were plated on LBA containing the appropriate antibiotics and incubated at 28 °C for 2 days.

2.2.4 Polymerase Chain Reaction (PCR)

PCR was performed using a PTC-200 Peltier Thermal Cycler (MJ Research, Massachusetts, USA). MyTaq DNA Polymerase (Bioline, London, UK) was used for general purposes whereas Phusion DNA Polymerase (New England Biolabs, Ipswich, Massachusetts, USA) was used for high fidelity DNA amplification. Generally, PCR was conducted using 1X PCR Buffer (see below) containing 200 µM of each dNTP, 0.5 µM forward primer, 0.5 µM reverse primer, 2–10 ng DNA template, and 1 unit of DNA Polymerase. For high-fidelity PCR, Phusion HF Buffer (Thermo Fisher Scientific, Waltham, MA, USA) was used whereas for low-fidelity PCR, MyTaq buffer (Bioline, London, UK) was used.

For general purposes, PCR was performed with an initial denaturation step of 95 °C for 1 min, followed by 29 cycles of denaturation at 95 °C for 15 s, primer annealing at 50–55 °C for 15 s and extension at 72 °C allowing 15–30 s for every 1 kb of product expected. For high fidelity DNA amplification, PCR was performed with an initial denaturation step of 98 °C for 30 s, followed by 35 cycles of denaturation at 98 °C for 10 s, primer annealing at 55–65 °C for 20 s and extension at 72 °C allowing 15–30 s for every 1 kb of product expected.

2.2.5 DNA gel electrophoresis

DNA was size fractionated by electrophoresis through agarose gels using a Bio-Rad gel apparatus. Electrophoresis buffer comprising 0.5X TBE buffer was prepared from a 5X stock (1.1 M Tris, 900 mM borate, 25 mM EDTA, pH 8.3) and used in the preparation of 1% (w/v) agarose gels and as a running buffer. DNA was visualised by incorporating 1X RedSafe (INtRON Biotechnology, Summit, NJ, USA) into the gel and viewing it under UV light using a Molecular Imager® Gel Doc™ XR+ System and Image Lab™ 3.0 software from Bio-Rad.

2.2.6 Preparation of plasmid DNA

Crude plasmid DNA was prepared by alkaline-lysis plasmid DNA extraction according to the protocol of Sambrook and Russell (2001). High-quality plasmid preparations for DNA sequencing and cloning procedures were obtained using the Plasmid DNA Extraction Mini kit (Favorgen Biotech Corp, Ping-Tung, Taiwan).

2.2.7 DNA sequencing

DNA sequencing was performed using the ABI Big-Dye Terminator V3.1 reaction mix (Thermo Fisher Scientific, Waltham, MA, USA) with PCR conditions following the manufacturer's protocol. The sample was purified by adding 5 µl of 125 mM EDTA and 60 µl of 100% ethanol and then incubated at RT for 15 min. The sample was then centrifuged at 10,000 x *g* at room temperature for 20 min. The pellet was washed by adding 250 µl of a freshly made 70% ethanol and centrifuging the sample again at room temperature for 5 min. The pellet was air-dried for 15 min at room temperature and then sent to the Biomedical Resource Facility at the John Curtin School of Medical Research ANU for sequencing.

2.2.8 Ligation Independent Cloning (LIC)

Most of the AvrP constructs were prepared in the pL vector (see Appendix 2) using the Ligation Independent Cloning (LIC) method. The method is illustrated in Figure 2.2 below. The pL vector, constructed by Laura Rolston in the Jones Laboratory, Research School of Biology, ANU, was based on pGreenII (Hellens et al. 2000), a binary vector containing a *npt*II gene for selection of transformed plants using kanamycin. It contains

LIC sites flanking a lethal *ccdB* gene and is in turn flanked by a Cauliflower mosaic virus (CaMV) 35S promoter and terminator. Sequences to be cloned by LIC were amplified by adding the LIC extension 5'-ACTATTTACAATTACG-3' on the forward primers and 5'-TCCTCTCCAAATTACG-3' on the reverse primers (Table 2.2) and the purified PCR product was treated with T4 DNA Polymerase (New England Biolabs [NEB], Ipswich, MA, USA) in 1X Buffer 2 (NEB), 1X BSA and 2.5 µM dCTP at 22 °C for 30 min and 75 °C for 20 min. To prepare the vector, pL was digested with *Sna*BI, purified and treated with T4 DNA polymerase in 1X Buffer 2, 1X BSA and 2.5 µM dGTP at 22 °C for 30 min and 75 °C for 20 min. PCR products (6 ng) and vector (50 ng) were mixed together and annealed at room temperature or 22 °C for 30 min prior to transformation of *E. coli* cells. Transformants were screened by colony PCR using pL primers (Table 2.2) and the integrity of the LIC constructs was confirmed by sequencing using individual pL primers. The vector was extracted from *E. coli* and transformed together with pSoup, a helper plasmid (Hellens et al. 2000), into *Agrobacterium tumefaciens* by electroporation. Once the plasmids were in *Agrobacterium* cells, the transformants were then screened by colony PCR using pL and pSoup primers (Table 2.2).

Table 2.2 Primers used in LIC

Name of construct / plasmid	Primer sequence (5'–3')	Usage
pLdSP-AvrP	F: ACTATTTACAATTACGATGCAGTCTAATCCTAATCAAGAG R : TCCTCTCCAAATTACGCTAACCTCCGTACTCCACACTG	Amplification of dSP-AvrP for LIC
pLdSP-271	F: ACTATTTACAATTACGATGCAGTCTAACCCTAATCAACAG R: TCCTCTCCAAATTACGCTAACCTCCGTACTGCACACTG	Amplification of dSP-271 for LIC
pL	LIC 1F : CACTATCCTTCGCAAGACCC LIC 2R : CCTATAAGAACCCTAATTCCC	Colony PCR & sequencing
pSoup	F: CGTGATTGCCAAGCACGTCC R: CATCATCTGTGGGAAACTCGC	Colony PCR in *Agrobacterium*
pSoup	F: CTTGGAGCCACTATCGACTACG R: GACTCCTGCATTAGGAAGCAGC	Colony PCR in *Agrobacterium*

Table showing primers used in Ligation Independent Cloning (LIC) with LIC extensions highlighted in red.

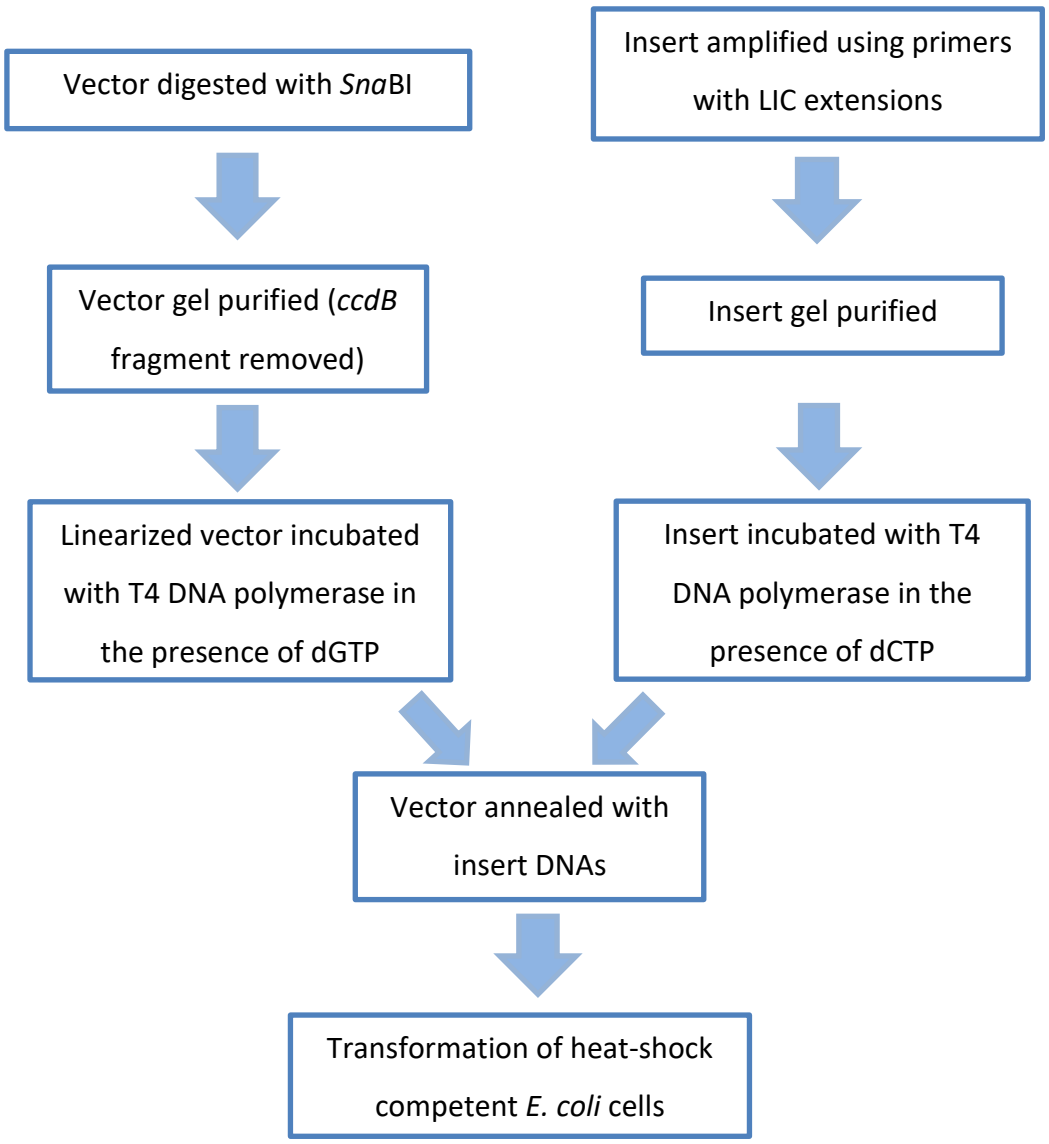

Figure 2.2 Ligation Independent Cloning (LIC). Both PCR product and vector were treated with T4 DNA Polymerase in the presence of dCTP or dGTP, respectively. The 5' to 3' polymerase and 3' to 5' exonuclease activities of T4 DNA Polymerase result in a constant cycle of removal and addition of the corresponding G or C nucleotide following exonuclease removal of sequence lacking G or C, respectively. Vector and insert can then be annealed and transformed without using DNA ligase as ligation occurs *in vivo*.

2.2.9 Construction of C-terminal HA-tag LIC vector

The sequence encoding a triple hemagglutinin (3X HA) epitope tag was introduced into the pL vector to enable C-terminal tagging of proteins expressed using the pL vector. The first step was introducing the 3X HA tag into pL and re-creating the *Sna*BI restriction site. The 3X HA sequence was amplified from an existing 3X HA tag (Hcr9 vector, Figure 2.3) with some sequence modification introduced via the HA LIC FOR and HA LIC REV

primers (Table 2.3) to facilitate LIC and to introduce the *SnaB*I site and stop codon. The 3X HA tag was then cloned into pL as per the LIC protocol (see section 2.2.8). The ligated insert-vector was then transformed into *E. coli* and confirmed by sequencing using the LIC 1F or LIC 2R primers (Table 2.2). At this stage, the *Sna*BI restriction site was restored to enable re-insertion of the *ccdB* gene. The LIC procedure used to insert the 3X HA sequence into the pL vector had removed the *ccdB* gene but recreated the *Sna*BI restriction site at the 5' end of the 3X HA sequence. The new pL::3xHA vector then contained only one *Sna*BI site.

The next step was to introduce the *ccdB* gene into the pL::3xHA to facilitate cloning with LIC. Firstly, the pL::3xHA vector was linearized by digestion with *Sna*BI and dephosphorylated with calf intestinal alkaline phosphatase (CIAP) (Promega, Madison, Wisconsin, USA) to prevent recircularisation. The *ccdB* gene (insert) was released from pL vector using *Sna*BI restriction enzyme. The small fragment corresponding to the *ccdB* gene was then purified via electrophoresis and extraction from the gel and ligated into the prepared pL::3xHA vector. The ligated vector-insert was then used to transform the *E. coli* DB3.1 cells which are resistant to the lethal effect of the *ccdB* gene. Transformants were confirmed by colony PCR using ccdB For and ccdB Rev primers (Table 2.3) and further investigated for insert orientation. The new vector (pLH) was then confirmed by sequencing using the LIC 1F or LIC 2R primers (Table 2.2) and used for cloning via LIC protocol.

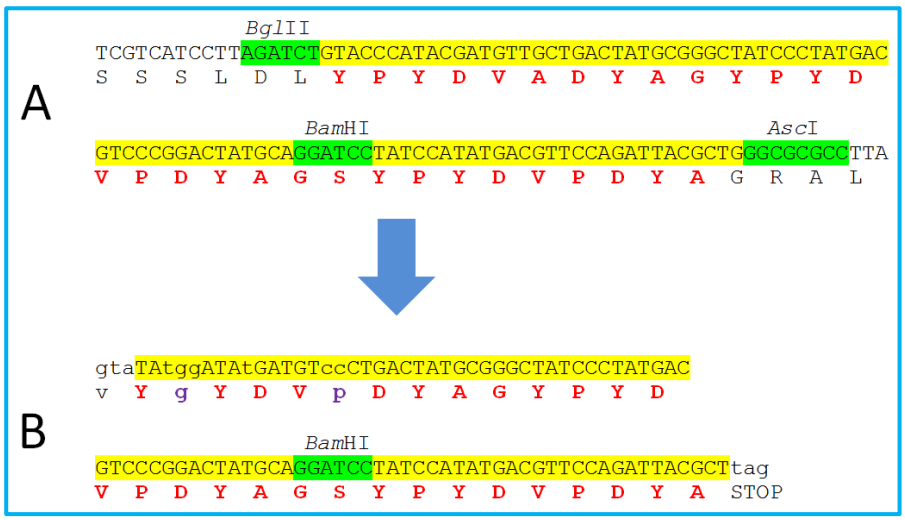

Figure 2.3 Modified bases and amino acids of the 3X HA tag used in this study. (A) The original sequence of the 3X HA tag used as a template. (B) The modified version of the 3X HA tag used in this study. Three copies of the epitope sequence YPYDVPDYA are present in the 3X HA tag. The sequence at the 5' end of the 3X HA tag was modified to remove C's to enable generation of an LIC site. In addition, an in-frame stop codon was added at the 3' end. 3X HA tag nucleotides are highlighted in yellow; restriction sites are in green; the amino acid sequence of the 3X HA tag is shown in red capitals. Modified bases and amino acids are shown in lower case.

Table 2.3 Primers used in generating a C-terminal 3X HA tag LIC vector

Name of primer	Sequence (5'–3')	Usage
HA LIC FOR	actatttacaattacgtaTAtggATAtGATGTccCTGACTATGCGG	Amplification of 3x HA tag
HA LIC REV	tcctctccaaattacgctaAGCGTAATCTGGAACGTC	
ccdB For	GAGCCGTTATCGTCTGTTTG	Colony PCR
ccdB Rev	GTGTATAACGGAGCCTGAC	Colony PCR

Table showing primers used in generating a C-terminal 3X HA tag LIC vector. The LIC extensions (highlighted in red) were introduced to enable the cloning into the pL vector. The nucleotides ta (highlighted in green) were introduced to recreate the *SnaB*I site (TACGTA, underlined) and place the 3X HA tag in the correct reading frame.

2.2.10 Domain swaps

Domain swaps were prepared using the Restriction-site Independent Cloning method (RIC, Anderson, unpublished), which was adapted from LIC. Primer design is illustrated in Figure 2.4 using an AvrP-271 swap as an example. Two PCR products are amplified so that Product 1 will contain a 5' LIC extension in combination with the 5' end of the AvrP coding region and a 3' end with at least four bases deficient in Cs and Gs (blue arrows Figure 2.4) whereas Product 2 will contain contain a complementary 5' end with at least four bases deficient in Cs and Gs and the 3' end of the 271 coding region in combination with a 3' LIC extension (green arrows Figure 2.4).

The LIC vector was prepared as per standard LIC protocol. However, at the T4 DNA polymerase treatment, the reaction was modified by replacing the NEB2 buffer used for *Sna*BI digestion with ligation buffer. Sticky ends on the inserts (two PCR products) were prepared using T4 DNA polymerase and dCTP and T4 polynucleotide kinase (PNK) was used to phosphorylate the 5' ends. The two PCR products and the LIC vector were then annealed and ligated in a 10 µl reaction as follows: 50 ng vector DNA, 10 ng PCR product 1, 10 ng PCR product 2, 1X ligation buffer (NEB), 10 mM ATP, 1 µl T4 DNA ligase (NEB, 400 U/µl). The reaction was incubated at room temperature for 2 hr to overnight, followed by a standard *E. coli* heat shock transformation. Domain swaps between AvrP and 271 (section 2.3.4) were prepared using the primer pairs shown in Table 2.4.

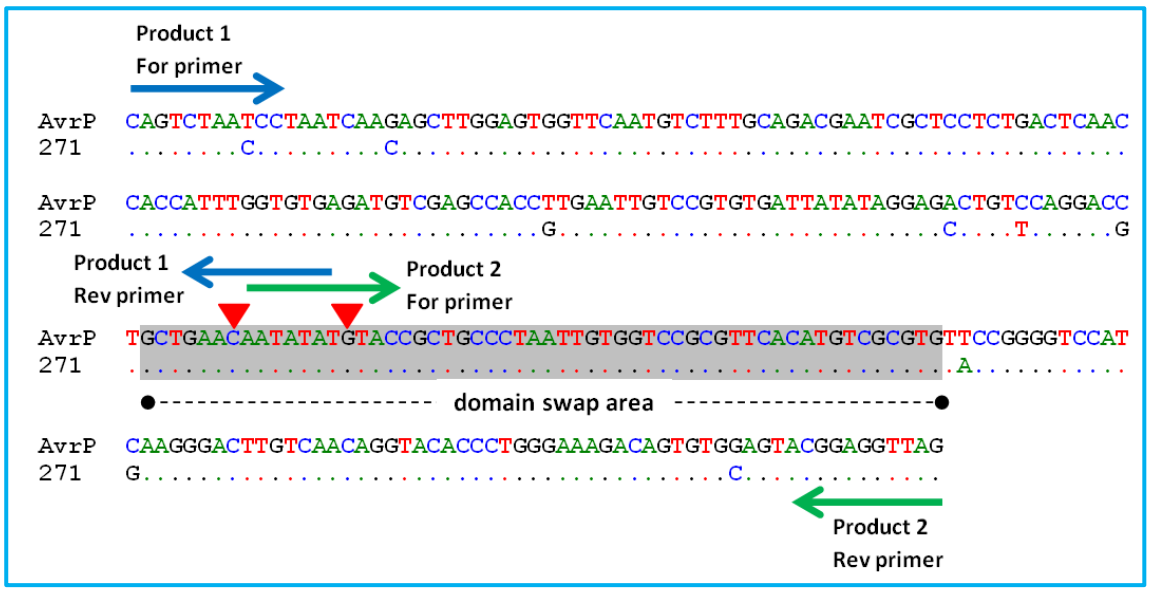

Figure 2.4 Primer design for the RIC method. The chosen domain swap area is highlighted in grey. Internal forward and reverse primers were chosen from locations where a C is separated from a G (red triangles) by a stretch of As and Ts in order to produce complementary sticky ends following treatment with T4 DNA polymerase and dCTP. AvrP sequence was amplified using a forward primer with a LIC extension and an internal reverse primer (blue arrows) whereas 271 sequence was amplified using an internal forward primer and a reverse primer with a LIC extension (green arrows).

Table 2.4 Primer pairs used in AvrP-271 domain swaps

Name of construct	DNA Template	Primer pairs
3 (5' end)	271	F : ACTATTTACAATTACGATGCAGTCTAACCCTAATCAACAG R : ATATATTGTTCAGCACGTCCTG
3 (3' end)	AvrP	F : AATATATGTACCGCTGCCC R : TCCTCTCCAAATTACGCTAACCTCCGTACTCCACACTG
1,2 (5' end)	AvrP	F : ACTATTTACAATTACGATGCAGTCTAATCCTAATCAAGAG R : ATATATTGTTCAGCAGGTCCTG
1,2 (3' end)	271	F : AATATATGTACCGCTGCCC R : TCCTCTCCAAATTACGCTAACCTCCGTACTGCACACTG

Table showing primer pairs used in AvrP-271 domain swaps. The LIC extension nucleotides are highlighted in red. A start codon (ATG) was introduced (highlighted in blue).

2.2.11 Site-Directed Mutagenesis

Site-directed mutagenesis (SDM) was performed according to the protocol from the Phusion Site-Directed Mutagenesis Kit (Thermo Fisher Scientific, Waltham, MA, USA). Primers were designed using SDM Assist (http://www.psrg.org.uk/sdm-assist.html) with the addition of a restriction site for mutant screening. Plasmid was amplified using 5' phosphorylated mutagenic primers (Table 2.5) in PCR reactions containing a high fidelity DNA Polymerase such as Phusion as described in section 2.2.2, with the addition of DMSO to 3% (v/v) for GC-rich templates. Thermal cycling was performed according to the manufacturer's instructions. PCR products were purified using a DNA Clean & Concentrator kit (Zymo Research, Irvine, CA, USA) according to the manufacturer's instructions followed by ligation using T4 DNA ligase in a 10 µl reaction. Ligation reactions were incubated for 45 min at room temperature followed by transformation into *E. coli*. Positive colonies were confirmed by digestion and sequencing.

Table 2.5 Primer pairs used for site-directed mutagenesis

Name of construct	DNA Template	Primer pairs	Restriction enzyme used for screening
1	1,2	F : GTGATTATATAGGAGCCTGTTCCGGACGTGCTGAACAATATAT R : ACGGACAATTCAAGGTGGCTCGACATCTCACAC	*Bsp*EI : TCCGGA
2	271	F : GTGATTATATAGGAGACTGTCCAGGACCAGCTGAACAATATATG R : ACGGACAATTCACGGTGGCTCGACATCTCACAC	*Pvu*II : CAGCTG
1,2 E30Q	1,2	F : ACGAATCGCTCCTCTGACTCAACCACCATTTGGTG R : CTGCAAAGACATTGTACAACTCCAAGTTGTTGATTAGGATT	*Bsr*GI : TGTACA
1,2 L57V	1,2	F : CCATTTGGTGTGCGCTGCAGAGCCACCGTTAATTGTCCGTGTG R : TGGTTGAGTCAGAGGAGCGATTCGTCTGCAAAGAC	*Pst*I : CTGCAG
1,3	AvrP	F : GTGATTATATAGGAGCCTGTTCCGGACGTGCTGAACAATATAT R : ACGGACAATTCAAGGTGGCTCGACATCTCACAC	*Bsp*EI : TCCGGA
2,3	3	F : GTGATTATATAGGAGACTGTCCAGGACCAGCTGAACAATATATG R : ACGGACAATTCACGGTGGCTCGACATCTCACAC	*Pvu*II : CAGCTG
2,3 S90T	2,3	F : TCACATGTCGCGTGTACTGGTGTACATCAAGGGACTTGTCA R : ACGCGGACCACAATTAGGGCAGCGGTACATATATTG	*Bsr*GI : TGTACA
2,3 Q94E	2,3	F : TCACATGTCGCGTGTTCCGGTGTACATGAAGGGACTTGTCAAC R : ACGCGGACCACAATTAGGGCAGCGGTACATATATTG	*Bsr*GI : TGTACA

D66A	AvrP	F : GTGATTATATAGGAGCCTG**TCCCGGG**CCTGCTGAACAATATAT R : ACGGACAATTCAAGGTGGCTCGACATCTCACAC	*Sma*I : CCCGGG
P68S	AvrP	F : GTGATTATATAGGAGACTGT**TCCGGA**CCTGCTGAACAATATAT R : ACGGACAATTCAAGGTGGCTCGACATCTCACAC	*Bsp*EI : TCCGGA
P70R	AvrP	F : GTGATTATATAGGAGACTGT**CCCGGG**CGTGCTGAACAATATAT R : ACGGACAATTCAAGGTGGCTCGACATCTCACAC	*Sma*I : CCCGGG
P68S + P70R	AvrP	F : GTGATTATATAGGAGACTGT**TCCGGA**CGTGCTGAACAATATAT R : ACGGACAATTCAAGGTGGCTCGACATCTCACAC	*Bsp*EI : TCCGGA

Table showing primer pairs used in site-directed mutagenesis. Nucleotide changes are highlighted in red; restriction sites introduced are in bold and underlined.

2.2.12 Selection of homozygous transgenic W38::*P* tobacco

Seventeen progeny sown from seed of the primary transformant of a transgenic tobacco W38::*P* line (supplied by CSIRO Agriculture and Food, Canberra) were screened by PCR for the presence of the *P* resistance gene. DNA was extracted from 100–200 mg of young tobacco leaf. Leaf tissues were ground in a chilled mortar and pestle with liquid nitrogen. The powdered tissues were then transferred to a 2 ml microcentrifuge tube and put on ice before adding 900 µl of nuclear extraction buffer (7.5 ml nuclear lysis buffer (200 mM Tris-HCl pH 7.5; 50 mM EDTA; 2 M NaCl; 2% (w/v) CTAB), 5 ml sterile milliQ water, 0.1 g sodium bisulphite) and vortexing to mix. Following addition of 90 µl of 10% (v/v) N-lauroylsarcosine each sample was inverted 4–6 times to mix. Samples were then incubated at 65 °C for 20 min and chilled on ice. An equal volume (900 µl) of 25:24:1 phenol:chloroform:isoamyl alchohol were then added to each sample and vortexed to mix. After centrifugation for 15 min at 10,000 x g, the supernatants were transferred to clean 2 ml microcentrifuge tubes. A 0.6 volume of isopropanol was then added to each sample and inverted 4–6 times to mix. After centrifugation for 20 min at 10,000 x g, pellets were washed with 80% (v/v) ethanol. Pellets were air dried and resuspended in TE buffer.

PCR positive and negative progeny were then grown for seed production following self fertilisation. A homozygous line was identified by screening the self seed from each PCR positive plant on MS (Murashige-Skoog; 4.3 g MS basal medium (Sigma Aldrich), 30 g sucrose, 5 g Agargel pH 5.8) media containing 50 µg/ml spectinomycin, using self-seed from PCR negative progeny as negative controls.

2.2.13 *Agrobacterium*-mediated gene expression in tobacco

Cultures of *Agrobacterium* strain GV3101 (pMP90) containing binary vector expression constructs were prepared to OD_{600} of 1.0 in 10 mM MES (pH 5.5) with 10 mM $MgCl_2$ and 200 µM acetosyringone. The cell suspension was incubated in the dark at room temperature for at least 2 hr prior to infiltration. Six- to seven-week-old W38 and W38::*P* tobacco plants were used for infiltration. Agroinfiltration was performed using a 1 ml syringe (without a needle) on the abaxial side of the leaves. The plants were grown in a controlled growth chamber at 24 °C with an 8 hr light (200 µmol m^{-2} s^{-1})/16 hr dark cycle from 1–2 days prior to infiltration until 4–5 days post infiltration. Co-expression of an *R*

gene with the corresponding *Avr* gene triggers host-defence responses that result in necrosis within the infiltrated leaf area.

2.2.14 Western blots

Tissue (2 leaf discs, approximately 0.9 cm in diameter) from agroinfiltrated W38 *N. tabacum* or *N. benthamiana* leaves was sampled at 2 days post infiltration, frozen and briefly ground in a microtube using a plastic pestle, and resuspended in 100 µl of 2X sample loading buffer (125 mM Tris pH 7.5, 4% (w/v) SDS, 20% glycerol (v/v), 0.02% (w/v) bromophenol blue, 0.2 M dithiothreitol). The samples were then boiled for 5 min at 95 °C and centrifuged at 10,000 x g for 5 min to remove cellular debris.

Twelve to fifteen µl of protein samples were fractionated by 12.5–14% gradient sodium dodecyl sulphate-polyacrylamide gel electrophoresis (SDS-PAGE) with the Precision Plus protein standards (Bio-Rad, Hercules, California, USA) used as a protein ladder. The SDS-PAGE gel was prepared using a standard separating and stacking gel as described in Laemmli (1970). The gel was then transferred onto Amersham Protran 0.2 NC membrane (GE Healthcare, Little Chalfont, UK). After transfer, the membrane was blocked overnight using 5% skim milk in 1X TBST (10 mM Tris-HCl pH 7.5, 150 mM NaCl, 0.1% Tween20). The membrane was then incubated with a 1 : 1000 primary antibody 3F10 clone anti-HA from rat (Roche Diagnostics Ltd, Basel, Switzerland) and a 1 : 5000 α-rat IgG horseradish peroxidase-linked secondary antibody from goat (Sigma, St. Louis, Missouri, USA) for one hour each at room temperature. Between the incubation with primary and secondary antibody, the membrane was washed three times for 5 minutes with 1X TBST. The blot was then treated with Amersham ECL Western Blotting Detection Reagent (GE Healthcare) and labelled proteins detected using the Image Quant LAS 4000 instrument (GE Healthcare). After detection, the membrane was stained with Ponceau S staining (0.1% (w/v) Ponceau S, 5% (v/v) acetic acid) for visualisation of protein loading.

2.3 Results

2.3.1 Screening of transgenic tobacco W38::*P* homozygous line

Seventeen progeny of the primary transformant were screened for the presence of the *P* transgene using the P_For and P_Rev primer pair (Table 2.6), which amplified ~ 600 bp

of the *P* gene. The hsr203A and hsr203B primer pair (Table 2.6) were used as an internal positive control for the PCR reaction and amplified two PCR products of ~ 934 bp and ~ 200 bp (Figure 2.5A). Both primer pairs were used in a single PCR reaction (i.e. multiplex PCR).

Table 2.6 Primer pairs used in screening of transgenic *P* tobacco

Name of primer	Sequence (5'–3')
P_For	TACCGGAGAATGGGAGTACG
P_Rev	TTTCCACAACCGCCTTAATC
hsr203A	GAGGAAGTATCCGGCTGGCTTAG
hsr203B	CAGAACCAGTTACAGGGTCCATTC

Based on PCR screening, ten progeny (1, 3, 4, 6, 11, 12, 13, 14, 16, and 17) contained the *P* gene whereas 4 progeny (2, 8, 10, and 15) did not contain the *P* gene (Figure 2.4A). Three progeny (5, 7 and 9) were excluded from analysis as they failed to amplify either the *P* gene or the internal control. A 10 : 4 ratio of *P* positive to negative progeny fitted a Mendelian 3 : 1 ratio (χ^2 with 1 degree of freedom = 0.095, $p > 0.75$) suggesting a single transgene locus.

Progeny of these 14 plants were screened on MS media containing 50 µg/ml spectinomycin, which inhibits plastid biosynthesis. Plants containing the *P* transgene will be green owing to the presence of the spectinomycin resistance gene used for selection of the primary transformants, while those lacking the *P* gene will have bleached cotyledons. A line homozygous for the *P* transgene did not contain any bleached cotyledons (Figure 2.5B) whereas lines derived from heterozygous plants segregated for green and bleached seedlings (Figure 2.5C). From the ten *P* positive plants, only one line was homozygous whereas the other nine were segregating. A line derived from one of the *P* negative progeny was used as a negative control (Figure 2.5D).

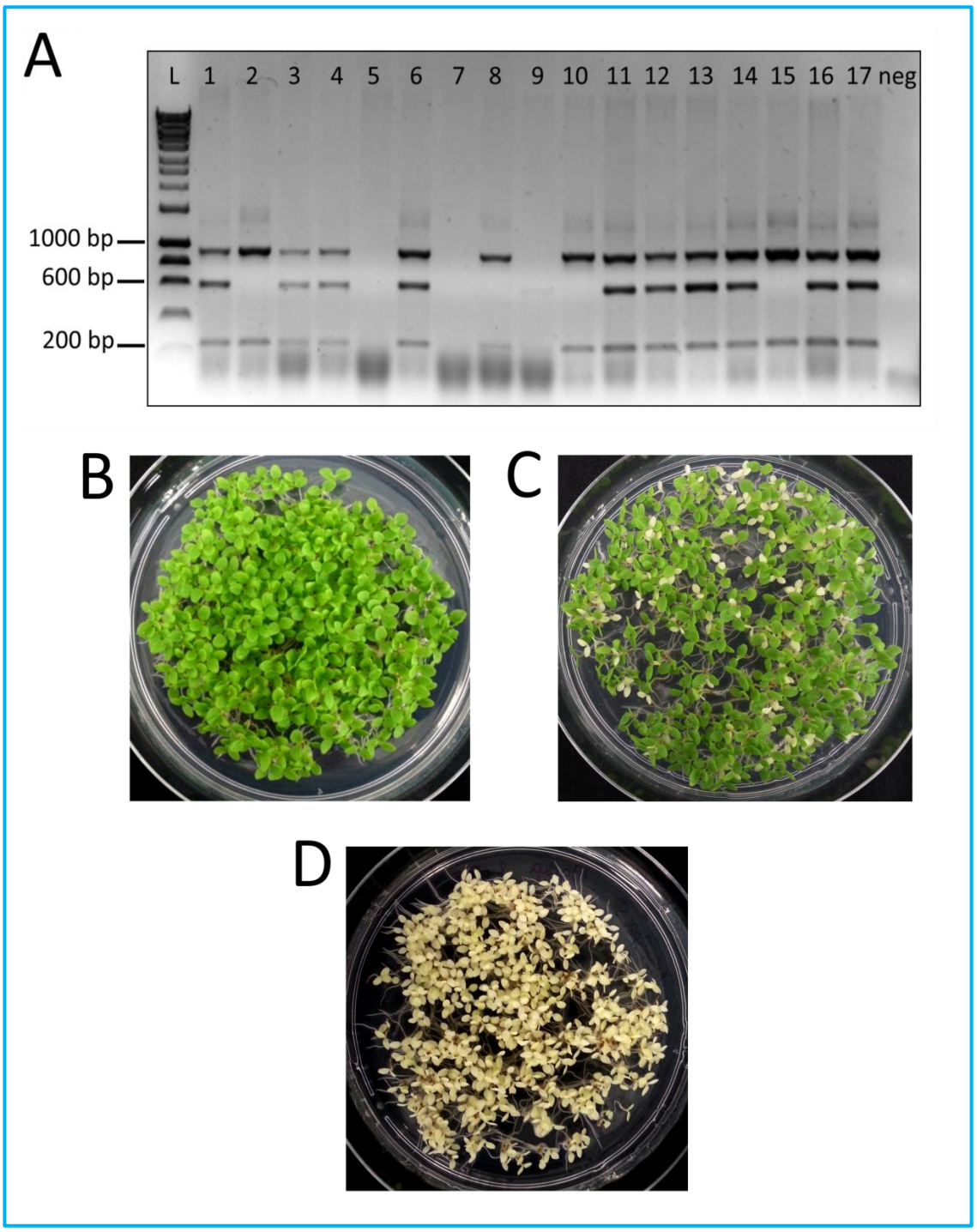

Figure 2.5 Screening for a homozygous transgenic W38::*P* tobacco line. (A) PCR screening of 17 progeny of a tobacco W38::*P* primary transformant using *P*-gene specific primers and a tobacco housekeeping gene as an internal control. L = Hyperladder I (Bioline). (B) Seedlings of a homozygous *P* line. (C) Seedlings of a segregating line. (D) Bleached seedlings indicating the absence of the *P* gene. Seedlings were photographed 7 days after sowing on MS media containing 50 µg/ml spectinomycin.

2.3.2 Full-length AvrP is important for recognition

In order to determine whether full-length of AvrP is important for recognition by P, three large deletions were made based on the AvrP structure, one at the N-terminus (Δ25-35), one at the C-terminus (Δ96-111), and one internal deletion (Δ58-64) (Figure 2.6A). A mutant carrying both the C-terminal and internal deletions (Δ58-64 + Δ96-111) was also made (Figure 2.6A).

The deletion at the N-terminus was based on the previous studies on AvrM and AvrL567 where the signal for plant uptake was found at the N-terminus (Rafiqi et al. 2010). Based on the structure, the deletion at the N-terminus omits beta-sheet 1 (β1, Figure 2.1D). However, no protein was detected for the N-terminal deletion (Figure 2.6C), so it was not possible to determine whether AvrP recognition was affected by this mutation.

The C-terminal deletion (Δ96-111) omits alpha helix 1 (α1, Figure 2.1D) and nine C-terminal residues not represented in the structure. This deletion also disrupted the Zn3 binding site via the loss of C97 and H101 whereas the internal deletion (Δ58-64) disrupted the Zn3 binding site via the loss of C59 and C61. In *P* tobacco leaves, both deletions failed to trigger cell death (Figure 2.6B), suggesting that both the internal region (residues 58-64) and the C-terminus (residues 96-111) are important for AvrP recognition, most probably because residues within these two regions binding with Zn3 were deleted. A combination of the internal deletion and C-terminal deletion (Δ58-64 + Δ96-111) also resulted in the loss of recognition by P (Figure 2.6B). In conclusion, full length AvrP seems to be required for recognition by P.

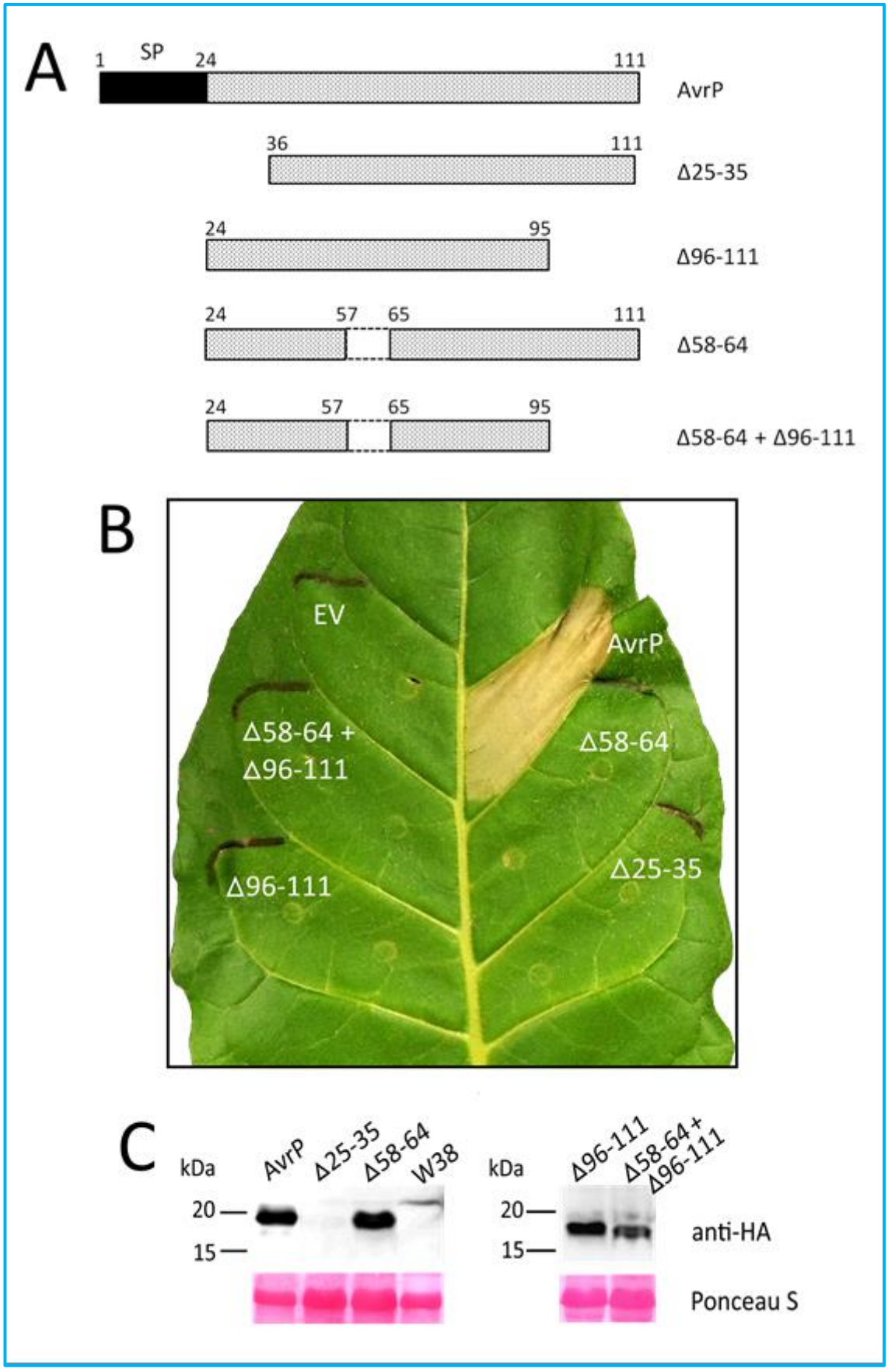
A
1
SP
24
111
AvrP
36
111
Δ25-35
24
95
Δ96-111
24
57
65
111
Δ58-64
24
57
65
95
Δ58-64 + Δ96-111
B
EV
AvrP
Δ58-64 +
Δ96-111
Δ58-64
Δ96-111
Δ25-35
C
kDa
AvrP
Δ25-35
Δ58-64
W38
20
15
kDa
Δ96-111
Δ58-64+
Δ96-111
20
15
anti-HA
Ponceau S

Figure 2.6 Effect of AvrP deletion mutants on necrosis induced in *P* tobacco. (A) Diagram of AvrP deletions which includes an N-terminal deletion (Δ25-35), a C-terminal deletion (Δ96-111), an internal deletion (Δ58-64), and an internal deletion + C-terminal deletion (Δ58-64 + Δ96-111). AvrP and all deletions were constructed without a signal peptide. (B) Agroinfiltration results for constructs described in (A) on W38::*P* transgenic tobacco. Empty vector (EV) was used as a negative control. The photograph was taken 5 days after agroinfiltration. The experiment was repeated at least two times with six leaves per experiment. (C) Upper panel shows a gel blot of HA-tagged AvrP (without signal peptide), Δ25-35, Δ96-111, Δ58-64, and Δ58-64+Δ96-111 proteins expressed under the control of the 35S promoter in agroinfiltrated W38 tobacco leaves. Untreated W38 leaf was used as a negative control. Protein was extracted 2 days after agroinfiltration and the blot was probed with the anti-HA antibody. Positions and sizes (kDa) of protein molecular mass standards are indicated. The lower panel shows the Ponceau-S-stained membrane confirming approximately equal protein loading.

2.3.3 Zn^{2+} binding is important for recognition of AvrP by P

Zhang et al. (2018) reported that Zn^{2+} ions are required for AvrP protein production and crystallisation. They also suggested that Zn^{2+} may play a role in the structural integrity of AvrP. Based on the structure determined for AvrP, Zn^{2+} ions bind to AvrP at three positions. Zn1 comprising four cysteines (C36, C38, C78, C81) and Zn2 and Zn3 each comprising three cysteines and one histidine (C53, C67, C89, H93 and C59, C61, C97, H101, respectively). To investigate the importance of Zn^{2+} binding in AvrP recognition by P, three mutations were generated each targeting the four residues that correspond to one of the Zn^{2+} binding sites and replacing them with alanines i.e. C36A, C38A, C78A and C81A for Zn1, C53A, C67A, C89A and H93A for Zn2 and C59A, C61A, C97A and H101A for Zn3.

Derivatives of AvrP carrying mutations in each of the three Zn^{2+} binding sites failed to trigger cell death following *Agrobacterium*-mediated expression in *P* tobacco leaves (Figure 2.7A), suggesting that these binding sites are each important for AvrP recognition by the P resistance protein. Each of the HA-tagged mutant proteins was detectable following gel electrophoresis and immunoblotting for the HA-tag (Figure 2.7B), although the Zn1 and Zn2 mutants were not as abundant as the Zn3 mutant and

wild type (AvrP-HA) proteins. Lack of ability to trigger cell death is therefore not due to lack of protein expression, but most likely due to changes in the structural integrity of AvrP. It seems that AvrP needs to bind to all three Zn^{2+} ions in order to maintain its structure and be recognised by P.

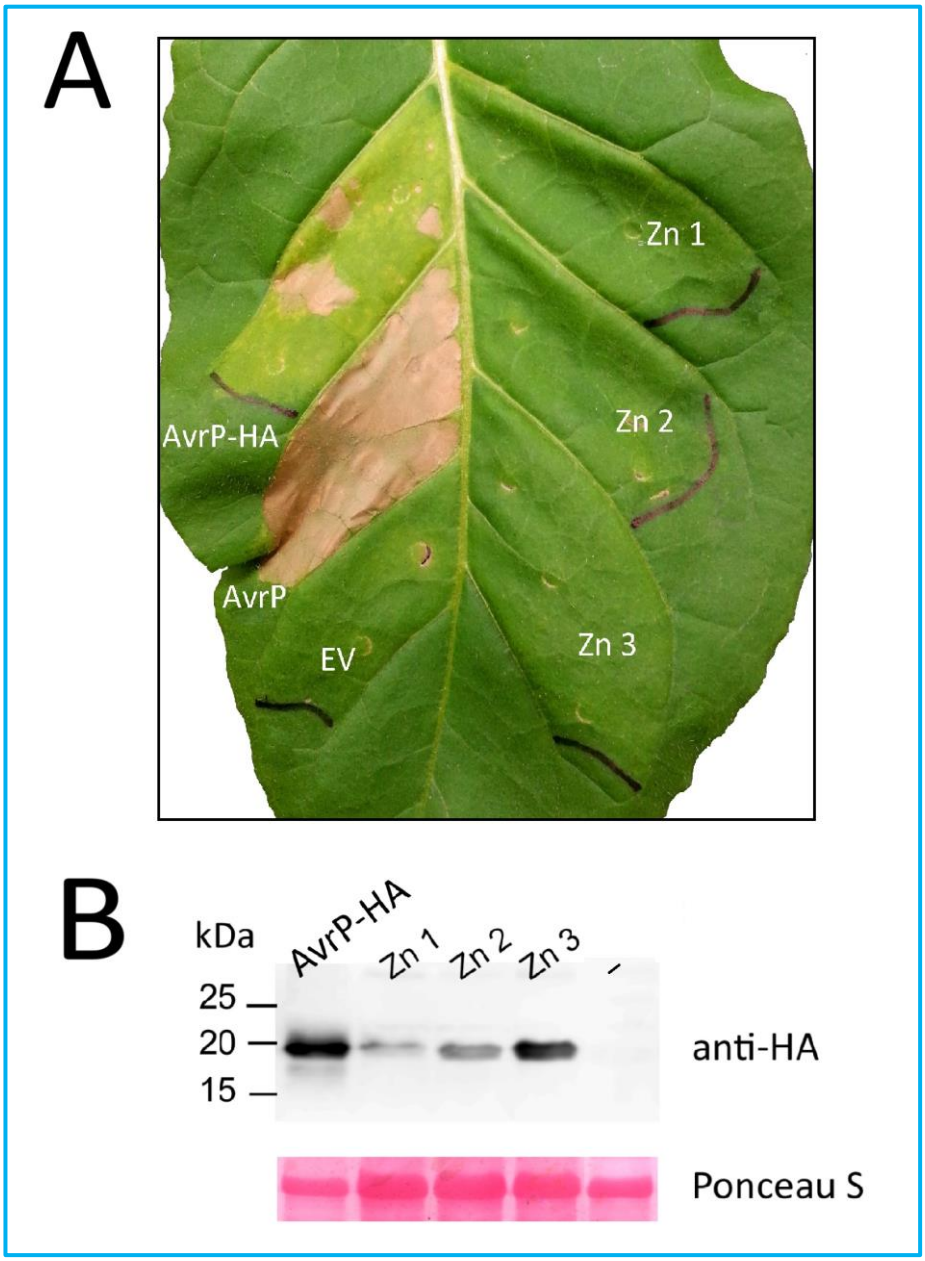

Figure 2.7 Effect of zinc (Zn)-binding motif mutants of AvrP on necrosis induced in *P* tobacco. (A) AvrP protein (lacking the signal peptide) fused with a haemagglutinin (HA) tag (AvrP-HA) or without a tag (AvrP) and AvrP-HA containing mutations in the Zn-binding residues (Zn1, Zn2, Zn3) were expressed in W38::*P* transgenic tobacco. Empty vector (EV) was used as a negative control. The photograph was taken 5 days after agroinfiltration. The experiment was repeated at least two times with six leaves per

experiment. (B) Upper panel shows a gel blot of HA-tagged AvrP and Zn1, Zn2 and Zn3 mutants expressed under the control of the 35S promoter in agroinfiltrated W38 tobacco leaves. Non-infiltrated leaf tissue (-) was used as a negative control. Protein was extracted 2 days after agroinfiltration and the blot was probed with anti-HA antibody. Positions and sizes (kDa) of protein molecular mass standards are indicated. The lower panel shows the Ponceau S stained membrane confirming approximately equal protein loading.

2.3.4 Identification of amino acid residues important for AvrP recognition

2.3.4.1 Domain swaps with the 271 variant of AvrP

In order to determine regions in AvrP that contribute to recognition by P, domain swaps were made using the 271 variant of AvrP, which is not recognised by P. There are eight polymorphic residues between AvrP and the 271 variant (Figure 2.8A). For the purposes of domain swaps, these proteins were divided into three regions designated 1, 2 and 3 each containing two or three of the polymorphic sites. Domain swaps were named according to the region of AvrP they contained e.g. domain swap 1 contains AvrP region 1, domain swap 1,2 contains AvrP regions 1 and 2 and so on. Agroinfiltration with domain swaps 1 and 3 did not induce necrosis on *P* tobacco but domain swap 2 did induce some necrotic spots suggesting a slight gain of AvrP recognition (Figure 2.8). This result suggested that polymorphic residues D66, P68 or P70 in region 2 may be important for AvrP recognition. The importance of this region was confirmed by domain swap 1,3, which did not induce any necrosis in *P* tobacco (Figure 2.9). On the other hand, domain swaps 1,2 and 2,3 showed greater necrosis than domain swap 2 alone indicating that polymorphic residues in regions 1 and 3, whilst not sufficient to trigger necrosis by themselves, contributed to the necrotic response triggered by polymorphic residues in region 2 (Figure 2.9).

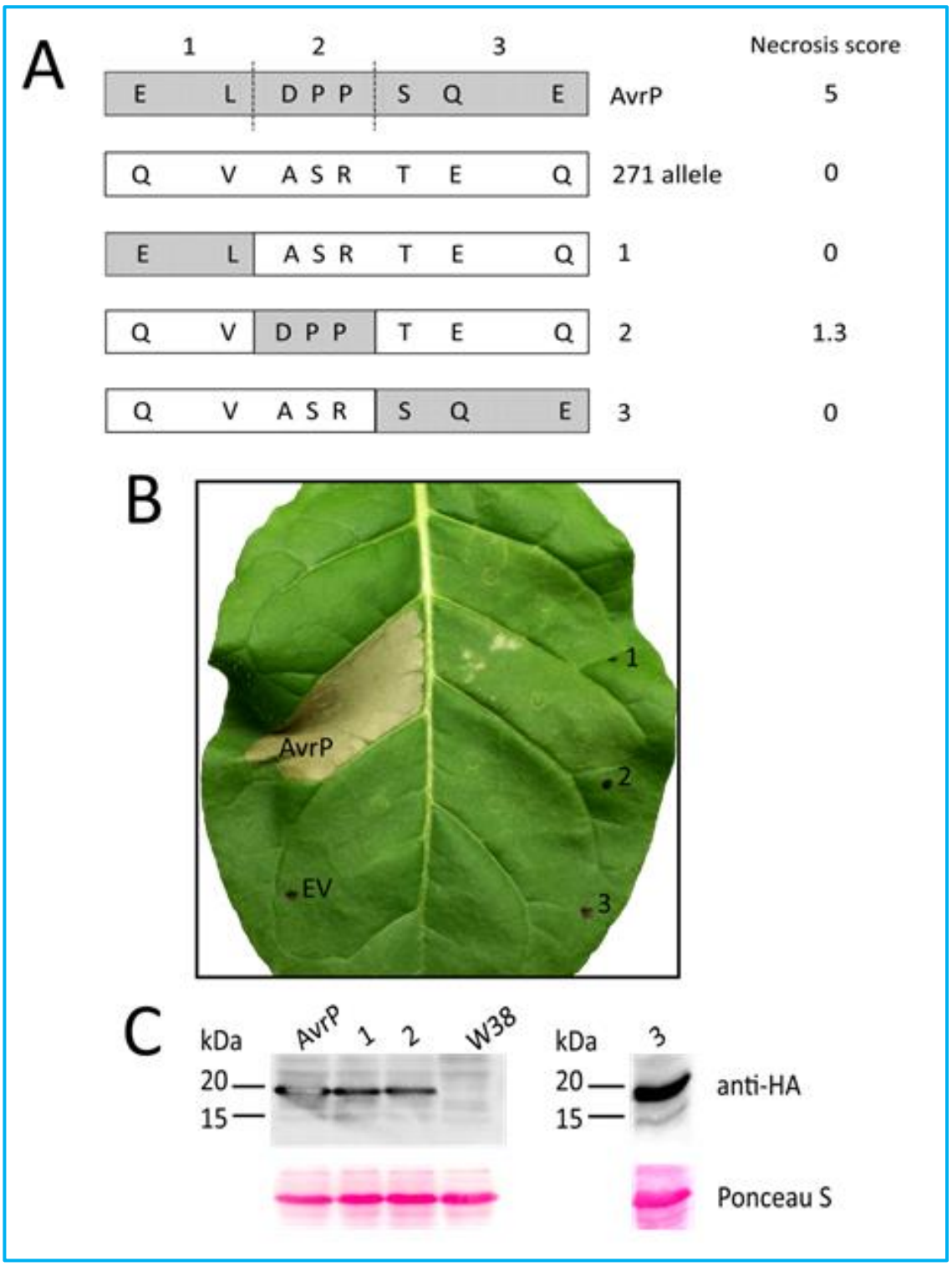
A
1
2
3
Necrosis score
E L D P P S Q E
AvrP
5
Q V A S R T E Q
271 allele
0
E L A S R T E Q
1
0
Q V D P P T E Q
2
1.3
Q V A S R S Q E
3
0
B
AvrP
EV
1
2
3
C
kDa
AvrP
1
2
W38
20
15
kDa
3
20
15
anti-HA
Ponceau S

Figure 2.8 Effect of domain swaps between regions 1, 2 and 3 of AvrP and its 271 variant on necrosis induced in *P* tobacco. (A) Diagram of domain swaps generated between AvrP and its 271 variant. The eight amino acid residues polymorphic between the two proteins are shown in capital letters on grey (AvrP) and white (271) bars. AvrP and its 271 variant were divided into three regions for the purposes of domain swapping and the domain swaps were named according to the AvrP region they contained. All constructs were made without a signal peptide coding sequence. Necrosis scores were determined as the average of the necrosis scores for each construct ranging from 0 (lowest) to 5 (highest) where 1 = 10-20% of the infiltrated area showing necrosis, 2 = 21-40% , 3 = 41 – 60% , 4 = 61-80%, 5 = 81-100%. The experiment was repeated at least two times with six leaves per experiment. (B) Agroinfiltration results for constructs described in (A) on W38::*P* transgenic tobacco. Photograph was taken at 3 dpi. Empty vector (EV) was used as a negative control. (C) Protein extracts from *N. tabacum* leaf tissue (W38) and infiltrated leaf tissue expressing the AvrP-271 variants described in (A) were size fractionated by gel electrophoresis and analysed by immunoblotting with anti-HA antibody. Positions and sizes (kDa) of protein molecular mass standards are indicated. The lower panel shows Ponceau S staining of protein bands on the blotted nitrocellulose membranes showing protein loading.

2.3.4.2 Site-directed mutagenesis of residues polymorphic between AvrP and its 271 variant

To investigate the contribution of residues in region 1 to the necrosis induced by domain swap 1,2, the AvrP-specific residues (E30 and L57) in region 1 of domain swap 1,2 were converted individually to their 271 counterparts (Q and V respectively) by site-directed mutagenesis. Both 1,2 E30Q and 1,2 L57V showed a reduction in necrosis on *P* tobacco compared to domain swap 1,2 indicating that both region 1 residues contribute to the necrosis induced by region 2 (Figure 2.9). However, 1,2 L57V showed a much greater reduction in necrosis induced than 1,2 E30Q suggesting that L57 makes a greater contribution to AvrP recognition than E30.

Domain swap 1,2 showed a lower average necrosis score than domain swap 2,3 (Figure 2.9) suggesting that polymorphic residues in region 3 of AvrP played a more important role in the necrosis triggered by region 2 of AvrP than the polymorphic residues in region

1 of AvrP. To investigate the contribution of residues in region 3 to the necrosis induced by domain swap 2,3, the AvrP-specific residues (S90, Q94 and E108) in region 3 of domain swap 2,3 were converted individually to their 271 counterparts (T, E and Q respectively) by site-directed mutagenesis. 2,3 S90T showed only a slight reduction in necrosis on *P* tobacco compared to domain swap 2,3 (Figure 2.10) suggesting that S90 plays only a minor role in AvrP recognition. 2,3 Q94E and 2,3 E108Q both showed a much greater reduction in necrosis on *P* tobacco compared to domain swap 2,3 (Figure 2.10) suggesting that both contribute to AvrP recognition. Investigation of residue E108 alone in combination with residues in region 2 (2,3 S90T + Q94E, Figure 2.10) resulted in a lower necrosis score compared to domain swap 2,3 suggesting that this residue is needed in combination with another residue, presumably Q94E.

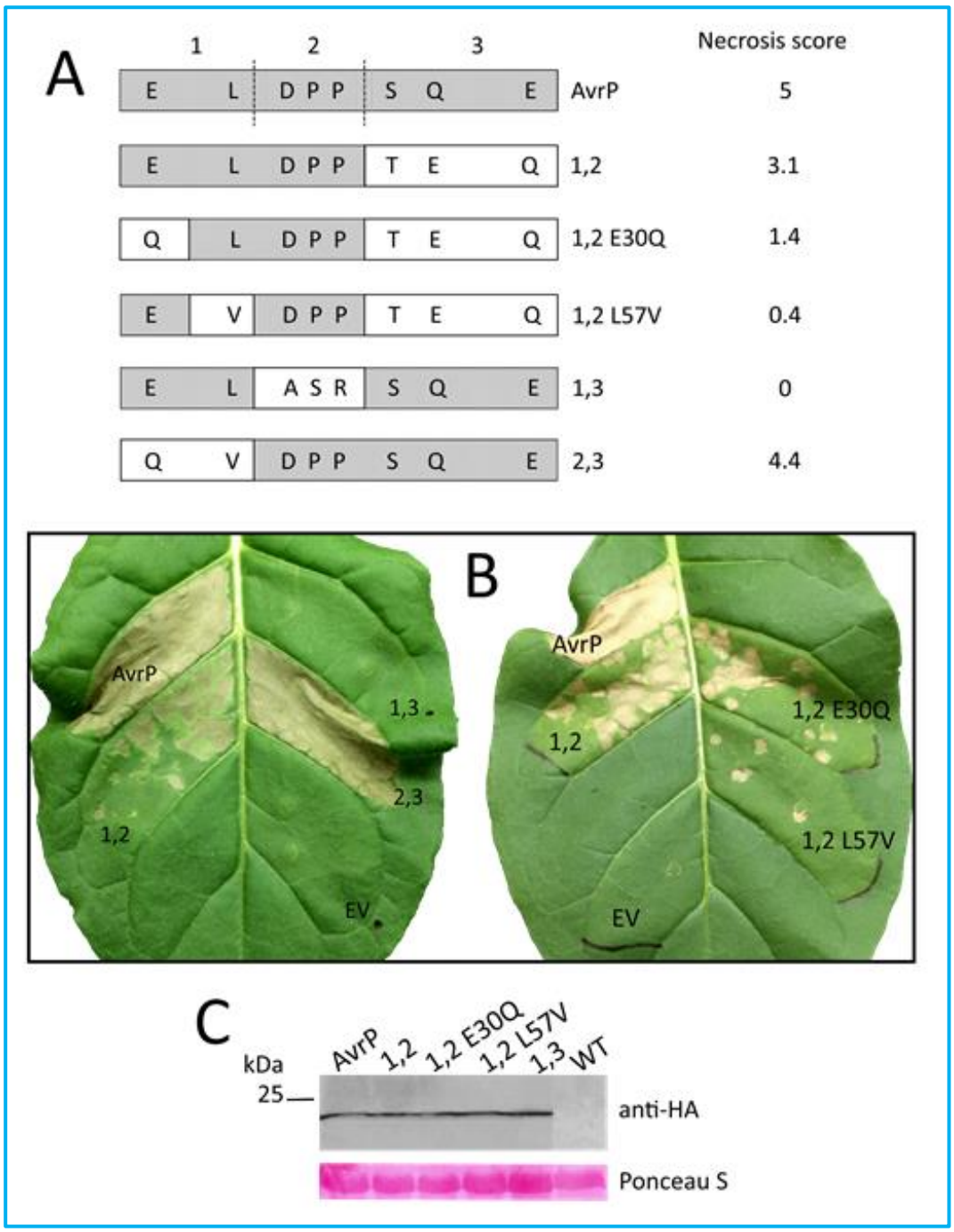

Figure 2.9 Effect of combining regions of AvrP and its 271 variant on necrosis induced in *P* tobacco. (A) Diagram of constructs combining regions of AvrP and its 271 allele and mutants thereof. The eight amino acid residues polymorphic between the two proteins are shown in capital letters on grey (AvrP) and white (271) bars. All constructs were made without a signal peptide coding sequence. Necrosis scores were determined as the average of the necrosis scores for each construct ranging from 0 (lowest) to 5 (highest) where 1 = 10-20% of the infiltrated area showing necrosis, 2 = 21-40% , 3 = 41 – 60% , 4 = 61-80%, 5 = 81-100%. The experiment was repeated at least two times with six leaves per experiment. (B) Agroinfiltration results for constructs described in (A) on

W38::*P* transgenic tobacco. Photographs were taken at 3 dpi (left) and 5 dpi (right). Empty vector (EV) was used as a negative control. (C) Protein extracts from *N. benthamiana* leaf tissue (WT) and infiltrated *N. benthamiana* leaf tissue expressing the AvrP-271 variants described in (A) were size fractionated by gel electrophoresis and analysed by immunoblotting with anti-HA antibody. Positions and sizes (kDa) of protein molecular mass standards are indicated. The lower panel shows Ponceau S staining of protein bands on the blotted nitrocellulose membranes showing protein loading.

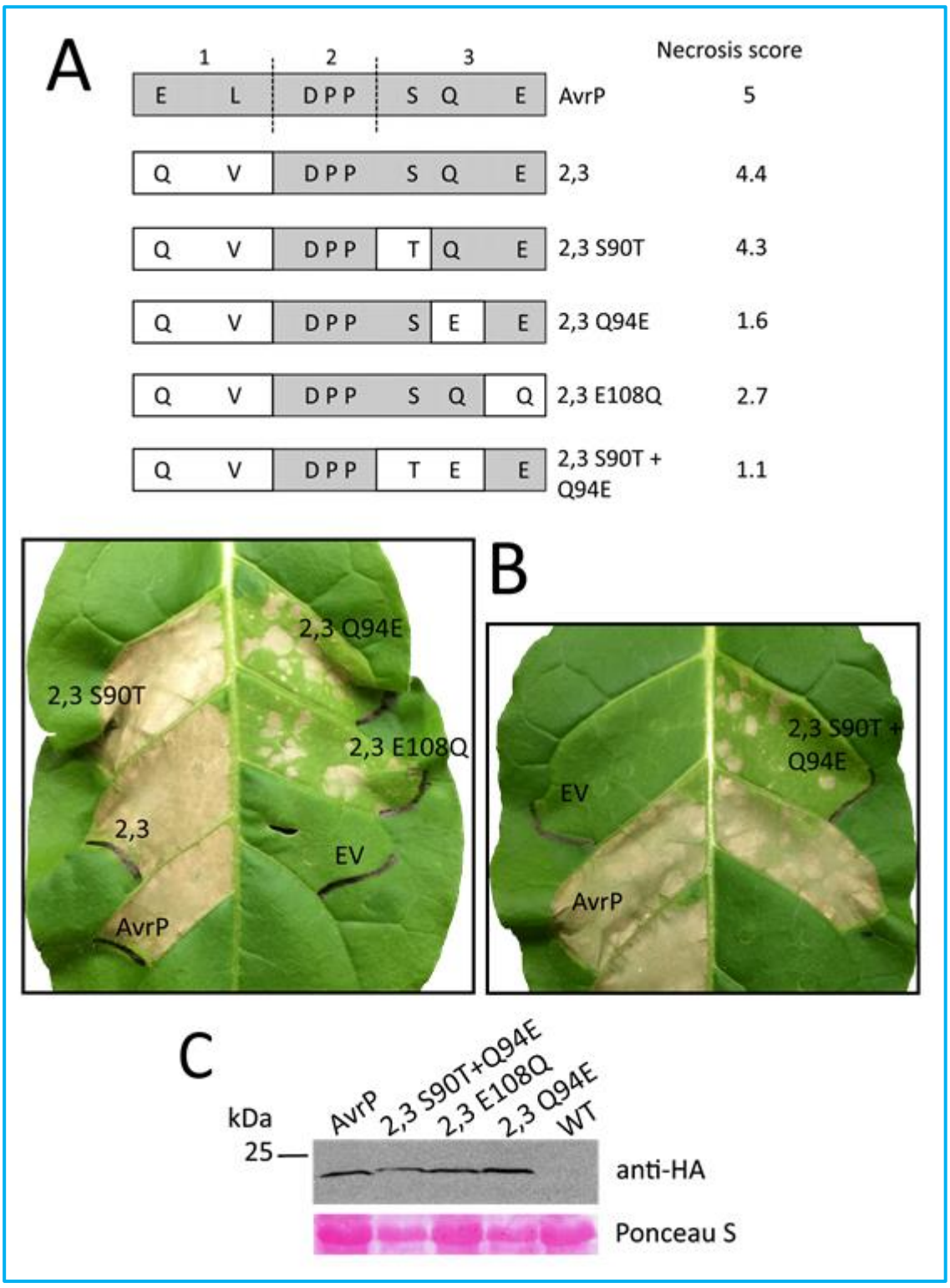

Figure 2.10 Effect of individual residues in region 3 of AvrP on necrosis induced in *P* tobacco. (A) Diagram of constructs used to investigate individual residues from region 3 of AvrP. The eight amino acid residues polymorphic between the two proteins are shown in capital letters on grey (AvrP) and white (271) bars. All constructs were made without a signal peptide coding sequence. Necrosis scores were determined as the average of the necrosis scores for each construct ranging from 0 (lowest) to 5 (highest) where 1 =

10-20% of the infiltrated area showing necrosis, 2 = 21-40% , 3 = 41 – 60% , 4 = 61-80%, 5 = 81-100%. The experiment was repeated at least two times with six leaves per experiment. (B) Agroinfiltration results for constructs described in (A) on W38::*P* transgenic tobacco. Photographs were taken at 4 dpi (left) and 5 dpi (right). Empty vector (EV) was used as a negative control. (C) Protein extracts from *N*. *benthamiana* leaf tissue (WT) and infiltrated *N*. *benthamiana* leaf tissue expressing the AvrP-271 variants described in (A) were size fractionated by gel electrophoresis and analysed by immunoblotting with anti-HA antibody. Positions and sizes (kDa) of protein molecular mass standards are indicated. The lower panel shows Ponceau S staining of protein bands on the blotted nitrocellulose membranes showing protein loading.

To investigate the contribution of residues in region 2 to the necrosis induced by AvrP, three AvrP-specific residues (D66, P68, P70) in region 2 were converted individually to their 271 counterparts (A, S and R respectively) by site-directed mutagenesis (Figure 2.11A). A double mutation of P68 and P70 (P68S + P70R, Figure 2.11A) was also introduced to determine the contribution of these two residues to the necrosis induced by AvrP (Figure 2.11A). A single mutation of D66A abolished AvrP-induced necrosis on *P* tobacco whereas both single mutation and double mutation of P68 and P70R did not reduce necrosis on *P* tobacco (Figure 2.11B). This finding suggests that residue D66 from region 2 is important and contributes to AvrP recognition.

Lastly, to investigate the minimum number of AvrP-specific residues required to trigger a strong cell death on *P* tobacco, two variants were made, namely 2,3 P68S+P70R and 2,3 P68S+P70R+S90T (Figure 2.11A). Variant 2,3 P68S+P70R investigated the role of residue D66 from region 2 of AvrP and all three residues from region 3 (S90, Q94 and E108) whereas variant 2,3 P68S+P70R+S90T investigated the role of residue D66 from region 2 and residues Q94 and E108 from region 3 for recognition by P. In *P* tobacco, both variants (2,3 P68S+P70R and 2,3 P68S+P70R+S90T) were able to trigger a strong cell death response (Figure 2.11B), suggesting that the D66, Q94 and E108 residues of AvrP are important for AvrP recognition.

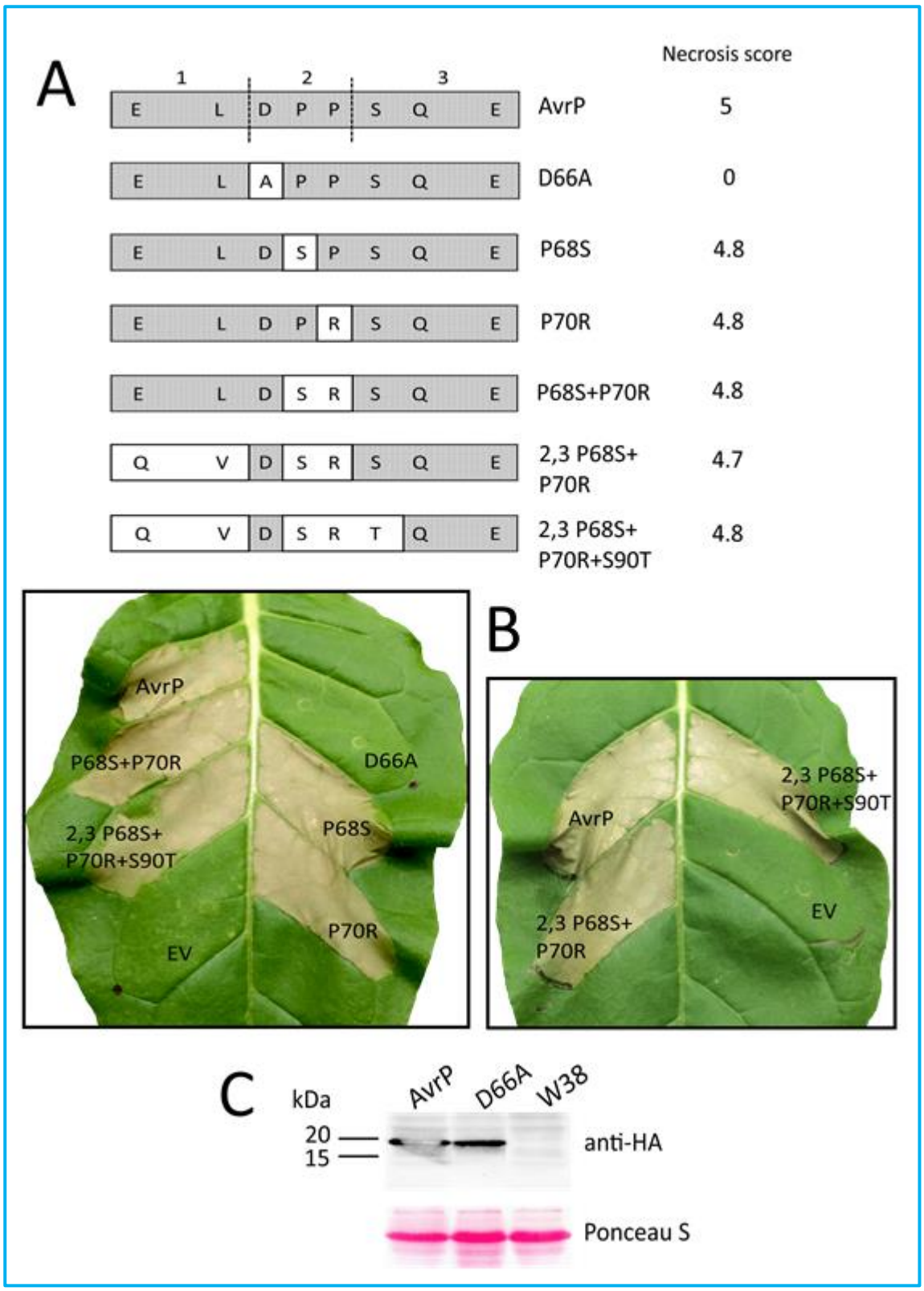

Figure 2.11 Effect of individual residues from regions 2 and 3 of AvrP on necrosis induced in *P* tobacco. (A) Diagram of constructs investigating individual residues from regions 2 and 3 of AvrP. The eight amino acid residues polymorphic between the two proteins are shown in capital letters on grey (AvrP) and white (271) bars. All constructs were made without a signal peptide coding sequence. Necrosis scores were determined as the

average of the necrosis scores for each construct ranging from 0 (lowest) to 5 (highest) where 1 = 10-20% of the infiltrated area showing necrosis, 2 = 21-40% , 3 = 41 – 60% , 4 = 61-80%, 5 = 81-100%. The experiment was repeated at least two times with six leaves per experiment. (B) Agroinfiltration results for constructs described in (A) on W38::*P* transgenic tobacco. The photographs were taken 3 dpi. Empty vector (EV) was used as a negative control. (C) Protein extracts from *N. tabacum* leaf tissue (W38) and infiltrated W38 leaf tissue expressing the AvrP proteins were size fractionated by gel electrophoresis and analysed by immunoblotting with anti-HA antibody. Positions and sizes (kDa) of protein molecular mass standards are indicated. The lower panel shows Ponceau S staining of protein bands on the blotted nitrocellulose membranes showing protein loading.

2.4 Discussion

2.4.1 Zinc binding is important for AvrP recognition

Based on the structure determined by Zhang et al. (2018), AvrP binds to three Zn^{2+} ions. This binding seems to be crucial for the structural integrity of AvrP and hence recognition by the P resistance protein (Figure 2.7). The binding of Zn^{2+} ions and the C4–HC3 (Zn1 Zn2) signature in AvrP structure resembles the Plant Homeodomain (PHD) finger or RING finger, which are found to be conserved and present in most eukaryotic genomes (Schindler et al. 1993; Aasland et al. 1995). The PHD finger is a small protein domain that spans approximately 50–80 amino acids, contains zinc-binding domains and appears in many chromatin-associated proteins (Aasland et al. 1995). Structurally, it has a conserved two-strand anti-parallel β-sheet and a C-terminal α-helix that is stabilized by two zinc atoms anchored by the Cys4–His–Cys3 motif (Sanchez and Zhou 2011). With this similarity in structure to the PHD finger, it is possible that AvrP may, like many PHD proteins, play a role in transcription.

2.4.2 Full-length AvrP is required for recognition by P

Deletion of the N-terminal residues preceding the first cysteine residue involved in zinc binding (Δ25-35), besides removing E30, which contributes to AvrP recognition, led to a loss of protein available for detection by P (Figure 2.6) and was therefore uninformative with respect to the role of the deleted residues in recognition by P. The internal (Δ58-64) and C-terminal (Δ96-111) deletions allowed protein accumulation but abolished

AvrP recognition (Figure 2.6) most likely due to the loss of protein structural integrity caused by the loss of two Zn3-binding residues (C59 and C61 for internal deletion and residues C97 and H101 for the C-terminal deletion). A combination of the internal and C-terminal deletions (Δ58-64 + Δ96-111), which removed Zn3 completely, also resulted in the loss of recognition by P, as might be expected. The C-terminal deletion (Δ96-111) also results in the loss of E108, which is important for AvrP recognition (section 2.3.4.2). In conclusion, full length AvrP protein is required for recognition by P as the N-terminal, internal and C-terminal deletions in AvrP all abolished AvrP recognition albeit for different reasons.

2.4.3 D66 residue is crucial for AvrP recognition

Domain swaps with the 271 allele revealed five residues to be important for AvrP recognition, which are the E30, L57, D66, Q94 and E108 residues (section 2.3.4.2). Based on the AvrP structure, the E30, D66 and Q94 residues are on the exposed surface, whereas the L57 residue can be found inside the protein. Surface exposure of the E108 residue, however, cannot be determined as it isn't represented in the structure.

A single mutation of D66 to alanine (A) resulted in the abolition of AvrP recognition (Figure 2.11), suggesting that this residue is crucial for AvrP recognition. Aspartic acid (D), present at position 66 in AvrP, is an acidic and polar amino acid whereas its counterpart alanine residue in the 271 allele is hydrophobic and nonpolar. Changing the D residue to A possibly affects AvrP protein folding and therefore its recognition by P.

Despite L57 being buried inside the protein and therefore unlikely to be recognised directly by P, the L57V mutation, although a relatively conservative mutation (both leucine and valine are branched hydrophobic residues), results in a less bulky amino acid at position 57 that could potentially affect protein structure including the conformation of residues on the surface of the protein that are involved in recognition by P. The side chain of L57 is very close to the peptide backbone of D66 in the three-dimensional structure of AvrP and could therefore affect the conformation of D66 on the surface of the protein.

2.4.4 Three key residues of AvrP recognition

Investigation on each residue from region 3 of AvrP (Figure 2.10) revealed that the S90 residue was not important for AvrP recognition whereas the last two polymorphic residues (Q94 and E108) are important for AvrP recognition. Mutation of the S90 residue to T (threonine) (2,3 S90T, Figure 2.10A) did not affect recognition of AvrP by P (Figure 2.10B), most likely because serine and threonine have very similar chemical properties (non-aromatic, hydroxyl and polar). E108 (glutamic acid), however, is acidic and charged whereas Q94 (glutamine, an amide of glutamic acid) is neutral and uncharged. In combination with D66, these two residues appear to complement one another in the recognition of AvrP by P. D66 in combination with E94+E108 (variant 2,3 Q94E and variant 2.3 S90T+Q94E, Figure 2.10A) and Q94+Q108 (variant 2,3 E108Q, Figure 2.10A) resulted in decreased necrosis (Figure 2.10B), suggesting that not only is each residue important by itself, but also that the combination of these two residues is important for AvrP recognition. The complementation of Q and E residues can also be inferred from the investigation of region 1 of AvrP (Figure 2.9). The necrosis score of variant 1,2, which has E94+Q108, was lower than that of variant 2,3, which has Q94+E108 the same as AvrP. In conclusion, the three key residues found to be important for AvrP recognition are D66, Q94 and E108.

2.4.5 Key residues for AvrP recognition are on the surface of the AvrP protein

Three key residues found in this study to be important for AvrP recognition were D66, Q94 and E108. When these residues were plotted on the AvrP structure, the D66 and Q94 residues are in the surface of AvrP while the E108 residue is not represented in the structure (Figure 2.12). Residues that lie in the accessible surface area (ASA), of a protein are believed to be important for determining the secondary structure of a protein. Mutations or deletions of ASA residues may affect protein proper folding. In AvrP, mutations of the D66 and Q94 residue may have changed its proper folding, hence reduced its ability to be recognised by the P resistance protein.

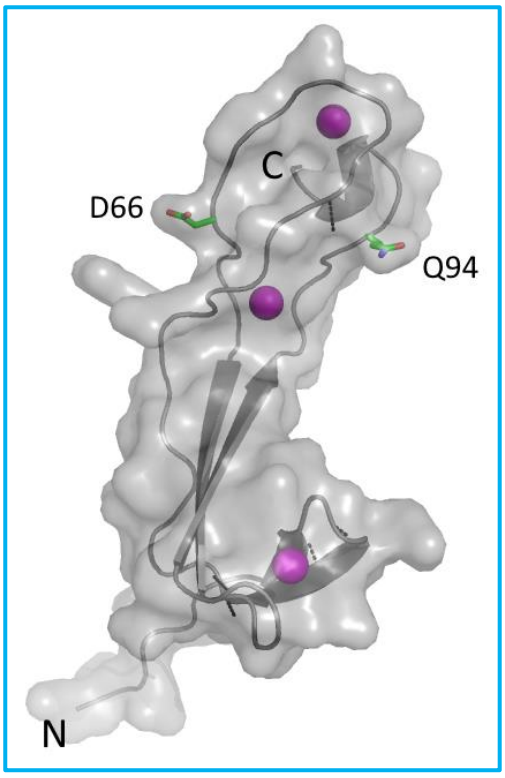

Figure 2.12 Key residues of AvrP recognition plotted onto the AvrP structure. The side chains of D66 and Q94 residues are shown. The tree zinc ions bound to AvrP are represented as magenta spheres. The N-terminus and C-terminus of AvrP are shown as N and C respectively. This figure was prepared using PyMOL (https://pymol.org).

Chapter 3
Recognition of AvrP123

3.1 Introduction

AvrP123 is recognised by the P1, P2 and P3 resistance proteins but not the P resistance protein. The *AvrP123* gene was identified after screening a flax-rust haustorium-specific cDNA library for transcripts encoding haustorially-expressed secreted proteins (Catanzariti et al. (2006). Initially, AvrP123 was predicted to have a Kazal serine protease-inhibitor signature (Catanzariti et al. 2006), but, following identification of the allelic *AvrP* gene (Barrett et al. 2009) and structural characterisation of the AvrP protein (Zhang et al. 2018), it was found to have a Plant Homeodomain (PHD) zinc finger motif. AvrP123 is predicted to have a similar structure to AvrP (Zhang et al. 2018) and, like AvrP, has ten cysteines and two histidines that bind to three zinc ions (Figure 3.1A). However, AvrP123 has an extra six C-terminal residues that are not present in AvrP.

Beside *AvrP*, other *AvrP123* variants have been found in flax rust isolates such as 271, 339, bs25 and WA (Figure 3.1) (Barrett et al. 2009; Dodds and Thrall 2009). The 271 allele, which is not recognised by P, P1, P2 or P3, was used in the investigation of AvrP recognition described in Chapter 2. Among the other *AvrP123* variants, the WA allele (here designated *AvrP-WA*) encodes a protein with high similarity to AvrP123 but, unlike AvrP123, is not recognised by the P1 resistance protein (Figure 3.1). Seven of the ten residues polymorphic between AvrP-WA and AvrP123 are near the N-terminus of the mature protein. These residues were investigated for their role in recognition by P1 (section 3.3.1.1).

Unlike *AvrP-WA*, the 339 allele (here designated *AvrP-339*) is more similar to *AvrP* than *AvrP123*. Interestingly, it is recognised by P, P2 and P3, but not by P1 (Figure 3.1B). It encodes a protein with seven polymorphic residues compared to AvrP, with five of these residues near the C-terminus (Figure 3.1A). These residues were investigated for P2 and P3 specificity (section 3.3.2.2).

The bs25 allele (here designated *AvrP-bs25*) is a product of recombination between AvrP and AvrP123 that was recovered by selection for virulence on flax plants heterozygous for *P* and *P1* (Lawrence et al. 1981b). It was found to encode a domain swap comprising the N-terminal 60–63 amino acids of AvrP and the C-terminal 54–57 amino acids of AvrP123 and is recognised by P2, but not by P, P1 or P3 (Figure 3.1). A reciprocal domain swap was therefore made and tested for recognition by P, P1, P2 and P3 (section 3.3.3).

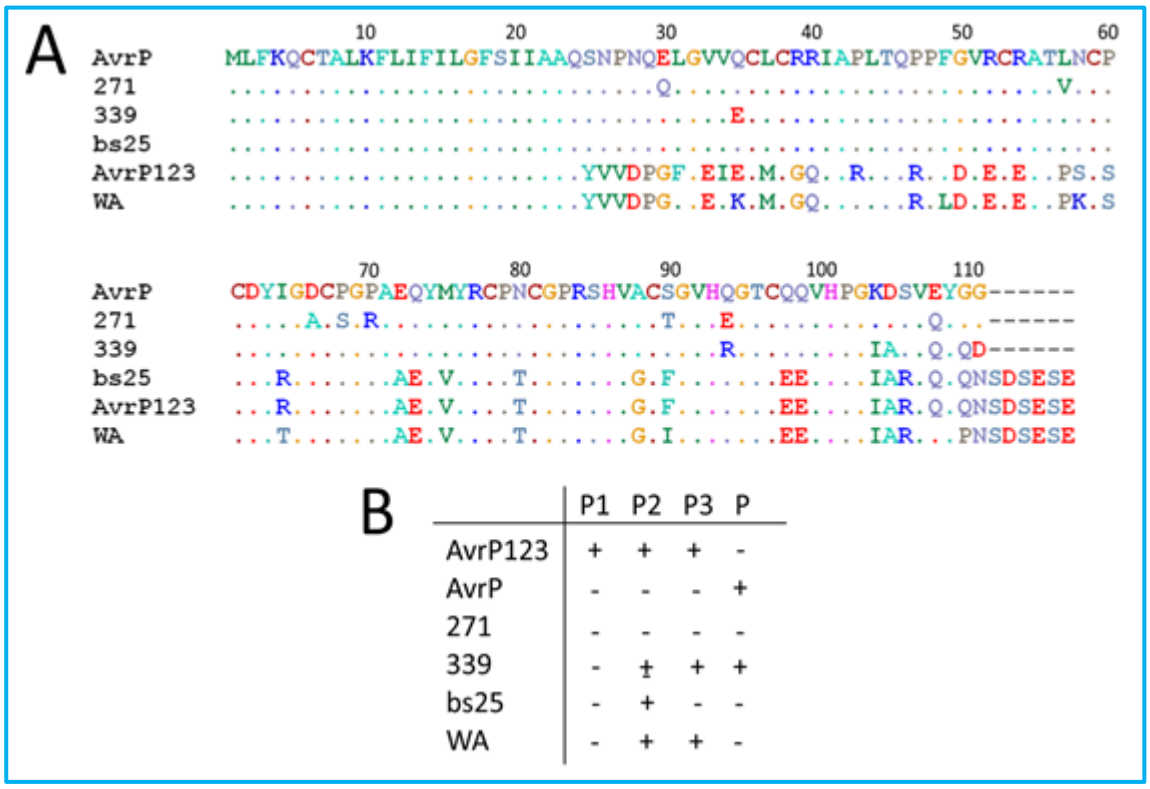

Figure 3.1 AvrP/P123 variants and their recognition by the P, P1, P2 and P3 resistance proteins. (A) Alignment of AvrP/P123 with other variants encoded by alleles present in the 271, 339, bs25 and WA isolates of flax rust. Identical residues are represented by dots (.) (B) Recognition of AvrP/P123 variants (left) by *P*, *P1*, *P2*, and *P3* lines of flax (top). Table taken from Dodds and Thrall (2009). + indicates necrosis; - indicates no necrosis; ± indicates weak necrosis/chlorosis.

This chapter describes several approaches used to investigate the domains of AvrP123 recognised by the P1, P2 and P3 resistance proteins. These approaches include deletions, domain swaps and site-directed mutations. All mutants were expressed in flax plants containing the *P*, *P1*, *P2* or *P3* resistance gene via *Agrobacterium*-mediated transformation of infiltrated leaves (agroinfiltration).

3.2 Materials and Methods

3.2.1 Generation of control, C6 and C8 constructs via Gateway cloning

AvrP123 and its variants were cloned using the Gateway pENTRY Directional TOPO Cloning kit (Invitrogen, Carlsbad, California, USA) following the manufacturer's protocol. The genes of interest, including controls (*AvrP123*, *AvrP*, *AvrP-339*, *AvrP-WA*, *AvrP-bs25* and *AvrP-271*), deletions or additions of the C-terminal six amino acids of AvrP123 (C6 constructs, section 3.3.2.1) and swaps of the preceding 8 amino acids (C8 constructs, section 3.3.2.2), were amplified by PCR using gene-specific primers containing an additional 5'-CACCATG nucleotide sequence on the forward primers (Table 3.1). The amplified gene was then cloned into the pENTRY TOPO vector (Appendix 2) by TOPO cloning. Positive clones were confirmed by PCR and sequencing using TOPO M13F (5'-GATGTTTTCCCAGTCACGAC-3') and TOPO M13R (5'-CAGGAAACAGCTATGAC-3') primers. The cloned genes were then transferred into a destination vector such as pEarlyGate104 vector (Appendix 2) (Earley et al. 2006) using the Clonase® II for LR recombination kit (Invitrogen) according to the manufacturer's protocol. After recombination, the pENTRY TOPO vector was linearized by restriction enzyme (*Pvu*I) to reduce the incidence of false positives owing to the fact that both donor and destination vectors confer kanamycin resistance. Positive transformants were confirmed by colony PCR and sequencing using forward primer pEG104seqFOR (5'-AGTCCGGACTCAGATCTC-3') and sequence-specific reverse primers (Table 3.1).

Table 3.1 Primer pairs used in generating control, C6 and C8 constructs

Name of construct	Name of primers	Primer pairs (5'–3')
AvrP123	dSP123 FOR P123 REV	F : CACCATGCAGTATGTTGTTGATCCAGGG R : TCATTCTGACTCCGAGTCAG
AvrP	dSP-AvrP FOR AvrP REV	F : CACCATGCAGTCTAATCCTAATCAAGAGC R : CTAACCTCCGTACTCCACACTG
339	339 FOR 339 REV	F : CACCATGCAGTCTAACCCTAATCAAGAGC R : CTAATCTTGGTACTGCACACTGG
WA	dSP123 FOR P123 REV	F : CACCATGCAGTATGTTGTTGATCCAGGG R : TCATTCTGACTCCGAGTCAG
bs25	dSP-AvrP FOR P123 REV	F : CACCATGCAGTCTAATCCTAATCAAGAGC R : TCATTCTGACTCCGAGTCAG
271	dSP-271 FOR 271 REV	F : CACCATGCAGTCTAACCCTAATCAACAGC R : CTAACCTCCGTACTGCACACTG
AvrP123ΔC6	dSP123 FOR dC6 REV	F : CACCATGCAGTATGTTGTTGATCCAGGG R : CTAATTTTGGTATTGCACCCTGG
AvrP+C6	dSP-AvrP FOR AvrP-C6 REV	F : CACCATGCAGTCTAATCCTAATCAAGAGC R : TCATTCTGACTCCGAGTCAGAACCTCCGTACTCCACACTG
AvrP-C8^{339}	dSP-AvrP FOR 339-C8 REV	F : CACCATGCAGTCTAATCCTAATCAAGAGC R : TCAATCTTGGTACTGCACACTGGCTATCCCAGGGTGTACCT GTTG
AvrP-C8^{P123}	dSP-AvrP FOR P123-C8 REV	F : CACCATGCAGTCTAATCCTAATCAAGAGC R : TCAATTTTGGTATTGCACCCTGGCTATCCCAGGGTGTACCT GTTG
AvrP-C14^{P123}	dSP-AvrP FOR AvrP-C14 REV	F : CACCATGCAGTCTAATCCTAATCAAGAGC R : TCATTCTGACTCCGAGTCAGAATTTTGGTATTGCACCCTG

3.2.2 Domain swaps

Domain swaps between AvrP123 and AvrP-WA (section 3.3.1.1) and between AvrP and AvrP123 (section 3.3.3) were made based on the RIC method developed by Claire Anderson as described in Chapter 2 section 2.2.10. The swaps were amplified and cloned into the LIC (pL) vector (Chapter 2, section 2.2.8) using the primer pairs shown in Table 3.2.

Table 3.2 Primer pairs used for generating domain swaps between AvrP123 and WA and between AvrP123 and AvrP

Name of construct	DNA Template	Primer pairs (5'– 3')
1,2	AvrP123 (5' end)	F : ACTATTTACAATTACGATGCAGTATGTTGTTGATCCAGGG R : GCGGACCACAAGTAGGGCAGCGGTACACATATTC
	AvrP-WA (3' end)	F : GTTCACATGTCGGGTGTATC R : TCCTCTCCAAATTACGTCATTCTGACTCCGAGTCAG
3	AvrP-WA (5' end)	F : ACTATTTACAATTACGATGCAGTATGTTGTTGATCCAGGG R : GCGGACCACAAGTAGGGCAGCGGTACACATATTC
	AvrP123 (3' end)	F : GTTCACATGTCGGGTGTTTC R : TCCTCTCCAAATTACGTCATTCTGACTCCGAGTCAG
1	AvrP123 (5' end)	F : ACTATTTACAATTACGATGCAGTATGTTGTTGATCCAGGG R : GTTGAGTCAGACGAGCGATTTG
	AvrP-WA (3' end)	F : GACCACTTGATGTGGAATGTG R : TCCTCTCCAAATTACGTCATTCTGACTCCGAGTCAG
2,3	AvrP-WA (5' end)	F : ACTATTTACAATTACGATGCAGTATGTTGTTGATCCAGGG R : GTTGAGTCAGAGGAGCGATTTG
	AvrP123 (3' end)	F : GACCATTTGATGTGGAATGTG R : TCCTCTCCAAATTACGTCATTCTGACTCCGAGTCAG
bs25^{R}	AvrP123 (5' end)	F : ACTATTTACAATTACGATGCAGTATGTTGTTGATCCAGGG R : GAACAACTTGGGGTGGCTTCACATTC
	AvrP (3' end)	F : GTGTGATTATATAGGAGACTGTCC R : TCCTCTCCAAATTACGCTAACCTCCGTACTCCACACTG

LIC extensions are highlighted in red; introduced methionine codons (ATG) are highlighted in blue.

Once the domain swaps were made in the LIC vector (pL), they were then cloned into the pENTRY TOPO vector using the TOPO cloning method. Firstly, the gene of interest was amplified by PCR using sequence-specific primers with an additional 5'-CACCATG nucleotide on the forward primers (Table 3.3). Domain swaps 1,2; 3; 1; and 2,3 were all amplified using dSP123 FOR and P123 REV primers (Table 3.3) whereas domain swap bs25^{R} was amplified using dSP123 FOR and AvrP REV primers (Table 3.3). Positive transformants were confirmed by colony PCR and sequencing as described in section 3.2.1. Constructs were then transferred to the destination vector pEarlyGate104 via Gateway cloning as described in section 3.2.1.

Table 3.3 Primers used for generating AvrP123-WA and AvrP123-AvrP domain swap in pENTRY TOPO

Name of primer	Primers (5'–3')
dSP123 FOR	CACCATGCAGTATGTTGTTGATCCAGGG
P123 REV	TCATTCTGACTCCGAGTCAG
AvrP REV	CTAACCTCCGTACTCCACACTG

3.2.3 Site-Directed Mutagenesis

Mutants were made using the site-directed mutagenesis method described in Chapter 2 section 2.2.11, using the primer pairs shown in Table 3.4. Mutations were made in the pENTRY TOPO constructs and the mutants were then transferred to pEarlyGate104 as described in section 3.2.1.

Table 3.4 Primer pairs used for site-directed mutagenesis

Name of construct	Primer pairs	Restriction enzyme used for screening
AvrP123 D66A	F : GATTATAGAGGAGCTTGT**CCCGGG**CCTGCTGCAGAAT R : ACACGAACAACTTGGGGTGGCTTCACATTCCACATC	*Sma*I
1 E35K	F : GTATGTTGTTGAT**CCCGGG**TTTGGAGAGATTAAATGTATGTGCG R : TGCATGGTGAAGGGGGCGGCCGCGGAGCCTGCTTTTTTG	*Sma*I
271-C8[339] I64R	F : GTCCGTGTGATTATCGTGGAGCCTGT**TCCGGA**CGTGCTGAAC R : AATTCACGGTGGCTCGACATCTCACACCAAATGGTGGTTG	*Bsp*EI

Nucleotide changes are highlighted in red; introduced restriction sites are in bold and underlined.

3.2.4 DNA sequencing

DNA was sequenced as described in Chapter 2 section 2.2.7.

3.2.5 *Agrobacterium*-mediated transformation of flax and tobacco leaves

Cultures of *Agrobacterium* strain GV3101 (pMP90) containing the binary vector (pEarlyGate104) expression constructs were prepared as described in Chapter 2 section 2.2.13. Three- to four-week-old *P, P1, P2* and *P3* flax plants were used for infiltration. These included lines that had been backcrossed multiple times to the susceptible Bison or Hoshangabad (Hosh) lines of flax as well as the parental lines Koto (*P*), Akmolinsk (*P1*), Abyssinian (*P2*) and Leona (*P3*). Bison backcross lines were used to ensure a near-isogenic background so that variation in responses could be ascribed to the different resistance proteins rather than differences in genetic background. Hosh backcross lines were also used to compensate for the presence of a chlorotic background response in Bison for AvrP123. Agroinfiltration was performed using a 1 ml syringe (without a needle) on the abaxial side of flax and tobacco leaves. Flax plants were grown in a temperature-controlled glasshouse (23 °C day, 13 °C night) and observed 8 to 15 days post infiltration (dpi).

For P specificity, agroinfiltration of *P* tobacco leaves were performed using the same method as described in Chapter 2 section 2.2.13. W38 tobacco and *Nicotiana benthamiana* leaves were also used for co-infiltration experiments with the *P2* resistance gene (in pTN35S vector). *N. benthamiana* plants were grown in a controlled-environment room with a 22 °C constant temperature with a 16 hr day (approximately 200 µmol/m^{-2}s light intensity)/8 hr night cycle. Necrosis was scored 6-8 days post infiltration. W38 tobacco were grown in the same temperature-controlled glasshouse as *P* tobacco, but were co-infiltrated and observed in the same controlled-environment room as *N. benthamiana.* Co-infiltrations were performed using a 1:1 ratio of *Agrobacterium* suspensions carrying *Avr* constructs and *P2*.

3.2.6 Western blots

The destination vector pEarlyGate104 adds a YFP-tag at the N-terminus. Western blots of the YFP-fusion proteins extracted from two Bison or Hoshangabad leaves at 3 dpi were generated and probed with anti-GFP mouse IgG mononclonal antibody (Roche, Basel, Switzerland) and anti-mouse horseradish peroxidase-linked secondary antibody (GE Healthcare) as described in Chapter 2 section 2.2.14, except that Hybond-C-extra nitrocellulose membranes (Amersham Biosciences, Piscataway, NJ, USA) were used instead of Amersham Protran 0.2 NC membranes.

3.3 Results

3.3.1 Recognition by P1

3.3.1.1 N-terminal residues of AvrP123 are important for recognition by P1

To determine the residues/regions important for P1 specificity, four domain swaps were made between AvrP123 and AvrP-WA (Figure 3.2A). There are ten polymorphic residues between AvrP123 and AvrP-WA with seven of them located near the N-terminus of the mature protein. The domain swaps were made and named based on three regions of AvrP123, designated regions 1, 2 and 3. Region 1 contains four polymorphic residues (F31, I34, E35, R43), whereas regions 2 and 3 each contain three polymorphic residues (F49, S58, R64 and F90, Q108, Q110 respectively) (Figure 3.2A).

Domain swap 1,2 contains seven AvrP123 polymorphic residues from regions 1 and 2, and three AvrP-WA polymorphic residues from region 3 (I90, E108, P110) (Figure 3.2A). Its reciprocal (domain swap 3) contains seven AvrP-WA polymorphic residues from regions 1 and 2 (L31, V34, K35, P43, L49, K58, T64) and three AvrP123 polymorphic residues from region 3 (Figure 3.2A). Both constructs were tested for recognition on H^3 x Koto (*P*), Akmolinsk (*P1*), H^3 x Abyssinian (*P2*) and Leona (*P3*) flax plants, where H^3 indicates these lines had been backcrossed three times to Hoshangabad (Figure 3.2B). Domain swap 1,2 triggered cell death on *P1*, *P2* and *P3* flax plants whereas domain swap 3 only triggered cell death on *P2* and *P3* flax plants (Figure 3.2B). This finding suggests that regions 1 and 2 are important for AvrP123 recognition by P1.

To determine the residues in regions 1 and 2 of AvrP123 important for recognition by P1, another two domain swaps were made, namely domain swaps 1 and 2,3 (Figure 3.2A). Domain swap 1 contains four AvrP123 polymorphic residues from region 1, and six AvrP-WA polymorphic residues from regions 2 and 3. Unexpectedly, not only did domain swap 1 trigger cell death on the *P1*, *P2*, and *P3* flax plants, it also triggered cell death on the *P* flax plants (Figure 3.2B). Its reciprocal domain swap (2,3), also triggered strong cell death on the *P2* and *P3* flax plants, but a weaker (intermediate) response on the *P1* flax plants (Figure 3.2B). Additional experiments were conducted with a dilution series of *Agrobacterium* to confirm this observation. *Agrobacterium* suspensions with OD_{600} of 1.0, 0.5 or 0.4 were used for this experiment and tested on *P1* flax plants (Figure 3.3). Domain swap 1 consistently produced a stronger cell-death response compared to domain swap 2,3. Altogether, these results suggest that polymorphic residues in both regions 1 and 2 of AvrP123 are involved in AvrP123 recognition by P1, but those in region 1 appear to play a more important role in recognition than those in region 2.

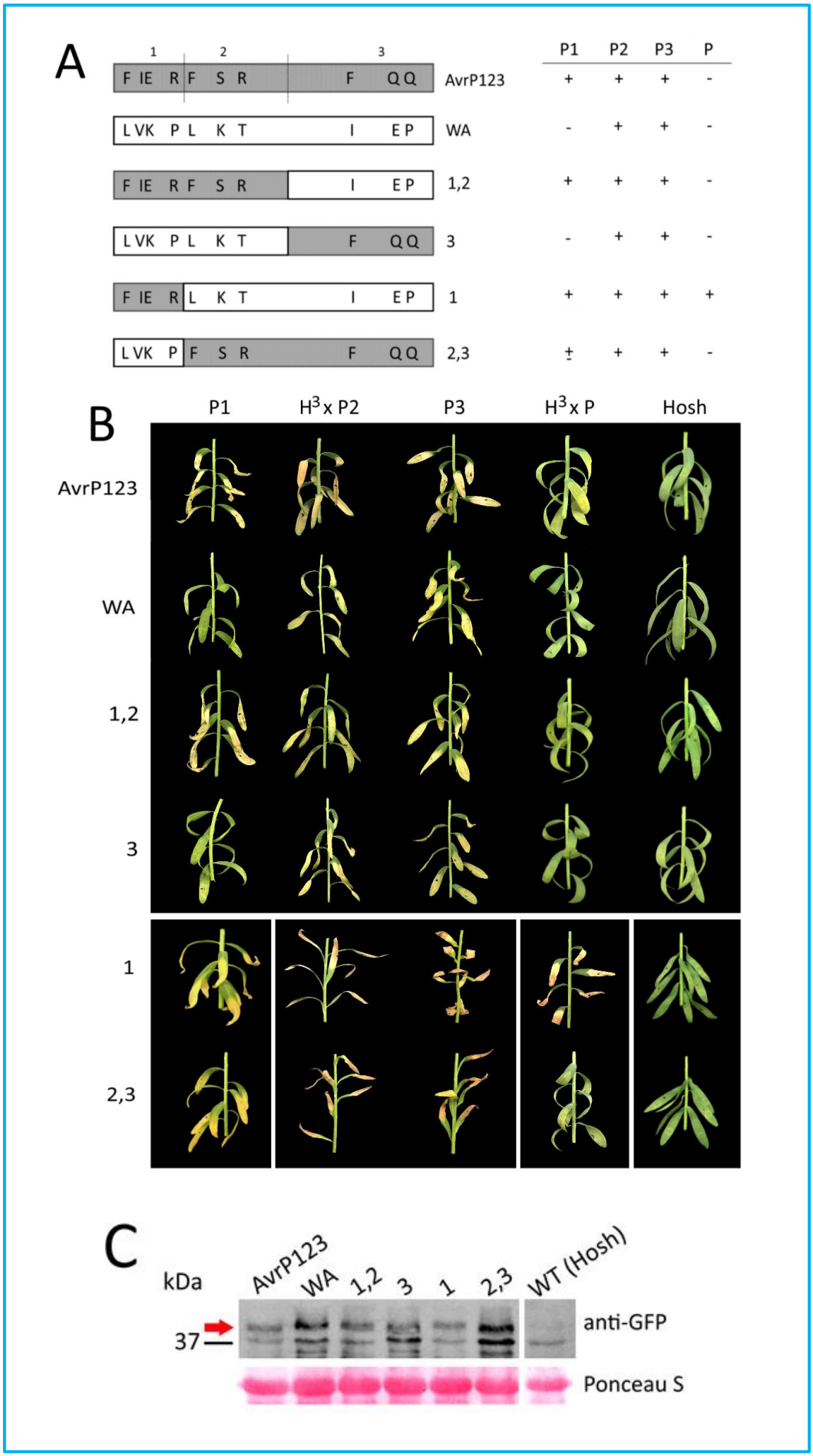
A
1
2
3
F IE R F S R F Q Q
AvrP123
L VK P L K T I E P
WA
F IE R F S R I E P
1,2
L VK P L K T F Q Q
3
F IE R L K T I E P
1
L VK P F S R F Q Q
2,3
P1 P2 P3 P
+ + + -
- + + -
+ + + -
- + + -
+ + + +
± + + -
B
P1
H3 x P2
P3
H3 x P
Hosh
AvrP123
WA
1,2
3
1
2,3
C
kDa
AvrP123
WA
1,2
3
1
2,3
WT (Hosh)
37
anti-GFP
Ponceau S

Figure 3.2 Necrosis induced by domain swaps between AvrP123 and AvrP-WA in *P*, *P1*, *P2* and *P3* flax. (A) Diagram of domain swaps between AvrP123 and AvrP-WA (WA) with their corresponding patterns of necrosis induction on *P*, *P1*, *P2* and *P3* flax. AvrP123 sequence is represented by a grey bar whereas AvrP-WA sequence is represented by a white bar. + = necrosis; - = no necrosis. All constructs were made without a signal peptide coding sequence. (B) Agroinfiltration results for constructs described in (A) on Koto (*P*), Akmolinsk (*P1*), Abyssinian (*P2*) and Leona (*P3*) flax plants. The *P2* and *P* flax cultivars had been backcrossed three times (H^3) with Hoshangabad (Hosh). The domain swap 1,2 and 3 were tested separately from swap 1 and 2,3. Each domain swap was tested on three flax plants with 6-8 leaves tested per plant (only one plant shown per treatment). The photographs were taken at least 8 days after infiltration from two independent tests. (C) Upper panel shows a gel blot of YFP-tagged AvrP123, AvrP-WA and four domain swaps between AvrP123 and AvrP-WA expressed without a signal peptide coding sequence under the control of the 35S promoter in agroinfiltrated Hosh leaves. Protein was extracted 4 days after infiltration and the blot was probed with anti-GFP antibody. Positions and sizes (kDa) of protein molecular mass standards are indicated. The position of protein bands of interest is indicated by a red arrow. The lower panel shows the Ponceau-S-stained membrane confirming approximately equal protein loading.

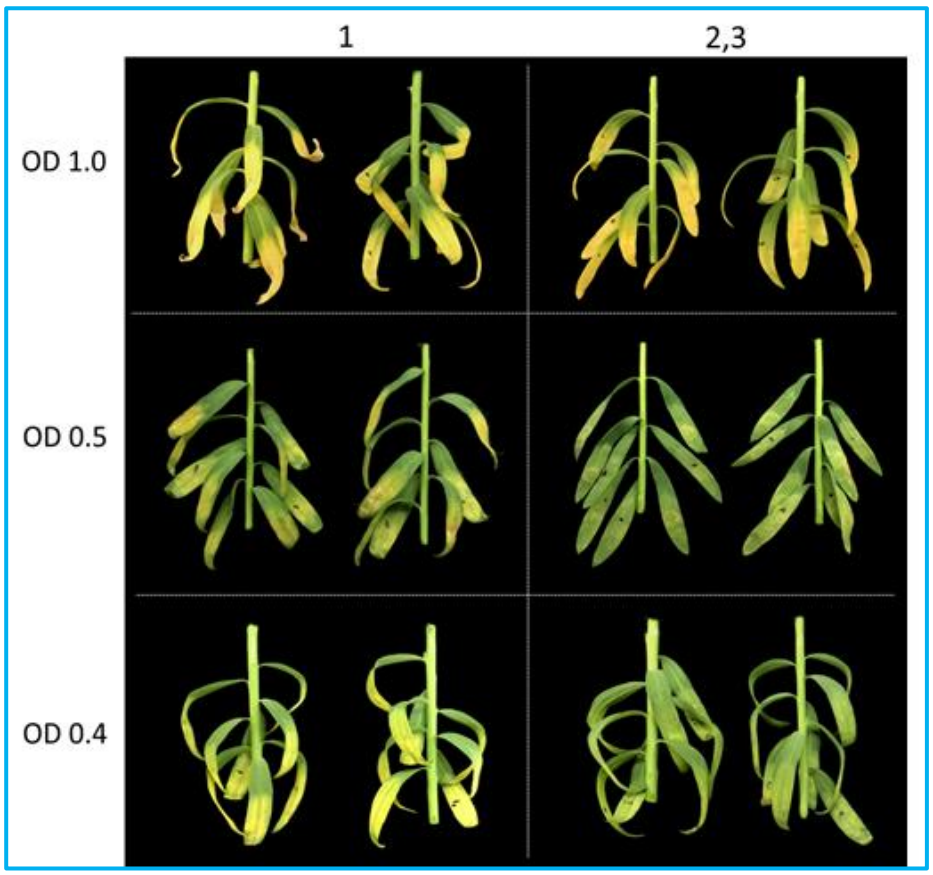

Figure 3.3 Necrosis/chlorosis induced by a dilution series of domain swaps 1 and 2,3 on *P1* flax plants. An OD_{600} dilution series of 1.0, 0.5 and 0.4 of *Agrobacterium* carrying domain swaps 1 and 2,3 were infiltrated into the leaves of *P1* flax plants. Seven to eight leaves were infiltrated on each of three flax plants (only two plants shown per treatment). Photographs were taken 8 days after infiltration.

3.3.1.2 E35 is important for recognition of domain swap 1 by P and P1

Surprisingly, domain swap 1 was not only recognised by P1, but also recognised by P (section 3.3.1.1). Two of the four polymorphic residues in region 1 of AvrP123 represent non-conservative amino acid differences compared to AvrP-WA. Of these residues, E35 was chosen for further analysis to test its role in the recognition of domain swap 1 by P and P1. The E35 residue was mutated into its AvrP-WA counterpart, K, in the domain swap 1 background (designated 1 E35K, Figure 3.4A).

The 1 E35K mutant was tested on *P*, *P1*, *P2* and *P3* flax plants (Figure 3.4B) and *P* tobacco plants (Figure 3.5A) for recognition. In flax, the E35K mutation abolished necrosis on *P* and *P1* flax plants (Figure 3.4B), suggesting that E35 is indeed important for recognition

of domain swap 1 by P and P1 and most likely for recognition of AvrP123 by P1. In *P* tobacco, domain swap 1 produced a low level of necrosis (Figure 3.5A) suggesting weaker recognition compared to AvrP. The domain swap 1 E35K mutant completely abolished necrosis in *P* tobacco (Figure 3.5A), confirming that the E35 residue is important for recognition of domain swap 1 by P.

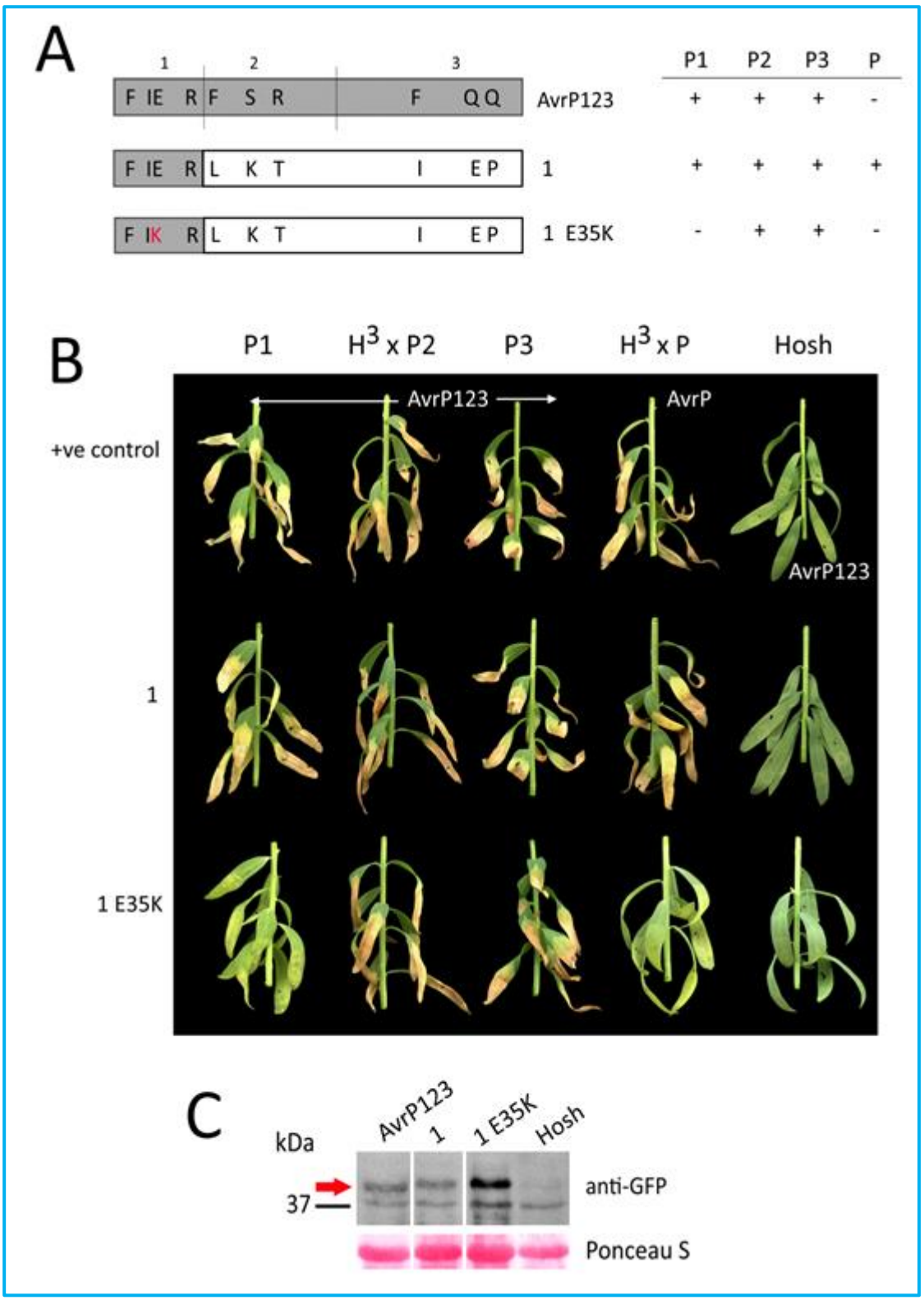

Figure 3.4 Necrosis induced by the E35K mutation of domain swap 1 in *P*, *P1 P2* and *P3* flax. (A) Diagram of domain swap 1 and the 1 E35K mutant with their corresponding patterns of necrosis induction on *P*, *P1*, *P2* and *P3* flax. AvrP123 sequence is represented by a grey bar whereas AvrP-WA sequence is represented by a white bar. + = necrosis; - = no necrosis. All constructs were made without a signal peptide coding sequence. (B)

Agroinfiltration results for constructs described in (A) on Koto (*P*), Akmolinsk (*P1*), Abyssinian (*P2*) and Leona (*P3*) flax plants. The *P* and *P2* flax cultivars had been backcrossed three times (H^3) with Hoshangabad (Hosh). Each construct was tested on three flax plants with 6-8 leaves tested per plant (only one plant shown per treatment). The experiment was conducted at least two times. The photograph was taken 11 days after infiltration. (C) Upper panel shows a gel blot of YFP-tagged AvrP123, domain swap 1 and domain swap 1 E35K mutant proteins expressed without a signal peptide coding sequence under the control of the 35S promoter in agroinfiltrated Hosh leaves. Protein was extracted 4 days after infiltration and the blot was probed with anti-GFP antibody. Positions and sizes (kDa) of protein molecular mass standards are indicated. The position of protein bands of interest is indicated by a red arrow. The lower panel shows the Ponceau-S-stained membrane confirming approximately equal protein loading.

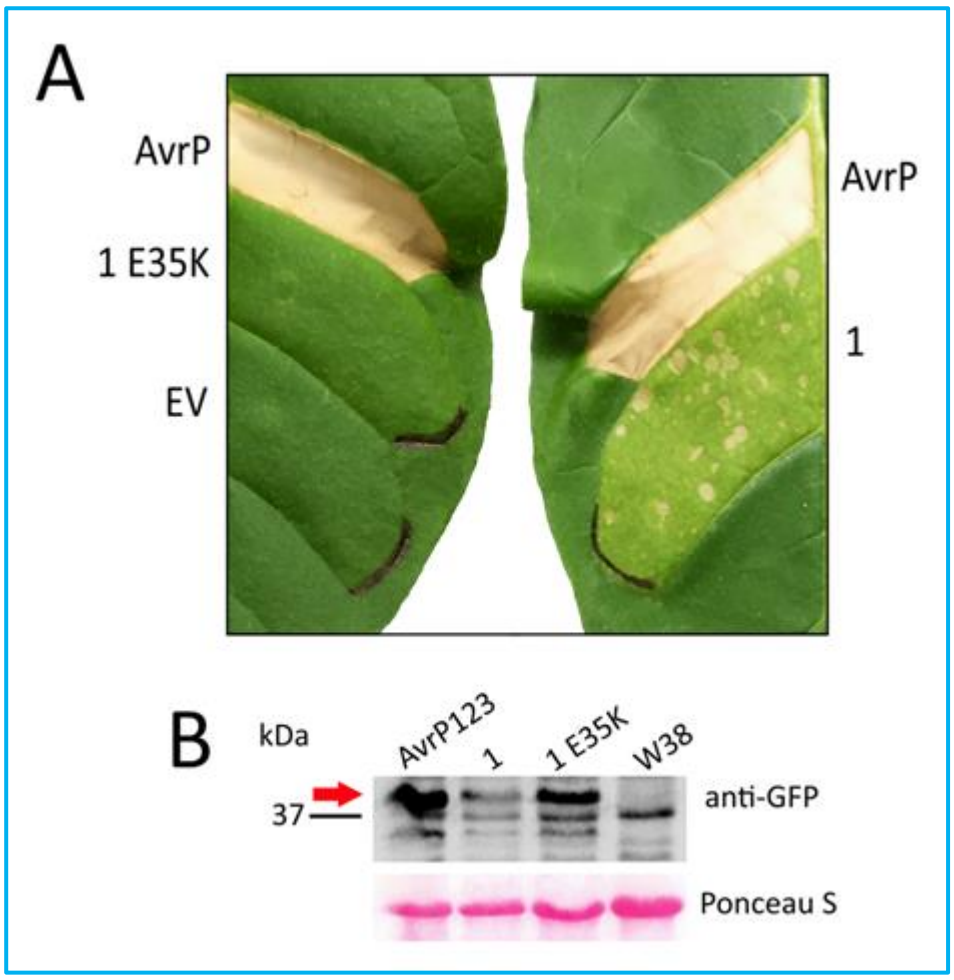

Figure 3.5 Necrosis/chlorosis induced by domain swap 1 and the domain swap 1 E35K mutant on *P* tobacco. (A) Agroinfiltration results of domain swap 1 and the domain swap 1 E35K mutant on W38::*P* transgenic tobacco. The experiment was conducted at least two times with six leaves per experiment. Photographs were taken 4 days (left) and 5 days (right) after infiltration. (B) Upper panel shows a gel blot of YFP-tagged AvrP123, domain swap 1 and domain swap 1 E35K mutant proteins expressed without a signal peptide coding sequence under the control of the 35S promoter in W38 tobacco leaves. Protein was extracted 2 days after agroinfiltration and the blot was probed with anti-GFP antibody. Positions and sizes (kDa) of protein molecular mass standards are indicated. The position of protein bands of interest is indicated by a red arrow. The lower panel shows the Ponceau-S-stained membrane confirming approximately equal protein loading.

3.3.1.3 D66 is important for recognition of AvrP123 by P1

In Chapter 2, it was shown that the D66 residue of AvrP is important for recognition by the P resistance protein (section 2.3.4.2). AvrP123 shares this residue with AvrP. To determine whether this residue is also important for AvrP123 recognition by P1, P2, or P3, a D66A mutation was made in AvrP123 and tested in flax (Figure 3.6A).

The D66A mutant triggered a strong cell death response in *P2* and *P3* flax plants and no necrotic response in *P* flax plants, but produced an intermediate response in *P1* flax plants (Figure 3.6A). This response was greater than the background response observed in negative control plants (Bison). The decreased necrotic response induced by this mutant on *P1* flax plants suggests that D66 is important for recognition of AvrP123 by P1.

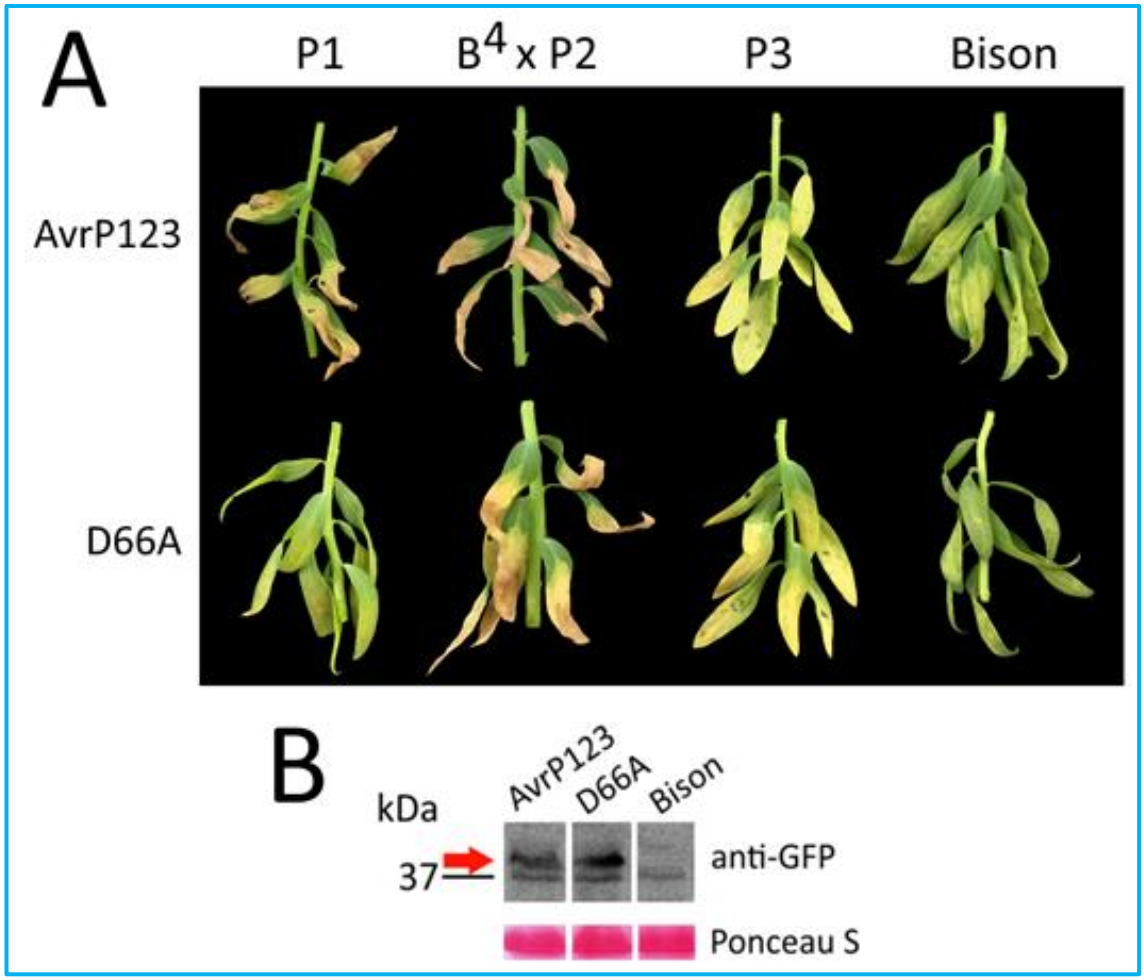

Figure 3.6 Necrosis induced by the D66A mutation of AvrP123 in *P1*, *P2* and *P3* flax. (A) Agroinfiltration results for the D66A mutation of AvrP123 on plants of Akmolinsk (*P1*), Abyssinian (*P2*) and Leona (*P3*) flax lines. Abyssinian (*P2*) had been backcrossed four

times (B^4) to Bison. All constructs were made without a signal peptide coding sequence. Each construct was tested on three flax plants with 6-8 leaves tested per plant (only one plant shown per treatment). The experiment was conducted at least two times. The photograph was taken 11 days after infiltration. (B) Upper panel shows a gel blot of YFP-tagged AvrP123 and D66A mutant proteins expressed without a signal peptide coding sequence under the control of the 35S promoter in Bison leaves. Protein was extracted 2 days after agroinfiltration and the blot was probed with anti-GFP antibody. Positions and sizes (kDa) of protein molecular mass standards are indicated. The position of protein bands of interest is indicated by a red arrow. The lower panel shows the Ponceau-S-stained membrane confirming approximately equal protein loading.

3.3.2 Recognition by P2 and P3

3.3.2.1 Investigation of the role of the six C-terminal residues (C6) of AvrP123 in recognition

Compared to AvrP, AvrP123 has a six residue (C6; SDSESE) extension at the C-terminus, which could potentially play a role in AvrP123 recognition. To investigate the role of C6 in AvrP123 recognition, a deletion of these residues was made (designated AvrP123ΔC6; Figure 3.7A). AvrP123ΔC6 was tested in flax and, like unmodified AvrP123, triggered cell death on *P1*, *P2* and *P3* flax plants but not *P* flax plants (Figure 3.7B), suggesting that C6 did not play a role in AvrP123 recognition.

To further investigate the role of C6, a derivative of AvrP was made with the C6 residues added (designated AvrP+C6; Figure 3.8A) and tested in flax (Figure 3.8B). Addition of C6 did not trigger cell death on *P1*, *P2* and *P3* flax plants and did not affect the cell death response on *P* flax plants (Figure 3.8B). This result further supports the conclusion that C6 is not involved in recognition.

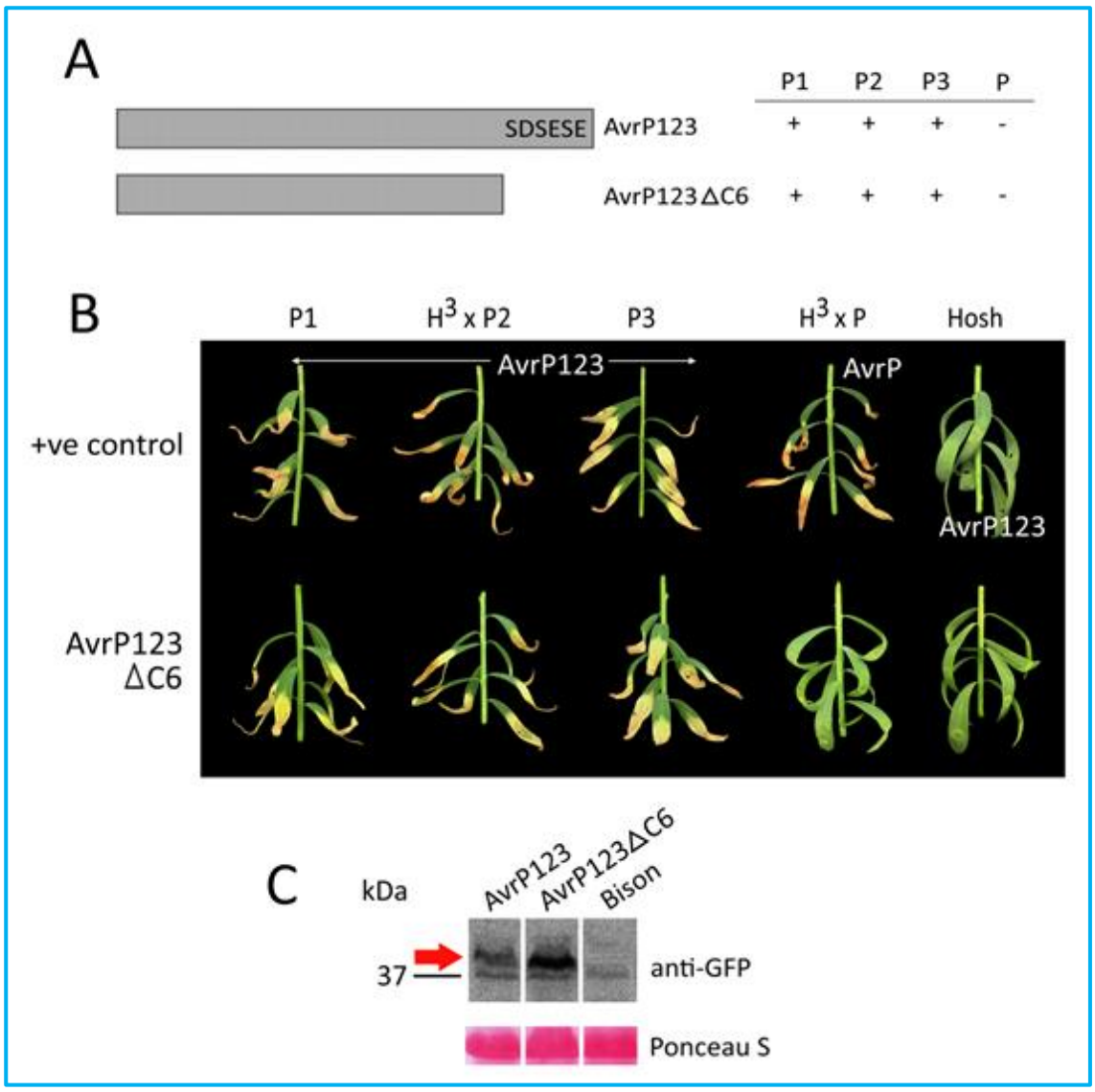

Figure 3.7 Necrosis induced by the C6 deletion mutant of AvrP123 in *P*, *P1*, *P2* and *P3* flax. (A) Diagram of AvrP123 and a deletion mutant lacking the six C-terminus residues of AvrP123 (AvrP123ΔC6) with their corresponding patterns of necrosis induction on *P*, *P1*, *P2* and *P3* flax. + = necrosis; - = no necrosis. All constructs were made without a signal peptide coding sequence. (B) Agroinfiltration results for a construct described in (A) on flax plants cultivars Koto (*P*), Akmolinsk (*P1*), Abyssinian (*P2*) and Leona (*P3*). The *P* and *P2* flax cultivars had been backcrossed three times (H^3) with Hoshangabad (Hosh). Each construct was tested on three flax plants with 6-8 leaves tested per plant (only one plant shown per treatment). The experiment was conducted at least two times. The photograph was taken 8 days after infiltration. (C) Upper panel shows a gel blot of YFP-tagged AvrP123 and AvrP123ΔC6 proteins expressed without a signal peptide coding sequence under the control of the 35S promoter in agroinfiltrated Hosh flax leaves. Protein was extracted 3 days after infiltration and the blot was probed with anti-GFP

antibody. Positions and sizes (kDa) of protein molecular mass standards are indicated. The position of protein bands of interest is indicated by a red arrow. The lower panel shows the Ponceau-S-stained membrane confirming approximately equal protein loading.

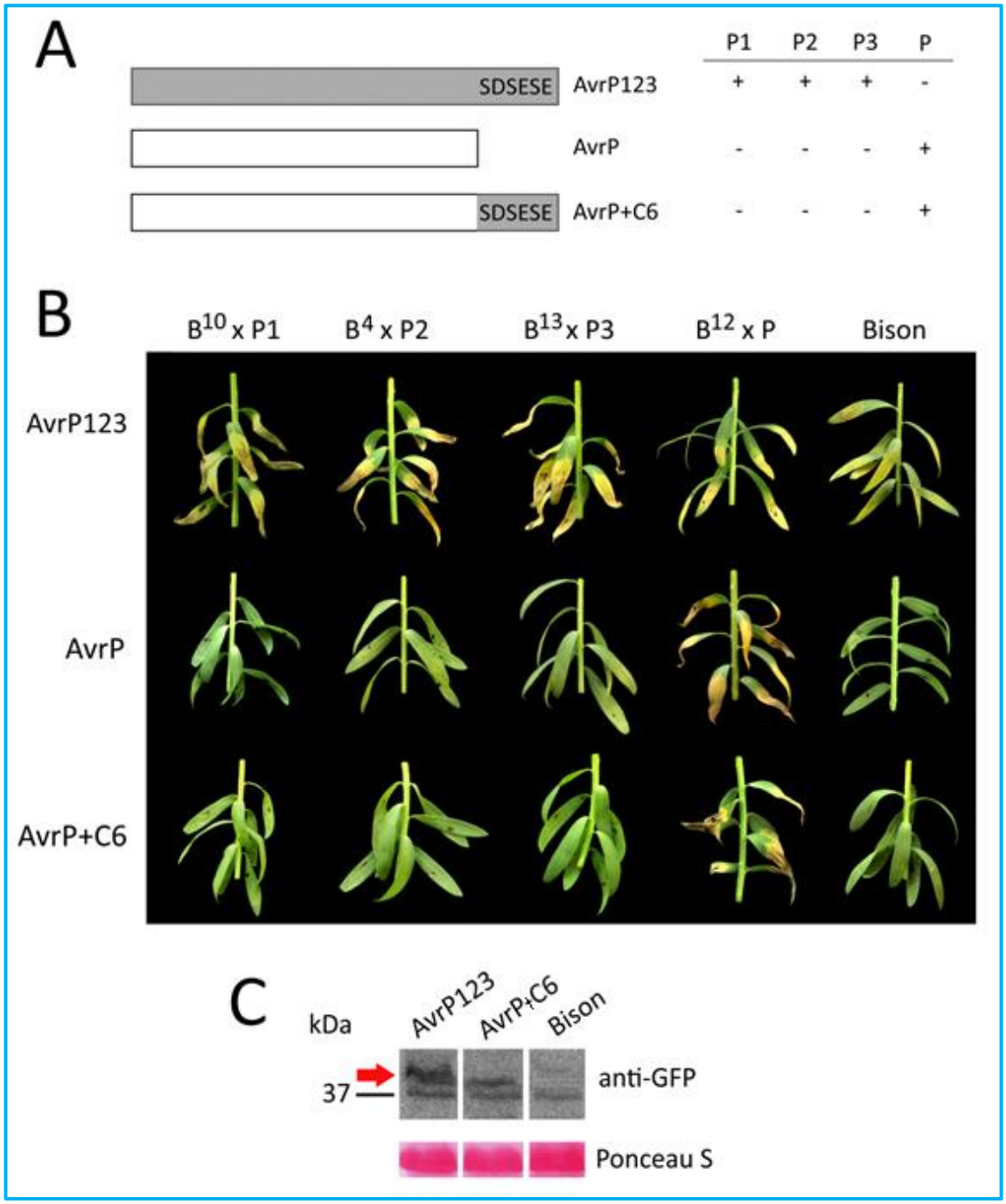

Figure 3.8 Necrosis induced by the C6 addition mutant of AvrP in *P*, *P1*, *P2* and *P3* flax. (A) Diagram of AvrP123, AvrP and the C6 addition mutant of AvrP (AvrP+C6) with their corresponding patterns of necrosis induction on *P*, *P1*, *P2* and *P3* flax. AvrP123 sequence is represented by a grey bar whereas AvrP sequence is represented by a white bar. + =

necrosis; - = no necrosis. All constructs were made without a signal peptide coding sequence. (B) Agroinfiltration results for constructs described in (A) on plants on plants from Koto (*P*), Akmolinsk (*P1*), Abyssinian (*P2*) and Leona (*P3*) flax lines that had been backcrossed to Bison twelve (B^{12}), ten (B^{10}), four (B^{4}) and thirteen (B^{13}) times to Bison, respectively. Each construct was tested on three flax plants with 6-8 leaves tested per plant (only one plant shown per treatment). The experiment was conducted at least two times. The photograph was taken at least 8 days after infiltration. (C) Upper panel shows a gel blot of YFP-tagged AvrP123 and AvrP+C6 proteins expressed without a signal peptide coding sequence under the control of the 35S promoter in agroinfiltrated Bison flax leaves. Protein was extracted 3 days after infiltration and the blot was probed with anti-GFP antibody. Positions and sizes (kDa) of protein molecular mass standards are indicated. The position of protein bands of interest is indicated by a red arrow. The lower panel shows the Ponceau-S-stained membrane confirming approximately equal protein loading.

3.3.2.2 Investigation of the role of the eight C-terminal residues (C8) of AvrP-339 and the corresponding residues of AvrP123 in recognition

To investigate the role of the eight C-terminal residues (C8) of AvrP-339 and the corresponding C8 preceding C6 of AvrP123, two constructs were made in which C8 of AvrP-339 (IASVQYQD) and AvrP123 (IARVQYQN) replaced C8 of AvrP (KDSVEYGG). These constructs were designated AvrP-$C8^{339}$ and AvrP-$C8^{P123}$, respectively (Figure 3.9A). A third construct was also made in which C6 from AvrP123 (see section 3.3.2.1) was added to AvrP-$C8^{P123}$. This construct was designated AvrP-$C14^{P123}$ (Figure 3.9A). The AvrP-339 was used as a control (Figure 3.9A).

All constructs were tested on *P*, *P1*, *P2* and *P3* flax plants (Figure 3.9B) and *P* tobacco (Figure 3.10A). In flax, AvrP-339 triggered strong cell death in *P2* flax plants (Figure 3.9B), which differs from the previous finding of weak necrosis reported by Dodds and Thrall (2009). Both AvrP-$C8^{339}$ and AvrP-$C8^{P123}$ triggered strong cell death in *P*, *P2* and *P3* flax plants (Figure 3.9B), suggesting that C8 is important for recognition by P2 and P3. AvrP-$C14^{P123}$ also triggered strong cell death in *P*, *P2*, and *P3* flax plants (Figure 3.9B), suggesting that C6 plays no modifying role in the recognition mediated by C8.

AvrP-C8^{339}, AvrP-C8^{P123} and AvrP-C14^{P123} were also tested along with AvrP+C6 (section 3.3.2.1) in *P* tobacco (Figure 3.10)**.** All triggered strong cell death responses in *P* tobacco leaves except for AvrP+C6, which, surprisingly, only produced weak necrosis (Figure 3.10A). C6 from AvrP123 apparently inhibited AvrP recognition by P in tobacco, but not in flax (section 3.3.2.1) and not when combined with C8 from AvrP123 (AvrP-C14^{P123}, Figure 3.10A).

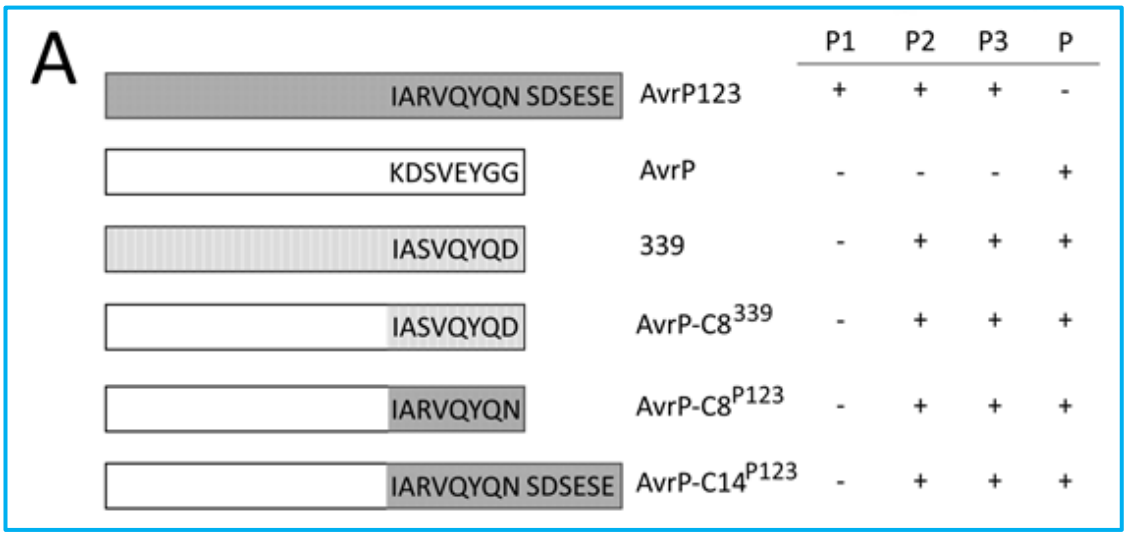

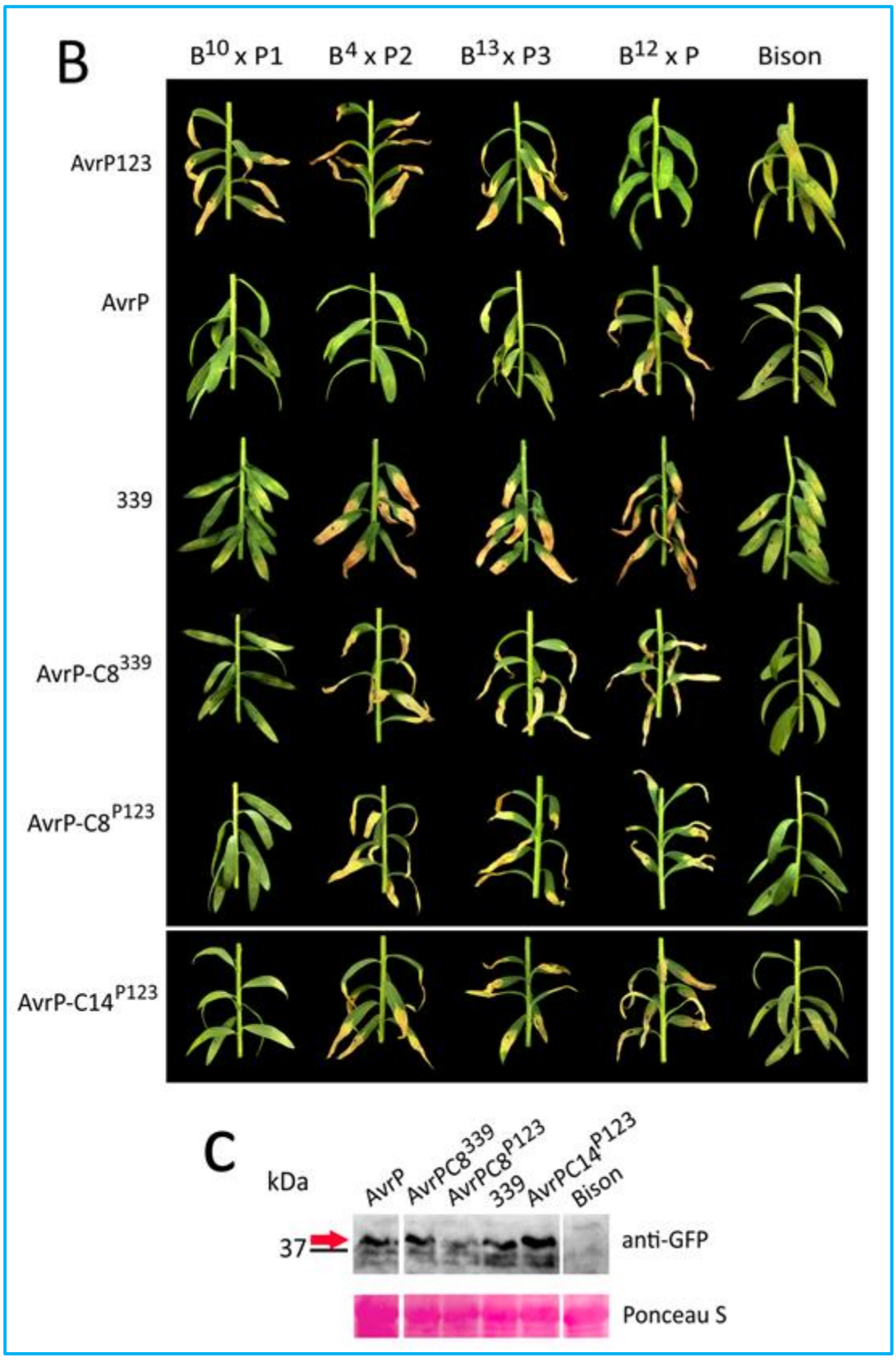

Figure 3.9 Necrosis induced by C8 substitution mutants of AvrP in *P*, *P1*, *P2* and *P3* flax. (A) Diagram of AvrP123, AvrP, AvrP-339 and the C8 substitution mutants AvrP-C8^{339}, AvrP-C8^{P123} and AvrP-C14^{P123} and their corresponding patterns of necrosis induction on *P*, *P1*, *P2* and *P3* flax. AvrP123 sequence is represented by a grey bar, AvrP sequence is

represented by a white bar and AvrP-339 sequence is represented as a light grey and white striped bar. + = necrosis; - = no necrosis. All constructs were made without a signal peptide coding sequence. (B) Agroinfiltration results for constructs described in (A) on plants from Koto (*P*), Akmolinsk (*P1*), Abyssinian (*P2*) and Leona (*P3*) flax lines that had been backcrossed to Bison twelve (B^{12}), ten (B^{10}), four (B^{4}) and thirteen (B^{13}) times to Bison, respectively. AvrP-$C14^{P123}$ was tested separately from AvrP-$C8^{339}$ and AvrP-$C8^{P123}$. Each construct was tested on three flax plants with 6-8 leaves tested per plant (only one plant shown per treatment). The experiment was conducted at least two times. Photographs were taken at least 8 days after infiltration. (C) Upper panel shows a gel blot of YFP-tagged AvrP, AvrP-$C8^{339}$, AvrP-$C8^{P123}$, AVrP-339 and AvrP-$C14^{P123}$ proteins expressed without a signal peptide coding sequence under the control of the 35S promoter in agroinfiltrated Bison flax leaves. Protein was extracted 3 days after infiltration and the blot was probed with anti-GFP antibody. Positions and sizes (kDa) of protein molecular mass standards are indicated. The position of protein bands of interest is indicated by a red arrow. The lower panel shows the Ponceau-S-stained membrane confirming approximately equal protein loading.

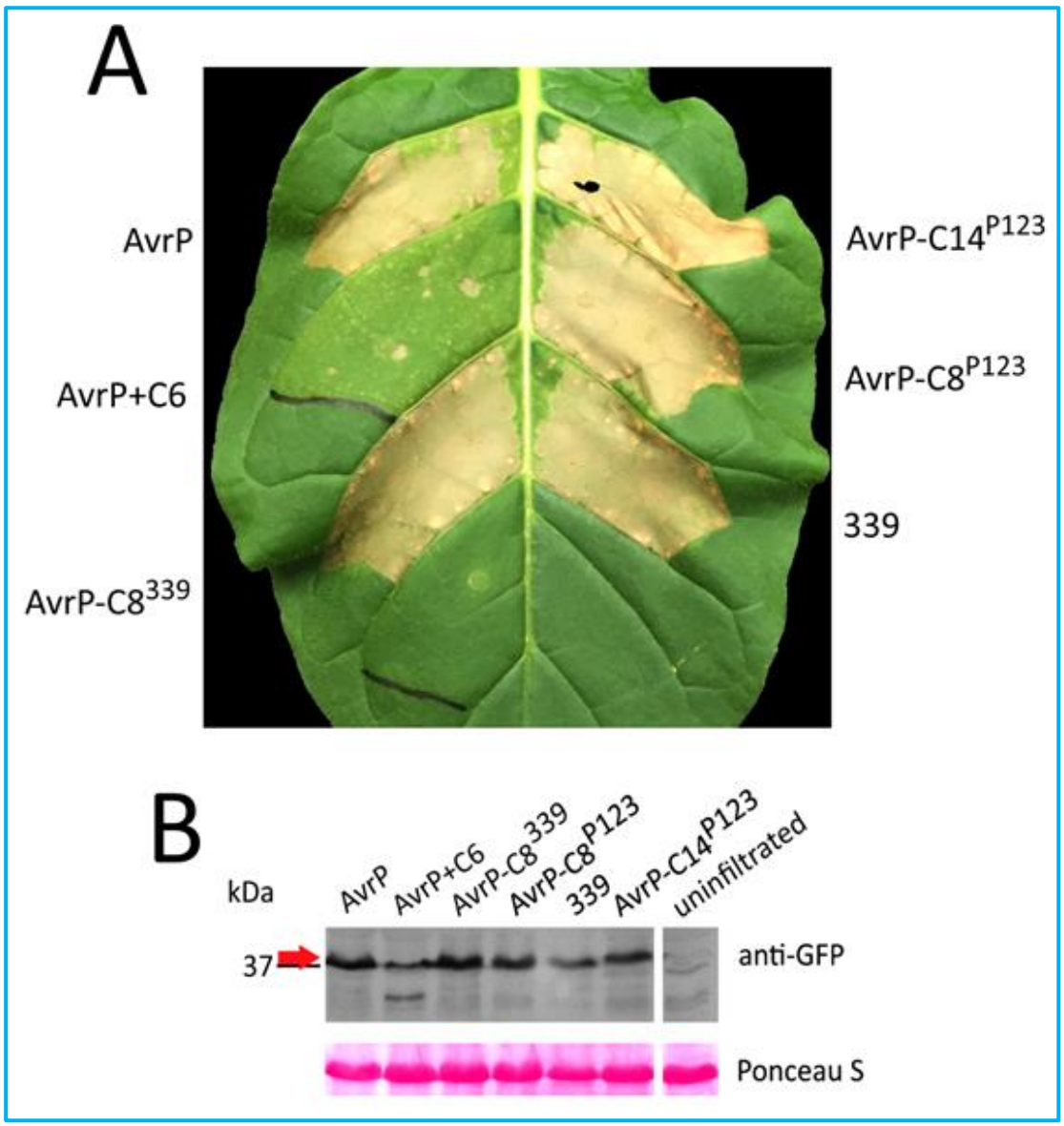

Figure 3.10 Necrosis induced by C8 substitution mutants of AvrP in *P* tobacco (A) Agroinfiltration results for AvrP, AvrP+C6, AvrP-339 and the C8 substitution mutants AvrP-C8^{339}, AvrP-C8^{P123} and AvrP-C14^{P123} in *W38::P* transgenic tobacco. The photograph was taken 4 days after infiltration. The leaf shown is representative of at least three replicates. (B) Upper panel shows a gel blot of YFP-tagged AvrP123, AvrP+C6, AvrP-C8^{339}, AvrP-C8^{P123}, AvrP-339 and AvrP-C14^{P123} proteins expressed without a signal peptide coding sequence under the control of the 35S promoter in *N. benthamiana* leaves. Protein was extracted 2 days after agroinfiltration and the blot was probed with anti-GFP antibody. Positions and sizes (kDa) of protein molecular mass standards are indicated. The position of protein bands of interest is indicated by a red arrow. The lower panel shows the Ponceau-S-stained membrane confirming approximately equal protein loading.

The necrosis induced by AvrP-C8^{339} in *P2* flax plants with a Bison background often appeared stronger than that induced by AvrP-C8^{P123} (Figure 3.9B). There are two polymorphic residues differing between C8 of AvrP-339 (IASVQYQD) and C8 of AvrP123 (IARVQYQN). To investigate whether these polymorphisms affected the strength of necrosis/cell death, AvrP-C8^{339} and AvrP-C8^{P123} were compared more closely in *P2* flax plants that had been backcrossed to Hosh, with Avr-339 used as a control (Figure 3.11). AvrP-C8^{339} still triggered a stronger cell death response compared to the AvrP-C8^{P123} in the *P2* flax plants with a Hosh background (Figure 3.11), suggesting that the two polymorphic residues in C8 of AvrP-339 (S106 and D111) enhanced recognition by the P2 resistance protein.

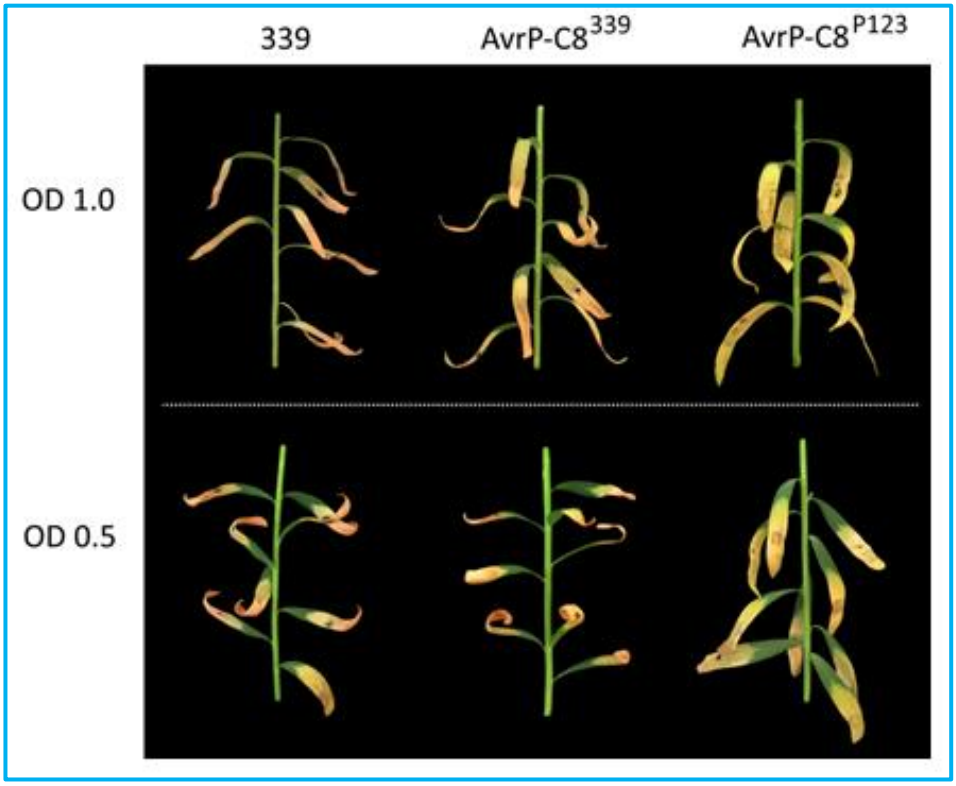

Figure 3.11 Necrosis induced by AvrP-C8^{339} and AvrP-C8^{P123} in *P2* flax plants with a Hosh background. OD600 dilutions of 1.0 and 0.5 of *Agrobacterium* carrying AvrP-339, AvrP-C8^{339} and AvrP-C8^{P123} were infiltrated into leaves of *P2* flax plants with a Hosh background. Seven to eight leaves were infiltrated on each of three flax plants (only one plant shown per treatment). Experiments using an *Agrobacterium* suspension with OD600 of 1.0 were conducted at least three times. The photograph was taken 8 days after infiltration.

To further test the role of C8 in recognition by P2 and P3, another construct was made by replacing the C8 residues in AvrP-271 with the C8 residues from AvrP-339. This construct, designated AvrP-271-C8^{339} (Figure 3.12A), was then tested in flax and *P* tobacco leaves. AvrP-271-C8^{339} did not trigger cell death in *P1* and *P3* flax plants, but triggered cell death slightly in *P2* and more strongly in *P* flax plants (Figure 3.12B). However, the necrosis produced by this construct was only observed 10-15 days after infiltration rather than 6-8 days as found for AvrP123 in *P2* flax plants, suggesting only weak recognition by the P and P2 resistance proteins. AvrP-271-C8^{339} did not trigger any cell death in *P* tobacco (Figure 3.13A), confirming the weak recognition by the P resistance protein. Nevertheless, this result further supports a role for C8 residues in recognition by P2. Interestingly, it also suggests that C8 of AvrP-271 may be suppressing its own recognition by P.

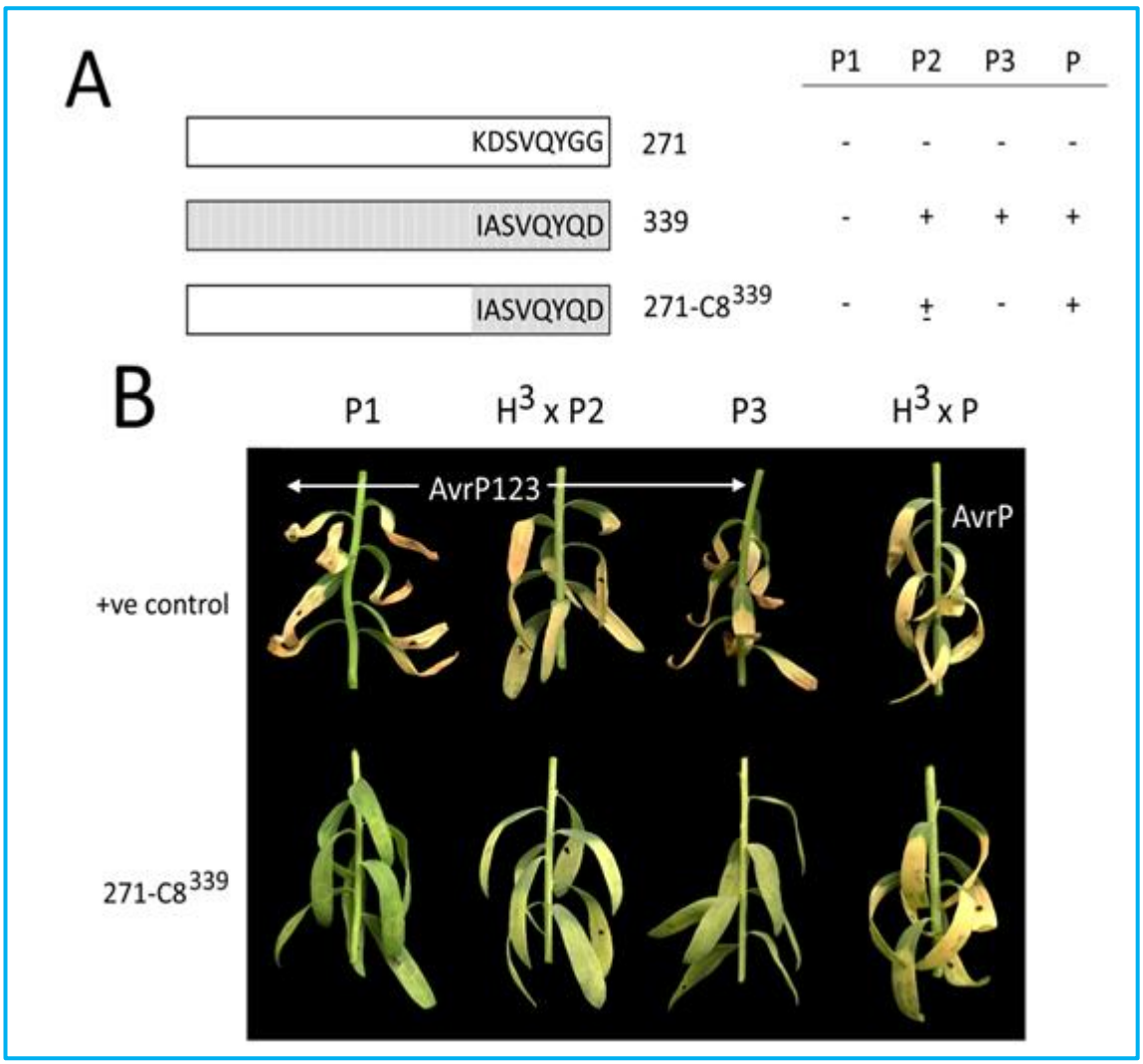

Figure 3.12 Necrosis induced by a C8 substitution mutant of AvrP-271 in *P*, *P1*, *P2* and *P3* flax. (A) Diagram of AvrP-271, AvrP-339 and the C8 substitution mutant AvrP-271-C8^{339} and their corresponding patterns of necrosis induction on *P*, *P1*, *P2* and *P3* flax. AvrP-271 sequence is represented by a white bar and AvrP-339 sequence is represented as a light grey and white striped bar. + = necrosis; - = no necrosis. All constructs were made without a signal peptide coding sequence. (B) Agroinfiltration results for AvrP-271-C8^{339} on plants from Koto (*P*), Akmolinsk (*P1*), Abyssinian (*P2*) and Leona (*P3*) flax lines where *P2* and *P* had been backcrossed three times to Hoshangabad (H^3). Each construct was tested on three flax plants with 6-8 leaves tested per plant (only one plant shown per treatment). The experiment was conducted at least two times. The photograph was taken 15 days after infiltration.

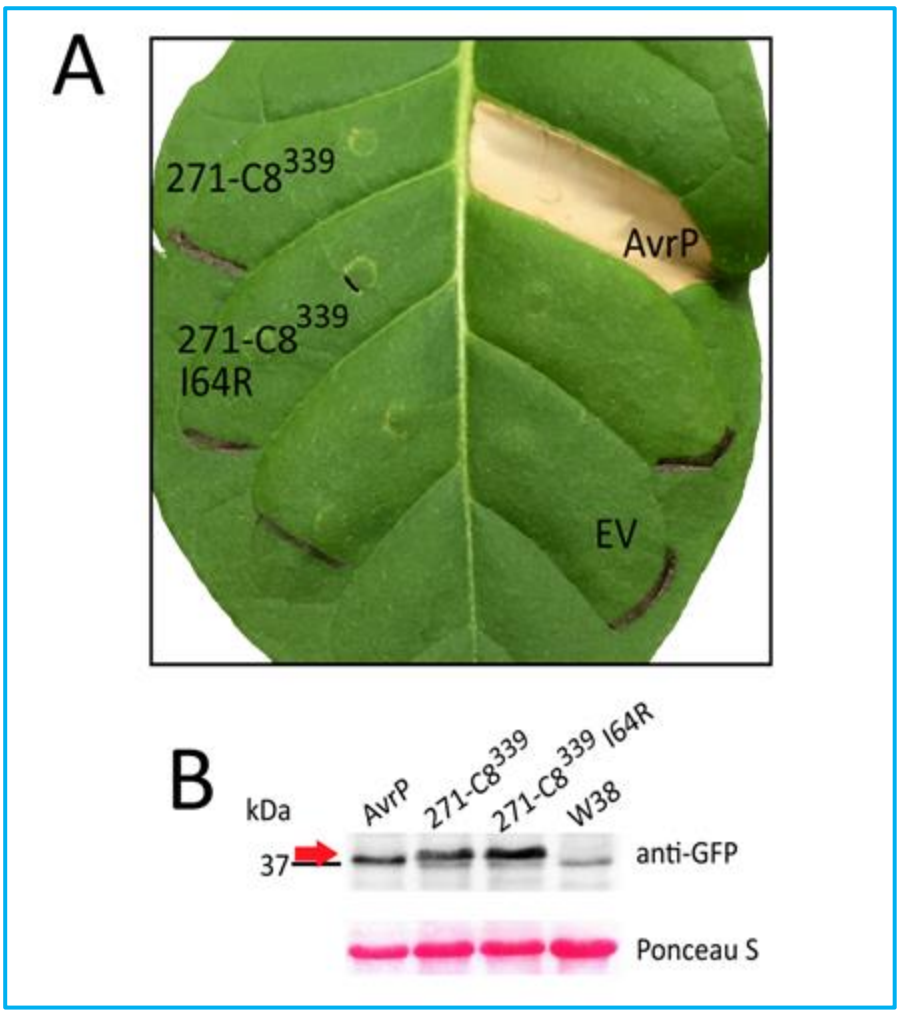

Figure 3.13 Necrosis induced by AvrP-271-C8^{339} and its I64R mutant in *P* tobacco. (A) Agroinfiltration results for AvrP-271-C8^{339} and its I64R mutant on W38::*P* transgenic tobacco. The experiment was conducted at least two times with six leaves per experiment. The photograph was taken 4 days after agroinfiltration. (B) Upper panel shows a gel blot of YFP-tagged AvrP, AvrP-271-C8^{339} and AvrP-271-C8^{339} I64R proteins expressed without a signal peptide coding sequence under the control of the 35S promoter in W38 tobacco leaves. Protein was extracted 2 days after agroinfiltration and the blot was probed with anti-GFP antibody. Positions and sizes (kDa) of protein molecular mass standards are indicated. The position of protein bands of interest is indicated by a red arrow. The lower panel shows the Ponceau-S-stained membrane confirming approximately equal protein loading.

3.3.2.3 I64 is important for recognition of AvrP-271-C8^{339} by P and P2

The I64 residue of AvrP has been shown to be important for recognition by P (Zhang et al, 2018) and is present in both AvrP-271 and AvrP-339. To determine whether I64 was also important for recognition of AvrP-271-C8^{339} by P, it was mutated into the corresponding R residue present in AvrP123 (Figure 3.13A) as described in section 3.2.3. The AvrP-271-C8^{339} I64R mutant was then tested on the *P*, *P1*, *P2* and *P3* flax plants (Figure 3.14B) and *P* tobacco leaves (Figure 3.13A).

In flax, the I64R mutation abolished the ability of AvrP-271-C8^{339} to trigger cell death in *P* and *P2* flax plants (Figure 3.14B). This result shows that the I64 residue is also important for P recognition in the context of AvrP-271-C8^{339}. However, the I64R mutation also abolished the recognition of 271-C8^{339} by the P2 resistance protein, suggesting that whilst the I64 residue is not required for recognition of AvrP123 by P2, it is important for recognition of AvrP-271-C8^{339} by P2. The I64R mutation did not alter the inability of AvrP-271-C8^{339} to trigger cell death in *P* tobacco (Figure 3.13A).

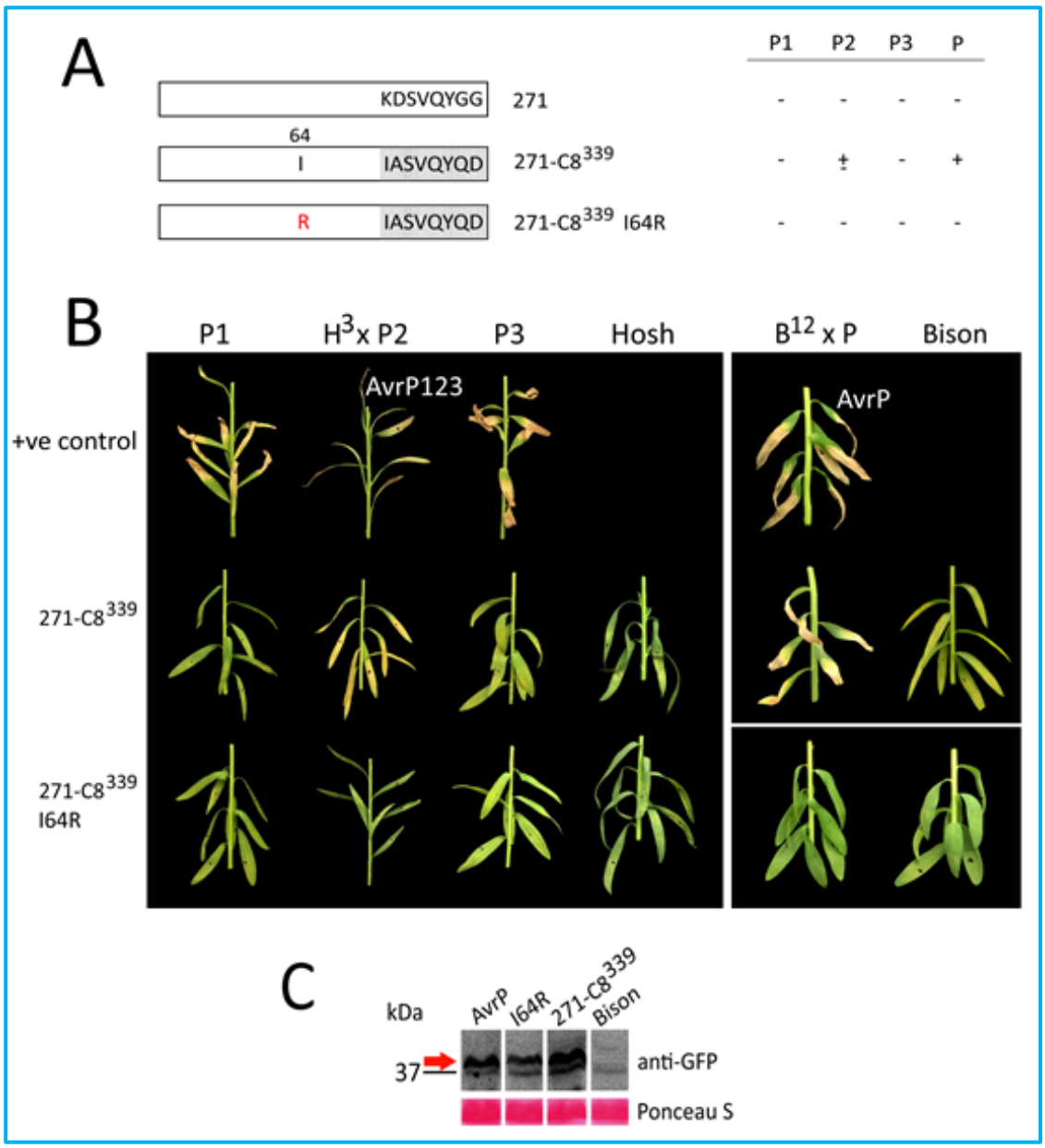

Figure 3.14 Necrosis induced by AvrP-271-C8^{339} and its I64R mutant in *P*, *P1*, *P2* and *P3* flax. (A) Diagram of AvrP-271-C8^{339} and its I64R mutant, and their corresponding patterns of necrosis induction on *P*, *P1*, *P2* and *P3* flax. AvrP-271 sequence is represented by a white bar and AvrP-339 sequence is represented as a light grey and white striped bar. + = necrosis; - = no necrosis. All constructs were made without a signal peptide coding sequence. (B) Agroinfiltration results for construct described in (A) on plants from Koto (*P*), Akmolinsk (*P1*), Abyssinian (*P2*) and Leona (*P3*) flax lines backcrossed to Hosh in the case of Abyssinian or to Bison in the case of Koto. Each construct was tested on three flax plants with 6-8 leaves tested per plant (only one plant shown per treatment). The experiment was conducted at least two times. Photographs were taken 11 days (left panel) and 15 days (right panels) after infiltration. Bison exhibited a background

response to 271-C8^{339} so only the clear difference in necrosis observed in Bison backcross plants carrying *P* is shown. (C) Upper panel shows a gel blot of YFP-tagged AvrP, 271-C8^{339} I64R and 271-C8$^{\mathbf{339}}$ proteins expressed without a signal peptide coding sequence under the control of the 35S promoter in agroinfiltrated Bison flax leaves. Protein was extracted 3 days after infiltration and the blot was probed with anti-GFP antibody. Positions and sizes (kDa) of protein molecular mass standards are indicated. The position of protein bands of interest is indicated by a red arrow. The lower panel shows the Ponceau S stained membrane confirming approximately equal protein loading.

3.3.3 The six C-terminal residues of AvrP123 (C6) improve recognition of AvrP-C8^{P123} by P2

To further investigate the role of C6 in AvrP123 recognition, C8 constructs (AvrP-C8^{339}, AvrP-C8^{P123}, AvrP-C14^{P123} and 271-C8^{339}, section 3.3.2.2) were co-infiltrated with the *P2* resistance gene into leaves of *Nicotiana benthamiana* (Figure 3.15A) and *N. tabacum* W38 (Figure 3.15B). AvrP123 and AvrP-C8^{339} were used as controls. AvrP-C8^{P123} triggered no response or slight chlorosis in both tobacco species compared to a stronger response for AvrP-C8^{339}, confirming the previous results observed in P2 flax plants (Figure 3.11). However, the further addition of C6 from AvrP123 to AvrP-C8^{P123} enabled AvrP-C14^{P123} to trigger stronger chlorosis compared to AvrP-C8^{P123} although not as strong as the chlorosis produced by AvrP-C8^{339} or AvrP123. This result suggested that C6 of AvrP123 improved recognition of AvrP-C8^{P123} by the P2 resistance protein.

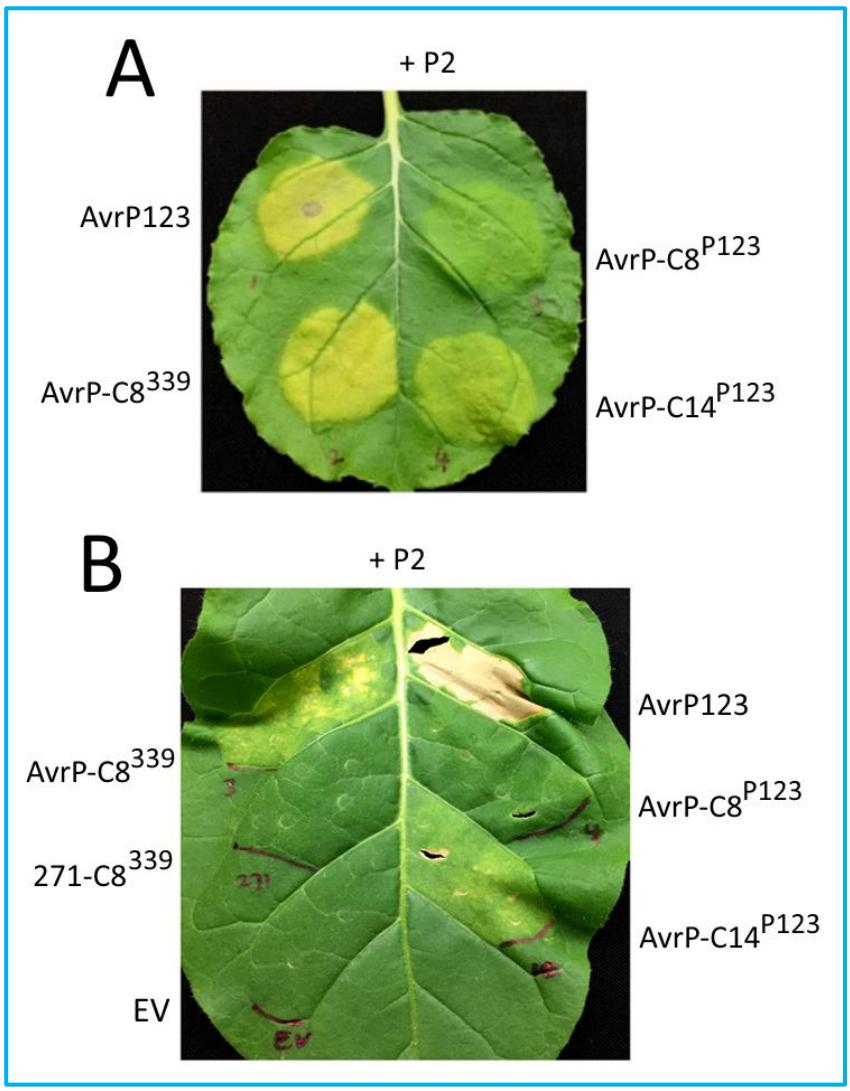

Figure 3.15 Investigating the effect of adding six C-terminal residues of AvrP123 (C6) onto AvrP-C8^{P123} on necrosis induced following co-expression with the *P2* resistance gene in tobacco. (A) Agroinfiltration results for AvrP-C8^{P123} and AvrP-C14^{P123} on *Nicotiana benthamiana* leaves. The experiment was conducted twice with six leaves per experiment. The photograph was taken 8 days after infiltration. (B) Agroinfiltration results for AvrP-C8^{339} and AvrP-C14^{P123} on W38 tobacco. The experiment was conducted twice with six leaves per experiment. The photograph was taken 9 days after infiltration. AvrP123, AvrP-C8^{339} and Empty Vector (EV) were used as controls.

3.3.4 AvrP-AvrP123 domain swap proteins

AvrP-bs25 is a natural domain swap between AvrP and AvrP123 (Figure 3.16A). It is unique because it is only recognised by the P2 resistance protein and not by the P, P1 or P3 resistance proteins. A reciprocal domain swap, AvrP-bs25^{R} (Figure 3.16A), was then made as described in section 3.2.2 with AvrP123 at the N-terminus and AvrP at the C-terminus starting from the I64 residue of AvrP. This domain swap was then tested in *P*, *P1*, *P2* and *P3* flax plants (Figure 3.16B) and *P* tobacco leaves (Figure 3.17A). Surprisingly, bs25^{R} was able to trigger strong cell death on all four flax lines (Figure 3.16B), suggesting recognition by P, P1, P2 and P3. However, in *P* tobacco leaves bs25^{R} produced weaker necrosis compared to AvrP (Figure 3.17A), suggesting weak recognition by P.

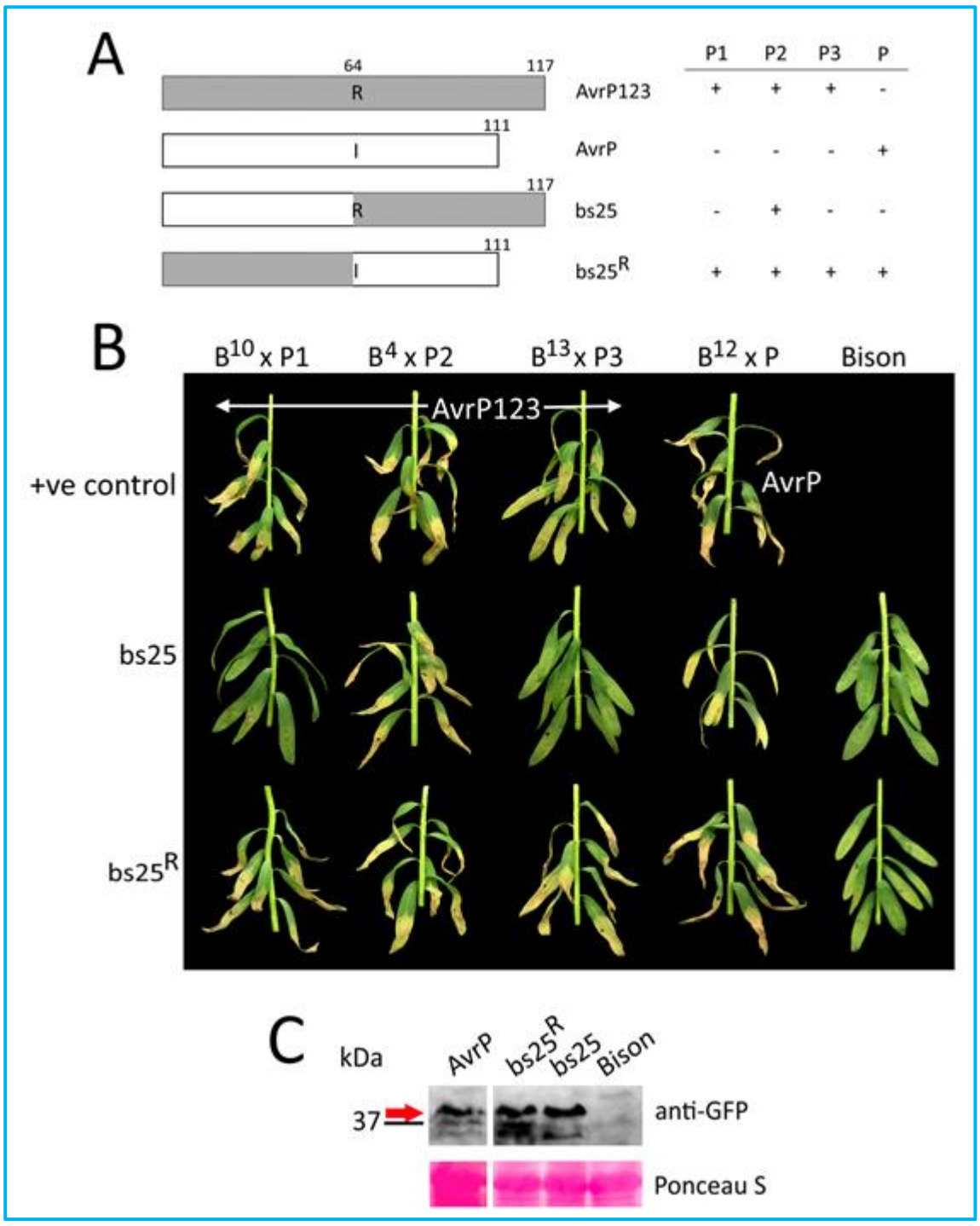

Figure 3.16 Necrosis induced by the AvrP-bs25^{R} domain swap in *P*, *P1*, *P2* and *P3* flax. (A) Diagram of AvrP-bs25 and AvrP-bs25^{R}, and their corresponding patterns of necrosis induction on *P*, *P1*, *P2* and *P3* flax. AvrP123 sequence is represented by a grey bar and AvrP sequence is represented by a white bar. + = necrosis; - = no necrosis. All constructs are without a signal peptide coding sequence. (B) Agroinfiltration results for a construct described in (A) on flax plants cultivars Koto (*P*), Akmolinsk (*P1*), Abyssinian (*P2*) and Leona (*P3*) flax lines that had been backcrossed to Bison twelve (B^{12}), ten (B^{10}), four (B^{4}) and thirteen (B^{13}) times to Bison, respectively. Each construct was tested on three flax

plants with 6-8 leaves tested per plant (only one plant shown per treatment). The experiment was conducted two times. The photograph was taken 8 days after infiltration. (C) Upper panel shows a gel blot of YFP-tagged AvrP, AvrP-bs25^{R} and AvrP-bs25 proteins expressed without a signal peptide coding sequence under the control of the 35S promoter in agroinfiltrated Bison flax leaves. Protein was extracted 3 days after infiltration and the blot was probed with anti-GFP antibody. Positions and sizes (kDa) of protein molecular mass standards are indicated. The position of protein bands of interest is indicated by a red arrow. The lower panel shows the Ponceau-S-stained membrane confirming approximately equal protein loading.

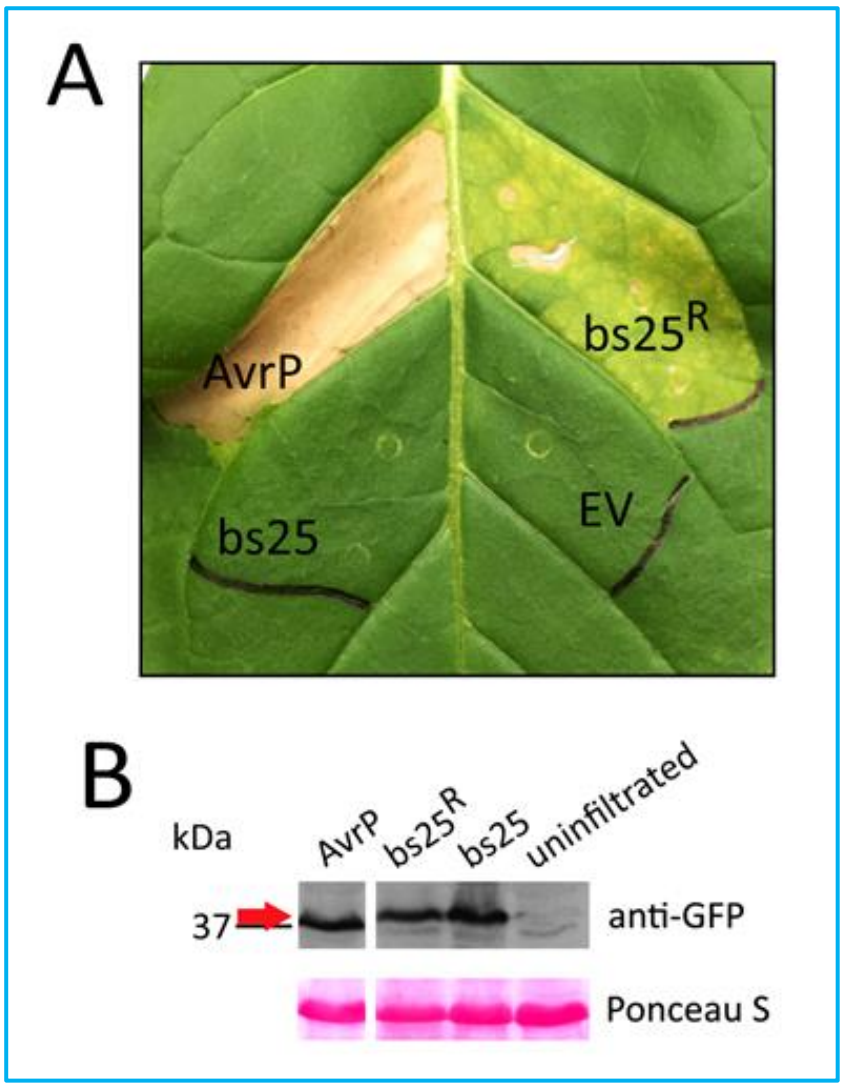

Figure 3.17 Necrosis induced by the AvrP-bs25^{R} domain swap in *P* tobacco. (A) Agroinfiltration results for AvrP, AvrP-bs25 and AvrP-bs25^{R} on W38::*P* transgenic tobacco. The photograph was taken 5 days after agroinfiltration. The leaf shown is representative of at least three replicates. (B) Upper panel shows a gel blot of YFP-tagged AvrP, bs25^{R} and bs25 proteins expressed without a signal peptide coding sequence under the control of the 35S promoter in *N. benthamiana* leaves. Protein was extracted 2 days after agroinfiltration and the blot was probed with anti-GFP antibody. Positions and sizes (kDa) of protein molecular mass standards are indicated. The position of protein bands of interest is indicated by a red arrow. The lower panel shows the Ponceau-S-stained membrane confirming approximately equal protein loading.

3.4 Discussion

3.4.1 Residues near the N-terminus of AvrP123 are important for P1 recognition and specificity

The variants of AvrP and AvrP123 have given valuable information regarding the recognitional specificity of the P, P1, P2 and P3 resistance proteins. Among the AvrP/P123 variants, AvrP-WA has the greatest similarity with AvrP123 (Figure 3.1). The seven polymorphic residues near the N-terminus of AvrP-WA and AvrP123 were shown by domain swaps to be important for P1 specificity (section 3.3.1.1). Interestingly, domain swap 1 was recognised not only by P1, P2 and P3 but also by P (Figure 3.2B). In domain swap 1, three residues shown to be important for AvrP recognition by P (D66, Q94 and E108; Chapter 2, section 2.3.4.2) were contributed by the WA isolate.

Domain swap 1 also contains E35 contributed by AvrP123. Analysis of an E35K mutation confirmed that E35 is indeed important for recognition of domain swap 1 by P1 and P (section 3.3.1.2). Overall, it seems likely that Q35 (as in AvrP) or E35 (as in AvrP-339 and domain swap 1) but not K35 (as in AvrP-WA) are compatible with recognition by P but neither is sufficient for recognition by P (Q35 is present in both AvrP-271 and AvrP-bs25, which are not recognised by P, and E35 is present in AvrP123, which is not recognised by P). Similarly, whilst E35 (as in AvrP123 and domain swap 1) but not K35 (as in AvrP-WA or the E35K mutant of domain swap 1) is compatible with recognition by P1, it is not sufficient for recognition by P1 (E35 is present in AvrP-339, which is not recognised by P1).

The D66A mutation of AvrP abolished necrosis induced in *P* tobacco (Chapter 2, Figure 2.11B), whereas the D66A mutation of AvrP123 only diminished necrosis induced by P1 and did not affect necrosis induced by P2 or P3 (section 3.3.1.3, Figure 3.6B). Whilst D66 may be important for recognition of both AvrP and AvP123 it would not seem to contribute to their specificity of recognition given that AvrP, AvrP-339, AvrP-bs25 and AvrP-WA all carry D66 but are not recognised by P1, and AvrP123, AvrP-bs25 and AvrP-WA all carry D66 but are not recognised by P.

Overall, five polymorphic residues near the N-terminus are unique (F31, I34, R43 and S58) or almost unique (R64) to AvrP123 (Figure 3.18) and are therefore candidates for

residues controlling the specificity of recognition of AvrP123 by the P1 resistance protein. The AvrP-bs25^{R} domain swap between AvrP123 and AvrP is recognised by P1 and contains the four unique AvrP123 residues but not R64 (Figure 3.15). Domain swap 1 between AvrP123 and AvrP-WA contains the first three of these unique residues and is recognised by P1 whereas domain swap 2,3, which carries only the fourth unique residue (S58), gives an intermediate response on *P1* flax as opposed to domain swap 3, which lacks S58 and gives no response. Taken together these data suggest that at least two of these unique residues (including S58) and possibly all four are involved in P1 recognitional specificity. A mutational analysis of these four residues is needed to test their role further. Cloning and sequencing of the *P1* gene might also help reveal how AvrP123 is recognised by the P1 resistance protein.

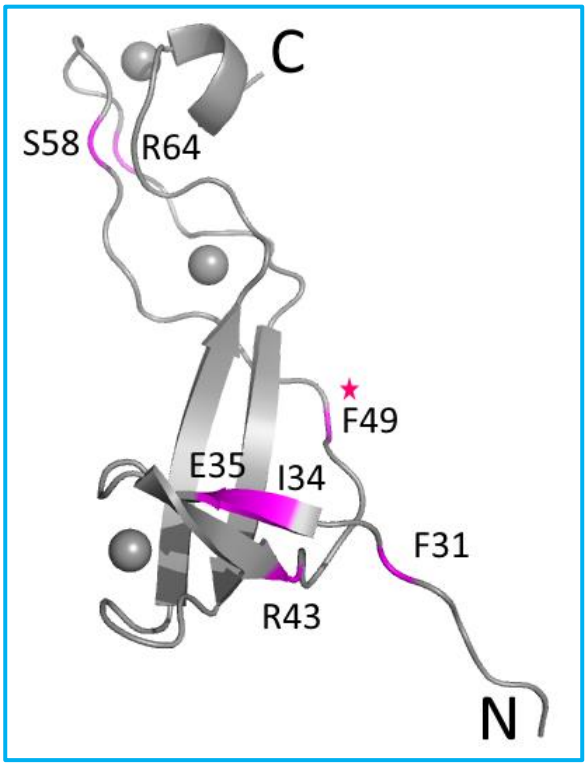

Figure 3.18 Seven polymorphic residues near the N-terminal of AvrP123 projected onto the structural model of AvrP. At least two of these unique residues and possibly four (F31, I34, R43 and S58) are candidates for residues controlling the specificity of AvrP123 recognition by the P1 resistance protein. The polymorphic residues are represented in magenta on the protein backbone. Residue F31, I34, E35, R43, S58 and R64 are polymorphic relative to AvrP whereas F49, highlighted with a pink star, is shared with AvrP. The N-terminus and C-terminus are represented as N and C, respectively.

3.4.2 The eight C-terminal residues (C8) of AvrP-339 and the corresponding eight residues of AvrP123 are important for P2 and P3 recognitional specificity

AvrP123 carries a six amino acid C-terminal extension relative to AvrP (Figure 3.1). Removal of this extension from AvrP123 or adding it to AvrP did not alter recognition by the P, P1, P2 or P3 resistance proteins (Figures 3.7 and 3.8), suggesting that this extension is not important for recognition or recognitional specificity. However, the C-terminal eight residues of AvrP-339 and the corresponding eight residues of AvrP123 preceding the six amino acid extensions were shown to be important for P2 and P3 recognition. Substitution of AvrP C8 (KDSVEYGG) by AvrP123 C8 (IARVQYQN) or AvrP-339 C8 (IASVQYQD) enabled recognition by P2 and P3 (sections 3.3.2.2).

There are two polymorphic residues between the C8 regions of AvrP-339 (IASVQYQD) and AvrP123 (IARVQYQN), but these two polymorphisms did not affect the specificity of recognition by the P2 and P3 resistance proteins. However, AvrP-C8^{339} was able to trigger a stronger cell death response in *P2* flax plants compared to AvrP-C8^{P123} (Figure 3.11). The first of these polymorphisms (S at position 3 in C8 of AvrP-339, Figure 3.19A) is shared with C8 of AvrP and AvrP-271, which are not recognised by P2 or P3. However, the second of these polymorphisms (D or N at position 8) is also polymorphic with C8 of AvrP and AvrP-271 (G at position 8). There are also two residues shared between all four C8s (V at position 4 and Y at position 6) and one residue (Q at position 5) shared between the C8s of AvrP-123 and AvrP-339, which are recognised by P2 and P3, and AvrP-271, which is not. Taken together, these findings suggest that residues at position 1, 2, 7 and 8 (I, A, Q/P and D/N, Figure 3.19A) may play a role in the specificity of recognition by P2 and P3. A mutational analysis of these four residues is needed to test their role further. However, the fact that AvrP-bs25 contains the same C8 sequence as AvrP123 but is not recognised by P3 indicates that other residues outside the C8 region must also influence recognition specificity.

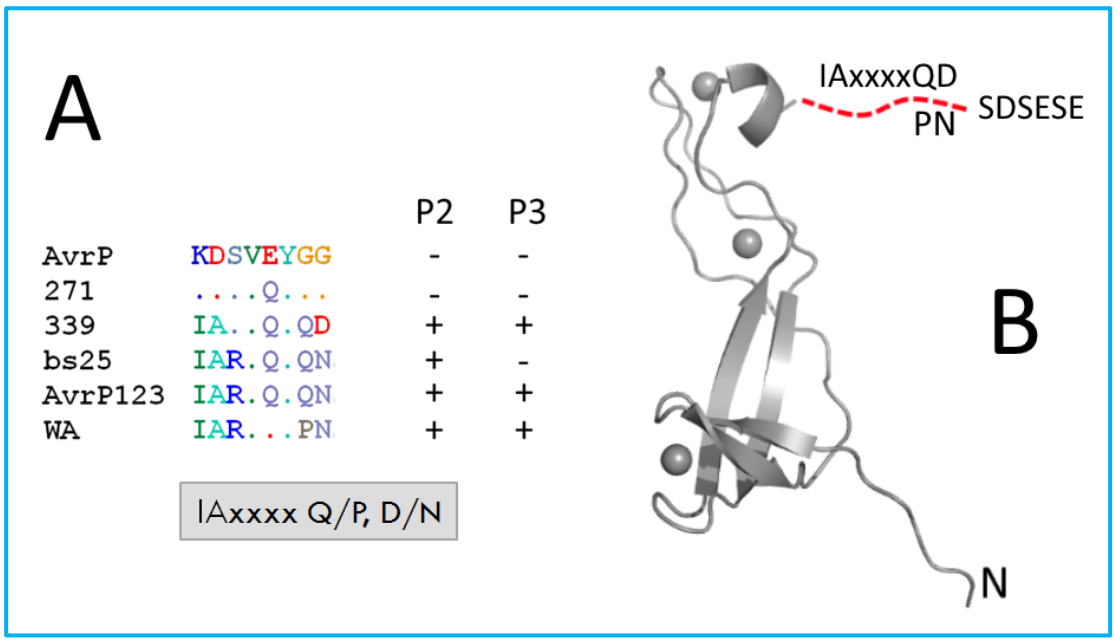

Figure 3.19 Comparison of C8 residues between AvrP/P123 variants and their location on the AvrP structure. (A) Comparison of C8 residues between AvrP/P123 variants in conjunction with their recognitional specificity by P2 and P3 resistance proteins. A consensus of potential candidates of residues involved in AvrP123 recognition by P2 and P3 is in a grey box. (B) The location of C8 residues at the C-terminus of AvrP123 prior to the C6 residues of AvrP123 (SDSESE).

3.4.3 The I64 residue is important for P specificity

Zhang et al. (2018) showed that the I64R mutation abolishes recognition of AvrP by the P resistance protein in *P*-containing flax plants and *P* tobacco. The I64R mutation also abolishes recognition of 271-C8^{339} by the P and P2 resistance proteins (Figure 3.14B). Converting the hydrophobic isoleucine residue into a charged arginine residue may have changed the overall folding of the 271-C8^{339} protein, thus affecting the ability of 271-C8^{339} to be recognised by the P and P2 resistance proteins.

AvrP-bs25 is only recognised by the P2 resistance protein (Dodds and Thrall 2009). However, the reciprocal recombinant AvrP-bs25^{R} is recognised by *P*, *P1*, *P2* and *P3* flax plants (Figure 3.16B). Structurally, AvrP-bs25 has the AvrP sequence at the N-terminus and AvrP123 sequence at the C-terminus whereas the reciprocal AvrP-bs25^{R} contains the reverse (Figure 3.16A). It is understandable that AvrP-bs25 is not recognised by the P1 resistance protein because the seven polymorphic residues of AvrP123 responsible

for P1 specificity are not present. It is also understandable that AvrP-bs25 is not recognised by P because two of the key residues required for P recognition are not present (I64 and E108). However, the reciprocal swap, AvrP-bs25^{R}, contains all seven of the AvrP123 residues important for P1 specificity thus enabling recognition by the P1 resistance protein. AvrP-bs25^{R} also has four of the residues important for P recognition (I64, D66, Q94 and E108), thus enabling recognition by the P resistance protein. However, with two of the residues contributing to P recognition (E30 and L57) replaced by AvrP123 residues, the response was not as strong as that for AvrP in *P* tobacco (Figure 3.17A). In AvrP-bs25^{R}, the R64 residue present in AvrP-bs25 was replaced by the I64 residue. This replacement may have enabled it to be recognised by both the P2 and P3 resistance proteins (Figure 3.16B). Further investigation of the I64 residue is needed to determine its role in AvrP123 recognition.

Chapter 4

Identifying and characterising AvrP interactor proteins

4.1 Introduction

Protein-protein interactions play an important role in many biological processes. One of the methods that has been used extensively to investigate protein-protein interactions is yeast two-hybrid analysis. In the yeast two-hybrid system, yeast is used as an expression system for genetic assays designed to detect protein-protein interactions *in vivo*. Not only can it be used to investigate interaction between two known proteins, it can also be used to screen for proteins that interact with a target protein from genomic or cDNA expression libraries. For the latter application, unlike many other methods for detection of interacting proteins, the gene encoding the protein that interacts with a target protein is immediately available on a plasmid. The method can also be used to investigate protein domains or specific residues that are involved in the protein-protein interaction (Fields and Song 1989).

The yeast-two-hybrid method is based on the work of Fields & Song (1989) using the GAL4 transcriptional activator of yeast (*Saccharomyces cerevisiae*) required for expression of galactose-induced genes. The GAL4 transcription factor can be divided into two separate and functionally independent domains: a DNA-binding domain (BD) and a transcription activating domain (AD). The DNA-binding domain binds to specific upstream activating sequences (UAS), whereas the activating domain, which contains an acidic region, is required to activate transcription. In the yeast two-hybrid system based on the GAL4 promoter, the BD is fused to protein “X” (bait) while the AD is fused to protein “Y” (prey). When proteins “X” and “Y” interact and form a protein-protein complex, the BD and AD are brought into close proximity and a fully functional transcription factor is re-formed. This allows the transcription of genes regulated by the UAS including GAL4 promoter fusions to reporter genes that allow screening of yeast cells showing bait-prey interaction using a visible marker or their selection using a nutritional marker (Fields and Song 1989; Chien et al. 1991).

Generally, in a yeast-two-hybrid assay, yeast cells are grown on a selective media lacking one or more essential amino acids corresponding to one or more mutations in amino acid biosynthesis. The corresponding wild type genes are placed under the control of the GAL4 promoter, so that they are only transcribed when bait-prey protein interaction reconstitutes the GAL4 promoter. The yeast cells are then able to grow on the selective media (Fields and Song 1989; Chien et al. 1991).

In this chapter, a yeast-two-hybrid screen was conducted using the AvrP-C8^{339} protein as bait to identify host proteins targeted by AvrP. The AvrP-C8^{339} was fused to the GAL4-BD and a cDNA library generated from rust infected-flax leaves was fused to the GAL4-AD. Several putative interactors of AvrP-C8^{339} have been identified by screening the prey cDNA library using AvrP-C8^{339} as bait.

4.2 Materials and Methods

4.2.1 Yeast cultures

The two *Saccharomyces cerevisiae* strains used in this study, AH109 and Y187, were grown in liquid Peptone Dextrose (YPDA) media containing 20 g/L peptone, 10 g/L yeast extract, 2% (w/v) glucose and 30 mg/L of L-adenine hemisulphate, or on a YPDA plate containing 2% (w/v) agar. Synthetic dropout (SD) media lacking appropriate amino acids was used to select transformed yeast and for selection of interactor candidates. The SD media contained 6.7 g/L yeast nitrogen base (Difco) without added amino acids, 2% (w/v) glucose and 2% (w/v) agar. The appropriate amino acids and two nitrogenous bases (adenine and uracil) were added into SD media according to plasmid selection and/or corresponding biosynthesis reporter genes with standard concentration of: 20 mg/L adenine, 20 mg/L arginine, 20 mg/L histidine, 30 mg/L isoleucine, 100 mg/L leucine, 30 mg/L lysine, 20 mg/L methionine, 50 mg/L phenylalanine, 200 mg/L threonine, 20 mg/L tryptophan, 30 mg/L tyrosine, 20 mg/L uracil, 150 mg/L valine (Yeast Protocols Handbook, Clontech Laboratories, Mountain View, California, USA).

4.2.2 Yeast heat-shock transformation

4.2.2.1 Preparation of yeast competent cells

Yeast heat-shock transformation was conducted according to the Yeast Protocols Handbook (Clontech) with modification. Before transformation, the yeast strain was

made competent for transformation. One colony of AH109 or Y187 yeast strain was grown in 25 mL of YPDA and incubated at 30 °C for 12 h with shaking until the OD_{600} reached 0.125–0.2. The liquid culture was centrifuged at 1,000 x g for 5 min and the pellet was re-suspended in 50 mL of YPDA and grown again until the OD_{600} reached 0.4–0.5. For library construction, the culture was re-grown in 100 mL of YPDA. The culture was centrifuged again at 1,000 x g for 5 min and the pellet was then washed with 30 mL of sterile water. The washed culture was then centrifuged at 1,000 x g for 5 min and the pellet was then re-suspended in 1.5 mL of 1.1x TE/LiAc (Clontech kit). The resuspended cells were transferred into two 1.5 mL microcentrifuge tubes and centrifuged at 12,000 x g for 30 sec. The pellet was resuspended again in 600 µL of 1.1x TE/LiAc and the cells were then ready for transformation.

4.2.2.2 Small scale yeast transformation

For small scale yeast transformation, 100–300 ng of plasmid was combined with 50 µg of denatured carrier DNA in a pre-chilled 1.5 mL microcentrifuge tube. The carrier DNA had been denatured previously by boiling at 95–100 °C for 5 min. Fifty µL of competent cells and 500 µL of 1.1x PEG/LiAc (Clontech kit) were then added into the microcentrifuge tube and mixed. The cells were then incubated at 30 °C for 30 min with mixing every 10 min by tapping or gently vortexing. Twenty µL of DMSO was then added prior incubation at 42 °C for 30 min with mixing every 10 min by gently vortexing. The transformed cells were then centrifuged at 12,000 x g for 30 sec and resuspended in 1 mL of YPD Plus Medium (Clontech kit). The cells could then be grown at 30 °C with shaking for 90 min, but this was optional. Cells were centrifuged at 12,000 x for 30 sec and then resuspended in 1 mL of 0.9% (w/v) NaCl. One hundred µL of 1/10 and 1/100 dilutions of cells were spread onto SD media containing appropriate amino acids and grown at 30 °C for 3–5 days.

4.2.2.3 Library scale yeast transformation

For library scale yeast transformation, 5–15 µg of plasmid was combined with 200 µg of denatured carrier DNA in a pre-chilled 15 mL tube. The carrier DNA had been denatured previously by boiling at 95–100 °C for 5 min. Six hundred µL of competent cells and 2.5 mL of 1.1x PEG/LiAc were then added into the tube and mixed. The cells were then incubated at 30 °C for 45 min with mixing every 15 min by tapping or gently vortexing.

One hundred and sixty µL of DMSO was then added prior to incubation at 42 °C for 30 min with mixing every 10 min by gently vortexing. The transformed cells were then centrifuged at 7000 x g for 5 min and resuspended in 3 mL of YPD Plus Medium (Clontech kit). The cells were grown in 30 °C with shaking for 90 min. Cells were centrifuged at 7000 x g for 5 min and then resuspended in 15 mL of 0.9% (w/v) NaCl. One hundred µL of 1/10 and 1/100 dilutions of cells were spread onto SD media containing appropriate amino acids and grown at 30 °C for 3–5 days.

4.2.3 Construction of GAL4BD-AvrP and -AvrP-C8^{339}

AvrP-C8^{339} binding domain (BD) constructs was tested as baits for cDNA library screening. The BD-AvrP construct was obtained from Xiaoxiao Zhang (CSIRO Agriculture and Food, Black Mountain) whereas BD-AvrPC8^{339} was made in a Gateway compatible vector pGBG-NSC-GWY-Y2H (modified version of pGBT9; Appendix 2) obtained from Maud Bernoux (CSIRO Agriculture and Food, Black Mountain). For simplicity, pGBG-NSC-GWY-Y2H will be referred as pGBT9. The AvrP-C8^{339} construct in pENTRY (from Chapter 3) was transferred into the modified Gateway vector pGBT9 using the LR reaction (as described in section 3.2.1 of Chapter 3). The positive clone was confirmed by PCR using a specific forward primer for AvrP and the ADH1 terminator primer 5'-CTATACCTGAGAAAGCAACCTGACCT-3'. The sequence was confirmed by sequencing using the ADH1 terminator primer. BD-AvrP and BD-AvrP-C8^{339} constructs were then inserted into competent Y187 (MATα) yeast cells using the small-scale transformation protocol described in section 4.2.2.

4.2.4 Autoactivity and toxicity tests of GAL4-BD candidates

The pGBT9-AvrP and pGBT9-AvrPC8^{339} constructs were tested for autoactivity and toxicity to confirm that the bait constructs do not autonomously activate the reporter genes in Y187 in the absence of a prey protein. One hundred ng of the pGBT9-AvrP and pGBT9-AvrPC8^{339} constructs were used to transform competent Y187 yeast cells using the small-scale transformation protocol described in section 4.2.2. One hundred µl of 1/10 and 1/100 dilutions of the transformation mixture were spread onto separate SD/-Trp/X-α-Gal plates (i.e. without tryptophan but with 5-bromo-4-chloro-3-indolyl α-D-galactopyranoside). If the bait is autoactive in this assay then distinct blue colonies will

grow on SD/-Trp/X-α-Gal selection plates. The pGBT9-AvrPC8^{339} construct was then tested for stringency by mating Y187 yeast cells carrying pGBT9-AvrPC8^{339} with AH109 yeast cells carrying an Empty-AD construct and plated on SD/-Trp/-Leu, SD/-Ade/-His/-Trp/X-α-Gal and SD/-Ade/-His/-Trp/-Leu/X-α-Gal plates (i.e. quadruple dropout without adenine, histidine, tryptophan and leucine but with 5-bromo-4-chloro-3-indolyl α-D-galactopyranoside) and grown at 30 °C for 3–5 days. Empty-AD was made in a Gateway compatible vector pGAD-GWY-Y2H (modified version of pGADT7; Appendix 2) obtained from Maud Bernoux (CSIRO Agriculture and Food, Black Mountain). The pGBT9-L6 TIR and pGADT7-L6 TIR constructs were obtained from Maud Bernoux (CSIRO Agriculture and Food, Black Mountain) and used in combination as a positive control for reporter activation. To test for toxicity, 1/10 and 1/100 dilutions of the transformation mixtures were also spread onto SD/-Trp agar plates and inoculated into SD/-Trp liquid medium. The cultures were grown at 30 °C for 3–5 days. If the bait is toxic to the yeast cells, both solid and liquid cultures will grow more slowly compared to the positive control.

4.2.5 Generating cDNA and construction of a GAL4-AD fusion library

4.2.5.1 RNA isolation and electrophoresis

RNA was isolated from leaves of the flax cultivar Hoshangabad infected by the flax rust strain CH5, which was generated by crossing flax rust strains C and H (Lawrence et al. 1981a). Infection was conducted by Greg Lawrence (CSIRO Agriculture and Food, Canberra). The leaves were harvested 6 days after infection. One gram of infected flax leaves was ground to a fine powder in liquid N_2 with mortar and pestle. The fine powder was then mixed into 2 mL of NTES buffer (0.1 M NaCl, 10 mM Tris-HCl pH 8, 1 mM Na_2EDTA, 1% (w/v) SDS, 1% (v/v) β-mercaptoethanol) and 3 mL of phenol : chloroform (1:1). Samples were then mixed for 15 min at room temperature on a mixing rotor followed by centrifugation for 10 min at 11,200 x g. The aqueous phase was then carefully pipetted into a 15 ml centrifuge tube. An equal volume of 4 M LiCl was then added and mixed by inversion. Samples were put on ice at 4 ^{o}C overnight. On the following day, samples were centrifuged for 10 min at 11,200 x g and the supernatants discarded. The pellets were dissolved in 450 µL of H_2O by gentle mixing and transferred to a microcentrifuge tube. Forty five µL of 20% (w/v) NaOAc pH 5.5 and 1 mL of ice-cold absolute ethanol were added into the samples and mixed by inversion. Samples were

left at -20 °C for a minimum of 1 hr followed by centrifugation at 18,900 x g for 10 min. The supernatants were discarded and the pellets were washed three times with 80% (v/v) ethanol (no set volume) and then "pulsed" briefly in a microcentrifuge. The RNA pellet was resuspended in 200 µL RNase free water and RNA concentration measured using a Nanodrop 2000 (Thermo Fisher Scientific, Waltham, MA USA).

RNA quality was assessed by gel electrophoresis. In a fume cupboard, a formaldehyde gel was prepared by adding 10 mL formaldehyde to 90 mL of molten agarose containing 1.4 g agarose and 10 mL of 10x MOPS (0.2 M MOPS, 0.05 M NaOAc, 0.01 M Na_2EDTA, adjusted to pH 7). RNA denaturation solution was prepared in a final volume of 20 µL consisting of 10 µL formamide, 3.5 µL formaldehyde, 2 µL of 10x MOPS and 1 µL of 10 mg/ml ethidium bromide. The solution was then put on ice for a few minutes until it turned orange. One to five µL of RNA was added into the denaturation solution. Samples were then heated at 65 °C for 5–10 min and 5 µL of RNA loading dye (8% (w/v) Ficoll, 0.02% (w/v) Bromophenol Blue, 0.04% (w/v) Xylene Cyanol) was added to each sample. The RNA samples were then loaded onto the formaldehyde gel and subjected to electrophoresis at 20 mV until the bromophenol-blue dye front had migrated at least 2–3 cm into the gel.

4.2.5.2 mRNA isolation

mRNA was isolated from total RNA using the PolyATtract® mRNA Isolation Systems III and IV (Promega, Madison, Wisconsin, USA), according to the manufacturer's protocol, starting from 0.52 mg of total RNA yielding 3.15 µg of mRNA (eluted in 250 µL). The mRNA was then precipitated and concentrated by additional of 0.1 volume of 3 M NaOAc pH 5.2 and one volume of isopropanol. The mixture was then incubated at -20 °C overnight and then centrifuged at 12,000 x g for 10 min at 4 °C. The pellet was then washed one time with 70% (v/v) ethanol, dried and resuspended in 6 µL of RNAse-free water, yielding 2.58 µg of mRNA in total.

4.2.5.3 Generation of a cDNA library

There were three steps conducted in generating the cDNA required for library preparation: 1) first-strand cDNA synthesis; 2) amplification of cDNA by long distance

PCR (LD-PCR); 3) purification of cDNA. The Make Your Own "Mate & Plate" Library System kit (Clontech) was used to generate the two cDNA samples from 0.5 µg and 1.0 µg of mRNA. All reagents and primers were from Clontech. To generate first-strand cDNA, mRNA (0.5 µg or 1.0 µg) was annealed with CDSIII oligo-dT primer in a total volume of 4 µL and incubated for 2 min at 72 °C before adding 2 µL of 5x first strand buffer, 1 µL of 20 mM DTT , 1 µL of 10 mM dNTPs and 1 µL of SMART Moloney Murine Leukemia Virus (MMLV) reverse transcriptase (10 U/µL) and incubating at 42 °C for 10 min. After addition of 1 µL of SMART III-modified oligo, the reaction mixture was incubated at 42 °C for 1 hr and the reaction was terminated by incubation at 75°C for 10 min. The mixture was cooled to room temperature and 1 µL of RNase H (2 units) was added to the mixture and incubated at 37 °C for 20 min.

First strand cDNA was amplified using the LD-PCR protocol. All reagents and primers were from Clontech. Amplification was carried out in a 100 µL reaction containing 2 µL first strand cDNA, 1x Advantage 2 PCR Buffer (1x dNTP Mix, 0.2 µM 5' PCR primer, 0.2 µM 3' PCR primer, 1x Melting solution and 1x Advantage 2 Polymerase mix. The PCR conditions were as follow: 95 °C for 30 sec, then 20 cycles at 95°C for 10 sec and 68 °C for 6 min with a 5 sec addition to the extension time with each successive cycle, followed by 68 °C for 5 min. The LD-PCR amplification was conducted five times in total in order to generate 2–5 µg of cDNA.

A 5 µL sample of the cDNA amplification was analysed by gel electrophoresis on a 1% (w/v) agarose gel to determine whether the cDNA was larger than 200 bp. The cDNA was column purified and concentrated using a DNA Clean & Concentrator™-5 kit (Zymo Research, Irvine, CA). In total, 4.16 µg of purified cDNA was used to generate a cDNA library by recombination with the pGADT7-Rec plasmid (Clontech). The purified cDNA was combined with 6 µL of pGADT7-Rec plasmid and used to transform competent AH109 yeast cells following the library scale yeast transformation protocol (section 4.2.2.3). The transformed cells were resuspended in 15 mL of 0.9% (w/v) NaCl and 100 µL of 1/10 and 1/100 dilutions of cells were spread onto 90-mm-diameter SD/-Leu plates and grown at 30°C for 3–4 days. The remainder of the cells were spread onto 66 150-mm-diameter SD/-Leu plates with 160-200 µL of cells spread on each plate. The aim was to have at least 133 colonies on the 1/100 dilution plate as an indication that a library of

2 million clones was made. A count of 183 colonies was obtained on the 1/100 dilution plate indicating that the library contained 2.2 million clones and was therefore suitable for further analysis.

Once the library was confirmed to have more than one million clones, cells were harvested. Prior to harvesting, plates were chilled at 4 °C for 3–4 hr. Five mL of freezing media (25% (v/v) glycerol in YPD) was added to each plate. Colonies were detached from each plate using sterile disposable spreader and all liquids were combined into a single sterile flask. The cell density was measured and adjusted to 2 x 10^7 cells per mL. The library was aliquoted into several 1 mL aliquots for short-term use and 50 mL aliquots for long-term storage and then stored at -80 °C.

4.2.6 Screening for two-hybrid interactions and confirmation of interaction

4.2.6.1 Two-Hybrid library screening using yeast mating

A 1 mL aliquot of frozen cDNA library was thawed at room temperature and 10 µL was removed for library titration. Roughly 1 x 10^8 Y187 cells containing the bait plasmid pGBT9-AvrPC8^{339} were combined with cells containing the cDNA library and resuspended in 45 mL of 2x YPDA plus 50 µg/mL kanamycin in a sterile 2 L flask. The cells were incubated for 20 hr at 30 °C with gentle swirling (30 rpm). After 20 hr, the mating was considered complete as zygotes were no longer visible under a phase-contrast microscope. The mating mix was centrifuged at 1,000 g for 10 min and the supernatant was discarded. The 2 L flask was rinsed twice with 50 mL 0.5x YPDA plus 50 µg/mL kanamycin and then the pelleted cells were resuspended in 50 mL 0.5x YPDA plus 50 µg/mL kanamycin. The cells were then centrifuged again for 10 min at 1,000 x g and the supernatant was discarded. The pelleted cells were resuspended in 10 mL of 0.5x YPDA plus 50 µg/mL kanamycin. One hundred µL of 1/10, 1/100, 1/1,000 and 1/10,000 dilutions of the mating mixture were spread onto SD/-Leu, SD/-Trp and SD/-Leu/-Trp plates to determine the mating efficiency. The remainder of the culture were plated on SD/-Ade/-His/-Trp/-Leu/X-α-Gal plates with 200 µL cells per plate (twenty 150-mm-diameter plates in total). All plates were incubated for 3–8 days at 30 °C.

4.2.6.2 Confirmation of interaction

Positive colonies were re-streaked on QDO + X-α-Gal plates to obtain individual clones. Plasmid DNA was isolated from the candidates using a lysis buffer containing 2% (v/v) Triton X-100, 1% (w/v) SDS, 100 mM NaCl, 10 mM TRIS (pH 8) and 1 mM EDTA (Hoffman and Winston 1987). A loopful of cells was picked from the plate and resuspended in 200 µL lysis buffer, 200 µL of phenol/chloroform/isoamyl alcohol (25:24:1) and 0.3 g of acid washed glass beads (Sigma, St. Louis, Missouri, USA). The mixture was then vortexed for 2 min and centrifuged at 12,000 x g for 30 sec. The mixture was then incubated at -20°C for 3 hr and centrifuged at 12,000 x g for 30 sec. The pellet was washed with 70% (v/v) EtOH, dried for 30 min at room temperature and resuspended in 20 µL of sterile deionised water. One µL of this solution was used for PCR analysis with vector specific primers for pGADT7-Rec (MATCHMAKER AD LD-insert screening amplimer set, 5' AD primer: 5'-CTATTCGATGATGAAGATACCCCACCAAACCC-3' and 3' AD primer: 5'-GTGAACTTGCGGGGTTTTTCAGTATCTACGAT-3'.

Isolated total DNA for each putative interactor was transformed into electrocompetent *E. coli* DH5α cells and grown on LB media with ampicillin (100 µg/mL) plates overnight at 37 °C. Plasmid DNA was then isolated and sequenced as described below. AH109 yeast cells were then transformed using 100–200 ng of plasmid DNA , plated on SD/-Leu media and grown at 30 °C for 3–4 days. A small-scale yeast mating was performed to re-test the interaction between the bait AvrP-C8^{339} in Y187 and putative interactors in AH109 as described in section 4.2.3.3.

4.2.6.3 Sequencing and sequence analysis

DNA sequencing was performed using the same protocol as described in Chapter 2 section 2.2.7. For sequencing of putative interactors, direct sequencing of PCR products was performed using the following protocol. Firstly, the putative interactors inserts were analysed by colony PCR using the MATCHMAKER AD LD-insert screening amplimer set (section 4.2.6.2). Twenty ng of purified PCR product of the selected clones were sequenced using the 5' AD primer. The sequencing results were analysed using BLASTN and BLASTP searches of the NCBI nucleotide and protein sequence databases (https://blast.ncbi.nlm.nih.gov/Blast.cgi) and the flax genome database available at JGI

Phytozome 11 (https://phytozome.jgi.doe.gov/pz/portal.html#!info?alias=Org_Lusitatissimum).

4.3 Results

4.3.1 Determination of the bait used in the Y2H screen

4.3.1.1 Autoactivity and toxicity tests

In yeast two-hybrid analysis it is important to confirm that the bait:BD fusion protein does not activate the yeast expression system in the absence of a prey:AD fusion protein. Based on the autoactivity test conducted in this study, Y187 yeast carrying pGBT9-AvrP (BD-AvrP) produced more blue pigment compared to those carrying the pGBT9-AvrP-C8^{339} (BD-AvrP-C8^{339}) after growth on SD/-Trp selection media plus X-α-Gal (SD-T/X, Figure 4.1A), suggesting that the BD-AvrP was more autoactive compared to BD-AvrP-C8^{339}. The BD-AvrP-C8^{339} was then tested for stringency on selection media. Y187 yeast cells only carrying the *LacZ* and *MEL1* reporter genes whereas AH109 yeast cells carry all four reporter genes (*HIS3, ADE2*, *LacZ* and *MEL1*). The *MEL1* reporter will produce blue color X-α-Gal (5-bromo-4-chloro-3-indolyl α-D-galactopyranoside) is added to the growth medium. Hence, to confirm the stringency of the selection media, Y187 cells carrying the BD-AvrP-C8^{339} construct were mated with AH109 cells carrying Empty-AD construct and plated on the SD/-Trp/-Leu (SD-TL) which selected for both plasmids, and on the SD/-His/-Trp/-Leu/X-α-Gal (SD-HTL/X) and SD/-Ade/-His/-Trp/-Leu/X-α-Gal (SD-AHTL/X) plates for more stringent selection (Figure 4.1B).

When grown on the SD-HTL/X plates, BD-AvrP-C8^{339}+ Empty-AD produced blue color (Figure 4.1B), suggesting that the selection was not stringent enough and that the BD construct was still able to activate the GAL4 transcription system. However, when grown on more stringent media (SD – AHTL/X, Figure 4.1B), BD-AvrP-C8^{339}+ Empty-AD could not grow and activate the GAL4 transcription system. Based on this this result, BD-AvrP-C8^{339} could still be used as a bait for screening of the rust-infected flax cDNA library.

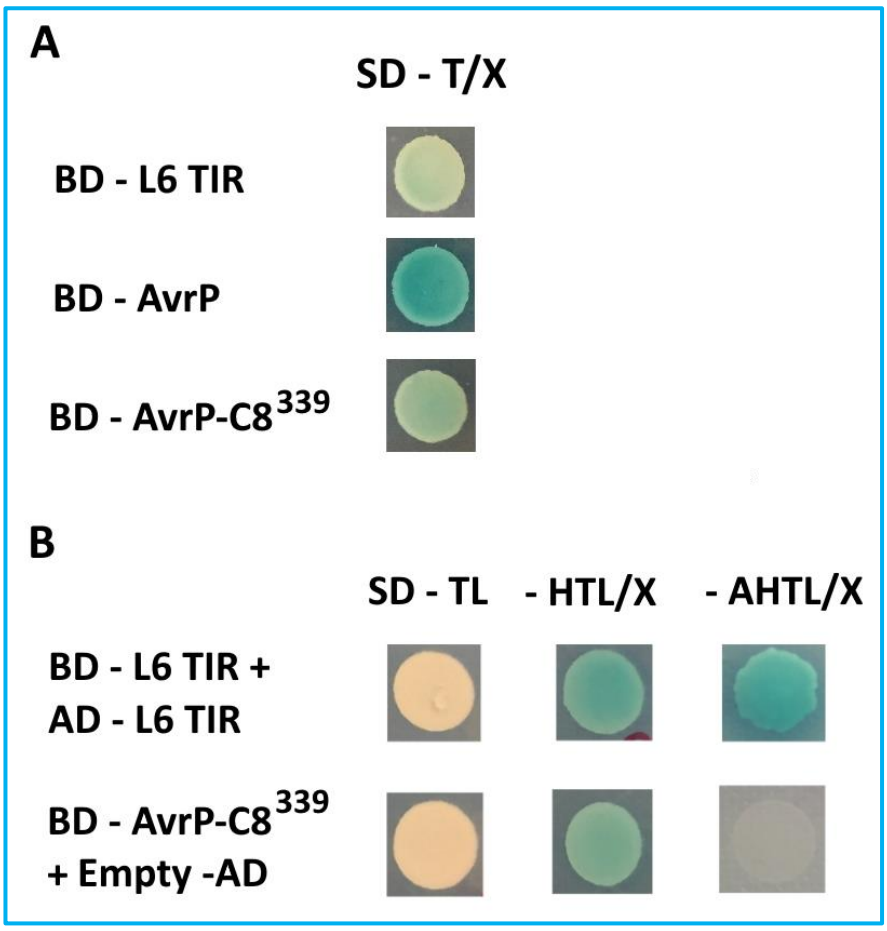

Figure 4.1 Autoactivity of the bait candidates (BD-AvrP and BD-AvrP-C8^{339}). A) Yeast expressing AvrP and AvrP-C8^{339} BD fusion proteins were tested on SD/-Trp selection media plus X-α-Gal (SD-T/X). BD-L6 TIR was used as a control. The blue color indicates autoactivation of BD-AvrP and BD- AvrP-C8^{339} as they activated the GAL4 transcription system without the presence of an AD construct. B) BD-AvrP-C8^{339} was tested for more stringent selection on SD/-Trp/-Leu (SD-TL), Triple Dropout SD/-His/-Trp/-Leu/X-α-Gal (SD-HTL/X) and Quadruple Dropout SD/-Ade/-His/-Trp/-Leu/X-α-Gal (SD-AHTL/X). The SD-TL media selected both BD- and AD- plasmids (pGBT9 and pGADT7, respectively). Yeast growth and the blue color on Dropout media indicate activation of the GAL4 transcription system. The experiment was conducted two times.

4.3.2 Construction of a cDNA library from rust-infected flax

Total RNA was isolated from rust-infected flax leaves 6 days after infection and analysed by gel electrophoresis (Figure 4.2). The RNA was found to contain distinct 5S, 18S and 28S rRNA subunits, suggesting the RNA to be intact and not degraded.

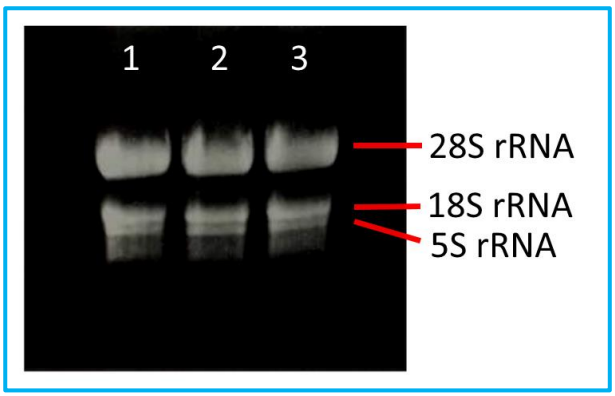

Figure 4.2 Gel electrophoresis of total RNA extracted from rust-infected flax. An ethidium-bromide-stained agarose gel showing the distinctive ribosomal RNA subunits (28S, 18S and 5S). Three RNA samples were analysed and labelled as indicated.

mRNA was isolated as described in section 4.2.5.2 and a total of 3.15 µg of mRNA was eluted in 250 µL of RNAse-free water. The mRNA was then precipitated and resuspended in 6 µL of RNAse-free water with a final concentration of 0.43 µg/µL Two first strand synthesis reactions were performed as described in section 4.2.5.3 using 0.5 µg and 1.0 µg of mRNA, followed by LD-PCR, to produce the cDNA.

The cDNA was then analysed by gel electrophoresis to determine whether it had a good size range of cDNA greater than 200 bp. Both samples were found to contained cDNAs ranging mostly from 400–2,500 bp (Figure 4.3). LD-PCR amplification was then conducted up to four more times for each first strand. The cDNA was then combined and purified using the purification kit from Zymo Research (section 4.2.5.3). A total of 4.16 µg of purified cDNA was recovered in 50 µL. The combined cDNA was then used to make a cDNA library that was estimated as described in section 4.2.5.3 to have at least 2.2 million cDNA clones.

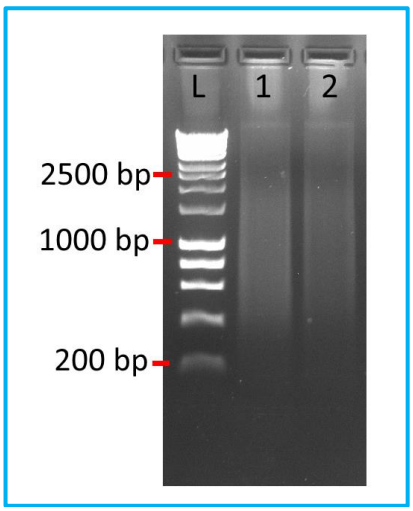

Figure 4.3 Gel electrophoresis of cDNA obtained from rust-infected flax. Two lanes of cDNA obtained after LD-PCR amplification of first strand cDNA synthesised from 0.5 µg (lane 1) and 1.0 µg (lane 2) mRNA. HyperladderTM 1 kb (Bioline, Toronto, Canada) was used as a size marker. Some of the sizes are marked for reference.

4.3.3 Y2H screen of the rust-infected flax cDNA library using AvrP-C8^{339} as bait

In order to identify AvrP-C8^{339} protein interactors, the cDNA library was screened with the pGBT9-AvrPC8^{339} bait construct as described in section 4.2.6.1. The library titration produced 400 colonies after two days plating of the 10^{-4} dilution on the SD/-Leu plate, suggesting that 2 x 10^7 cells/mL of cDNA library were screened. Similarly, the numbers of colonies on SD/-Trp and SD/-Leu/-Trp suggested that the library had been screened with 9.12 x 10^7 cells/mL of bait and 1.28 x 10^7 diploid cells containing both bait and prey plasmids had been recovered indicating a mating efficiency of 64%.

The blue colonies produced on the QDO + X-α-Gal plates were then analysed by direct PCR sequencing. Firstly, they were screened by yeast colony PCR using the MATCHMAKER AD LD-insert screening amplimer set (section 4.2.6.2). Amplification products were generated from 101 blue colonies but unfortunately 15 samples dried out during PCR and could not be analysed further. Of the remaining 86 samples analysed by agarose gel electrophoresis (Figure 4.4), 50 that generated a single PCR product ≥ 600 bp were analysed further by sequencing using the 5' AD primer.

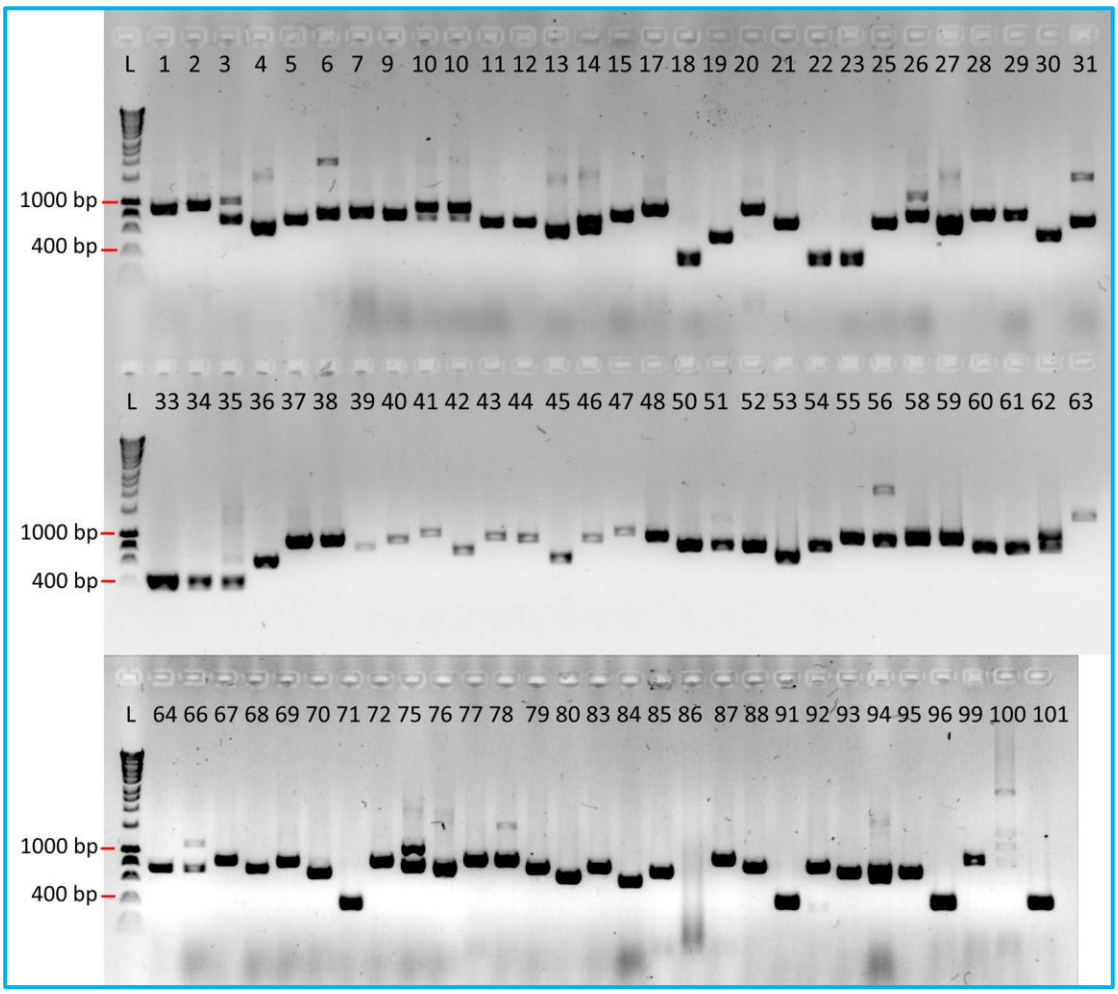

Figure 4.4 Gel electrophoresis of PCR products from a yeast colony PCR screen of 87 putative interactors from one Y2H screen of rust infected flax cDNA library. Colonies generating PCR products < 600 bp or multiple products were excluded from further analysis. Hyperladder^{TM} 1 kb (Bioline) was used as a size reference.

4.3.4 Sequence analysis

After checking that the colony PCR products contained coding sequence in frame with the activation domain, the inserted cDNA sequences were trimmed to remove upstream vector and activation domain sequences and non-coding sequences downstream of the stop codon. Analysis of the remaining coding sequences revealed five candidate AvrP-C8^{339}-interactors (Table 4.1) that were recovered two or more times. Based on BLASTN and BLASTP searches of the NCBI sequence database, two matched DEAD-box ATP-Dependent RNA helicase 56, five matched a cytosolic phosphoglucomutase (PGM), three matched a second cytosolic PGM, 11 matched a chloroplast PGM, and four matched peptidyl-prolyl cis-trans isomerase FKBP12 (Tables 4.1 and 4.2). These sequences also matched protein sequences with similar annotations in the JGI

Phytozome flax (*Linum usitatissimum*) protein sequence database with 99–100% identity (Table 4.3). Fourteen candidates matched a small, secreted, cysteine-rich protein of unknown function from poplar rust *Melampsora larici-populina* (Table 4.1). This sequence also matched a protein in the JGI Mycocosm flax rust (*Melampsora lini*) protein sequence database (https://genome.jgi.doe.gov/Melli1/Melli1.home.html) with 95.9% identity.

All sequences within each group had the same 5' junction with the activation domain, indicating that none of the duplicates were independent clones. Three flax sequences were recovered only once. One encoded a chloroplast or mitochondrial dnaJ chaperone and two encoded short peptides of 27 and 28 aa, respectively, with no high protein-sequence matches. All three are likely false positives. The remaining colony PCR products gave poor sequencing results and were not pursued further.

Table 4.1 Best annotated BLASTN matches in the NCBI nucleotide sequence database to 3' coding sequences (cds) encoding candidate AvrP-C8^{339} interactor proteins identified by Y2H analysis

Number of candidates	Size of cds (nt)	Top BLASTN hit	e-value	Putative function (organism)
14	367	XM_007414411.1	2e-108	Hypothetical protein (*Melampsora larici-populina*)
11	305	XM_012584776.1	7e-65	Phosphoglucomutase, chloroplastic (*Gossypium raimondii*)
5	400	XM_015724541.1	9e-103	Phosphoglucomutase, cytoplasmic (*Ricinus communis*)
4	217	XM_021788332.1	1e-53	Peptidyl-prolyl cis-trans isomerase FKBP12 (*Hevea brasiliensis*)
3	367	XM_023107093.1	4e-88	Phosphoglucomutase, cytoplasmic (*Cucurbita moschata*)
2	229	XM_018589904.1	4e-72	DEAD-box ATP-dependent RNA helicase 56 (*Raphanus sativus*)

Table 4.2 Best annotated BLASTP matches in the NCBI protein database to C-terminal fragments of candidate AvrP-C8^{339}-interacting host proteins expressed in the Y2H analysis.

Abbreviated name	Size of protein frag. (aa)	Top BLASTP hit	e-value	Putative function (organism)
SIAP	122	XP_007414473.1	4e-67	Hypothetical protein (*Melampsora larici-populina*)
pPGM	101	PHU22909.1	1e-59	Phosphoglucomutase, chloroplastic (*Capsicum chinense*)
cPGM1	133	XP_008389983.1	1e-73	Phosphoglucomutase, cytoplasmic (*Malus domestica*)
PPCTI FKBP12	72	XP_021829057.1	7e-41	Peptidyl-prolyl cis-trans isomerase FKBP12 (*Prunus avium*)
cPGM2	122	KZV51025.1	4e-70	Phosphoglucomutase, cytoplasmic (*Dorcoceras hygrometricum*)
DRH56	76	XP_002535684.2	9e-50	DEAD-box ATP-dependent RNA helicase 56 (*Ricinus communis*)

Table 4.3 Best BLASTP matches in the Phytozome *Linum usitatissimum* protein database to C-terminal fragments of candidate AvrP-C8^{339}-interacting host proteins expressed in the Y2H analysis

Abbreviated name	Size of protein frag. (aa)	Top BLASTP hit	e-value	Annotation
pPGM	101	Lus10031669	3e-62	Phosphoglucomutase (glucose-cofactor)
cPGM1	133	Lus10003712	5e-86	Phosphoglucomutase
PPCTI FKBP12	72	Lus10016586	1e-45	Peptidyl-prolyl cis-trans isomerase FKBP12
cPGM2	122	Lus10001596	5e-79	Phosphoglucomutase
DRH56	76	Lus10014260* Lus10002021*	5e-45 9e-45	ATP-dependent RNA helicase UAP56/SUB2

* both show 100% amino-acid sequence identity in the region matching the interactor sequence

4.4 Discussion

Four candidates for AvrP-interacting proteins have been identified; one candidate matching a fungal protein that has the hallmarks of an effector protein and three candidates matching host proteins. These candidates may provide important clues to the function of AvrP inside host plant cells.

4.4.1 Fungal protein interactor

The full-length *M. lini* sequence showing the best BLASTP match to the fungal protein interacting with AvrP in the Y2H analysis has been designated SIAP (Secreted Interactor of AvrP; Table 4.2). The interacting protein differs from SIAP by 5 amino acid residues clustered together within otherwise identical protein sequences (Figure 4.5), corresponding to 5 nucleotide differences in otherwise identical transcript sequences. This could reflect the existence of a paralogue with sequence polymorphisms, but the next nearest BLASTP match shows extensive polymorphism throughout the sequence compared to the interacting protein. The unusual distribution of sequence difference could instead reflect errors in the genomic sequence, given that the sequence of the Y2H interactor is quite unambiguous in this region. For the purposes of this discussion, the interacting sequence and SIAP are considered to be the same.

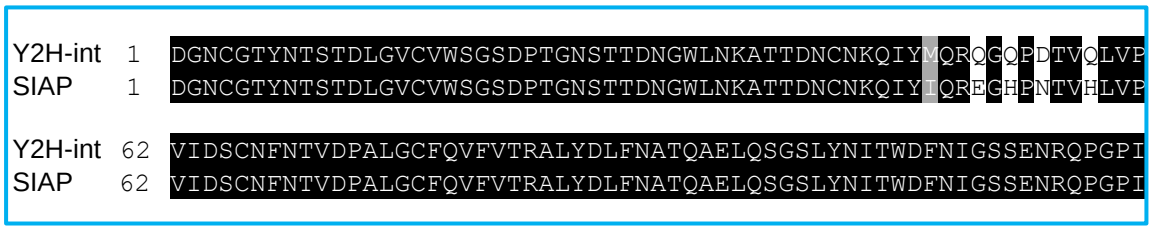

Figure 4.5 Alignment of predicted protein sequences for the AvrP interactor from flax rust detected in the Y2H analysis (Y2H-int) and the corresponding region of SIAP.

SIAP is a member of a multigene family with numerous homologues in *M. lini*, *M. larici-populina* and species of the genus *Puccinia* including wheat stem, stripe and leaf rust fungi. The best-matching *M. larici-populina* protein (XP_007414473.1), here designated *Mlp*SIAP, shows 78% identity and 85% similarity to SIAP (Figure 4.6). *SIAP* encodes a 225 amino-acid protein with eight cysteine residues and a predicted signal peptide of 22 amino acids (Figure 4.6), suggesting it is a small, secreted protein with four disulphide bonds. *MlpSIAP* encodes a 236 amino-acid protein with ten cysteine residues and a

predicted signal peptide of 22 amino acids (Figure 4.6), suggesting it is also a small, secreted protein with perhaps five disulphide bonds. With EffectorP (v2.0 beta http://effectorp.csiro.au/ (Sperschneider et al. 2016) probability scores of 0.769 and 0.847, respectively, SIAP and *Mlp*SIAP are predicted to be effector proteins translocated from fungal haustoria into the cytosol of host plant cells. Potentially, SIAP could be required for translocation of AvrP into flax cells, the activation of AvrP inside host cells or as a co-factor in AvrP effector function.

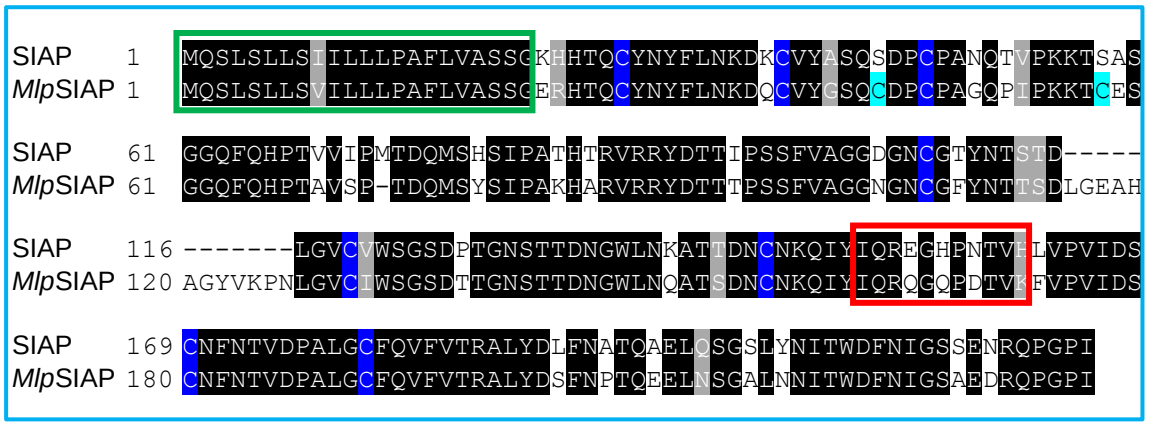

Figure 4.6 Alignment of predicted protein sequences for *M. lini* and *M. larici-populina* (*Mlp*) SIAPs. Predicted signal peptide sequences are boxed in green. Cysteine residues conserved between SIAP and *Mlp*SIAP are highlighted in dark blue. Additional cysteine residues in *Mlp*SIAP are highlighted in light blue. The region containing the sequence differences between SIAP and the interacting protein is boxed in red.

4.4.2 Phosphoglucomutase interactors

Phosphoglucomutase exists as both plastidial/chloroplastic (pPGM) and cytosolic (cPGM) isoforms. Both facilitate the interconversion of glucose-6-phosphate and glucose-1-phosphate. In the chloroplast, glucose 1-phosphate is a substrate for ADP-glucose pyrophosphorylase, which leads to starch synthesis. A lack of pPGM results in low levels of starch, and the amounts of soluble sugars, like glucose and sucrose, are higher in mutants lacking the ability to synthesize starch (Malinova et al. 2014). In the cytosol, however, glucose-1-phosphate is a substrate for UDP-glucose pyrophosphorylase, which leads to synthesis of UDP-glucose and ultimately sucrose as well as various cell wall components including β-glucans which are involved in plant defence (Morava 2014; Malinova et al. 2014). UDP-glucose pyrophosphorylase has also been shown to regulate plant cell death possibly via the accumulation of UDP-glucose

which may act as a damage-associated molecular pattern (reviewed by Janse van Rensburg and Van den Ende (2018)). Conversely, elicitor-induced plant cell death is reduced in a UDP-glucose pyrophosphorylase knockout possibly via reduced accumulation of UDP-glucose.

Rather than sucrose as suggested previously, it has been suggested from various studies that glucose is a likely candidate for nutrient uptake by biotrophic fungi (Mendgen and Nass 1988; Sutton et al. 1999; Aked and Hall 1993). It has been further proposed that enzymatic cleavage of sucrose into glucose and fructose is required for uptake into pathogen cells. In bean rust infections, the fungal invertase INV1p and plant enzymes cleave sucrose, and then the fungal hexose transporter HXT1p takes up the D-glucose and D-fructose (Voegele et al. 2006; Voegele and Mendgen 2011).

A multiple sequence alignment of the three interacting PGM fragments identified by Y2H analysis indicated a shared conserved C-terminal region of 92 amino acids, subdivided into two conserved regions of 57 amino acids and 28 amino acids (Figure 4.7). This domain includes a large portion of the C-terminal domain IV of PGM which contains residues involved in binding the phosphate of the phospho-glucose substrate (Figure 4.7).

Given that pPGM is located in the chloroplast and there is nothing to suggest that AvrP is targeted to the chloroplast (Zhang et al. 2018), it could be asked whether pPGM is a real target for AvrP. Chloroplast translocation is a post-translational process of cytosol to chloroplast transfer mediated by a N-terminal transit peptide sequence (Figure 4.8). The pPGM protein is therefore available in the cytosol for interaction with AvrP prior to protein translocation. Whether it would do so *in planta* is unknown.

Figure 4.7 Alignment of predicted protein sequences for the AvrP-interacting chloroplastic phosphoglucomutase (pPGM) and cytosolic phosphoglucomutase (cPGM1 and cPGM2) sequences detected in the Y2H analysis. Two regions of high sequence conservation between all three sequences are boxed in red. The region involved in phosphate binding is boxed in blue.

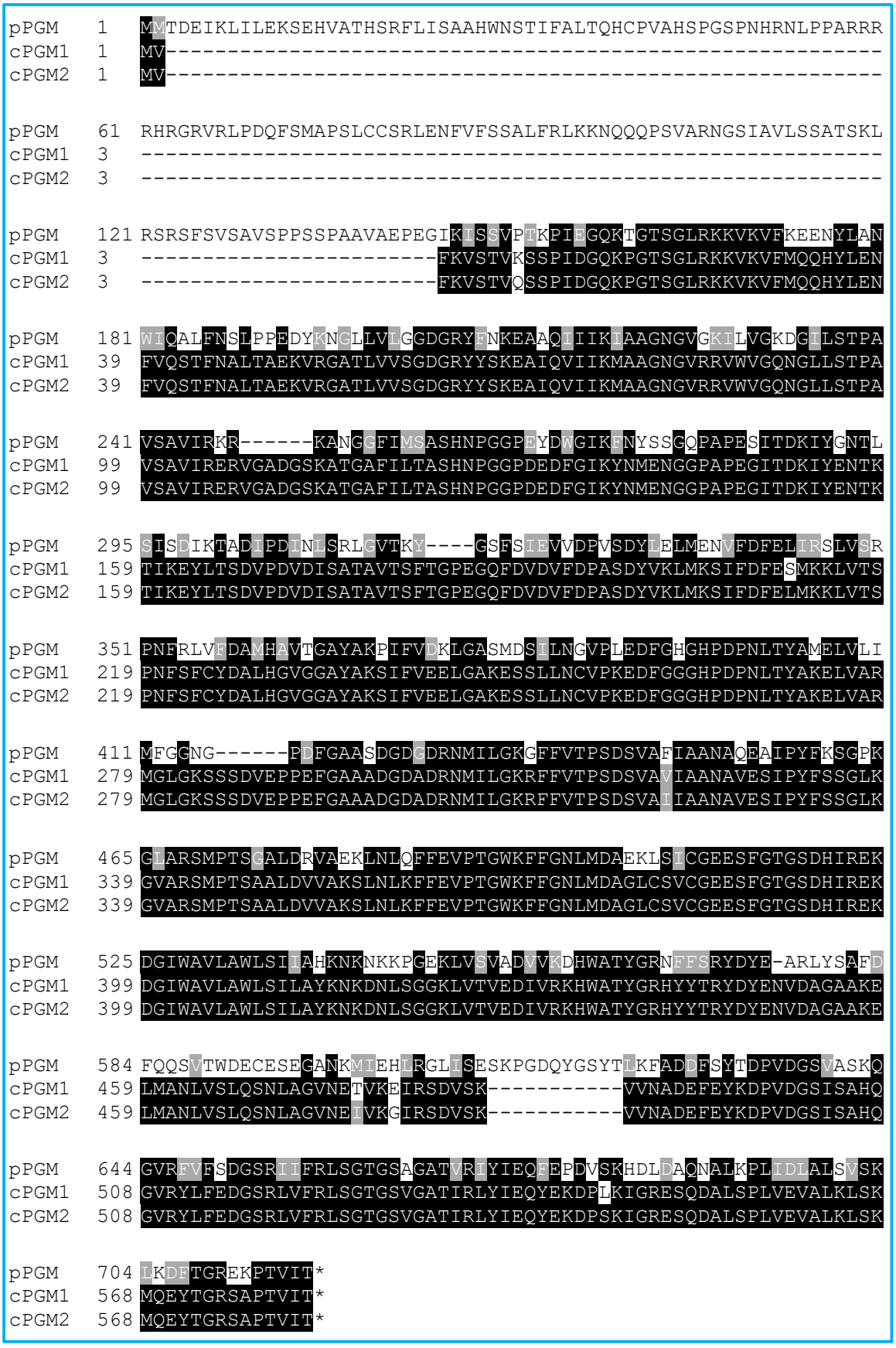

Figure 4.8 Alignment of predicted protein sequences for the full length chloroplastic (pPGM) and cystosolic (cPGM1 and cPGM2) phosphoglucomutases. The N-terminal extension of pPGM contains a chloroplast transit peptide sequence.

Potentially, the pathogen could use the interaction between AvrP and PGM to manipulate host metabolism to provide nutrients for the pathogen. In rice, metabolites, enzymatic activity (including PGM) and gene expression in the glycolysis pathway were increased after infection with the necrotrophic fungus *Rhizoctonia solani* (Mutuku and Nose 2012). It was also reported that the frequency of penetration and extent of hyphae formation of the hemibiotrophic fungus *Colletotrichum higginsianum* was greater in a starch-deficient *pgm* mutant of *Arabidopsis* than wild-type *Arabidopsis* (Engelsdorf et al. 2017). Whether AvrP could cause similar outcomes in the biotrophic interaction between flax and the flax rust fungus remains an open question requiring further investigation.

4.4.3 Peptidyl-prolyl cis-trans isomerase FKBP12 interactor

FKBPs (FK506-Binding Proteins), also known as peptidyl-prolyl isomerases (PPIases), are large protein families in most organisms, with the largest family found in higher plants. They catalyse rotation of peptide bonds immediately preceding proline residues between the *cis* and *trans* configurations. FKBPs are involved in several biochemical processes including protein folding, receptor signalling, protein trafficking and transcription (Gollan et al. 2012).

FKBP12 is the smallest isoform in plants (112 aa) and is localised to the cytosol, but its PPIase activity remains unknown (Gollan et al. 2012). However, human FKBP12 has been shown to have PPIase activity and plant FKBP12s share nine of the thirteen residues shown to be required for PPIase activity in human FKBP12 ((DeCenzo et al. 1996); Figure 4.9), so it is possible flax FKBP12 may be a functional PPIase. In *Arabidopsis*, FKBP12 interacts with AtFIP37, a protein suggested to be involved in mRNA splicing, affecting cell cycle regulation and embryo development (Faure et al. 1998; Vespa et al. 2004). In the conifer species *Picea wilsonii*, FKBP12 interacts with HAP5, a subunit of a histone-associated transcription factor, and plays a role in pollen tube development (Yu et al. 2011). *Vicia faba* FKBP12 shows a low-affinity interaction with bovine calcineurin that appears to be dependent on disulphide bond formation between two cysteine residues conserved among higher-plant FKBP12s ((Xu et al. 1998); Figure 4.9), raising the possibility of redox-sensitive regulation of FKBP12 via disulphide-bond formation and reduction. Interestingly, wheat FKBP12 is targeted by a lipase protein FGL15 from the

wheat scab fungus *Fusarium graminearum* and interacts with an elicitor-responsive protein ERG that contains a possible Ca^{++} binding domain and may play a role in plant defence (Niu et al. 2013).

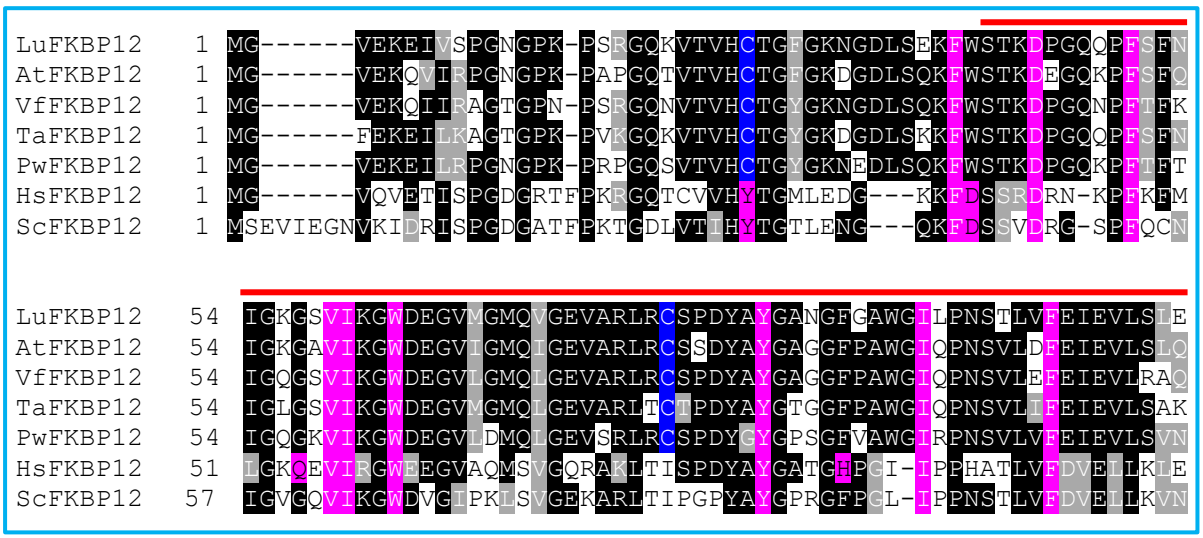

Figure 4.9 Alignment of predicted protein sequences for full-length FKBP12 proteins from flax (Lu) *Arabidopsis* (At), faba bean (Vf), wheat (Ta), Wilson's spruce (Pw) human (Hs) and yeast (Sc). Cysteine residues conserved among higher-plant FKBP12s are highlighted in blue. Nine residues conserved with the PPIase catalytic residues of human FKBP12 are shown in white text highlighted in pink and four residues that are not conserved are shown in black text highlighted in pink. The region of FKBP12 encoded by the interacting prey clone is overlined in red.

If flax FKBP12 has PPIase activity, it is possible that it could be required to activate AvrP *in planta* rather than being a target for AvrP effector function. AvrP has a proline in the cis conformation (Simon Williams, Australian National University, personal communication) that could make AvrP a substrate for the potential PPIase activity of flax FKBP12. Precedents for effector activation by PPIases are provided by the activation of *Pseudomonas syringae* AvrRpt2 and *Phytophthora sojae* Avr3b by plant cyclophilins (Coaker et al. 2005; Kong et al. 2015), which, although unrelated to FKBPs, also have PPIase activity. Whether PPIase activity would involve interaction detectable in a Y2H assay is unknown.

4.4.4 DEAD-box ATP-dependent RNA helicase 56 interactor

DEAD-box RNA helicases are members of a large protein family that plays a vital role in RNA metabolism such as pre-mRNA splicing, ribosome formation, the export of mRNA out of the nucleus and RNA degradation. Recent evidence also suggests that several DEAD box RNA helicases are crucial for regulating gene expression by acting as transcriptional co-activators (Sarkar and Ghosh 2016; Jarmoskaite and Russell 2014). Some DEAD-box proteins contribute to plant responses to various biotic and abiotic stresses (Li et al. 2008a; Xu et al. 2015). In *Arabidopsis*, UAP56, the equivalent to DRH56 (flax DEAD box RNA helicase 56; Table 4.3), forms part of the TREX (Transcription and Export) complex, which functions in RNA splicing and export, and plays a role in plant defence (Pan et al. 2012; Xu et al. 2015). DRH56 proteins are present in animals and fungi and the interacting fragment of flax DRH56 contains part of the conserved C-terminal helicase domain and includes all four of the ATP-binding site residues in this domain (Figure 4.10).

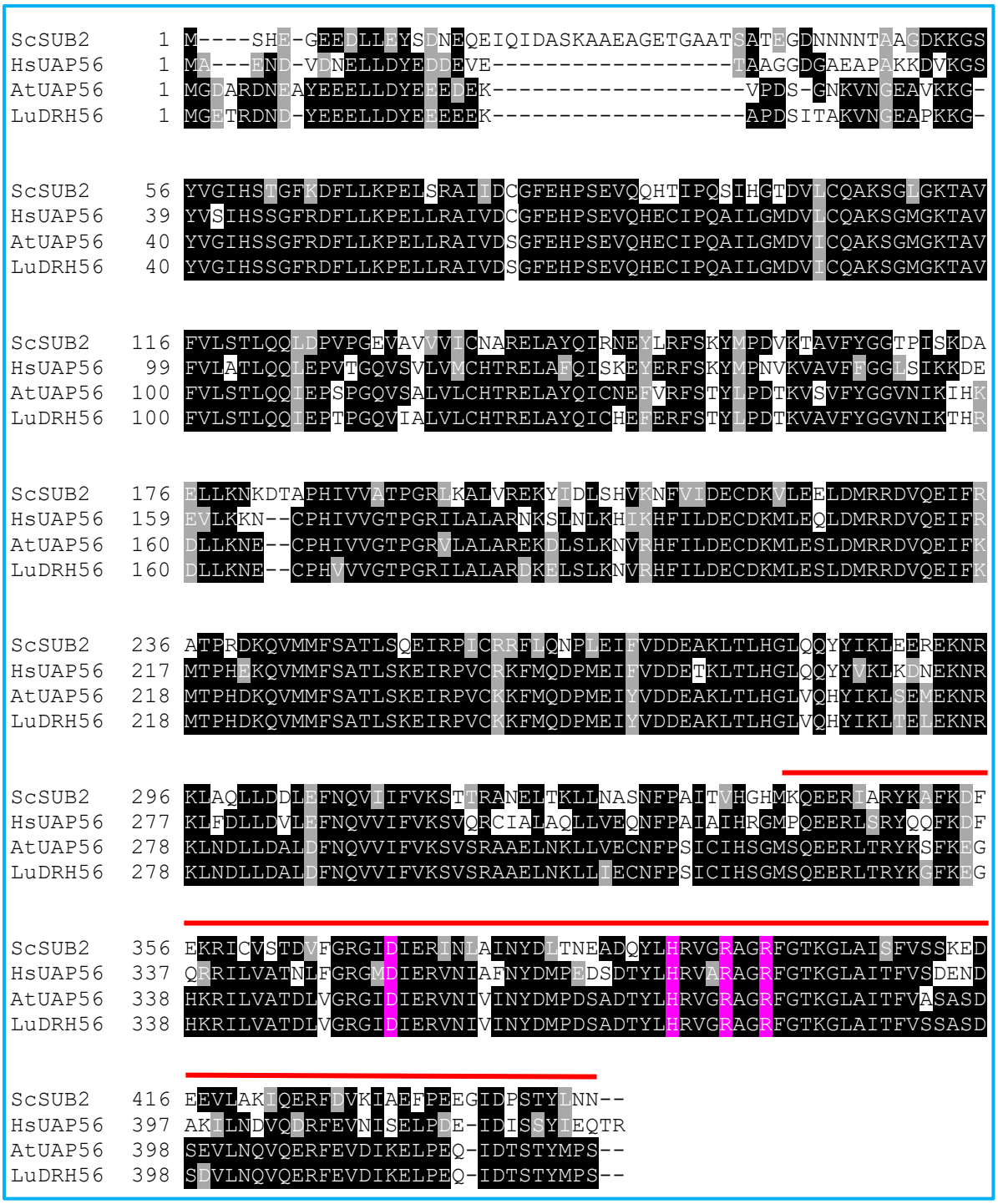

Figure 4.10 Alignment of predicted protein sequences for full-length DRH56 proteins from flax (Lu), *Arabidopsis* (At), yeast (Sc) and human (Hs). Four conserved residues involved in ATP binding are highlighted in pink. The region of DRH56 encoded by the interacting prey clone is overlined in red.

Interestingly, *Arabidopsis* UAP56 is localised to the nucleus, but largely excluded from the nucleolus (Figure 4.11) (Kammel et al. 2013). This is similar to the preferential localisation of AvrP and AvrP123 to the nucleus, but not the nucleolus, when expressed *in planta* (Figure 4.11) (Zhang et al. 2018). Interaction with flax DRH56 could potentially explain the localisation of AvrP, which has no known nuclear localisation signal of its own.

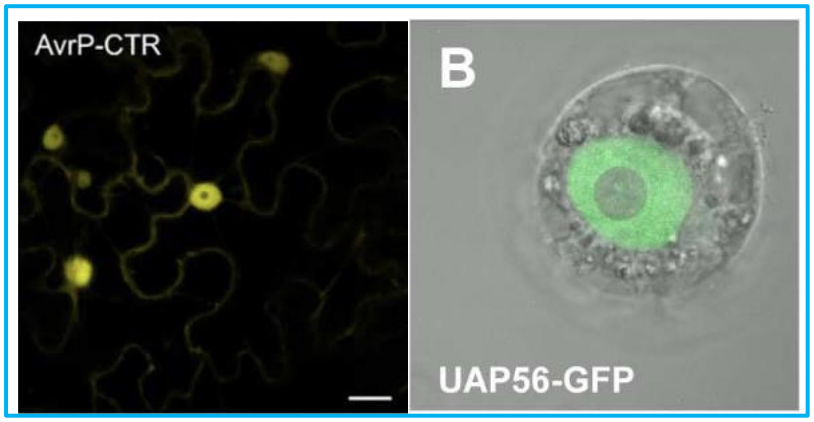

Figure 4.11 Localisation of AvrP-citrine in *N. benthamiana* epidermal cells (left panel) and AtUAP56-GFP in tobacco protoplasts (right panel). In both cases fluorescence is localised preferentially to the nucleus and largely excluded from the nucleolus. Images taken from Zhang et al. (2018) and Kammel et al. (2013).

4.4.5 Future work

In this study, AvrP-C8^{339} was used as bait to identify AvrP interactors. Several putative interactor proteins have been identified. However, these interactions need further confirmation. Firstly, full-length proteins need to be tested in Y2H assays to confirm their interaction with AvrP. This can be achieved by amplifying and cloning the corresponding full-length coding sequences from flax cDNA. Co-immunoprecipitation (co-IP) and/or Bimolecular Fluorescence Complementation (BiFC) (Bracha-Drori et al. 2004) should be used to provide independent confirmation of the interaction with AvrP. Co-IP and BiFC assays have been used extensively to confirm protein-protein interaction in plant-pathogen interactions (Berggard et al. 2007; Yue et al. 2016; Lyu et al. 2016). These experiments could also be used to test for interaction with AvrP123.

Once an interactor has been confirmed (or multiple interactors), experiments can be conducted to test the effect of AvrP on the interactor. Ideally, the interactor protein would be expressed in *E. coli* or insect cells using a baculovirus vector or another expression system, and purified for functional analysis. Functional assays could then be

developed for each of the interactors. Flax DRH56 could be tested for nucleic-acid-binding, ATPase and helicase activities as described by Kammel et al. (2013). The PGMs could be tested for enzymatic activity using a spectrophotometric assay to measure enzymatically coupled conversion of NAD+ to NADPH as described by Hattenbach and Heineke (1999). FKBP12 could be tested for proline isomerase activity using an assay based on the ability of chymotrypsin to cleave an Ala-Ala-Pro-Phe reporter substrate when the proline is in the trans conformation but not when it is in the cis conformation, as described by Fischer et al. (1984). Once these assays have been developed, the effect of AvrP could then be tested by assaying interactor protein function in the presence or absence of recombinant AvrP protein.

Chapter 5
General Discussion

5.1 AvrP and AvrP123 have different recognition sites

This study has shown that different residues in the flax rust AvrP/AvrP123 effectors and their variants are required for recognition by the flax P, P1, P2 and P3 resistance specificities. Key residues for AvrP recognition by the P resistance protein include D66, Q94 and E108 (chapter 2). D66 and Q94 are on the surface of AvrP near the C-terminal end of the structure whereas E108 is located in a region of the protein whose structure could not be determined (Figure 5.1). Residues E30 and L57 were also shown to contribute to AvrP recognition (chapter 2) and the side chain of L57, although buried in the hydrophobic core of the protein, is very close to the peptide backbone of D66 and may influence its structural conformation on the surface of the protein.

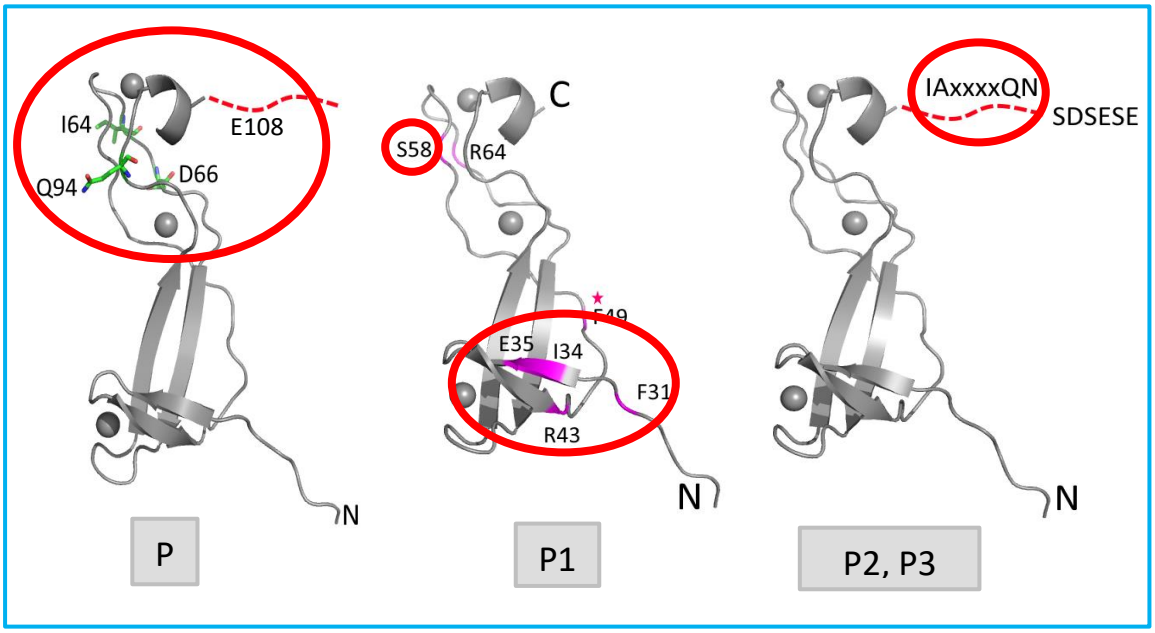

Figure 5.1 Structural representations of AvrP showing regions and residues within those regions important for recognition of AvrP by the P resistance protein and AvrP123 by the P1, P2 and P3 resistance proteins.

Interestingly, D66, Q94 and E108 are shared with the WA allele which is recognised by P2 and P3 but not by P or P1 (Figure 5.2). The WA allele lacks E30 and L57, instead having G30 and P57. Glycine and proline residues are associated with β turns and could potentially have a major impact on protein structure, including perhaps the surface

conformation of D66. In contrast, the 339 allele, which is recognised by P, P2 and P3 but not P1, has D66 but lacks Q94 and E108, instead having R94 and Q108 (Figure 5.2), suggesting that Q94 and E108 may not be critical for AvrP recognition per se if another pair of residues can serve the same complementary function. Interestingly, the 339 allele shares E30 and L57 with AvrP (Figure 5.2), consistent with the possibility that L57 affects the surface conformation of D66 allowing recognition by P.

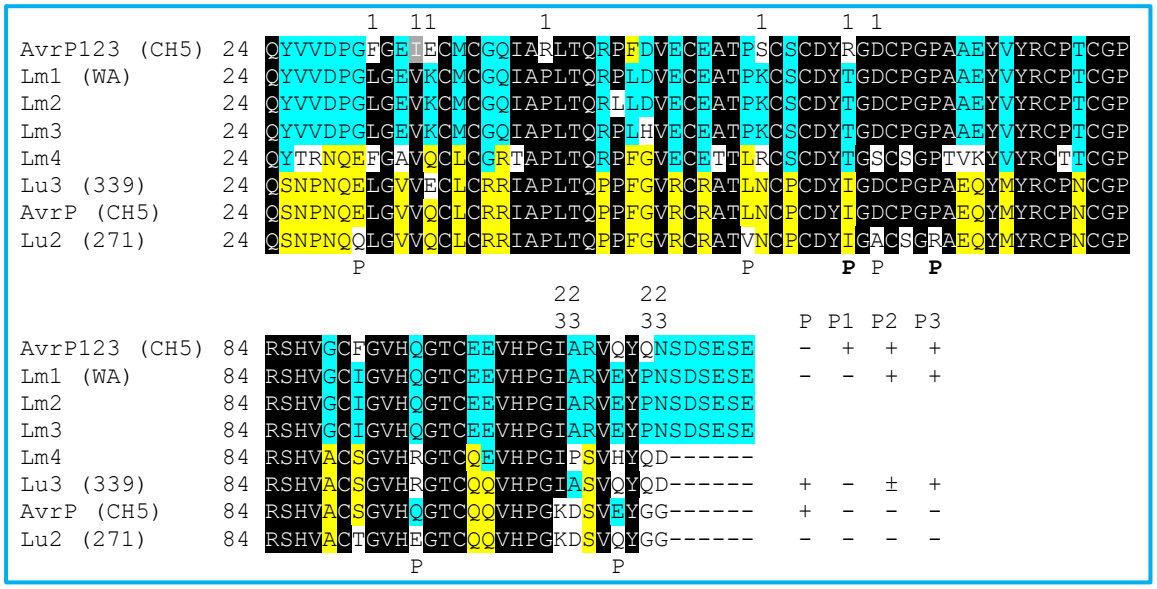

Figure 5.2 Sequence alignment of mature AvrP/AvrP123 proteins and their variants. Sequences are from Barrett et al. (2009). Lu sequences were obtained from *Melampsora lini* isolates found on cultivated flax (*Linum usitatissimum*) whereas Lm sequence were obtained from *M. lini* isolates found on native Australian flax (*L. marginale*). Names of *M. lini* isolates from which these sequences were isolated are shown in parentheses. Residues characteristic of the AvrP or AvrP123 subgroups are highlighted in yellow or blue, respectively. Residues conserved across both subgroups are highlighted in black. The CH5 allele of AvrP123 is identical to the Lu4 and Lm5 alleles and the CH5 allele of AvrP is identical to the Lu1 allele (Barrett et al. 2009). Necrosis scores following Agrobacterium-mediated expression of these variants on flax varieties carrying P, P1, P2 and P3 are shown to the right of the alignment. The letter P below the alignment indicates the position of residues in AvrP important for recognition by the P resistance protein (bold letters indicating residues identified by Zhang et al. (2018)). The numerals 1, 2 or 3 above the alignment indicate the positions of residues in AvrP123 important for recognition by the P1, P2 and P3 resistance proteins, respectively.

The D66A, S90T, Q94E and E108Q mutants produced in this study were also included in the study by Zhang et al. (2018) along with some additional mutants of residues shown by structural analysis to be exposed on the surface of AvrP. Two mutations, P68S and P70R, involved replacing AvrP residues with residues from the 271 allele of AvrP, and the rest involved replacing AvrP residues with residues from AvrP123. Of these additional mutants, G50D, R52E and E72A had little effect on necrosis induced in P tobacco, but I64R abolished necrosis, P70R reduced necrosis significantly, and P68S reduced necrosis slightly, suggesting that I64, P70 and perhaps P68 are also involved in AvrP recognition by P (Figure 5.2). Surprisingly, although the D66A, Q94E and E108Q mutants gave essentially the same results when retested for the Zhang et al. (2018) study, the S90T mutation seemed to abolish or weaken necrosis more severely than in the current study. Overall, six of the residues that appear to be important for AvrP recognition cluster near the C terminal end of the protein structure i.e. I64, D66, P68, P70, S90 and Q94 (Figures 5.1 and 5.2).

The P1 resistance protein recognises six polymorphic residues near the N-terminus which are unique (F31, I34, R43, and S58) or almost unique (E35 and R64) to AvrP123 (chapter 3). Four of these positions cluster near the N-terminal end of the structure determined for AvrP i.e. F31, I34, E35 and R43 (Figures 5.1 and 5.2), highlighting the importance of this part of the AvrP123 protein in recognition by P1. Of these residues, I34 is a buried bulky branched-hydrophobic residue whose side chain is located very close to the peptide backbone of R43 and is polymorphic with the smaller branched-hydrophobic residue valine in other members of the AvrP/AvrP123 family. Like L57, discussed above in relation to recognition of AvrP, changes at position 34 could potentially affect the surface conformation of the residue at position 43 or the flanking residue at position 35 to alter recognition by P1. Interestingly, a mutation of residue D66 that abolished recognition of AvrP by the P resistance protein also affected recognition of AvrP123 by the P1 resistance protein, suggesting that this residue is also crucial for recognition of AvrP123 by P1.

The P2 and P3 resistance proteins, however, recognise eight residues (IARVQYQN; residues 104-111) designated C8 near the C-terminus of AvrP123 (chapter 3). The residues at positions 1, 2, 7 and 8 (I, A, Q/P and D/N) of C8 appear to play a role in the

specificity of recognition by P2 and P3 (Figures 5.1 and 5.2). Unfortunately, these residues lie in a region of the protein for which no structural information is available and it therefore is not possible to understand how this region interacts with the remainder of the protein, if at all. It is likely that other residues outside of this region also play a role in AvrP123 recognition by P2 and P3 given that AvrP123 and AvrP-bs25 have identical C8 residues but are recognised differentially by P3 (Figure 5.2). However, rather than a difference in recognition specificity, it is possible that P3 is a poorer responder to activation than P2 and that AvrP-bs25 is a poorer inducer of activation than AvrP123.

Overall, recognition of AvrP/AvrP123 family members seems to be determined by different regions of the AvrP/AvrP123 protein structure, with P1 recognising residues near the N-terminal end of the structure, P near the C terminal end of the structure and P2 and P3 the very C-terminal sequences not represented in the structure (Figure 5.1), but with some overlap as shown in Figure 5.2. Given these differences in recognition, the question arises whether these sequence differences also reflect differences in effector function. The AvrP/AvrP123 protein family in *Melampsora lini* falls into two broad subgroups, AvrP-like and AvrP123-like (Figure 5.2), apart from the AvrP-Lm4 variant which possesses features of both groups and has not been tested for recognition by P, P1, P2 and P3 (Figure 5.2). Nevertheless, both groups share significant regions of sequence conservation (Figure 5.2) including surface exposed residues that could potentially be involved in a conserved effector function. It will therefore be important in future experiments to test whether AvrP123 also interacts with the putative AvrP interactors identified by yeast two hybrid analysis (chapter 4).

5.2 Role and function of PHD fingers in plants

Ten cysteines and two histidines of mature AvrP bind to three zinc atoms and this binding is crucial for structural integrity of the protein and for recognition of AvrP by the P resistance protein (chapter 2). The twelve zinc-binding residues of AvrP are conserved in AvrP123 and in the distantly-related Lm6 allele (described by Barrett et al., 2009) identified in the genome of *M. lini* (possibly present as a consequence of interspecific hybridisation) isolated from montane populations of *Linum marginale* (Figure 5.3). Similarly, these zinc-binding residues are conserved in MELLADRAFT_124530 a

predicted secreted protein of similar length from *Melampsora larici-populina* (Hacquard et al., 2012; Figure 5.3). However, the lack of conservation between Lm6 and MELLADRAFT_124530 and between these two proteins and the AvrP/AvrP123 protein family in *M. lini* suggests that whilst they may share the same structural platform they are likely to perform different functions and/or target different host proteins. This observation tends to support the idea that the conservation observed between AvrP and AvrP123 could indicate that they carry out identical or very similar effector functions and the differences between these two subgroups have evolved to avoid recognition by specific resistance proteins encoded by genes at the *P* locus.

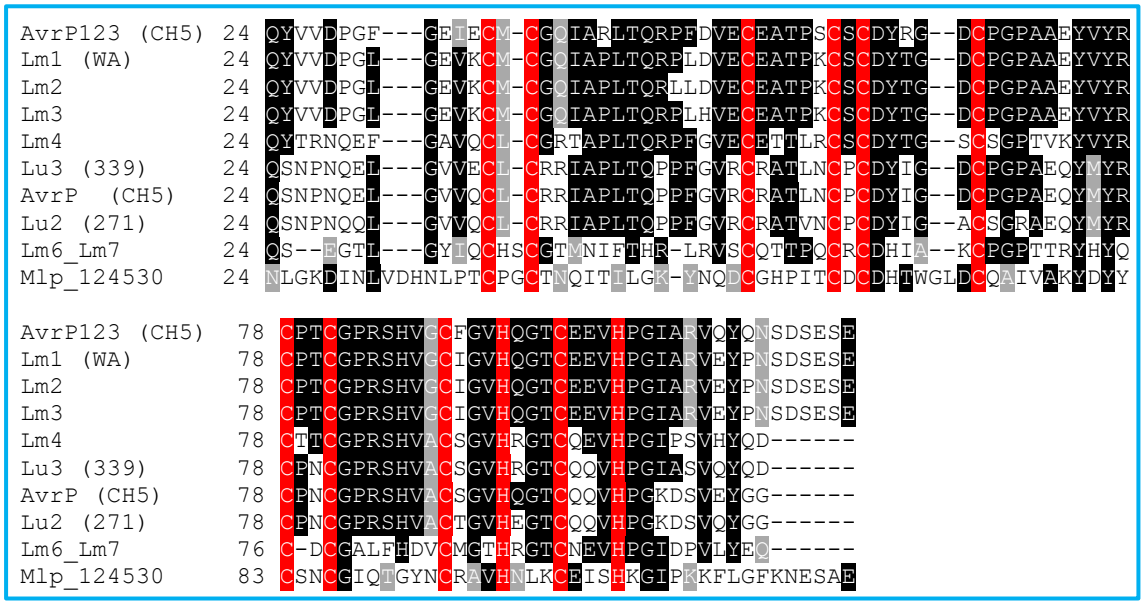

Figure 5.3 Sequence alignment of mature AvrP/AvrP123 proteins and their variants highlighting conserved cysteine and histidine residues involved in zinc binding. Conserved cysteine and histidine residues involved in zinc binding are highlighted in red. Lm6 and Lm7 are identical variants encoded by the B genome of *Melampsora lini* found on montane populations of native Australian flax (*Linum marginale*). Mlp_124530 corresponds to a predicted *Melampsora larici-populina* protein MELLADRAFT_124530 (GenBank Accession EGF98903.1) (Hacquard et al. 2012). Other sequence names are explained in the caption to Figure 5.1.

The Zn1 and Zn2 zinc-binding domains of AvrP are similar to the Plant Homeodomain (PHD) finger (Zhang et al. 2018). In eukaryotes, the PHD finger is a well-conserved protein domain. It was first discovered by Schindler et al. (1993) in the plant

homeodomain proteins HAT3.1 of *A. thaliana* and maize ZmHox1a, and has a characteristic signature of C4HC3 (four cysteines; one histidine, three cysteines) that resembles the RING (really interesting new gene) finger (C3HC4) and FYVE (domain shared by Fab1, YOTB, Vac1 and EEA1 proteins) domains. They also discovered that HAT3.1 was able to interact with any DNA fragment larger than 100 bp and that the N-terminal region of the protein was important for DNA binding purposes. PHD fingers have also been found in nuclear proteins that interact with chromatin (specifically histones) rather than binding directly to DNA (Aasland et al. 1995; Eberharter et al. 2004; Ragvin et al. 2004), leading to chromatin-mediated transcriptional regulation. PHD fingers have been shown to interact with N-terminal tails of H3 histones, either when the lysine 4 side chain was di- or trimethylated (H3K4me2/3) (Pena et al. 2006; Taverna et al. 2006; Cantu et al. 2013; Chung et al. 2016) or in the unmethylated state (H3K4me0) (Chignola et al. 2009; Lan et al. 2007; Saksouk et al. 2009). Other PHD fingers have been reported to interact with trimethylated lysines in H3K9me3 and H3K36me3 (Iwase et al. 2007; Karagianni et al. 2008; Li et al. 2008b).

Spanning approximately 50–80 amino acids in size and binding two zinc ions, PHD fingers are considered to be relatively small protein domains (Bienz 2006). Using X-ray crystallography or NMR spectroscopy, the structures of more that 30 PHD fingers have been determined either alone or in complex with different histone 3 peptides. Currently, 89 proteins have been identified in humans that contain at least one PHD finger, 44 in *Drosophila melanogaster*, 37 in *Caenorhabditis elegans*, 171 in *A. thaliana* and 16 in *Saccharomyces cerevisiae* according to the SMART database (http://smart.embl-heidelberg.de) (Lallous and Ramón-Maiques 2011).

If AvrP is mimicking the role of a plant PHD protein via interaction with histone 3 then it might be expected that the yeast two hybrid analysis described in chapter 4 should have identified interacting flax histone 3 clones. There are at least two reasons why a flax histone 3 clone may not have been identified. Firstly, the prey library was made using oligo dT priming which favours representation of the 3' end of transcripts and consequently the C-terminal ends of the proteins they encode, as was the case for the interactors that were identified in this study. Given that many PHD finger proteins interact with the N-terminal tails of histone 3 it is possible that clones encoding the N-

terminal region of flax histone 3 were not recovered because they were represented poorly or not at all in the prey library. Secondly, the prey library may not have been sufficiently large or sampled to sufficient depth to detect other interactors. Although 42 prey clones were sequenced only six independent putative interactor clones were identified. Most of the clones sequenced were duplicates arising from the PCR amplification step included during preparation of the cDNA library, suggesting that the library may have been 6-7-fold smaller than originally thought. These two potential problems could perhaps be overcome by making and screening a much larger prey library from random-primed-cDNA.

5.3 AvrP and AvrP123 potentially have multiple targets

Four categories of effector targets have been defined based on how they are affected by effectors and/or their role in pathogenicity (Khan et al. 2018): 1) targets that are altered by effectors to aid pathogen virulence, such as the rice RING E3 ubiquitin ligase APIP6, which is targeted by the fungal effector AvrPiz-t to suppress the PTI response and increase susceptibility of rice plants to *Magnaporthe oryzae* (Park et al. 2012); 2) targets that are required for effector function such as cofactors, for example the plant cyclophilin that activates the protease activity of *Pseudomonas syringae* AvrRpt2 (Coaker et al. 2005); 3) targets that act as "sensors" associated with NLR proteins and enabling them to trigger ETI, such as the RIN4 protein from *Arabidopsis*, which is "guarded" by NLR proteins RPM1 and RPS2 (Mackey et al. 2003); and 4) targets that do not affect pathogen fitness even after modification by effectors.

Based on the Y2H experiment discussed in Chapter 4, AvrP has six potential targets of four different kinds: SIAP from the fungus itself, the DEAD/DEAH box RNA helicase DRH56, one chloroplast and two cytoplasmic phosphoglucomutases (pPGM/cPGM), and the peptidyl-prolyl cis-trans isomerase FKBP12 (Figure 5.4). Although these findings are valuable, they still need validation by complementary approaches. SIAP and FKBP12 could fall into the second category described above, whereas the roles of pPGM/cPGM and DRH56, although likely to fall into the first category, still need further investigation and are yet to be determined. The question s whether any or all of these interactors are

real targets for AvrP. Is it possible for a single effector to have multiple unrelated targets?

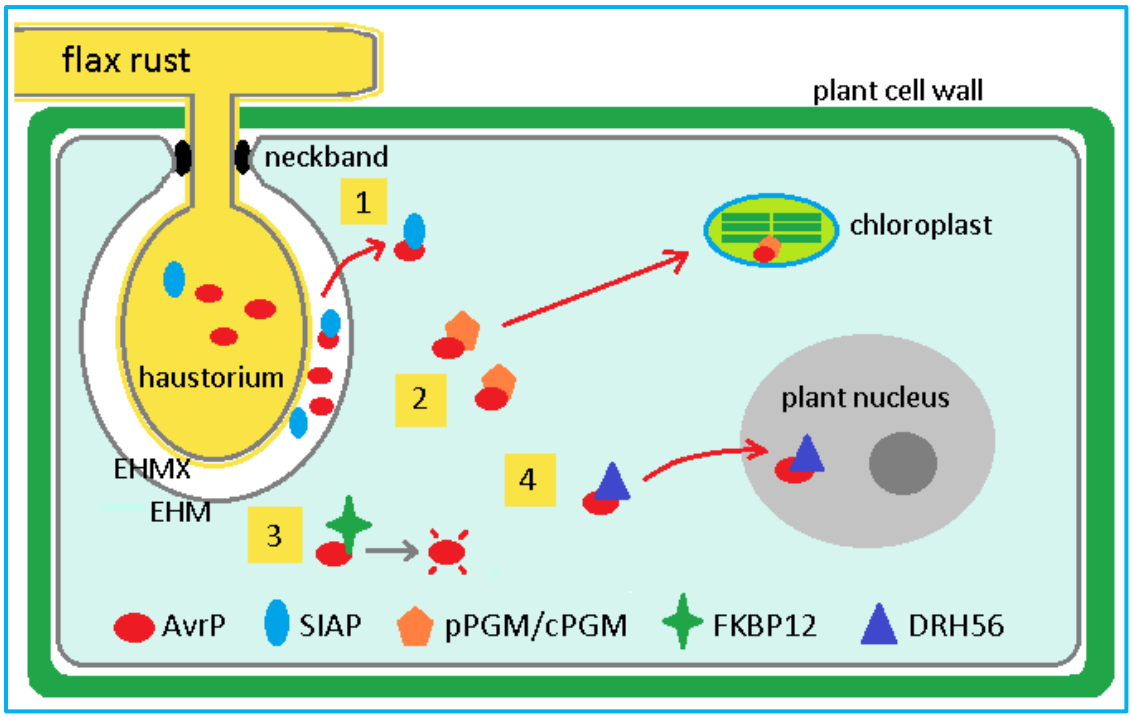

Figure 5.4 Hypothetical model of AvrP interaction with fungal and host proteins. 1) AvrP interacts with SIAP, a fungal effector, potentially required for translocation of AvrP into flax cells or activation of AvrP inside host cells or as a co-factor in AvrP effector function. 2) AvrP interacts with plastidial/chloroplastic PGM (pPGM) and cytosolic PGMs (cPGMs) in the host cytosol prior to translocation of pPGM into the chloroplast. Potentially, AvrP could manipulate host PGMs to obtain nutrients and suppress plant defence activation. 3) AvrP interacts with FKBP12, which, if it has PPIase activity, could potentially activate AvrP *in planta*. 4) AvrP interacts with flax DRH56, a DEAD-box RNA helicase that could "assist" AvrP translocation into the host nucleus and potentially enable AvrP to manipulate host transcription. EHMX = Extrahaustorial Matrix; EHM = Extrahaustorial Membrane. Image was adapted from Catanzariti et al. (2007).

In bacteria, a number of type-III effectors have been shown to target multiple host proteins, either to single or diverse classes of proteins. The Hrp outer protein Q (HopQ1) effector from *Pseudomonas syringae* pv. *tomato* has been shown to target multiple 14-3-3 proteins known to be responsible for regulation of many cellular processes by phosphorylation-dependent protein–protein interactions (Giska et al. 2013; Yoon and Kieber 2013; Li et al. 2013). Similarly, the HopX1 effector from *P. syringae* pv. *tabaci*

targets the JASMONATE-ZIM DOMAIN (JAZ) class of proteins which are key regulators of the jasmonate hormonal response (Gimenez-Ibanez et al. 2014) whereas the effector AvrPphB and HopAI1 target multiple PBS1-likekinases and mitogen-activated protein kinases (MAPKs), respectively (Zhang et al. 2010; Zhang et al. 2007). Effectors targeting multiple members of a single class of proteins are potentially disrupting multiple biological pathway to promote virulence as different kinases for example have distinct cellular functions (Khan et al. 2018).

HopM1 and HopZ1a are examples of type-III effectors that target multiple classes of proteins. In *Arabidopsis*, HopM1 interacts with ARF-GEF MIN7 (Nomura et al. 2006), 26S proteasome non-ATPase subunits (Ustun et al. 2016) and the 14-3-3 protein MIN10/GRF8 (Lozano-Duran et al. 2014). In soybean, HopZ1a, a member of HopZ/YopJ superfamily interacts with the isoflavone biosynthesis enzyme, 2-hydroxyisoflavanone dehydratase (GmHID1), leading to degradation of GmHID1 and promoting infection of *P. syringae* (Zhou et al. 2011). HopZ1a also interacts with host tubulin and polymerised microtubules, hence disrupting plant cellular trafficking (Lee et al. 2012). In addition, HopZ1a also interacts with the soybean GmJAZ1 and *Arabidopsis* JAZ6 proteins and activates JA signalling (Jiang et al. 2013).

Although fungal effectors may differ substantially from bacterial effectors, it is conceivable that the AvrP effector could also have multiple effector targets or could act as an adaptor protein between different effector targets as part of a multiprotein complex. For example, the plant homeodomain finger-like protein 5A acts as an adaptor between RNA helicases and proteins involved in RNA splicing and may also act as an adaptor to histone 3 in mouse (Rzymski et al. 2008).

5.4 Concluding remark and future directions

Plants and pathogens have developed a co-evolutionary relationship that determines their survival and co-existence. Biotrophic pathogens especially, need to “maintain” their fitness inside their hosts without being detected whilst conversely their plant hosts strive to counteract these pathogenic activities. Despite many attempts to understand the virulence-promoting activities of fungal effectors only the functions of a few have

been elucidated. In the flax rust system, the AvrL567 effector has been shown to bind and activate a cystosolic cytokinin oxidase thereby promoting the irreversible inactivation of cytosolic cytokinins (Wan et al. 2019), but how this acts to promote pathogencity is not understood. Similarly, the flax rust AvrM14 effector is a putative nudix hydrolase (Anderson et al. 2016), but its substrate in the host cell has not yet been identified and its role in pathogenicity remains unknown.

Many novel fungal effectors have been identified over the past decades. In oomycetes, the presence of RXLR motif has contributed greatly to effector prediction, especially for the hundreds of putative effectors from the *Phytophthora* genus and *Hyaloperonospora arabidopsidis* (Jiang et al. 2008; Baxter et al. 2010). For pathogenic fungi, however, identification of putative effectors has been more challenging. The advancement of high-throughput sequencing and post-genomic approaches have helped to identify effectors/avirulence proteins in various rust species (Hacquard et al. 2012; Petre et al. 2014; Nemri et al. 2014; Anderson et al. 2016; Chen et al. 2017; Salcedo et al. 2017) and provide new information regarding their genes, protein structure and recognition by their cognate resistance proteins. The *in silico* prediction of putative effectors using software such as EffectorP (Sperschneider et al. 2016; Sperschneider et al. 2018), combining the common features of fungal effectors discovered to date with *in planta* expression data (Duplessis et al. 2011b), has proven to be a reliable tool for effector prediction from fungal secretomes.

Three-dimensional structures of effector/avirulence proteins can provide valuable information regarding their possible function (e.g. enzymatic activity) which may lead to further experimentation. For example, the structure of AvrP is similar to the PHD finger and to investigate the possibilites of AvrP targeting host genomic DNA or host chromosomal proteins, a chromatin immunoprecipitation (ChIP) and sequencing (ChIP-seq) experiments can be performed (Siegel et al. 2009). Essentially, in the ChIP/CHIP-seq method cell samples are treated with a cross-linking agent to bind proteins to their DNA substrates; DNA is fragmented and the proteins of interest are then purified by immunoaffinity and identified by mass spectrometry; DNA samples are then sequenced and mapped to the reference genome (Lelandais et al. 2016). RNAseq could

also be used to investigate the possibility that AvrP effects host transcription (Hou et al. 2015).

To discover and validate the biological function of effectors, biochemical/biophysical studies can be performed. To do this, information regarding the effector target/target compartment (Petre et al. 2015) and/or effector/target protein function is required. Yeast-two-hybrid analysis can be used to identify effector interactor proteins and interactors can be validated using *in vitro* or *in vivo* pull-downs and/or BiFC. Expression and/or purification of interactors for *in vitro* or in *vivo* biochemical analysis of interactor function in the presence or absence of effector proteins can then be used to determine effector function as proposed in chapter 4 for the putative host targets of AvrP. Clearly, there is still a great deal of work to be done to understand the role of AvrP and AvrP123 in flax rust pathogenicity.

References

Aasland R, Gibson TJ, Stewart AF (1995) The PHD finger: implications for chromatin-mediated transcriptional regulation. Trends Biochem Sci 20 (2):56-59

Abramovitch RB, Janjusevic R, Stebbins CE, Martin GB (2006) Type III effector AvrPtoB requires intrinsic E3 ubiquitin ligase activity to suppress plant cell death and immunity. Proc Natl Acad Sci U S A 103 (8):2851-2856. doi:10.1073/pnas.0507892103

Abramovitch RB, Martin GB (2005) AvrPtoB: a bacterial type III effector that both elicits and suppresses programmed cell death associated with plant immunity. FEMS Microbiol Lett 245 (1):1-8. doi:10.1016/j.femsle.2005.02.025

Adhikari BN, Hamilton JP, Zerillo MM, Tisserat N, Levesque CA, Buell CR (2013) Comparative genomics reveals insight into virulence strategies of plant pathogenic oomycetes. PLoS One 8 (10):e75072. doi:10.1371/journal.pone.0075072

Aime MC (2006) Toward resolving family-level relationships in rust fungi (Uredinales). Mycoscience 47:112–122. doi:10.1007/s10267-006-0281-0

Aked J, Hall JL (1993) The uptake of glucose, fructose and sucrose into pea powdery mildew (*Erysiphe pisi* DC) from the apoplast of pea leaves. New Phytol 123:277–282

Amaro TM, Thilliez GJ, Motion GB, Huitema E (2017) A Perspective on CRN Proteins in the Genomics Age: Evolution, Classification, Delivery and Function Revisited. Front Plant Sci 8:99. doi:10.3389/fpls.2017.00099

Amselem J, Vigouroux M, Oberhaensli S, Brown JK, Bindschedler LV, Skamnioti P, Wicker T, Spanu PD, Quesneville H, Sacristan S (2015) Evolution of the EKA family of powdery mildew avirulence-effector genes from the ORF 1 of a LINE retrotransposon. BMC Genomics 16:917. doi:10.1186/s12864-015-2185-x

Anderson C, Khan MA, Catanzariti AM, Jack CA, Nemri A, Lawrence GJ, Upadhyaya NM, Hardham AR, Ellis JG, Dodds PN, Jones DA (2016) Genome analysis and avirulence gene cloning using a high-density RADseq linkage map of the flax rust fungus, *Melampsora lini*. BMC Genomics 17:667. doi:10.1186/s12864-016-3011-9

Anderson PA, Lawrence GJ, Morrish BC, Ayliffe MA, Finnegan EJ, Ellis JG (1997) Inactivation of the flax rust resistance gene M associated with loss of a repeated unit within the leucine-rich repeat coding region. Plant Cell 9 (4):641-651

Anderson RG, Deb D, Fedkenheuer K, McDowell JM (2015) Recent Progress in RXLR Effector Research. Mol Plant Microbe Interact 28 (10):1063-1072. doi:10.1094/MPMI-01-15-0022-CR

Axtell MJ, Staskawicz BJ (2003) Initiation of *RPS2*-specified disease resistance in *Arabidopsis* is coupled to the AvrRpt2-directed elimination of RIN4. Cell 112 (3):369-377

Bai S, Liu J, Chang C, Zhang L, Maekawa T, Wang Q, Xiao W, Liu Y, Chai J, Takken FL, Schulze-Lefert P, Shen QH (2012) Structure-function analysis of barley NLR immune receptor MLA10 reveals its cell compartment specific activity in cell death and disease resistance. PLoS Pathog 8 (6):e1002752. doi:10.1371/journal.ppat.1002752

Barrett LG, Thrall PH, Dodds PN, van der Merwe M, Linde CC, Lawrence GJ, Burdon JJ (2009) Diversity and evolution of effector loci in natural populations of the plant pathogen *Melampsora lini*. Mol Biol Evol 26 (11):2499-2513. doi:10.1093/molbev/msp166

Baxter L, Tripathy S, Ishaque N, Boot N, Cabral A, Kemen E, Thines M, Ah-Fong A, Anderson R, Badejoko W, Bittner-Eddy P, Boore JL, Chibucos MC, Coates M, Dehal P, Delehaunty K, Dong S, Downton P, Dumas B, Fabro G, Fronick C, Fuerstenberg SI, Fulton L, Gaulin E, Govers F, Hughes L, Humphray S, Jiang RHY, Judelson H, Kamoun S, Kyung K, Meijer H, Minx P, Morris P, Nelson J, Phuntumart V, Qutob D, Rehmany A, Rougon-Cardoso A, Ryden P, Torto-Alalibo T, Studholme D, Wang Y, Win J, Wood J, Clifton SW, Rogers J, Van den Ackerveken G, Jones JDG, McDowell JM, Beynon J, Tyler BM (2010) Signatures of adaptation to obligate biotrophy in the *Hyaloperonospora arabidopsidis* genome. Science 330 (6010):1549-1551. doi:10.1126/science.1195203

Berggard T, Linse S, James P (2007) Methods for the detection and analysis of protein-protein interactions. Proteomics 7 (16):2833-2842. doi:10.1002/pmic.200700131

Bernoux M, Burdett H, Williams SJ, Zhang X, Chen C, Newell K, Lawrence G, Kobe B, Ellis JG, Anderson P, Dodds PN (2016) Comparative analysis of the flax immune receptors L6 and L7 suggests an equilibrium-based switch activation model. Plant Cell. doi:10.1105/tpc.15.00303

Bernoux M, Ve T, Williams S, Warren C, Hatters D, Valkov E, Zhang X, Ellis JG, Kobe B, Dodds PN (2011) Structural and functional analysis of a plant resistance protein TIR domain reveals interfaces for self-association, signaling, and autoregulation. Cell Host Microbe 9 (3):200-211. doi:10.1016/j.chom.2011.02.009

Bienz M (2006) The PHD finger, a nuclear protein-interaction domain. Trends Biochem Sci 31 (1):35-40. doi:10.1016/j.tibs.2005.11.001

Bohm H, Albert I, Fan L, Reinhard A, Nurnberger T (2014) Immune receptor complexes at the plant cell surface. Curr Opin Plant Biol 20:47-54. doi:10.1016/j.pbi.2014.04.007

Bouwmeester K, de Sain M, Weide R, Gouget A, Klamer S, Canut H, Govers F (2011) The lectin receptor kinase LecRK-I.9 is a novel *Phytophthora* resistance component and a potential host target for a RXLR effector. PLoS Pathog 7 (3):e1001327. doi:10.1371/journal.ppat.1001327

Bracha-Drori K, Shichrur K, Katz A, Oliva M, Angelovici R, Yalovsky S, Ohad N (2004) Detection of protein-protein interactions in plants using bimolecular fluorescence complementation. Plant J 40 (3):419-427. doi:10.1111/j.1365-313X.2004.02206.x

Caillaud MC, Asai S, Rallapalli G, Piquerez S, Fabro G, Jones JD (2013) A downy mildew effector attenuates salicylic acid-triggered immunity in *Arabidopsis* by interacting with the host mediator complex. Plos Biol 11 (12):e1001732. doi:10.1371/journal.pbio.1001732

Cantu C, Valenta T, Hausmann G, Vilain N, Aguet M, Basler K (2013) The Pygo2-H3K4me2/3 interaction is dispensable for mouse development and Wnt signaling-dependent transcription. Development 140 (11):2377-2386. doi:10.1242/dev.093591

Casey LW, Lavrencic P, Bentham AR, Cesari S, Ericsson DJ, Croll T, Turk D, Anderson PA, Mark AE, Dodds PN, Mobli M, Kobe B, Williams SJ (2016) The CC domain structure from the wheat stem rust resistance protein Sr33 challenges paradigms for dimerization in plant NLR proteins. Proc Natl Acad Sci U S A. doi:10.1073/pnas.1609922113

Catanzariti AM, Dodds PN, Ellis JG (2007) Avirulence proteins from haustoria-forming pathogens. FEMS Microbiol Lett 269 (2):181-188. doi:10.1111/j.1574-6968.2007.00684.x

Catanzariti AM, Dodds PN, Lawrence GJ, Ayliffe MA, Ellis JG (2006) Haustorially expressed secreted proteins from flax rust are highly enriched for avirulence elicitors. Plant Cell 18 (1):243-256. doi:10.1105/tpc.105.035980

Catanzariti AM, Dodds PN, Ve T, Kobe B, Ellis JG, Staskawicz BJ (2010) The AvrM effector from flax rust has a structured C-terminal domain and interacts directly with the M resistance protein. Mol Plant Microbe Interact 23 (1):49-57. doi:10.1094/MPMI-23-1-0049

Cesari S, Bernoux M, Moncuquet P, Kroj T, Dodds PN (2014) A novel conserved mechanism for plant NLR protein pairs: the "integrated decoy" hypothesis. Front Plant Sci 5:606. doi:10.3389/fpls.2014.00606

Chen J, Upadhyaya NM, Ortiz D, Sperschneider J, Li F, Bouton C, Breen S, Dong C, Xu B, Zhang X, Mago R, Newell K, Xia X, Bernoux M, Taylor JM, Steffenson B, Jin Y, Zhang P, Kanyuka K, Figueroa M, Ellis JG, Park RF, Dodds PN (2017) Loss of *AvrSr50* by somatic exchange in stem rust leads to virulence for *Sr50* resistance in wheat. Science 358 (6370):1607-1610. doi:10.1126/science.aao4810

Chien CT, Bartel PL, Sternglanz R, Fields S (1991) The two-hybrid system: a method to identify and clone genes for proteins that interact with a protein of interest. Proc Natl Acad Sci U S A 88 (21):9578-9582

Chignola F, Gaetani M, Rebane A, Org T, Mollica L, Zucchelli C, Spitaleri A, Mannella V, Peterson P, Musco G (2009) The solution structure of the first PHD finger of autoimmune regulator in complex with non-modified histone H3 tail reveals the antagonistic role of H3R2 methylation. Nucleic Acids Res 37 (9):2951-2961. doi:10.1093/nar/gkp166

Chung HR, Xu C, Fuchs A, Mund A, Lange M, Staege H, Schubert T, Bian C, Dunkel I, Eberharter A, Regnard C, Klinker H, Meierhofer D, Cozzuto L, Winterpacht A, Di Croce L, Min J, Will H, Kinkley S (2016) PHF13 is a molecular reader and transcriptional co-regulator of H3K4me2/3. Elife 5. doi:10.7554/eLife.10607

Coaker G, Falick A, Staskawicz B (2005) Activation of a phytopathogenic bacterial effector protein by a eukaryotic cyclophilin. Science 308 (5721):548-550. doi:10.1126/science.1108633

Costanzo S, Ospina-Giraldo MD, Deahl KL, Baker CJ, Jones RW (2006) Gene duplication event in family 12 glycosyl hydrolase from *Phytophthora spp*. Fungal Genet Biol 43 (10):707-714. doi:10.1016/j.fgb.2006.04.006

Couto D, Zipfel C (2016) Regulation of pattern recognition receptor signalling in plants. Nat Rev Immunol 16 (9):537-552. doi:10.1038/nri.2016.77

Dangl JL, Horvath DM, Staskawicz BJ (2013) Pivoting the plant immune system from dissection to deployment. Science 341 (6147):746-751. doi:10.1126/science.1236011

de Jonge R, van Esse HP, Kombrink A, Shinya T, Desaki Y, Bours R, van der Krol S, Shibuya N, Joosten MHAJ, Thomma BPHJ (2010) Conserved fungal LysM effector Ecp6 prevents chitin-triggered immunity in plants. Science 329 (5994):953-955. doi:10.1126/science.1190859

de Wit PJGM (1995) *Cf9* and *Avr9*, two major players in the gene-for-gene game. Trends Microbiol 3 (7):251-252

DeCenzo MT, Park ST, Jarrett BP, Aldape RA, Futer O, Murcko MA, Livingston DJ (1996) FK506-binding protein mutational analysis:

defining the active-site residue contributions to catalysis and the stability of ligand complexes. Protein Eng 9 (2):173-180

Deslandes L, Olivier J, Theulieres F, Hirsch J, Feng DX, Bittner-Eddy P, Beynon J, Marco Y (2002) Resistance to *Ralstonia solanacearum* in *Arabidopsis thaliana* is conferred by the recessive *RRS1-R* gene, a member of a novel family of resistance genes. Proc Natl Acad Sci U S A 99 (4):2404-2409. doi:10.1073/pnas.032485099

Deslandes L, Rivas S (2012) Catch me if you can: bacterial effectors and plant targets. Trends Plant Sci 17 (11):644-655. doi:10.1016/j.tplants.2012.06.011

Dixon MS, Jones DA, Keddie JS, Thomas CM, Harrison K, Jones JD (1996) The tomato *Cf-2* disease resistance locus comprises two functional genes encoding leucine-rich repeat proteins. Cell 84 (3):451-459

Djamei A, Kahmann R (2012) *Ustilago maydis*: dissecting the molecular interface between pathogen and plant. PLoS Pathog 8 (11):e1002955. doi:10.1371/journal.ppat.1002955

Djamei A, Schipper K, Rabe F, Ghosh A, Vincon V, Kahnt J, Osorio S, Tohge T, Fernie AR, Feussner I, Feussner K, Meinicke P, Stierhof YD, Schwarz H, Macek B, Mann M, Kahmann R (2011) Metabolic priming by a secreted fungal effector. Nature 478 (7369):395-398. doi:10.1038/nature10454

Dodds P, Thrall P (2009) Recognition events and host-pathogen co-evolution in gene-for-gene resistance to flax rust. Funct Plant Biol 36 (5):395-408. doi:10.1071/FP08320

Dodds PN, Lawrence GJ, Catanzariti AM, Ayliffe MA, Ellis JG (2004) The *Melampsora lini AvrL567* avirulence genes are expressed in haustoria and their products are recognized inside plant cells. Plant Cell 16 (3):755-768. doi:10.1105/tpc.020040

Dodds PN, Lawrence GJ, Catanzariti AM, Teh T, Wang CI, Ayliffe MA, Kobe B, Ellis JG (2006) Direct protein interaction underlies gene-for-gene specificity and coevolution of the flax resistance genes and flax rust avirulence genes. Proc Natl Acad Sci U S A 103 (23):8888-8893. doi:10.1073/pnas.0602577103

Dodds PN, Lawrence GJ, Ellis JG (2001a) Contrasting modes of evolution acting on the complex *N* locus for rust resistance in flax. Plant J 27 (5):439-453

Dodds PN, Lawrence GJ, Ellis JG (2001b) Six amino acid changes confined to the leucine-rich repeat beta-strand/beta-turn motif determine the difference between the *P* and *P2* rust resistance specificities in flax. Plant Cell 13 (1):163-178

Dodds PN, Rathjen JP (2010) Plant immunity: towards an integrated view of plant-pathogen interactions. Nat Rev Genet 11 (8):539-548. doi:10.1038/nrg2812

Doehlemann G, van der Linde K, Assmann D, Schwammbach D, Hof A, Mohanty A, Jackson D, Kahmann R (2009) Pep1, a secreted effector protein of *Ustilago maydis*, is required for successful invasion of plant cells. PLoS Pathog 5 (2):e1000290. doi:10.1371/journal.ppat.1000290

Dong J, Xiao F, Fan F, Gu L, Cang H, Martin GB, Chai J (2009) Crystal structure of the complex between *Pseudomonas* effector AvrPtoB and the tomato Pto kinase reveals both a shared and a unique interface compared with AvrPto-Pto. Plant Cell 21 (6):1846-1859. doi:10.1105/tpc.109.066878

Dong S, Yin W, Kong G, Yang X, Qutob D, Chen Q, Kale SD, Sui Y, Zhang Z, Dou D, Zheng X, Gijzen M, Tyler BM, Wang Y (2011) *Phytophthora sojae* avirulence effector Avr3b is a secreted NADH and ADP-ribose pyrophosphorylase that modulates plant immunity. PLoS Pathog 7 (11):e1002353. doi:10.1371/journal.ppat.1002353

Dou D, Kale SD, Wang X, Jiang RH, Bruce NA, Arredondo FD, Zhang X, Tyler BM (2008) RXLR-mediated entry of *Phytophthora sojae* effector Avr1b into soybean cells does not require pathogen-encoded machinery. Plant Cell 20 (7):1930-1947. doi:10.1105/tpc.107.056093

Duplessis S, Cuomo CA, Lin YC, Aerts A, Tisserant E, Veneault-Fourrey C, Joly DL, Hacquard S, Amselem J, Cantarel BL, Chiu R, Coutinho PM, Feau N, Field M, Frey P, Gelhaye E, Goldberg J, Grabherr MG, Kodira CD, Kohler A, Kues U, Lindquist EA, Lucas SM, Mago R, Mauceli E, Morin E, Murat C, Pangilinan JL, Park R, Pearson M, Quesneville H, Rouhier N, Sakthikumar S, Salamov AA, Schmutz J, Selles B, Shapiro H, Tanguay P, Tuskan GA, Henrissat B, Van de Peer Y, Rouze P, Ellis JG, Dodds PN, Schein JE, Zhong S, Hamelin RC, Grigoriev IV, Szabo LJ, Martin F (2011a) Obligate biotrophy features unraveled by the genomic analysis of rust fungi. Proc Natl Acad Sci U S A 108 (22):9166-9171. doi:10.1073/pnas.1019315108

Duplessis S, Hacquard S, Delaruelle C, Tisserant E, Frey P, Martin F, Kohler A (2011b) *Melampsora larici-populina* transcript profiling during germination and timecourse infection of poplar leaves reveals dynamic expression patterns associated with virulence and biotrophy. Mol Plant Microbe Interact 24 (7):808-818. doi:10.1094/MPMI-01-11-0006

Earley KW, Haag JR, Pontes O, Opper K, Juehne T, Song K, Pikaard CS (2006) Gateway-compatible vectors for plant functional genomics and proteomics. Plant J 45 (4):616-629. doi:10.1111/j.1365-313X.2005.02617.x

Eberharter A, Vetter I, Ferreira R, Becker PB (2004) ACF1 improves the effectiveness of nucleosome mobilization by ISWI through PHD-histone contacts. Embo J 23 (20):4029-4039. doi:10.1038/sj.emboj.7600382

Ellis JG, Lawrence GJ, Luck JE, Dodds PN (1999) Identification of regions in alleles of the flax rust resistance gene *L* that determine differences in gene-for-gene specificity. Plant Cell 11 (3):495-506

Engelsdorf T, Will C, Hofmann J, Schmitt C, Merritt BB, Rieger L, Frenger MS, Marschall A, Franke RB, Pattathil S, Voll LM (2017) Cell wall composition and penetration resistance against the fungal pathogen *Colletotrichum higginsianum* are affected by impaired starch turnover in *Arabidopsis* mutants. J Exp Bot 68 (3):701-713. doi:10.1093/jxb/erw434

Faure JD, Gingerich D, Howell SH (1998) An Arabidopsis immunophilin, AtFKBP12, binds to AtFIP37 (FKBP interacting protein) in an interaction that is disrupted by FK506. Plant J 15 (6):783-789

Fields S, Song O (1989) A novel genetic system to detect protein-protein interactions. Nature 340 (6230):245-246. doi:10.1038/340245a0

Fischer G, Bang H, Mech C (1984) [Determination of enzymatic catalysis for the cis-trans-isomerization of peptide binding in proline-containing peptides]. Biomed Biochim Acta 43 (10):1101-1111

Flor HH (1942) Inheritance of pathogenicity in a cross between physiologic races 22 and 24 of *Melampsora lini*. Phytopathology 32 (1):5

Fu ZQ, Guo M, Jeong BR, Tian F, Elthon TE, Cerny RL, Staiger D, Alfano JR (2007) A type III effector ADP-ribosylates RNA-binding proteins and quells plant immunity. Nature 447 (7142):284-288. doi:10.1038/nature05737

Gassmann W, Hinsch ME, Staskawicz BJ (1999) The *Arabidopsis RPS4* bacterial-resistance gene is a member of the TIR-NBS-LRR family of disease-resistance genes. Plant J 20 (3):265-277

Germain H, Joly DL, Mireault C, Plourde MB, Letanneur C, Stewart D, Morency MJ, Petre B, Duplessis S, Seguin A (2018) Infection assays in *Arabidopsis* reveal candidate effectors from the poplar rust fungus that promote susceptibility to bacteria and oomycete pathogens. Mol Plant Pathol 19 (1):191-200. doi:10.1111/mpp.12514

Gimenez-Ibanez S, Boter M, Fernandez-Barbero G, Chini A, Rathjen JP, Solano R (2014) The bacterial effector HopX1 targets JAZ transcriptional repressors to activate jasmonate signaling and promote infection in *Arabidopsis*. Plos Biol 12 (2):e1001792. doi:10.1371/journal.pbio.1001792

Gimenez-Ibanez S, Hann DR, Ntoukakis V, Petutschnig E, Lipka V, Rathjen JP (2009) AvrPtoB targets the LysM receptor kinase CERK1 to promote bacterial virulence on plants. Curr Biol 19 (5):423-429. doi:10.1016/j.cub.2009.01.054

Giska F, Lichocka M, Piechocki M, Dadlez M, Schmelzer E, Hennig J, Krzymowska M (2013) Phosphorylation of HopQ1, a type III effector from *Pseudomonas syringae*, creates a binding site for host 14-3-3 proteins. Plant Physiol 161 (4):2049-2061. doi:10.1104/pp.112.209023

Gohre V, Spallek T, Haweker H, Mersmann S, Mentzel T, Boller T, de Torres M, Mansfield JW, Robatzek S (2008) Plant pattern-recognition receptor FLS2 is directed for degradation by the bacterial ubiquitin ligase AvrPtoB. Curr Biol 18 (23):1824-1832. doi:10.1016/j.cub.2008.10.063

Gollan PJ, Bhave M, Aro EM (2012) The FKBP families of higher plants: Exploring the structures and functions of protein interaction specialists. FEBS Lett 586 (20):3539-3547. doi:10.1016/j.febslet.2012.09.002

Gomez-Gomez L, Boller T (2000) FLS2: an LRR receptor-like kinase involved in the perception of the bacterial elicitor flagellin in *Arabidopsis*. Mol Cell 5 (6):1003-1011

Hacquard S, Joly DL, Lin YC, Tisserant E, Feau N, Delaruelle C, Legue V, Kohler A, Tanguay P, Petre B, Frey P, Van de Peer Y, Rouze P, Martin F, Hamelin RC, Duplessis S (2012) A comprehensive analysis of genes encoding small secreted proteins identifies candidate effectors in *Melampsora larici-populina* (poplar leaf rust). Mol Plant Microbe Interact 25 (3):279-293. doi:10.1094/MPMI-09-11-0238

Hahn M, Mendgen K (2001) Signal and nutrient exchange at biotrophic plant-fungus interfaces. Curr Opin Plant Biol 4 (4):322-327

Hattenbach A, Heineke D (1999) On the role of chloroplastic phosphoglucomutase in the regulation of starch turnover. Planta 207 (4):527-532. doi:10.1007/s004250050513

Hellens RP, Edwards EA, Leyland NR, Bean S, Mullineaux PM (2000) pGreen: a versatile and flexible binary Ti vector for Agrobacterium-mediated plant transformation. Plant Mol Biol 42 (6):819-832

Hemetsberger C, Herrberger C, Zechmann B, Hillmer M, Doehlemann G (2012) The *Ustilago maydis* effector Pep1 suppresses plant immunity by inhibition of host peroxidase activity. PLoS Pathog 8 (5):e1002684. doi:10.1371/journal.ppat.1002684

Hoffman CS, Winston F (1987) A ten-minute DNA preparation from yeast efficiently releases autonomous plasmids for transformation of Escherichia coli. Gene 57 (2-3):267-272

Hohmann U, Lau K, Hothorn M (2017) The Structural Basis of Ligand Perception and Signal Activation by Receptor Kinases. Annu Rev Plant Biol 68:109-137. doi:10.1146/annurev-arplant-042916-040957

Hou Z, Jiang P, Swanson SA, Elwell AL, Nguyen BK, Bolin JM, Stewart R, Thomson JA (2015) A cost-effective RNA sequencing protocol for large-scale gene expression studies. Sci Rep 5:9570. doi:10.1038/srep09570

Islam MR, Mayo GME (1990) A Compendium on Host Genes in Flax Conferring Resistance to Flax Rust. Plant Breeding 104 (2):89-100. doi:DOI 10.1111/j.1439-0523.1990.tb00409.x

Iwase S, Lan F, Bayliss P, de la Torre-Ubieta L, Huarte M, Qi HH, Whetstine JR, Bonni A, Roberts TM, Shi Y (2007) The X-linked mental retardation gene SMCX/JARID1C defines a family of histone H3 lysine 4 demethylases. Cell 128 (6):1077-1088. doi:10.1016/j.cell.2007.02.017

Jacob F, Vernaldi S, Maekawa T (2013) Evolution and conservation of plant NLR functions. Front Immunol 4:297. doi:10.3389/fimmu.2013.00297

Janse van Rensburg HC, Van den Ende W (2018) UDP-Glucose: A Potential Signaling Molecule in Plants? Front Plant Sci 8:2230. doi:10.3389/fpls.2017.02230

Jaouannet M, Rodriguez PA, Thorpe P, Lenoir CJ, MacLeod R, Escudero-Martinez C, Bos JI (2014) Plant immunity in plant-aphid interactions. Front Plant Sci 5:663. doi:10.3389/fpls.2014.00663

Jarmoskaite I, Russell R (2014) RNA helicase proteins as chaperones and remodelers. Annu Rev Biochem 83:697-725. doi:10.1146/annurev-biochem-060713-035546

Jiang RH, Tripathy S, Govers F, Tyler BM (2008) RXLR effector reservoir in two *Phytophthora* species is dominated by a single rapidly evolving superfamily with more than 700 members. Proc Natl Acad Sci U S A 105 (12):4874-4879. doi:10.1073/pnas.0709303105

Jiang S, Yao J, Ma KW, Zhou H, Song J, He SY, Ma W (2013) Bacterial effector activates jasmonate signaling by directly targeting JAZ transcriptional repressors. PLoS Pathog 9 (10):e1003715. doi:10.1371/journal.ppat.1003715

Jones DA, Thomas CM, Hammond-Kosack KE, Balint-Kurti PJ, Jones JD (1994) Isolation of the tomato *Cf-9* gene for resistance to

Cladosporium fulvum by transposon tagging. Science 266 (5186):789-793

Jones JDG, Dangl JL (2006) The plant immune system. Nature 444 (7117):323-329. doi:10.1038/nature05286

Joosten MHAJ, Vogelsang R, Cozijnsen TJ, Verberne MC, De Wit PJGM (1997) The biotrophic fungus *Cladosporium fulvum* circumvents *Cf-4*-mediated resistance by producing unstable AVR4 elicitors. Plant Cell 9 (3):367-379

Kammel C, Thomaier M, Sorensen BB, Schubert T, Langst G, Grasser M, Grasser KD (2013) *Arabidopsis* DEAD-box RNA helicase UAP56 interacts with both RNA and DNA as well as with mRNA export factors. PLoS One 8 (3):e60644. doi:10.1371/journal.pone.0060644

Karagianni P, Amazit L, Qin J, Wong J (2008) ICBP90, a novel methyl K9 H3 binding protein linking protein ubiquitination with heterochromatin formation. Mol Cell Biol 28 (2):705-717. doi:10.1128/MCB.01598-07

Kemen E, Kemen AC, Rafiqi M, Hempel U, Mendgen K, Hahn M, Voegele RT (2005) Identification of a protein from rust fungi transferred from haustoria into infected plant cells. Mol Plant Microbe In 18 (11):1130-1139. doi:10.1094/Mpmi-18-1130

Khan M, Seto D, Subramaniam R, Desveaux D (2018) Oh, the places they'll go! A survey of phytopathogen effectors and their host targets. Plant J 93 (4):651-663. doi:10.1111/tpj.13780

Kim HS, Desveaux D, Singer AU, Patel P, Sondek J, Dangl JL (2005) The *Pseudomonas syringae* effector AvrRpt2 cleaves its C-terminally acylated target, RIN4, from *Arabidopsis* membranes to block RPM1 activation. Proc Natl Acad Sci U S A 102 (18):6496-6501. doi:10.1073/pnas.0500792102

Kim YJ, Lin NC, Martin GB (2002) Two distinct *Pseudomonas* effector proteins interact with the Pto kinase and activate plant immunity. Cell 109 (5):589-598

Kong G, Zhao Y, Jing M, Huang J, Yang J, Xia Y, Kong L, Ye W, Xiong Q, Qiao Y, Dong S, Ma W, Wang Y (2015) The Activation of Phytophthora Effector Avr3b by Plant Cyclophilin is Required for the Nudix Hydrolase Activity of Avr3b. PLoS Pathog 11 (8):e1005139. doi:10.1371/journal.ppat.1005139

Krattinger SG, Lagudah ES, Spielmeyer W, Singh RP, Huerta-Espino J, McFadden H, Bossolini E, Selter LL, Keller B (2009) A putative ABC transporter confers durable resistance to multiple fungal pathogens in wheat. Science 323 (5919):1360-1363. doi:10.1126/science.1166453

Lallous N, Ramón-Maiques S (2011) Chromatin Recognition Protein Modules: The PHD Finger. doi:10.1002/9780470015902.a0023176

Lan F, Collins RE, De Cegli R, Alpatov R, Horton JR, Shi X, Gozani O, Cheng X, Shi Y (2007) Recognition of unmethylated histone H3 lysine 4 links BHC80 to LSD1-mediated gene repression. Nature 448 (7154):718-722. doi:10.1038/nature06034

Lanver D, Tollot M, Schweizer G, Lo Presti L, Reissmann S, Ma LS, Schuster M, Tanaka S, Liang L, Ludwig N, Kahmann R (2017) *Ustilago maydis* effectors and their impact on virulence. Nat Rev Microbiol 15 (7):409-421. doi:10.1038/nrmicro.2017.33

Lawrence GJ, Anderson PA, Dodds PN, Ellis JG (2010) Relationships between rust resistance genes at the *M* locus in flax. Mol Plant Pathol 11 (1):19-32. doi:10.1111/j.1364-3703.2009.00563.x

Lawrence GJ, Dodds PN, Ellis JG (2007) Rust of flax and linseed caused by *Melampsora lini*. Mol Plant Pathol 8 (4):349-364. doi:10.1111/j.1364-3703.2007.00405.x

Lawrence GJ, Finnegan EJ, Ayliffe MA, Ellis JG (1995) The *L6* gene for flax rust resistance is related to the *Arabidopsis* bacterial resistance gene *RPS2* and the tobacco viral resistance gene *N*. Plant Cell 7 (8):1195-1206. doi:10.1105/tpc.7.8.1195

Lawrence GJ, Mayo GME, Shepherd KW (1981a) Interactions between genes-controlling pathogenicity in the flax rust fungus. Phytopathology 71 (1):12-19. doi:DOI 10.1094/Phyto-71-12

Lawrence GJ, Shepherd KW, Mayo GME (1981b) Fine structure of genes controlling pathogenicity in flax rust, *Melampsora lini*. Heredity 46 (3):297-313

Lee AH, Hurley B, Felsensteiner C, Yea C, Ckurshumova W, Bartetzko V, Wang PW, Quach V, Lewis JD, Liu YC, Bornke F, Angers S, Wilde A, Guttman DS, Desveaux D (2012) A bacterial acetyltransferase destroys plant microtubule networks and blocks secretion. PLoS Pathog 8 (2):e1002523. doi:10.1371/journal.ppat.1002523

Lelandais G, Blugeon C, Merhej J (2016) ChIPseq in yeast species: from chromatin immunoprecipitation to high-throughput sequencing and bioinformatics data analyses. Methods Mol Biol 1361:185-202. doi:10.1007/978-1-4939-3079-1_11

Li D, Liu H, Zhang H, Wang X, Song F (2008a) OsBIRH1, a DEAD-box RNA helicase with functions in modulating defence responses against pathogen infection and oxidative stress. J Exp Bot 59 (8):2133-2146. doi:10.1093/jxb/ern072

Li F, Huarte M, Zaratiegui M, Vaughn MW, Shi Y, Martienssen R, Cande WZ (2008b) Lid2 is required for coordinating H3K4 and H3K9

methylation of heterochromatin and euchromatin. Cell 135 (2):272-283. doi:10.1016/j.cell.2008.08.036
Li W, Yadeta KA, Elmore JM, Coaker G (2013) The *Pseudomonas syringae* effector HopQ1 promotes bacterial virulence and interacts with tomato 14-3-3 proteins in a phosphorylation-dependent manner. Plant Physiol 161 (4):2062-2074. doi:10.1104/pp.112.211748
Lin ZJ, Liebrand TW, Yadeta KA, Coaker G (2015) PBL13 Is a Serine/Threonine Protein Kinase That Negatively Regulates *Arabidopsis* Immune Responses. Plant Physiol 169 (4):2950-2962. doi:10.1104/pp.15.01391
Link T, Seibel C, Voegele RT (2014) Early insights into the genome sequence of *Uromyces fabae*. Front Plant Sci 5:587. doi:10.3389/fpls.2014.00587
Liu T, Ye W, Ru Y, Yang X, Gu B, Tao K, Lu S, Dong S, Zheng X, Shan W, Wang Y, Dou D (2011) Two host cytoplasmic effectors are required for pathogenesis of *Phytophthora sojae* by suppression of host defenses. Plant Physiol 155 (1):490-501. doi:10.1104/pp.110.166470
Lozano-Duran R, Bourdais G, He SY, Robatzek S (2014) The bacterial effector HopM1 suppresses PAMP-triggered oxidative burst and stomatal immunity. New Phytol 202 (1):259-269. doi:10.1111/nph.12651
Lyu X, Shen C, Fu Y, Xie J, Jiang D, Li G, Cheng J (2016) A small secreted virulence-related protein is essential for the necrotrophic interactions of *Sclerotinia sclerotiorum* with its host plants. PLoS Pathog 12 (2):e1005435. doi:10.1371/journal.ppat.1005435
Mackey D, Belkhadir Y, Alonso JM, Ecker JR, Dangl JL (2003) *Arabidopsis* RIN4 is a target of the type III virulence effector AvrRpt2 and modulates RPS2-mediated resistance. Cell 112 (3):379-389
Mackey D, Holt BF, 3rd, Wiig A, Dangl JL (2002) RIN4 interacts with Pseudomonas syringae type III effector molecules and is required for RPM1-mediated resistance in Arabidopsis. Cell 108 (6):743-754
Maekawa T, Cheng W, Spiridon LN, Toller A, Lukasik E, Saijo Y, Liu P, Shen QH, Micluta MA, Somssich IE, Takken FLW, Petrescu AJ, Chai J, Schulze-Lefert P (2011) Coiled-coil domain-dependent homodimerization of intracellular barley immune receptors defines a minimal functional module for triggering cell death. Cell Host Microbe 9 (3):187-199. doi:10.1016/j.chom.2011.02.008
Mafurah JJ, Ma H, Zhang M, Xu J, He F, Ye T, Shen D, Chen Y, Rajput NA, Dou D (2015) A virulence essential CRN effector of *Phytophthora capsici* suppresses host defense and induces cell death in plant

nucleus. PLoS One 10 (5):e0127965. doi:10.1371/journal.pone.0127965

Mago R, Zhang P, Vautrin S, Simkova H, Bansal U, Luo MC, Rouse M, Karaoglu H, Periyannan S, Kolmer J, Jin Y, Ayliffe MA, Bariana H, Park RF, McIntosh R, Dolezel J, Berges H, Spielmeyer W, Lagudah ES, Ellis JG, Dodds PN (2015) The wheat *Sr50* gene reveals rich diversity at a cereal disease resistance locus. Nat Plants 1:15186. doi:10.1038/nplants.2015.186

Malinova I, Kunz HH, Alseekh S, Herbst K, Fernie AR, Gierth M, Fettke J (2014) Reduction of the cytosolic phosphoglucomutase in *Arabidopsis* reveals impact on plant growth, seed and root development, and carbohydrate partitioning. PLoS One 9 (11):e112468. doi:10.1371/journal.pone.0112468

Mathieu J, Schwizer S, Martin GB (2014) Pto kinase binds two domains of AvrPtoB and its proximity to the effector E3 ligase determines if it evades degradation and activates plant immunity. PLoS Pathog 10 (7):e1004227. doi:10.1371/journal.ppat.1004227

Mendgen K, Nass P (1988) The activity of powdery-mildew haustoria after feeding the host cells with different sugars, as measured with a potentiometric cyanine dye. Planta 174 (2):283-288. doi:10.1007/BF00394782

Mesarich CH, Griffiths SA, van der Burgt A, Okmen B, Beenen HG, Etalo DW, Joosten MH, de Wit PJ (2014) Transcriptome sequencing uncovers the *Avr5* avirulence gene of the tomato leaf mold pathogen *Cladosporium fulvum*. Mol Plant Microbe Interact 27 (8):846-857. doi:10.1094/MPMI-02-14-0050-R

Moore JW, Herrera-Foessel S, Lan C, Schnippenkoetter W, Ayliffe M, Huerta-Espino J, Lillemo M, Viccars L, Milne R, Periyannan S, Kong X, Spielmeyer W, Talbot M, Bariana H, Patrick JW, Dodds P, Singh R, Lagudah E (2015) A recently evolved hexose transporter variant confers resistance to multiple pathogens in wheat. Nat Genet 47 (12):1494-1498. doi:10.1038/ng.3439

Morava E (2014) Galactose supplementation in phosphoglucomutase-1 deficiency; review and outlook for a novel treatable CDG. Mol Genet Metab 112 (4):275-279. doi:10.1016/j.ymgme.2014.06.002

Mucyn TS, Clemente A, Andriotis VM, Balmuth AL, Oldroyd GE, Staskawicz BJ, Rathjen JP (2006) The tomato NBARC-LRR protein Prf interacts with Pto kinase in vivo to regulate specific plant immunity. Plant Cell 18 (10):2792-2806. doi:10.1105/tpc.106.044016

Mueller AN, Ziemann S, Treitschke S, Assmann D, Doehlemann G (2013) Compatibility in the *Ustilago maydis*-maize interaction requires

inhibition of host cysteine proteases by the fungal effector Pit2. PLoS Pathog 9 (2):e1003177. doi:10.1371/journal.ppat.1003177

Mutuku JM, Nose A (2012) Changes in the contents of metabolites and enzyme activities in rice plants responding to *Rhizoctonia solani* Kuhn infection: activation of glycolysis and connection to phenylpropanoid pathway. Plant Cell Physiol 53 (6):1017-1032. doi:10.1093/pcp/pcs047

Nemri A, Saunders DG, Anderson C, Upadhyaya NM, Win J, Lawrence GJ, Jones DA, Kamoun S, Ellis JG, Dodds PN (2014) The genome sequence and effector complement of the flax rust pathogen *Melampsora lini*. Front Plant Sci 5:98. doi:10.3389/fpls.2014.00098

Niu XW, Zheng ZY, Feng YG, Guo WZ, Wang XY (2013) The *Fusarium graminearum* virulence factor FGL targets an FKBP12 immunophilin of wheat. Gene 525 (1):77-83. doi:10.1016/j.gene.2013.04.052

Nomura K, Debroy S, Lee YH, Pumplin N, Jones J, He SY (2006) A bacterial virulence protein suppresses host innate immunity to cause plant disease. Science 313 (5784):220-223. doi:10.1126/science.1129523

Okmen B, Etalo DW, Joosten MHAJ, Bouwmeester HJ, de Vos RCH, Collemare J, de Wit PJGM (2013) Detoxification of alpha-tomatine by *Cladosporium fulvum* is required for full virulence on tomato. New Phytol 198 (4):1203-1214. doi:10.1111/nph.12208

Orsomando G, Brunetti L, Pucci K, Ruggeri B, Ruggieri S (2011) Comparative structural and functional characterization of putative protein effectors belonging to the *PcF toxin family* from *Phytophthora* spp. Protein Sci 20 (12):2047-2059. doi:10.1002/pro.742

Pan H, Liu S, Tang D (2012) The THO/TREX complex functions in disease resistance in Arabidopsis. Plant Signal Behav 7 (3):422-424. doi:10.4161/psb.18991

Park CH, Chen S, Shirsekar G, Zhou B, Khang CH, Songkumarn P, Afzal AJ, Ning Y, Wang R, Bellizzi M, Valent B, Wang GL (2012) The *Magnaporthe oryzae* effector AvrPiz-t targets the RING E3 ubiquitin ligase APIP6 to suppress pathogen-associated molecular pattern-triggered immunity in rice. Plant Cell 24 (11):4748-4762. doi:10.1105/tpc.112.105429

Pedersen C, Ver Loren van Themaat E, McGuffin LJ, Abbott JC, Burgis TA, Barton G, Bindschedler LV, Lu X, Maekawa T, Wessling R, Cramer R, Thordal-Christensen H, Panstruga R, Spanu PD (2012) Structure and evolution of barley powdery mildew effector

candidates. BMC Genomics 13:694. doi:10.1186/1471-2164-13-694

Pedley KF, Martin GB (2003) Molecular basis of *Pto*-mediated resistance to bacterial speck disease in tomato. Annu Rev Phytopathol 41:215-243. doi:10.1146/annurev.phyto.41.121602.143032

Pena PV, Davrazou F, Shi X, Walter KL, Verkhusha VV, Gozani O, Zhao R, Kutateladze TG (2006) Molecular mechanism of histone H3K4me3 recognition by plant homeodomain of ING2. Nature 442 (7098):100-103. doi:10.1038/nature04814

Periyannan S, Moore J, Ayliffe M, Bansal U, Wang X, Huang L, Deal K, Luo M, Kong X, Bariana H, Mago R, McIntosh R, Dodds P, Dvorak J, Lagudah E (2013) The gene *Sr33*, an ortholog of barley Mla genes, encodes resistance to wheat stem rust race Ug99. Science 341 (6147):786-788. doi:10.1126/science.1239028

Petre B, Joly DL, Duplessis S (2014) Effector proteins of rust fungi. Front Plant Sci 5:416. doi:10.3389/fpls.2014.00416

Petre B, Lorrain C, Saunders DG, Win J, Sklenar J, Duplessis S, Kamoun S (2016) Rust fungal effectors mimic host transit peptides to translocate into chloroplasts. Cell Microbiol 18 (4):453-465. doi:10.1111/cmi.12530

Petre B, Saunders DG, Sklenar J, Lorrain C, Win J, Duplessis S, Kamoun S (2015) Candidate effector proteins of the rust pathogen *Melampsora larici-populina* target diverse plant cell compartments. Mol Plant Microbe Interact 28 (6):689-700. doi:10.1094/MPMI-01-15-0003-R

Pretorius ZA, Singh RP, Wagoire WW, Payne TS (2000) Detection of virulence to wheat stem rust resistance gene *Sr31* in *Puccinia graminis* f. sp. *tritici* in Uganda. Plant Dis 84 (2):203

Pretsch K, Kemen A, Kemen E, Geiger M, Mendgen K, Voegele R (2013) The rust transferred proteins-a new family of effector proteins exhibiting protease inhibitor function. Mol Plant Pathol 14 (1):96-107. doi:10.1111/j.1364-3703.2012.00832.x

Qiao Y, Shi J, Zhai Y, Hou Y, Ma W (2015) *Phytophthora* effector targets a novel component of small RNA pathway in plants to promote infection. Proc Natl Acad Sci U S A 112 (18):5850-5855. doi:10.1073/pnas.1421475112

Rafiqi M, Ellis JG, Ludowici VA, Hardham AR, Dodds PN (2012) Challenges and progress towards understanding the role of effectors in plant-fungal interactions. Curr Opin Plant Biol 15 (4):477-482. doi:10.1016/j.pbi.2012.05.003

Rafiqi M, Gan PH, Ravensdale M, Lawrence GJ, Ellis JG, Jones DA, Hardham AR, Dodds PN (2010) Internalization of flax rust avirulence proteins into flax and tobacco cells can occur in the

absence of the pathogen. Plant Cell 22 (6):2017-2032. doi:10.1105/tpc.109.072983
Ragvin A, Valvatne H, Erdal S, Arskog V, Tufteland KR, Breen K, AM OY, Eberharter A, Gibson TJ, Becker PB, Aasland R (2004) Nucleosome binding by the bromodomain and PHD finger of the transcriptional cofactor p300. J Mol Biol 337 (4):773-788. doi:10.1016/j.jmb.2004.01.051
Ranf S, Gisch N, Schaffer M, Illig T, Westphal L, Knirel YA, Sanchez-Carballo PM, Zahringer U, Huckelhoven R, Lee J, Scheel D (2015) A lectin S-domain receptor kinase mediates lipopolysaccharide sensing in *Arabidopsis thaliana*. Nat Immunol 16 (4):426-433. doi:10.1038/ni.3124
Ravensdale M, Nemri A, Thrall PH, Ellis JG, Dodds PN (2011) Co-evolutionary interactions between host resistance and pathogen effector genes in flax rust disease. Mol Plant Pathol 12 (1):93-102. doi:10.1111/j.1364-3703.2010.00657.x
Redkar A, Hoser R, Schilling L, Zechmann B, Krzymowska M, Walbot V, Doehlemann G (2015) A secreted effector protein of *Ustilago maydis* guides maize leaf cells to form tumors. Plant Cell 27 (4):1332-1351. doi:10.1105/tpc.114.131086
Ridout CJ, Skamnioti P, Porritt O, Sacristan S, Jones JD, Brown JK (2006) Multiple avirulence paralogues in cereal powdery mildew fungi may contribute to parasite fitness and defeat of plant resistance. Plant Cell 18 (9):2402-2414. doi:10.1105/tpc.106.043307
Rooney HCE, van't Klooster JW, van der Hoorn RAL, Joosten MHAJ, Jones JDG, de Wit PJGM (2005) *Cladosporium* Avr2 inhibits tomato Rcr3 protease required for *Cf-2*-dependent disease resistance. Science 308 (5729):1783-1786. doi:10.1126/science.1111404
Rose JK, Ham KS, Darvill AG, Albersheim P (2002) Molecular cloning and characterization of glucanase inhibitor proteins: coevolution of a counterdefense mechanism by plant pathogens. Plant Cell 14 (6):1329-1345
Rosebrock TR, Zeng L, Brady JJ, Abramovitch RB, Xiao F, Martin GB (2007) A bacterial E3 ubiquitin ligase targets a host protein kinase to disrupt plant immunity. Nature 448 (7151):370-374. doi:10.1038/nature05966
Rzymski T, Grzmil P, Meinhardt A, Wolf S, Burfeind P (2008) PHF5A represents a bridge protein between splicing proteins and ATP-dependent helicases and is differentially expressed during mouse spermatogenesis. Cytogenet Genome Res 121 (3-4):232-244. doi:10.1159/000138890
Saintenac C, Zhang W, Salcedo A, Rouse MN, Trick HN, Akhunov E, Dubcovsky J (2013) Identification of wheat gene *Sr35* that confers

resistance to Ug99 stem rust race group. Science 341 (6147):783-786. doi:10.1126/science.1239022

Saksouk N, Avvakumov N, Champagne KS, Hung T, Doyon Y, Cayrou C, Paquet E, Ullah M, Landry AJ, Cote V, Yang XJ, Gozani O, Kutateladze TG, Cote J (2009) HBO1 HAT complexes target chromatin throughout gene coding regions via multiple PHD finger interactions with histone H3 tail. Mol Cell 33 (2):257-265. doi:10.1016/j.molcel.2009.01.007

Salcedo A, Rutter W, Wang S, Akhunova A, Bolus S, Chao S, Anderson N, De Soto MF, Rouse M, Szabo L, Bowden RL, Dubcovsky J, Akhunov E (2017) Variation in the *AvrSr35* gene determines *Sr35* resistance against wheat stem rust race Ug99. Science 358 (6370):1604-1606. doi:10.1126/science.aao7294

Salmeron JM, Oldroyd GE, Rommens CM, Scofield SR, Kim HS, Lavelle DT, Dahlbeck D, Staskawicz BJ (1996) Tomato *Prf* is a member of the leucine-rich repeat class of plant disease resistance genes and lies embedded within the *Pto* kinase gene cluster. Cell 86 (1):123-133

Sanchez-Vallet A, Saleem-Batcha R, Kombrink A, Hansen G, Valkenburg DJ, Thomma BPHJ, Mesters JR (2013) Fungal effector Ecp6 outcompetes host immune receptor for chitin binding through intrachain LysM dimerization. Elife 2:e00790. doi:10.7554/eLife.00790

Sanchez R, Zhou MM (2011) The PHD finger: a versatile epigenome reader. Trends Biochem Sci 36 (7):364-372. doi:10.1016/j.tibs.2011.03.005

Sarkar M, Ghosh MK (2016) DEAD box RNA helicases: crucial regulators of gene expression and oncogenesis. Front Biosci (Landmark Ed) 21:225-250

Schindler U, Beckmann H, Cashmore AR (1993) HAT3.1, a novel Arabidopsis homeodomain protein containing a conserved cysteine-rich region. Plant J 4 (1):137-150

Schmidt SM, Kuhn H, Micali C, Liller C, Kwaaitaal M, Panstruga R (2014) Interaction of a *Blumeria graminis* f. sp *hordei* effector candidate with a barley ARF-GAP suggests that host vesicle trafficking is a fungal pathogenicity target. Molecular Plant Pathology 15 (6):535-549. doi:10.1111/mpp.12110

Schornack S, van Damme M, Bozkurt TO, Cano LM, Smoker M, Thines M, Gaulin E, Kamoun S, Huitema E (2010) Ancient class of translocated oomycete effectors targets the host nucleus. Proc Natl Acad Sci U S A 107 (40):17421-17426. doi:10.1073/pnas.1008491107

Seitner D, Uhse S, Gallei M, Djamei A (2018) The core effector Cce1 is required for early infection of maize by *Ustilago maydis*. Mol Plant Pathol. doi:10.1111/mpp.12698

Shabab M, Shindo T, Gu C, Kaschani F, Pansuriya T, Chintha R, Harzen A, Colby T, Kamoun S, van der Hoorn RAL (2008) Fungal effector protein AVR2 targets diversifying defense-related cys proteases of tomato. Plant Cell 20 (4):1169-1183. doi:10.1105/tpc.107.056325

Shan L, He P, Li J, Heese A, Peck SC, Nurnberger T, Martin GB, Sheen J (2008) Bacterial effectors target the common signaling partner BAK1 to disrupt multiple MAMP receptor-signaling complexes and impede plant immunity. Cell Host Microbe 4 (1):17-27. doi:10.1016/j.chom.2008.05.017

Shao F, Golstein C, Ade J, Stoutemyer M, Dixon JE, Innes RW (2003) Cleavage of *Arabidopsis* PBS1 by a bacterial type III effector. Science 301 (5637):1230-1233. doi:10.1126/science.1085671

Shen QH, Zhou F, Bieri S, Haizel T, Shirasu K, Schulze-Lefert P (2003) Recognition specificity and RAR1/SGT1 dependence in barley Mla disease resistance genes to the powdery mildew fungus. Plant Cell 15 (3):732-744

Siegel TN, Hekstra DR, Kemp LE, Figueiredo LM, Lowell JE, Fenyo D, Wang X, Dewell S, Cross GA (2009) Four histone variants mark the boundaries of polycistronic transcription units in *Trypanosoma brucei*. Genes Dev 23 (9):1063-1076. doi:10.1101/gad.1790409

Singh RP, Hodson DP, Huerta-Espino J, Jin Y, Bhavani S, Njau P, Herrera-Foessel S, Singh PK, Singh S, Govindan V (2011) The emergence of Ug99 races of the stem rust fungus is a threat to world wheat production. Annu Rev Phytopathol 49:465-481. doi:10.1146/annurev-phyto-072910-095423

Skibbe DS, Doehlemann G, Fernandes J, Walbot V (2010) Maize tumors caused by *Ustilago maydis* require organ-specific genes in host and pathogen. Science 328 (5974):89-92. doi:10.1126/science.1185775

Song T, Ma Z, Shen D, Li Q, Li W, Su L, Ye T, Zhang M, Wang Y, Dou D (2015) An Oomycete CRN Effector Reprograms Expression of Plant HSP Genes by Targeting their Promoters. PLoS Pathog 11 (12):e1005348. doi:10.1371/journal.ppat.1005348

Spanu PD, Abbott JC, Amselem J, Burgis TA, Soanes DM, Stuber K, Ver Loren van Themaat E, Brown JK, Butcher SA, Gurr SJ, Lebrun MH, Ridout CJ, Schulze-Lefert P, Talbot NJ, Ahmadinejad N, Ametz C, Barton GR, Benjdia M, Bidzinski P, Bindschedler LV, Both M, Brewer MT, Cadle-Davidson L, Cadle-Davidson MM, Collemare J, Cramer R, Frenkel O, Godfrey D, Harriman J, Hoede C, King BC,

Klages S, Kleemann J, Knoll D, Koti PS, Kreplak J, Lopez-Ruiz FJ, Lu X, Maekawa T, Mahanil S, Micali C, Milgroom MG, Montana G, Noir S, O'Connell RJ, Oberhaensli S, Parlange F, Pedersen C, Quesneville H, Reinhardt R, Rott M, Sacristan S, Schmidt SM, Schon M, Skamnioti P, Sommer H, Stephens A, Takahara H, Thordal-Christensen H, Vigouroux M, Wessling R, Wicker T, Panstruga R (2010) Genome expansion and gene loss in powdery mildew fungi reveal tradeoffs in extreme parasitism. Science 330 (6010):1543-1546. doi:10.1126/science.1194573

Sperschneider J, Dodds PN, Gardiner DM, Singh KB, Taylor JM (2018) Improved prediction of fungal effector proteins from secretomes with EffectorP 2.0. Mol Plant Pathol. doi:10.1111/mpp.12682

Sperschneider J, Gardiner DM, Dodds PN, Tini F, Covarelli L, Singh KB, Manners JM, Taylor JM (2016) EffectorP: predicting fungal effector proteins from secretomes using machine learning. New Phytol 210 (2):743-761. doi:10.1111/nph.13794

Stam R, Jupe J, Howden AJ, Morris JA, Boevink PC, Hedley PE, Huitema E (2013) Identification and characterisation CRN effectors in *Phytophthora capsici* shows modularity and functional diversity. PLoS One 8 (3):e59517. doi:10.1371/journal.pone.0059517

Sukarta OCA, Slootweg EJ, Goverse A (2016) Structure-informed insights for NLR functioning in plant immunity. Semin Cell Dev Biol 56:134-149. doi:10.1016/j.semcdb.2016.05.012

Sutton PN, Henry MJ, Hall JL (1999) Glucose, and not sucrose, is transported from wheat to wheat powdery mildew. Planta 208:426–430

Takemoto D, Jones DA (2005) Membrane release and destabilization of *Arabidopsis* RIN4 following cleavage by *Pseudomonas syringae* AvrRpt2. Mol Plant Microbe Interact 18 (12):1258-1268. doi:10.1094/MPMI-18-1258

Tanaka S, Brefort T, Neidig N, Djamei A, Kahnt J, Vermerris W, Koenig S, Feussner K, Feussner I, Kahmann R (2014) A secreted *Ustilago maydis* effector promotes virulence by targeting anthocyanin biosynthesis in maize. Elife 3:e01355. doi:10.7554/eLife.01355

Tang D, Wang G, Zhou JM (2017) Receptor Kinases in Plant-Pathogen Interactions: More Than Pattern Recognition. Plant Cell 29 (4):618-637. doi:10.1105/tpc.16.00891

Tang X, Frederick RD, Zhou J, Halterman DA, Jia Y, Martin GB (1996) Initiation of plant disease resistance by physical interaction of AvrPto and Pto kinase. Science 274 (5295):2060-2063

Taverna SD, Ilin S, Rogers RS, Tanny JC, Lavender H, Li H, Baker L, Boyle J, Blair LP, Chait BT, Patel DJ, Aitchison JD, Tackett AJ, Allis CD (2006) Yng1 PHD finger binding to H3 trimethylated at K4

promotes NuA3 HAT activity at K14 of H3 and transcription at a subset of targeted ORFs. Mol Cell 24 (5):785-796. doi:10.1016/j.molcel.2006.10.026

Thomas CM, Jones DA, Parniske M, Harrison K, Balint-Kurti PJ, Hatzixanthis K, Jones JD (1997) Characterization of the tomato *Cf-4* gene for resistance to *Cladosporium fulvum* identifies sequences that determine recognitional specificity in Cf-4 and Cf-9. Plant Cell 9 (12):2209-2224

Tian M, Win J, Song J, van der Hoorn R, van der Knaap E, Kamoun S (2007) A *Phytophthora infestans* cystatin-like protein targets a novel tomato papain-like apoplastic protease. Plant Physiol 143 (1):364-377. doi:10.1104/pp.106.090050

Tissera P, Ayres PG (1986) Transpiration and the water relations of faba bean (*Vicia faba*) infected by rust (*Uromyces viciae-fabae*). New Phytol 102:385–395

Tyler BM (2001) Genetics and genomics of the oomycete-host interface. Trends Genet 17 (11):611-614

Tyler BM (2007) *Phytophthora sojae*: root rot pathogen of soybean and model oomycete. Mol Plant Pathol 8 (1):1-8. doi:10.1111/j.1364-3703.2006.00373.x

Ustun S, Sheikh A, Gimenez-Ibanez S, Jones A, Ntoukakis V, Bornke F (2016) The proteasome acts as a hub for plant immunity and is targeted by *Pseudomonas* type III effectors. Plant Physiol 172 (3):1941-1958. doi:10.1104/pp.16.00808

van Damme M, Bozkurt TO, Cakir C, Schornack S, Sklenar J, Jones AM, Kamoun S (2012) The Irish potato famine pathogen *Phytophthora infestans* translocates the CRN8 kinase into host plant cells. PLoS Pathog 8 (8):e1002875. doi:10.1371/journal.ppat.1002875

van den Burg HA, Harrison SJ, Joosten MHAJ, Vervoort J, de Wit PJGM (2006) *Cladosporium fulvum* Avr4 protects fungal cell walls against hydrolysis by plant chitinases accumulating during infection. Mol Plant Microbe Interact 19 (12):1420-1430. doi:10.1094/MPMI-19-1420

van der Hoorn RAL, Kamoun S (2008) From Guard to Decoy: A new model for perception of plant pathogen effectors. Plant Cell 20 (8):2009-2017. doi:10.1105/tpc.108.060194

van Esse HP, Bolton MD, Stergiopoulos I, de Wit PJGM, Thomma BPHJ (2007) The chitin-binding *Cladosporium fulvum* effector protein Avr4 is a virulence factor. Mol Plant Microbe Interact 20 (9):1092-1101. doi:10.1094/MPMI-20-9-1092

van Kan JAL, van den Ackerveken GFJM, de Wit PJGM (1991) Cloning and characterization of cDNA of avirulence gene *avr9* of the fungal

pathogen *Cladosporium fulvum*, causal agent of tomato leaf mold. Mol Plant Microbe Interact 4 (1):52 - 59

Vespa L, Vachon G, Berger F, Perazza D, Faure JD, Herzog M (2004) The immunophilin-interacting protein AtFIP37 from Arabidopsis is essential for plant development and is involved in trichome endoreduplication. Plant Physiol 134 (4):1283-1292. doi:10.1104/pp.103.028050

Voegele RT (2006) Uromyces fabae: development, metabolism, and interactions with its host *Vicia faba*. FEMS Microbiol Lett 259 (2):165-173. doi:10.1111/j.1574-6968.2006.00248.x

Voegele RT, Mendgen KW (2011) Nutrient uptake in rust fungi: how sweet is parasitic life? Euphytica 179 (1):41-55. doi:10.1007/s10681-011-0358-5

Voegele RT, Wirsel S, Moll U, Lechner M, Mendgen K (2006) Cloning and characterization of a novel invertase from the obligate biotroph *Uromyces fabae* and analysis of expression patterns of host and pathogen invertases in the course of infection. Mol Plant Microbe Interact 19 (6):625-634. doi:10.1094/MPMI-19-0625

Wan L, Koeck M, Williams SJ, Ashton AR, Lawrence GJ, Sakakibara H, Kojima M, Bottcher C, Ericsson DJ, Hardham AR, Jones DA, Ellis JG, Kobe B, Dodds PN (2019) Structural and functional insights into the modulation of the activity of a flax cytokinin oxidase by flax rust effector AvrL567-A. Mol Plant Pathol 20 (2):211-222. doi:10.1111/mpp.12749

Wang CI, Guncar G, Forwood JK, Teh T, Catanzariti AM, Lawrence GJ, Loughlin FE, Mackay JP, Schirra HJ, Anderson PA, Ellis JG, Dodds PN, Kobe B (2007) Crystal structures of flax rust avirulence proteins AvrL567-A and -D reveal details of the structural basis for flax disease resistance specificity. Plant Cell 19 (9):2898-2912. doi:10.1105/tpc.107.053611

Wawra S, Belmonte R, Lobach L, Saraiva M, Willems A, van West P (2012) Secretion, delivery and function of oomycete effector proteins. Curr Opin Microbiol 15 (6):685-691. doi:10.1016/j.mib.2012.10.008

Wawra S, Trusch F, Matena A, Apostolakis K, Linne U, Zhukov I, Stanek J, Kozminski W, Davidson I, Secombes CJ, Bayer P, van West P (2017) The RxLR motif of the host targeting effector AVR3a of *Phytophthora infestans* is cleaved before secretion. Plant Cell 29 (6):1184-1195. doi:10.1105/tpc.16.00552

Whisson SC, Boevink PC, Moleleki L, Avrova AO, Morales JG, Gilroy EM, Armstrong MR, Grouffaud S, van West P, Chapman S, Hein I, Toth IK, Pritchard L, Birch PR (2007) A translocation signal for delivery

of oomycete effector proteins into host plant cells. Nature 450 (7166):115-118. doi:10.1038/nature06203

Williams SJ, Sohn KH, Wan L, Bernoux M, Sarris PF, Segonzac C, Ve T, Ma Y, Saucet SB, Ericsson DJ, Casey LW, Lonhienne T, Winzor DJ, Zhang X, Coerdt A, Parker JE, Dodds PN, Kobe B, Jones JD (2014) Structural basis for assembly and function of a heterodimeric plant immune receptor. Science 344 (6181):299-303. doi:10.1126/science.1247357

Win J, Chaparro-Garcia A, Belhaj K, Saunders DG, Yoshida K, Dong S, Schornack S, Zipfel C, Robatzek S, Hogenhout SA, Kamoun S (2012) Effector biology of plant-associated organisms: concepts and perspectives. Cold Spring Harb Symp Quant Biol 77:235-247. doi:10.1101/sqb.2012.77.015933

Wu J, van der Burgh AM, Bi G, Zhang L, Alfano JR, Martin GB, Joosten M (2018) The bacterial effector AvrPto targets the regulatory coreceptor SOBIR1 and suppresses defense signaling mediated by the receptor-like protein Cf-4. Mol Plant Microbe Interact 31 (1):75-85. doi:10.1094/MPMI-08-17-0203-FI

Xiang T, Zong N, Zhang J, Chen J, Chen M, Zhou JM (2011) BAK1 is not a target of the *Pseudomonas syringae* effector AvrPto. Mol Plant Microbe Interact 24 (1):100-107. doi:10.1094/MPMI-04-10-0096

Xiang T, Zong N, Zou Y, Wu Y, Zhang J, Xing W, Li Y, Tang X, Zhu L, Chai J, Zhou JM (2008) *Pseudomonas syringae* effector AvrPto blocks innate immunity by targeting receptor kinases. Curr Biol 18 (1):74-80. doi:10.1016/j.cub.2007.12.020

Xiao F, He P, Abramovitch RB, Dawson JE, Nicholson LK, Sheen J, Martin GB (2007) The N-terminal region of *Pseudomonas* type III effector AvrPtoB elicits *Pto*-dependent immunity and has two distinct virulence determinants. Plant J 52 (4):595-614. doi:10.1111/j.1365-313X.2007.03259.x

Xing W, Zou Y, Liu Q, Liu J, Luo X, Huang Q, Chen S, Zhu L, Bi R, Hao Q, Wu JW, Zhou JM, Chai J (2007) The structural basis for activation of plant immunity by bacterial effector protein AvrPto. Nature 449 (7159):243-247. doi:10.1038/nature06109

Xu J, Liu C, Li M, Hu J, Zhu L, Zeng D, Yang Y, Peng Y, Ruan B, Guo L, Li H (2015) A rice DEAD-box RNA helicase protein, OsRH17, suppresses 16S ribosomal RNA maturation in *Escherichia coli*. Gene 555 (2):318-328. doi:10.1016/j.gene.2014.11.025

Xu Q, Liang S, Kudla J, Luan S (1998) Molecular characterization of a plant FKBP12 that does not mediate action of FK506 and rapamycin. Plant J 15 (4):511-519

Yoon GM, Kieber JJ (2013) 14-3-3 regulates 1-aminocyclopropane-1-carboxylate synthase protein turnover in *Arabidopsis*. Plant Cell 25 (3):1016-1028. doi:10.1105/tpc.113.110106

Yu Y, Li Y, Huang G, Meng Z, Zhang D, Wei J, Yan K, Zheng C, Zhang L (2011) PwHAP5, a CCAAT-binding transcription factor, interacts with PwFKBP12 and plays a role in pollen tube growth orientation in *Picea wilsonii*. J Exp Bot 62 (14):4805-4817. doi:10.1093/jxb/err120

Yue J, Xu W, Ban R, Huang S, Miao M, Tang X, Liu G, Liu Y (2016) PTIR: Predicted Tomato Interactome Resource. Sci Rep 6:25047. doi:10.1038/srep25047

Zhang D, Burroughs AM, Vidal ND, Iyer LM, Aravind L (2016) Transposons to toxins: the provenance, architecture and diversification of a widespread class of eukaryotic effectors. Nucleic Acids Res 44 (8):3513-3533. doi:10.1093/nar/gkw221

Zhang J, Li W, Xiang T, Liu Z, Laluk K, Ding X, Zou Y, Gao M, Zhang X, Chen S, Mengiste T, Zhang Y, Zhou JM (2010) Receptor-like cytoplasmic kinases integrate signaling from multiple plant immune receptors and are targeted by a *Pseudomonas syringae* effector. Cell Host Microbe 7 (4):290-301. doi:10.1016/j.chom.2010.03.007

Zhang J, Shao F, Li Y, Cui H, Chen L, Li H, Zou Y, Long C, Lan L, Chai J, Chen S, Tang X, Zhou JM (2007) A *Pseudomonas syringae* effector inactivates MAPKs to suppress PAMP-induced immunity in plants. Cell Host Microbe 1 (3):175-185. doi:10.1016/j.chom.2007.03.006

Zhang WJ, Pedersen C, Kwaaitaal M, Gregersen PL, Morch SM, Hanisch S, Kristensen A, Fuglsang AT, Collinge DB, Thordal-Christensen H (2012) Interaction of barley powdery mildew effector candidate CSEP0055 with the defence protein PR17c. Mol Plant Pathol 13 (9):1110-1119. doi:10.1111/j.1364-3703.2012.00820.x

Zhang X, Farah N, Rolston L, Ericsson DJ, Catanzariti AM, Bernoux M, Ve T, Bendak K, Chen C, Mackay JP, Lawrence GJ, Hardham A, Ellis JG, Williams SJ, Dodds PN, Jones DA, Kobe B (2018) Crystal structure of the *Melampsora lini* effector AvrP reveals insights into a possible nuclear function and recognition by the flax disease resistance protein P. Mol Plant Pathol 19 (5):1196-1209. doi:10.1111/mpp.12597

Zhou H, Lin J, Johnson A, Morgan RL, Zhong W, Ma W (2011) *Pseudomonas syringae* type III effector HopZ1 targets a host enzyme to suppress isoflavone biosynthesis and promote infection in soybean. Cell Host Microbe 9 (3):177-186. doi:10.1016/j.chom.2011.02.007

Zipfel C, Kunze G, Chinchilla D, Caniard A, Jones JD, Boller T, Felix G (2006) Perception of the bacterial PAMP EF-Tu by the receptor EFR restricts Agrobacterium-mediated transformation. Cell 125 (4):749-760. doi:10.1016/j.cell.2006.03.037

Appendix 1 Gene sequences

Signal Peptide, same sequence for all AvrP variants :
ATGCTTTTCAAACAATGCACTGCTTTGAAATTCTTAATCTTCATATTGGGATTTTCAATCATAGC
TGCA

- **AvrP**

CAGTCTAATCCTAATCAAGAGCTTGGAGTGGTTCAATGTCTTTGCAGACGAATCGCTCCTCTGA
CTCAACCACCATTTGGTGTGAGATGTCGAGCCACCTTGAATTGTCCGTGTGATTATATAGGAG
ACTGTCCAGGACCTGCTGAACAATATATGTACCGCTGCCCTAATTGTGGTCCGCGTTCACATGT
CGCGTGTTCCGGGGTCCATCAAGGGACTTGTCAACAGGTACACCCTGGGAAAGACAGTGTGG
AGTACGGAGGTTAG

- **271**

CAGTCTAACCCTAATCAACAGCTTGGAGTGGTTCAATGTCTTTGCAGACGAATCGCTCCTCTGA
CTCAACCACCATTTGGTGTGAGATGTCGAGCCACCGTGAATTGTCCGTGTGATTATATAGGAG
CCTGTTCAGGACGTGCTGAACAATATATGTACCGCTGCCCTAATTGTGGTCCGCGTTCACATGT
CGCGTGTACCGGGGTCCATGAAGGGACTTGTCAACAGGTACACCCTGGGAAAGACAGTGTGC
AGTACGGAGGTTAG

- **339**

CAGTCTAACCCTAATCAAGAGCTTGGAGTGGTTGAATGTCTTTGCAGACGAATCGCTCCTCTG
ACTCAACCACCATTTGGTGTGAGATGTCGAGCCACCTTGAATTGTCCGTGTGATTATATAGGA
GACTGTCCAGGACCTGCTGAACAATATATGTACCGCTGCCCTAATTGTGGTCCGCGTTCACAT
GTCGCGTGTTCCGGGGTCCATCGAGGGACTTGTCAACAGGTACACCCTGGGATAGCCAGTGT
GCAGTACCAAGATTAG

- **AvrP123**

CAGTATGTTGTTGATCCAGGGTTTGGAGAGATTGAATGTATGTGCGGACAAATCGCTCGTCTG
ACTCAACGACCATTTGATGTGGAATGTGAAGCCACCCCAAGTTGTTCGTGTGATTATAGAGGA
GACTGTCCAGGACCTGCTGCAGAATATGTGTACCGCTGCCCTACTTGTGGTCCGCGTTCACAT
GTCGGGTGTTTCGGGGTCCATCAAGGGACTTGTGAAGAGGTACACCCTGGGATAGCCAGGGT
GCAATACCAAAATTCTGACTCGGAGTCAGAATGA

- **WA**

CAGTATGTTGTTGATCCAGGGCTTGGAGAGGTTAAATGTATGTGCGGACAAATCGCTCCTCTG
ACTCAACGACCACTTGATGTGGAATGTGAAGCCACCCCAAAGTGTTCGTGTGATTATACAGGA
GACTGTCCAGGACCTGCTGCAGAATATGTGTACCGCTGCCCTACTTGTGGTCCGCGTTCACAT
GTCGGGTGTATCGGGGTCCATCAAGGGACTTGTGAAGAGGTACACCCTGGGATAGCCAGGGT
GGAATACCCAAATTCTGACTCGGAGTCAGAATGA

- **bs25**

CAGTCTAATCCTAATCAAGAGCTTGGAGTGGTTCAATGTCTTTGCAGACGAATCGCTCCTCTGA
CTCAACCACCATTTGGTGTGAGATGTCGAGCCACCTTGAATTGTCCGTGTGATTATAGAGGAG
ACTGTCCAGGACCTGCTGCAGAATATGTGTACCGCTGCCCTACTTGTGGTCCGCGTTCACATGT
CGGGTGTTTCGGGGTCCATCAAGGGACTTGTGAAGAGGTACACCCTGGGATAGCCAGGGTGC
AATACCAAAATTCTGACTCGGAGTCAGAATGA

- **3x HA tag**

gtaTAtggATAtGATGTccCTGACTATGCGGGCTATCCCTATGACGTCCCGGACTATGCAGGATCC
TATCCATATGACGTTCCAGATTACGCTtag

Sequences of putative AvrP interactors

DNA sequences highlighted in yellow matches to AvrP putative interactors based on the BLAST N search results.

- **Hypothetical protein *Melampsora larici-populina***

TGACGGAAATTGCGGAACCTACAACACCTCTACTGACCTTGGCGTGTGCGTTTGGTCAGCAGC
GATCCGACTGGAAACAGCACAACTGACAACGGGTGGTTGAACAAAGCCACTACTGACAACTG
CAACAAACAAATCTACATGCAACGTCAAGGCCAACCCGACACCGTTCAGCTTGTCCCCGTCATC
GACTCTTGCAACTTTAACACTGTGGACCCTGCGCTCGGCTGCTTCCAGGTTTTCGTGACCAGAG
CTCTGTACGACTTATTTAATGCGACTCAAGCGGAGTTACAATCTGGATCGTTGTACAACATCAC
CTGGGACTTCAACATTGGATCATCTGAGAACCGTCAGCCCGGCCCCATCTGATAGTGGTTCTT
GTATTGCTTGGTCTTACCGTCCTCCCGTCATGGAATTATGTTATCTCTGTGCC

- **cytoplasmic PGM1**

CGAGAATGTTGATGCAGGTGCAGCAAAAGAACTGATGGCAAATTTGGTCAGCCTCCAATCAA
ACCTTGCTGGAGTTAACGAGACTGTGAAGGAGATCCGATCAGATGTCTCCAAGGTCGTCAAC
GCTGATGAATTCGAGTACAAAGACCCTGTCGATGGTTCCATCTCAGCACACCAAGGTGTTCGA
TATTTGTTCGAGGATGGCTCTCGACTGGTTTTCCGCCTTTCAGGAACTGGATCAGTGGGCGCG
ACCATCCGTCTCTACATCGAACAGTACGAGAAGGATCCATTGAAGATCGGCAGAGAGTCTCTG
GACGCACTTTCACCTCTGGTTGAGGTCGCTTTGAAACTGTCCAAAATGCAAGAATACACCGGC
CGATCTGCTCCCACCGTCATCACATAGATCGCGTTTGCTCCACAAAGTTTGGATCCGATCGCAC
TTTTGAAATGGCGAAATTTTTTGGTTCTTTATGTTTGGCCACTATTCTGCTACTTTGACATGGTG
TTCTTCATGTTCTGAAATAATGTTGAGAGCCTGATTTTCTAGGTTGTTGATTGTTATAGATTCAC
CCATTAACCATAACAATCAAAACCGTTAGAAAAATTATAGTTTAATTTCATTTGG

- **cytoplasmic PGM2**

GATGGCCAATTTGGTCAGCCTTCAATCAAACCTGGCTGGAGTTAACGAGATTGTGAAGGGGA
TCCGATCAGATGTCTCCAAGGTCGTCAACGCTGACGAATTCGAGTACAAAGACCCTGTCGATG
GTTCCATCTCAGCTCACCAAGGTGTTCGATATTTGTTCGAGGATGGCTCTCGACTGGTTTTCCG
CCTTTCAGGAACTGGATCTGTGGGCGCGACAATCCGTCTCTATATTGAGCAGTACGAGAAGGA
TCCATCGAAGATCGGCAGAGAGTCTCAGGATGCACTTTCTCCTCTGGTTGAGGTAGCTTTGAA
ACTCTCTAAAATGCAAGAATACACCGGTCGATCTGCTCCGACAGTCATCACATAGTTCGCGTTT
GCTCCGCAAAATTTGGATATGATCGCACTCTCGAAATGGCGACGGTTTTTGGTTCTTTATGTTT
GGCCACTATTCTGCTCATTTGACACGGTGTTCTTCATGTTCTGAAATAATGTTGAGAGCCTGAT
TTTCTGGG

- **plastidial PGM**

ACCAATATGGAAGCTACACGCTGAAGTTTGCAGACGACTTCTCATACACCGATCCCGTTGATG
GTAGTGTGGCGTCGAAACAAGGTGTCCGGTTCGTGTTCAGTGATGGGTCAAGGATCATCTTCC
GCTTATCAGGAACCGGATCGGCAGGCGCAACAGTAAGAATCTACATCGAGCAGTTCGAACCG
GATGTCTCGAAACACGACCTGGATGCACAAAAGGCACTGAAGCCCCTCATAGATTTGGCACTC
TCGGTCTCGAAGCTGAAGGACTTCACCGGAAGAGAAAAACCCACTGTCATCACATAAAATGAC
AGATCAAATCCATCTCTAGCCGGTCCGAGATTTTGCGATATCTCGGTTAACTCAGAGCTGATTT
GGACGGGTGGGTCCACCTTTTTAGTAGTGGCTGCAGTAATTTAGTTTTAGTAGTATTAAAAGG

TGCGAAACAATAAAGAGAAGAGAGAAGCAAAAAATGAGATGCAAGCATAGAAGAGTCCTTG
ATCATGTCAAATAAATCTCAATCACTATATCG

- **FKBP12**

GAGCACCAAGGACCCTGGGCAGCAACCTTTCTCTTTCAATATTGGCAAGGGAAGCGTCATTAA
AGGATGGGATGAAGGTGTCATGGGAATGCAAGTGGGAGAAGTCGCTCGTTTACGGTGCTCCC
CAGACTACGCTTATGGAGCTAATGGATTTGGAGCATGGGGAATCTTGCCCAATTCGACTCTGG
TTTTTGAAATTGAAGTCCTGAGCTTAGAGTAATTCTATACTGAAGCCCTACCTCAGTGGTTGTT
GCACTACTTTCTTTCTTGGCCTTGTTTCTTTCTGTCTTTCTTATTGAATGTGCTTCAATAGTGCTT
AGAATAATGTCTACCTAGTGACTCTGGTA AAATGCCAGTTAAGTGTGGG AACTTTGATACC

- **DEAD-box RNA helicase 56**

AATTGACATAGAGCGTGTCAACATTGTTATCAACTACGACATGCCTGATTCTGCCGACACATAT
CTTCACAGGGTTGGTCGTGCTGGTAGGTTCGGAACAAAGGGTCTCGCAATTACGTTTGTTTCA
TCAGCTTCAGACTCAGATGTTCTCAATCAGGTTCAGGAGAGGTTCGAGGTGGACATTAAAGAA
CTTCCGGAGCAAATTGACACTTCAACATACATGCCCTCGTAATCGGAATAGTAGTGATGCAAG
TATGGAAATTGAGGATAATTCCAGATGAATTGAAGCTTGGATAATGCGTTAATGTAGCGGATA
GCTTTCTTGGTTTCGGAGGTGTAAGGTTGTTTGTTAGCAGGGAAAGGGTAGAGATGCAGGAC
GGTGGGCGCTCTGTTTGTCTTTCGTCGGCTGTGTAATCGATGAACAAAATGTTTTGATGCTCTT
AGTTTGCAGAATTTTTCGGGCCATCAGGACCTGTCAGTGGGTTGTGTAACAAATTTAGTTAAT
GAGCTTTATACAATAGTTACATTCTATT

Appendix 2 Plasmids

pL and pSoup

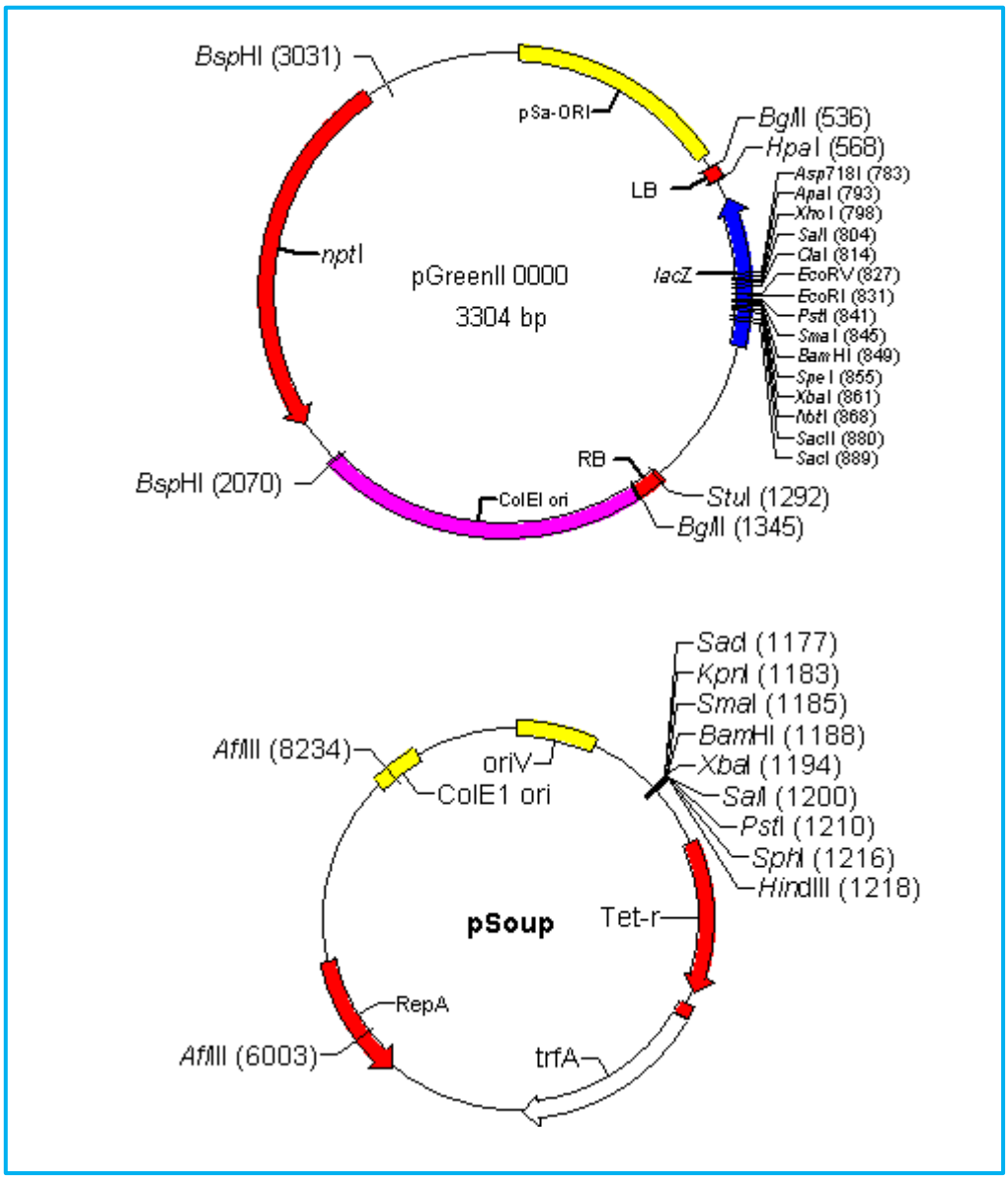

The ligation independent cloning (LIC) vectors are based on the pGreenII plant expression vector carrying *npt*I kanamycin resistance for selection in bacteria. The pSa-ori allows replication of pGreenII in *Agrobacterium,* but only if the corresponding replicase function is provided *in trans* by a separate plasmid called pSoup (note that pSoup is not required for replication of pGreenII in *E. coli*). pSoup carries the *TetR* tetracycline resistance gene for selection in bacteria. The pL vector contains:

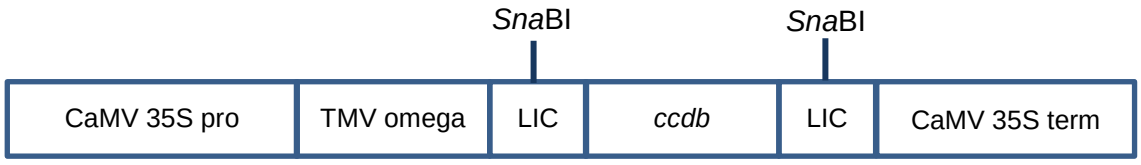

pENTRY TOPO Cloning

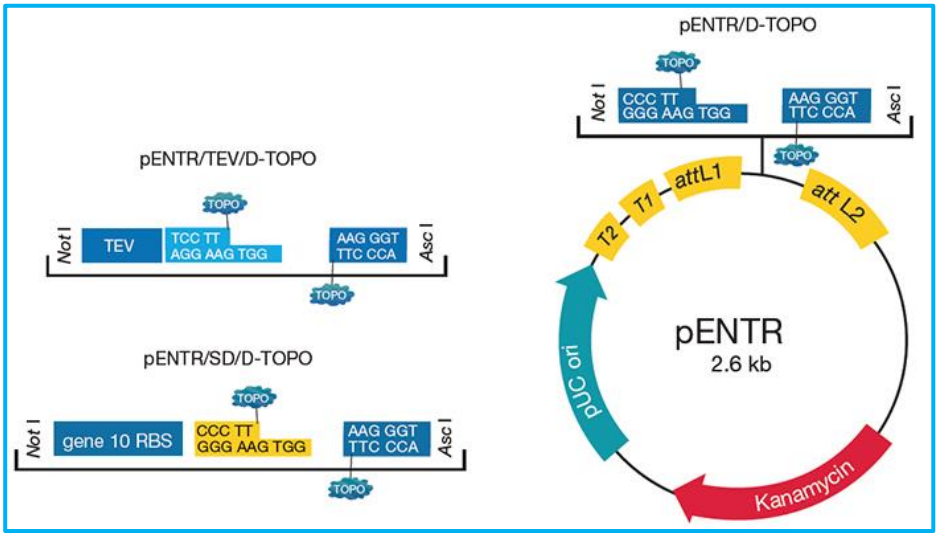

Source: Termo Fisher Scientific (www.thermofisher.com)

pEarlyGate104

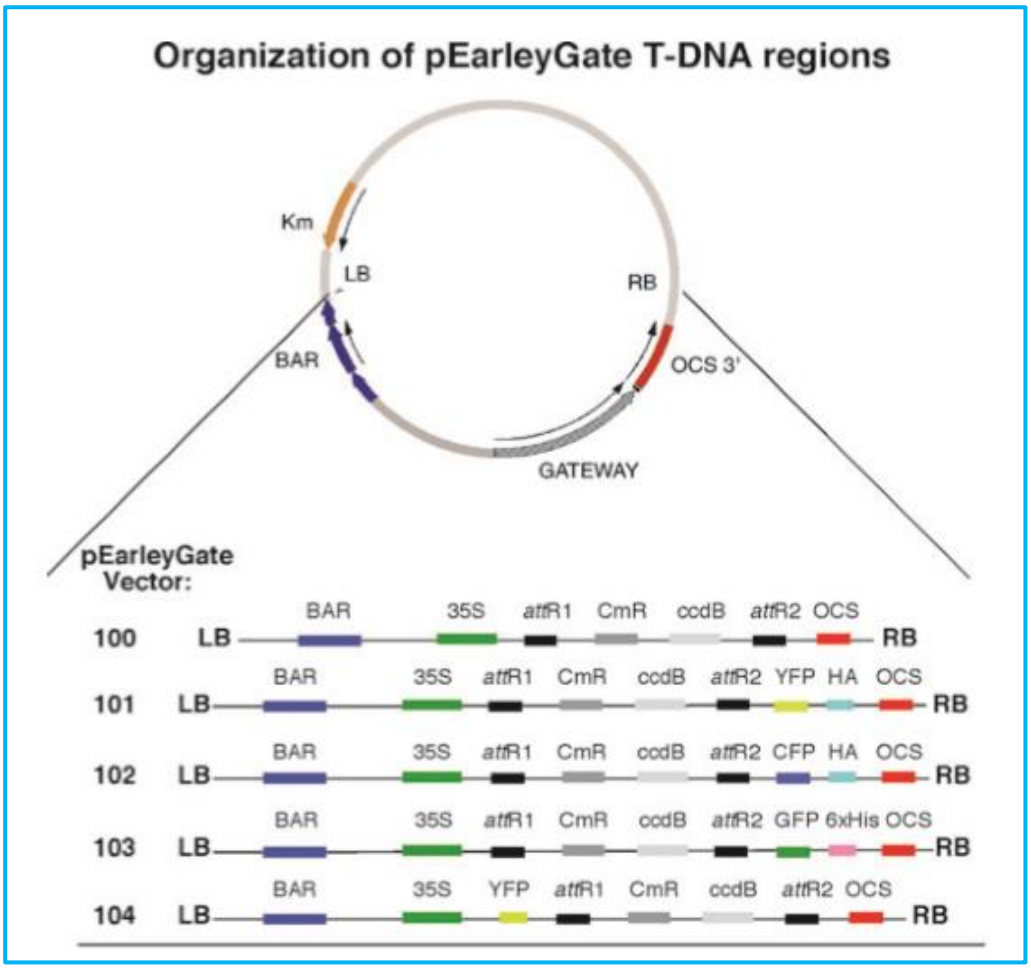

pGBG-NSC-GWY-Y2H (modified version of pGBT9; vector for bait AvrP-C8^{339})

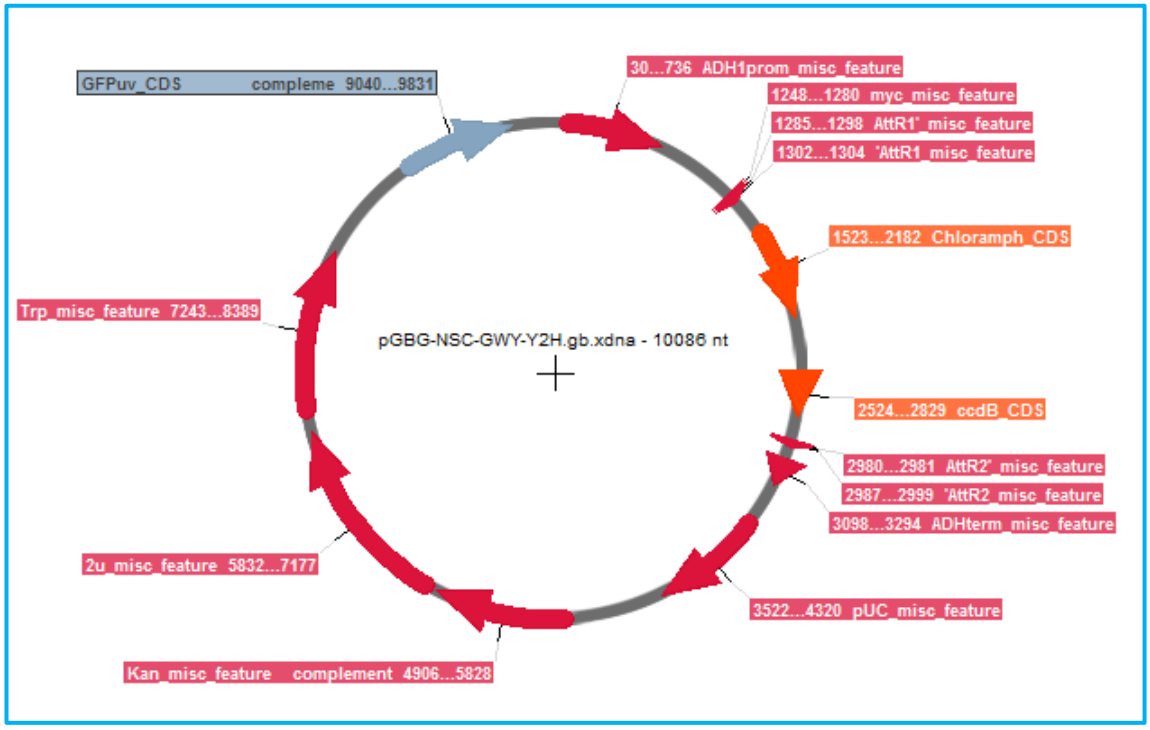

pGAD-GWY-Y2H (modified version of pGADT7; vector for Empty-AD)

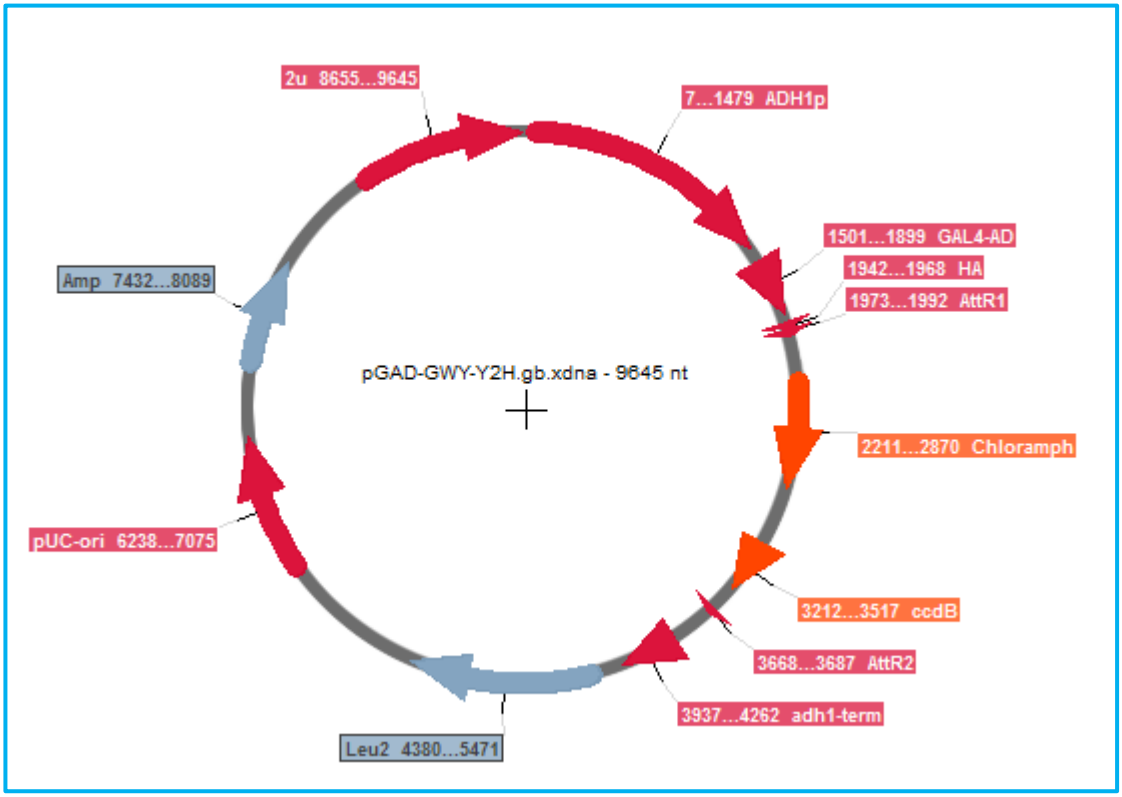

pGADT7-Rec (vector for cDNA library)

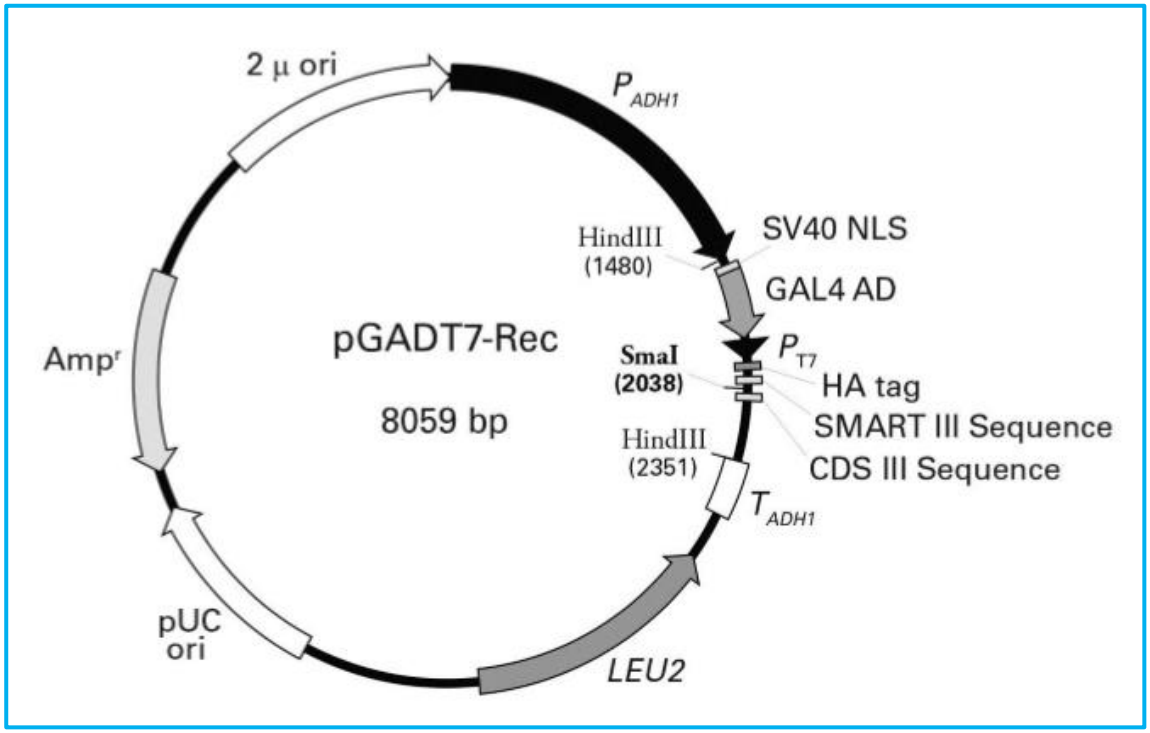

Appendix 3 Published paper

Molecular Plant Pathology

MOLECULAR PLANT PATHOLOGY (2018) 19(5), 1196–1209 DOI: 10.1111/mpp.12597

Crystal structure of the *Melampsora lini* effector AvrP reveals insights into a possible nuclear function and recognition by the flax disease resistance protein P

XIAOXIAO ZHANG[1,2,*], NADYA FARAH[3], LAURA ROLSTON[3], DANIEL J. ERICSSON[1,4], ANN-MAREE CATANZARITI[3], MAUD BERNOUX[2], THOMAS VE[1,5], KATERINA BENDAK[6], CHUNHONG CHEN[2], JOEL P. MACKAY[6], GREGORY J. LAWRENCE[2], ADRIENNE HARDHAM[3], JEFFREY G. ELLIS[2], SIMON J. WILLIAMS[1,3], PETER N. DODDS[2], DAVID A. JONES[3] AND BOSTJAN KOBE[1,*]

[1] *School of Chemistry and Molecular Biosciences, Australian Infectious Diseases Research Centre and Institute for Molecular Bioscience, University of Queensland, Brisbane, Queensland 4072, Australia*

[2] *Commonwealth Scientific and Industrial Research Organisation Agriculture and Food, Canberra, Australian Capital Territory 2601, Australia*

[3] *Division of Plant Sciences, Research School of Biology, Australian National University, Acton, Australian Capital Territory 2601, Australia*

[4] *Australian Synchrotron, Macromolecular crystallography, Clayton, Victoria 3168, Australia*

[5] *Institute for Glycomics, Griffith University, Southport, Queensland 4222, Australia*

[6] *School of Molecular Bioscience, University of Sydney, Sydney, New South Wales 2006, Australia*

SUMMARY

The effector protein AvrP is secreted by the flax rust fungal pathogen (*Melampsora lini*) and recognized specifically by the flax (*Linum usitatissimum*) P disease resistance protein, leading to effector-triggered immunity. To investigate the biological function of this effector and the mechanisms of specific recognition by the P resistance protein, we determined the crystal structure of AvrP. The structure reveals an elongated zinc-finger-like structure with a novel interleaved zinc-binding topology. The residues responsible for zinc binding are conserved in AvrP effector variants and mutations of these motifs result in a loss of P-mediated recognition. The first zinc-coordinating region of the structure displays a positively charged surface and shows some limited similarities to nucleic acid-binding and chromatin-associated proteins. We show that the majority of the AvrP protein accumulates in the plant nucleus when transiently expressed in *Nicotiana benthamiana* cells, suggesting a nuclear pathogenic function. Polymorphic residues in AvrP and its allelic variants map to the protein surface and could be associated with differences in recognition specificity. Several point mutations of residues on the non-conserved surface patch result in a loss of recognition by P, suggesting that these residues are required for recognition.

Keywords: crystal structure, effector-triggered immunity, flax rust (*Melampsora lini*) effector, NLR [nucleotide-binding and oligomerization domain (NOD)-like receptor, nucleotide-binding/leucine-rich repeat receptor], nuclear localization, plant disease resistance, zinc finger.

*Correspondence: Email: b.kobe@uq.edu.au; xiaoxiao.zhang@csiro.au

INTRODUCTION

During infection, many plant pathogens deliver proteins known as effectors into host cells to aid colonization. To counteract this infection strategy, plants have evolved intracellular receptors, known as resistance (R) proteins, which recognize effectors and initiate defence responses, collectively known as effector-triggered immunity (ETI) (Dodds and Rathjen, 2010; Jones and Dangl, 2006). ETI is typically defined by the hypersensitive response (HR), which results in death of the infected cell. Most R proteins contain nucleotide-binding (NB) and leucine-rich repeat (LRR) domains and are related to mammalian nucleotide-binding and oligomerization domain (NOD)-like receptors (NLRs) (Bonardi *et al.*, 2012). Effectors are often highly variable, both within and between species, and the recognition of effectors is highly specific. Pathogen effector–plant R protein interactions were described genetically in the 1950s by the gene-for-gene theory (Flor, 1956). Effectors recognized by R proteins are termed avirulence (Avr) proteins. The recognition of Avr proteins by R proteins is accomplished by direct association, indirect association through accessory proteins or the recognition of host proteins modified by Avr proteins (Dodds and Rathjen, 2010).

Effectors from filamentous eukaryotic plant pathogens, such as fungi and oomycetes, have a high level of genetic diversity, and few features have been identified in their protein sequences to help predict biological functions (Bozkurt *et al.*, 2012; Oliveira-Garcia and Valent, 2015; Rafiqi *et al.*, 2012). Fungal and oomycete intracellular effectors have been found to suppress immunity by interaction with host proteins to modulate plant metabolism, including hormone signalling and transcription; however, only a few have been assigned a specific function (Djamei *et al.*, 2011; McLellan *et al.*, 2013; Okmen and Doehlemann, 2014). Increasing

numbers of fungal and oomycete effectors have been reported to move into the host nucleus, suggesting that these effectors may interfere with host nuclear processes. For instance, the effector domains of oomycete Crinkler (CRN) effectors target the host nucleus and accumulate in specific subnuclear compartments, leading to necrosis (Ramirez-Garces *et al.*, 2016; Schornack *et al.*, 2010; Stam *et al.*, 2013a,b). The *Phytophthora* PSR (suppressor of RNA silencing) effector binds to the *Arabidopsis* PSR1-interacting protein 1 (PINP1), which regulates small RNA accumulation in the host nucleus, to promote infection (Qiao *et al.*, 2015). The *Ustilago maydis* effector See1 (seedling efficient effector 1) interacts with a maize homologue of yeast suppressor of the G2 allele of *skp1* (SGT1) in both the cytosol and nucleus of leaf cells, resulting in re-activation of plant DNA synthesis and tumour formation (Redkar *et al.*, 2015). A putative *Colletotrichum graminicola* effector, CgEP1 (*Colletotrichum graminicola* effector protein 1), targets the host nucleus and binds directly to maize genomic DNA (Vargas *et al.*, 2016).

Genetic studies of the interaction between flax (*Linum usitatissimum*) and its rust pathogen (*Melampsora lini*) have identified a number of *R* genes in the host and *Avr* genes in the rust pathogen. *R* genes at the *L*, *M*, *N* and *P* loci have been cloned and encode NLR proteins with an N-terminal Toll/interleukin-1 receptor (TIR) domain (Ravensdale *et al.*, 2011). In flax rust, *Avr* genes have been cloned from six loci, *AvrL567*, *AvrL2*, *AvrM*, *AvrM14*, *AvrP123* and *AvrP4*, and all encode secreted proteins (Anderson *et al.*, 2016; Barrett *et al.*, 2009; Catanzariti *et al.*, 2006; Dodds *et al.*, 2004). Apart from AvrM14, which shows homology to nudix hydrolases, these Avr proteins have no homologues with defined functions in current databases. Because these Avr proteins are recognized by intracellular host R proteins, they have been proposed to enter plant cells during infection, a process that has been observed for AvrM by confocal microscopy (Rafiqi *et al.*, 2010). A physical interaction between Avr and R proteins has been shown using yeast two-hybrid (Y2H) assays for the AvrL567:L5/L6/L7 pairs and the AvrM:M pair (Catanzariti *et al.*, 2010; Dodds *et al.*, 2006). Structure-guided mutagenesis studies have revealed that specific recognition of AvrL567 effectors results from multiple amino acid contacts between Avr and R proteins (Wang *et al.*, 2007). In the case of AvrM, the C-terminal domain of AvrM is required for M-dependent cell death and is directly involved in the interaction (Catanzariti *et al.*, 2010; Ve *et al.*, 2013).

The screening of an *M. lini* haustorium-specific cDNA library revealed a haustorially expressed secreted protein gene cosegregating with a gene at the *AvrP123* locus (Catanzariti *et al.*, 2006). So far, 10 *AvrP123* alleles have been identified from rust isolates collected from flax species *L. usitatissimum* and *Linum marginale*, including *AvrP* and *AvrP123* (Barrett *et al.*, 2009; Catanzariti *et al.*, 2006; Lawrence *et al.*, 1981b). In flax, at least six rust resistance genes (P, P1–P5) occur at the complex *P* locus (Islam and Mayo, 1990). The P and P1–P3 resistance specificities are defined by the recognition of allelic variants of AvrP123 (Barrett *et al.*, 2009; Catanzariti *et al.*, 2006; Dodds and Thrall, 2009). Transient expression of *AvrP123* induces cell death activities in flax plants containing the *P1*, *P2* or *P3* resistance genes, and *AvrP* induces *P*-dependent cell death activity (Catanzariti *et al.*, 2006; Dodds and Thrall, 2009). AvrP123 and its allelic variants, including AvrP, are cysteine (Cys)-rich proteins. They contain a sequence motif resembling that found in Kazal family serine protease inhibitors, where the Cys residues form disulfide bonds (Barrett *et al.*, 2009; Catanzariti *et al.*, 2006). However, recent biochemical studies of purified AvrP protein have suggested that the Cys residues may instead bind metal ions, and the arrangement of Cys residues in AvrP is similar to that in the plant homeodomain (PHD) motif, which binds zinc (Zn) ions (Zhang *et al.*, 2017).

To further investigate fungal effector function and recognition by R proteins, we determined the crystal structure of AvrP. Structural comparisons reveal similarities to proteins involved in gene regulation, and microscopic analysis indicates nuclear enrichment of AvrP when expressed *in planta*. Structure-guided mutagenesis and transient expression assays reveal surface residues of AvrP that are required for recognition by the P resistance protein.

RESULTS

Crystal structure of AvrP

The *AvrP* and *AvrP123* genes are alleles at the *AvrP123* locus, encoding proteins with a 23-amino-acid N-terminal signal peptide (Barrett *et al.*, 2009; Catanzariti *et al.*, 2006). The predicted mature forms of the AvrP and AvrP123 proteins, consisting of residues 24–111 and 24–117, respectively, were expressed in *Escherichia coli* and purified as described previously (Zhang *et al.*, 2017). AvrP was crystallized using $ZnCl_2$ as an additive; however, AvrP123 failed to crystallize (Zhang *et al.*, 2017). The structure of AvrP was solved using the multi-wavelength anomalous diffraction (MAD) approach (Table S1, see Supporting Information). The final model of AvrP contains two molecules in the asymmetric unit with a root-mean-square deviation of 0.5 Å. The refined model of the AvrP structure encompasses residues 26–102; the N-terminal residues 24–25 and the C-terminal residues 103–111 have no interpretable electron density, suggesting that they are flexible within the crystal. The structure adopts an elongated shape, containing four β-strands (β1–β4) and a C-terminal α-helix (α1) connected by loops (Fig. 1a). The structure shows three Zn ions bound in each protein molecule. Each Zn ion has a tetrahedral coordination with either four Cys or three Cys and one histidine (His) residue (Fig. 1b–d). The four β-strands form an elongated and twisted β-sheet, and coordinate Zn1 by residues C36, C38, C78 and C81 (Fig. 1a,b,e). Zn2 is coordinated by residues C53 and C67 in the elongated β2β3 loop, C89 in the β4 strand and H93 in the β4α1

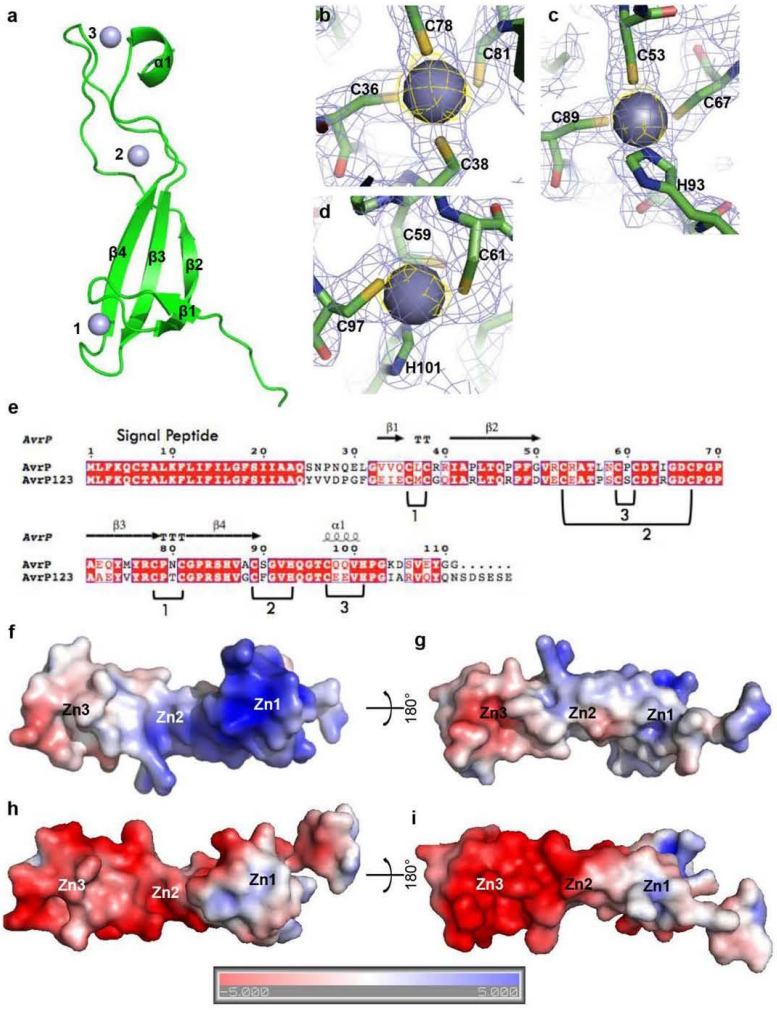

Fig. 1 The crystal structure of AvrP. (a) Ribbon diagram showing the overall structure of AvrP. Zinc (Zn) ions are shown as numbered spheres. (b–d) Tetrahedral coordination of Zn ions with CCCC (b) and CCCH (c, d) residue combinations. The images show the electron density map (blue mesh) of AvrP contoured at 1.0 σ and the anomalous difference map (yellow mesh) for the Zn ions contoured at 4.0 σ. The AvrP residues are shown as sticks and the Zn ions are shown as spheres. (e) Sequence alignment of AvrP and AvrP123. The secondary structure elements of AvrP are displayed above the alignment. 'T' corresponds to a β-turn. The Zn-binding motifs are numbered and the Zn-binding residues are indicated under the alignment. (f–i) Surface electrostatic potentials of AvrP (f, g) and AvrP123 (h, i). Positive potential is shown in blue and negative potential is shown in red (coloured continuously between −5 and 5 kT/e). Zn1, Zn2 and Zn3 indicate the relative positions of the Zn ions.

loop. Zn3 is coordinated by residues C59 and C61 in the β2β3 loop, C97 in the α1 helix and H101 in the C-terminal loop.

The interface between the two molecules within the asymmetric unit of AvrP crystals features few side-chain interactions and does not appear to be biologically relevant. Size-exclusion chromatography coupled with multi-angle light scattering (SEC-MALS) showed that both AvrP and AvrP123 are monomers in solution (experimental and theoretical molecular weights correspond to

10.5 and 9.8 kDa for AvrP, and 10.7 and 10.6 kDa for AvrP123, respectively) (Fig. S1a, see Supporting Information).

Examination of the surface electrostatic potential of AvrP reveals an uneven distribution. The Zn1-binding region forms a positively charged head (Fig. 1f). The C-terminal α-helix and the β2β3 loop within the Zn3-binding motif feature a negatively charged surface patch (Fig. 1g). Modelling the AvrP123 structure using AvrP as a template (sequence identity, 60%) reveals an extended negatively charged surface area in the Zn3-binding region of AvrP123 (Fig. 1h,i), whereas the positively charged surface patch in the Zn1-binding region is much smaller than that of AvrP (Fig. 1h). The flax rust AvrM effectors contain positively charged surface patches that mediate binding to head-groups of negatively charged phospholipids, such as phosphatidylinositol phosphates (PIPs), but this binding ability is not essential for plant intracellular accumulation of secreted AvrM (Ve *et al.*, 2013). AvrP and AvrP123 did not bind to PIPs in a dot-blot lipid-binding assay (Fig. S1b), indicating that they are unlikely to enter the plant cells through a PIP-binding pathway. Both AvrP and AvrP123 showed weak binding to phosphatidic acid at protein concentrations of 0.3 μg/mL. However, this is likely to be non-specific, given the significantly lower affinity compared with the positive control AvrM.

Zn-binding motifs in AvrP have features of Zn-finger domains

The Zn-binding topology of AvrP is similar to the treble-clef Zn-finger domain family, which includes PHD, RING (really interesting new gene), B-box and FYVE (domain shared by Fab1, YOTB, Vac1 and EEA1) domains. These domains each bind to two Zn ions through interleaved Zn-binding motifs, known as the 'cross-brace' topology, in which the first and third C/C or C/H pairs bind to the first Zn ion and the second and fourth C/C or C/H pairs bind to the second Zn ion (Grishin, 2001) (Fig. S2a, see Supporting Information). Each subgroup of the treble-clef Zn-finger family is characterized by distinct arrangements of the Zn ion-coordinating residues. However, they have similar protein folds consisting of two orthogonally positioned β-hairpins and C-terminal α-helices (ββα) (Fig. S2a,b). Each β-turn of the β-hairpins contains a pair of residues that are involved in binding two different Zn ions. The AvrP structure contains a similar, but distinct, 'cross-brace' topology, with six C/C or C/H pairs bound to three Zn ions (Fig. 1e and S2c,d). The secondary structure of AvrP has a ββα order similar to the treble-clef Zn-finger family proteins with a Cys pair located in each β-turn. The second β-hairpin of AvrP (in the Zn1 region) contains the sequence motif CPXCG, which is common in treble-clef Zn-finger domains (Wang *et al.*, 1998). However, in AvrP, the two β-hairpins are separated by a long loop and are involved in the binding of one Zn ion.

Zn-binding motifs are required for AvrP-triggered cell death

The addition of $ZnCl_2$ to the growth medium enhanced the production of AvrP protein in *E. coli* and Zn was required for AvrP crystallization (Zhang *et al.*, 2017). Therefore, we tested the effect of site-directed mutations in Zn-binding motifs on the ability of AvrP to trigger P-dependent cell death *in planta*. Three mutants were made, targeting each of the Zn-binding sites separately by replacing all four coordinating Cys and His residues of Zn1, Zn2 or Zn3 with alanine. Mature wild-type AvrP protein and its mutant variants were expressed in transgenic *Nicotiana tabacum* (tobacco) leaves containing the flax *P* resistance gene by *Agrobacterium* infiltration. The AvrP constructs, either with or without a haemagglutinin (HA) tag, triggered cell death in *P*-containing tobacco leaves, whereas the Zn-binding motif mutants (HA-tagged) failed to trigger cell death (Fig. 2a). All AvrP proteins are detectable by immunoblotting, although the Zn1 and Zn2 mutant variants accumulated to lower levels than the wild-type and Zn3 mutant proteins (Fig. 2b), indicating that the Zn1 and Zn2 mutations may affect protein stability. The low protein accumulation of the Zn1 and Zn2 mutants may be insufficient to trigger P-dependent cell death. Collectively, these data suggest that the integrity of each of the three Zn-binding sites is important for AvrP recognition by P, probably because they are required for the adoption of the correct folded structure of the protein.

Structural comparisons and functional implications

To investigate the similarity of AvrP to other known structures in the Protein Data Bank (PDB), structure-based similarity searches were performed using the Dali server (Holm and Rosenstrom, 2010). Dali reports structural similarities based on a Z-score, where proteins with Z-scores > 2 are considered to have similar folds (Holm and Rosenstrom, 2010). Although no high-scoring structural similarities were found that encompassed the entire AvrP structure, a region involving both hairpin β-strands and the Zn1-binding site in AvrP showed structural similarities with several proteins (Fig. 3a–e). The structural similarities in this region are unlikely to have been detected based on sequence alone, as the protein sequence identities with AvrP are low (~10%) (Fig. 3f). Of the four most closely related structures, ZPR1 is the only protein shown to bind Zn (Fig. 3d) (Mishra *et al.*, 2007). The proteins that showed similarity to AvrP in this region are over-represented by proteins involved in transcription and translation, suggesting that AvrP may possess a similar function. We therefore performed nucleic acid-binding assays with AvrP and AvrP123, but no significant nucleic acid-binding activity was observed under the conditions used (Fig. S3, References S1, see Supporting Information). AvrP showed weak single-stranded RNA (ssRNA) binding at high (15 μM) protein concentrations but, given the concentrations used, this appears unlikely to be of biological significance.

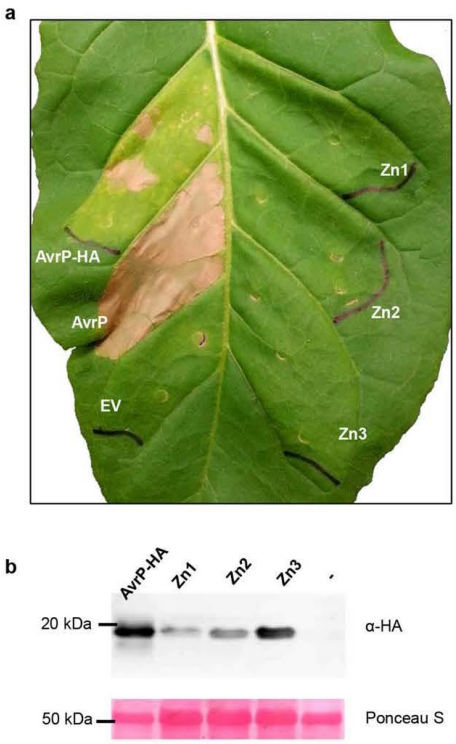

Fig. 2 *Agrobacterium*-mediated expression of zinc (Zn)-binding motif mutants of AvrP. AvrP protein (lacking the signal peptide) fused with a haemagglutinin (HA) tag (AvrP-HA) or without a tag (AvrP), and HA-tagged AvrP containing mutations in the Zn-binding residues (Zn1, Zn2 and Zn3), were expressed in a transgenic tobacco leaf containing the *P* resistance gene. (a) Leaf photographed at 5 days post-infiltration (dpi). Empty vector (EV) was used as a negative control. (b) Protein extracts from infiltrated leaf tissue expressing HA-tagged AvrP or Zn mutant proteins as in (a) or from non-infiltrated leaf tissue (–) were size fractionated by gel electrophoresis and analysed by immunoblotting with antibodies against HA. Samples were collected 2 days after infiltration. The positions and sizes (kDa) of protein molecular mass standards are indicated. The lower panel shows Ponceau S staining of ribulose-1,5-bisphosphate carboxylase/oxygenase (Rubisco) on the blotted nitrocellulose membrane to indicate relative protein loading. The western blot shows representative images from two independent experiments.

AvrP and AvrP123 localize preferentially to the nuclei of plant cells

The localization of AvrP and AvrP123 inside plant cells was investigated by *Agrobacterium*-mediated expression of C-terminal citrine (CTR) fusion proteins in *N. benthamiana* leaves (Fig. 4a). Compared with CTR alone, which showed a nuclear–cytoplasmic distribution, both AvrP-CTR and AvrP123-CTR fusion proteins showed nuclear accumulation, although some cytosolic fluorescence was also detected. To quantify the nuclear enrichment of AvrP and AvrP123, the ratio of nuclear to cytosolic fluorescence intensity was calculated. Compared with CTR alone, AvrP-CTR and AvrP123-CTR showed more than a two-fold and six-fold increase in nuclear relative to cytosolic fluorescence, respectively (Fig. 4b; Table S2, see Supporting Information). The expected molecular masses of AvrP and AvrP123 fused with the CTR tag are 36.9 and 37.7 kDa, respectively, and so these proteins may be small enough to diffuse into the plant nucleus (Wang and Brattain, 2007). However, the enhanced accumulation of AvrP and AvrP123 in the nucleus, compared with the cytosol, suggests that they are retained in the nucleus. No nuclear localization motifs were evident in these protein sequences, and so the mechanism of nuclear targeting is unknown. CTR-tagged AvrP and AvrP123 were able to trigger cell death in transgenic flax containing *P* and *P2*, respectively, indicating that they remained recognizable by their corresponding R proteins (Fig. S4, see Supporting Information).

Non-conserved positions are enriched on one side of the AvrP structure

A number of different *AvrP123* alleles have been identified from rust isolates collected from flax, *L. marginale* (Lm) or *L. usitatissimum* (Lu), including an intra-allelic recombinant between *AvrP* and *AvrP123*, designated as bs25 (Barrett *et al.*, 2009; Catanzariti *et al.*, 2006; Lawrence *et al.*, 1981b). They show varying recognition specificities by the corresponding P, P1, P2 and P3 resistance proteins (Fig 5a and S5, see Supporting Information) (Dodds and Thrall, 2009). A high level of polymorphism is observed amongst these seven AvrP123 variants (Fig. 5b), with 36 differences found between the mature AvrP (Lu4) and AvrP123 (Lu1) proteins. However, the 10 Cys and two His residues involved in Zn binding are strictly conserved amongst all the variants. Two sequence-related subgroups can be defined. The first, designated here as the AvrP group, includes Lu2, Lu3, Lu6 and AvrP, which share sequence identities of 86%–98%. The second group, designated here as the AvrP123 group, includes AvrP123 and Lm1, which share an identity of 89% and contain a six-amino-acid extension at the C-terminus compared with the AvrP group. The sequence identity between the two groups is ~60%. The bs25 protein is identical to AvrP for the first 60 amino acids and to AvrP123 for the remainder of the protein, and is recognized exclusively by the P2 resistance protein (Dodds and Thrall, 2009). Therefore, the C-terminal region of the AvrP protein most probably influences recognition by the P resistance protein, and the N-terminal region may influence recognition by P1 and P3. The Lu2 protein has eight amino acid differences compared with AvrP and

a

PDB ID	Z score	Description of the full-length protein
1IZ6	4.2	Translation Initiation Factor 5A (Putative RNA binding protein)
3QII	3.6	PHD finger protein 20 (Histone binding protein)
2QKD	3.4	Zinc finger protein ZPR1 (Regulation of translation elongation factor)
3KXT	2.8	Chromatin protein CREN7 (DNA binding)

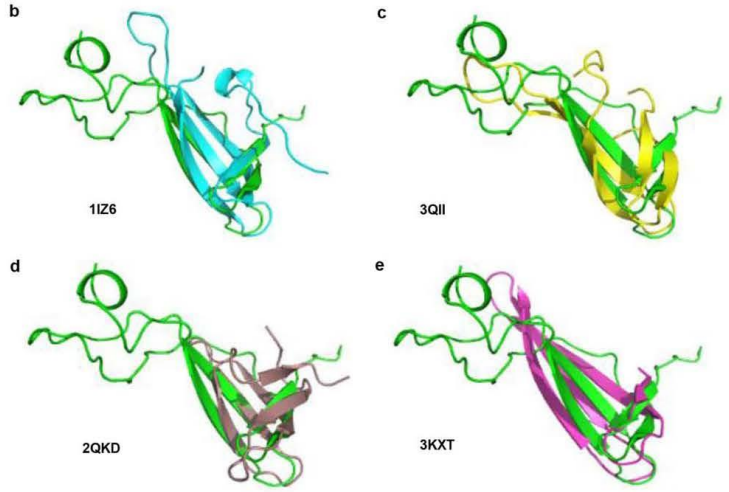

f

```
AvrP  GVVQCLCRRIAPLTQPPFGVPAEQYMYRCPNCGPRSHVACSG
1IZ6  RYIII-DDEPCRIVN-ITVSAKARIEAVGIDGKVRSIVKPTS
3QII  EQVLACWFYPAKVTA-VNKD--GTYTVKFYDGVVQTVKHI--
2QKD  IESLCMCYRNGTT--RLLLTEIIVSSFSCECGWNNTEIQSAG
3KXT  KPVKVKKEAELVPEK-VWALGVKIGLFKDPEGKYFRHKL---

AvrP  LEEELLLLLEEEEEEEEELLEEEEEEELLLEEEEEEELL
1IZ6  LEEEE-LLEEEEEEE-EEEELEEEEEEELLLLEEEEEELL
3QII  LEEEELEEEEEEE-ELLL--LEEEEELLLLEEEEHH—
2QKD  LEEELLLLLEEEE--EEEEEEEEEEEELLLLEEEEEEEE
3KXT  LLEEEELEEEELLLE-EEEELEEEEEELLLLEEEEL---
```

Fig. 3 Structural alignment of AvrP and Dali hits with low sequence similarity. (a) Representative hits from Dali structure search. (b–e) Structure superimposition of AvrP and the hits, showing the similarities in the Zn1-binding region. The AvrP structure is shown in green. The Protein Data Bank (PDB) IDs of the superimposed structures are indicated below each image. The residue regions aligned with AvrP and their corresponding domains are 16–63 (SH3-like β-barrel), 26–66 (Tudor domain), 11–58 (zinc finger) and 6–49 (not assigned) for 1IZ6 (Yao *et al.*, 2003), 3QII (Adams-Cioaba *et al.*, 2012), 2QKD (Mishra *et al.*, 2007) and 3KXT (Feng *et al.*, 2010), respectively. (f) Structure-based sequence alignment (top) generated using Dali, showing that AvrP has low sequence identities with the Dali hits. Only sequences of the superimposed structures are shown. Cysteine and histidine residues are highlighted in red. The bottom panel shows the alignment of elements of secondary structure; helices, β-strands and loops are shown as H, E and L, respectively.

is not detected by any of the P protein variants. Most of the residues that differ between Lu2 and AvrP localize to the C-terminal region, which further supports the role of this region in the recognition by P.

The polymorphic residues of the AvrP123 variants are spread over the entire protein sequence. To investigate their structural distribution, we scored residue conservation using Clustal Omega (Sievers *et al.*, 2011) and mapped the non-conserved residues onto the surface of the AvrP structure. This analysis showed conserved surface patches on the concave side of the structure and the surface of the β3 and β4 strands (Fig. 5c,d), whereas non-conserved residues are enriched on the opposite side of the protein (designated the variable surface) (Fig. 5e,f). On the variable surface, eight residues at non-conserved positions occur close to one another, including residues I64, D66, P68 and P70 in the β2β3 loop, and residue S90 in the β4α1 loop (using AvrP numbering), which form a line threaded across the surface of the structure. In addition to these five residues, P47 in the β2 strand and E72 in the β3 strand are located on the same relatively flat surface. The non-conserved N-terminal residues N26, P27, Q29 and

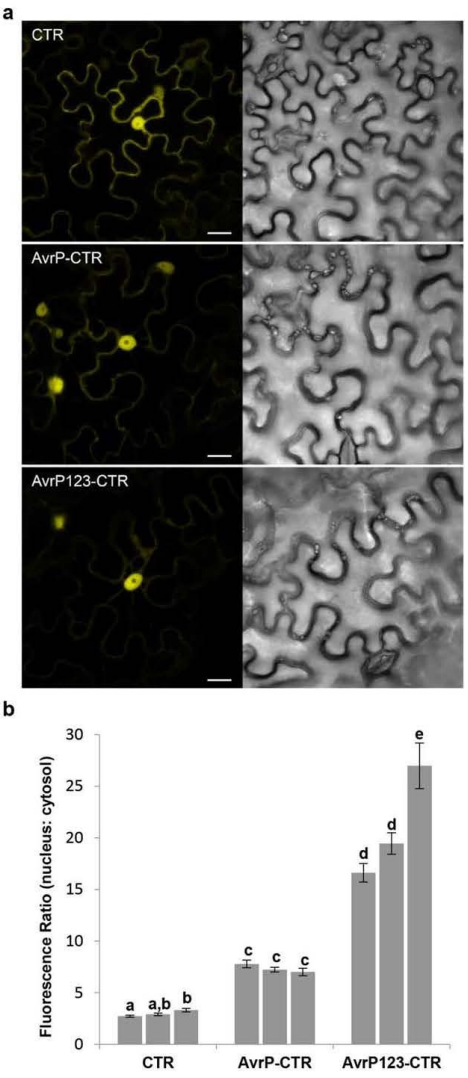

Fig. 4 Subcellular localization of citrine (CTR)-tagged AvrP and AvrP123. (a) Confocal images of *Nicotiana benthamiana* cells showing an increased ratio of fluorescence in the nucleus relative to the cytosol in leaves expressing AvrP-CTR and AvrP123-CTR, compared with CTR alone. The fluorescence image (left) and corresponding transmitted light image (right) were taken at 2 days post-infiltration (dpi). Bars, 20 μm. (b) Ratio of average fluorescence intensity of nucleus to cytosol in transformed cells. Column values represent mean ratios ± standard error (SE) ($n = 30$) from three independent experiments for each protein. Different letters denote a significant difference, whereas the same letters denote no significant difference (two-tailed *t*-test, $P < 0.05$).

E30 further extend the variable surface. The non-conserved residues in the C-terminal region (103–111) could not be mapped as this region is missing from the structure. Amongst the eight residues polymorphic between the AvrP and Lu2 proteins, four are in the variable surface at positions 66, 68, 70 and 90. Notably, residue 66 changes from aspartate (containing a negatively charged side-chain) in AvrP to alanine in Lu2, and residue 70 changes from proline to arginine (containing a positively charged side-chain). These observations suggest that residues 66, 68, 70 and 90 may be involved in P recognition. However, residues D66, P68 and P70 do not differ between AvrP and AvrP123, and their roles in P1, P2 or P3 recognition are currently unknown.

Surface polymorphic residues of AvrP are involved in R protein recognition

To further investigate the variable surface, we tested whether mutations of non-conserved residues in the variable surface of AvrP affect the P-mediated cell death response. Mutations were introduced into the non-conserved residues of AvrP, including P47R, I64R, E72A, D66A, P68S, P70R and S90T. As the C-terminal region of AvrP may be responsible for P recognition, we also tested Q94E and E108Q, which differ between AvrP and Lu2, although Q94 is not in the variable surface, and E108 is not modelled in the structure of AvrP, as well as residues G50 and R52, which differ between AvrP and AvrP123 and occur at the periphery of the variable surface. When expressed in P-containing flax as yellow fluorescent protein (YFP) fusions, the P47R, I64R and P70R mutants of AvrP did not trigger cell death, whereas the other mutants triggered cell death responses comparable with that of the wild-type protein (Fig. 6a). Although protein expression of the YFP-tagged AvrP and mutants could not be detected in flax (Fig. S6a, see Supporting Information), the same constructs were transiently expressed in *N. benthamiana* and stable protein overexpression was detected for all of them, except for the P47R and P70R mutants (Fig. S6b), which seemed to accumulate at a lower level, indicating that these proteins may be unstable. When expressed in P-containing transgenic tobacco as HA fusions, the P47R, I64R and D66A mutants abolished P-mediated cell death activity, whereas the P68S, P70R, S90T, Q94E and E108Q mutations led to weaker cell death activity compared with the wild-type protein (Figs 6b and S7, see Supporting Information). All proteins were detectable in *N. tabacum*, except for the P47R mutant (Fig. 6c). Collectively, these data show that mutations of several residues in the variable surface and the C-terminal Q94 and E108 residues of AvrP affect P-mediated cell death activity.

Testing for direct interaction of AvrP and AvrP123 with P and P2

Recognition by direct interaction between effector and R proteins has been shown for the AvrM:M and AvrL567:L6 pairs (Catanzariti

a

	P	P1	P2	P3
AvrP (Lu4)	+	-	-	-
Lu2	-	-	-	-
Lu6	±	-	-	-
Lu3	+	-	±	+
AvrP123 (Lu1)	-	+	+	+
Lm1	-	-	+	+
bs25	-	-	+	-

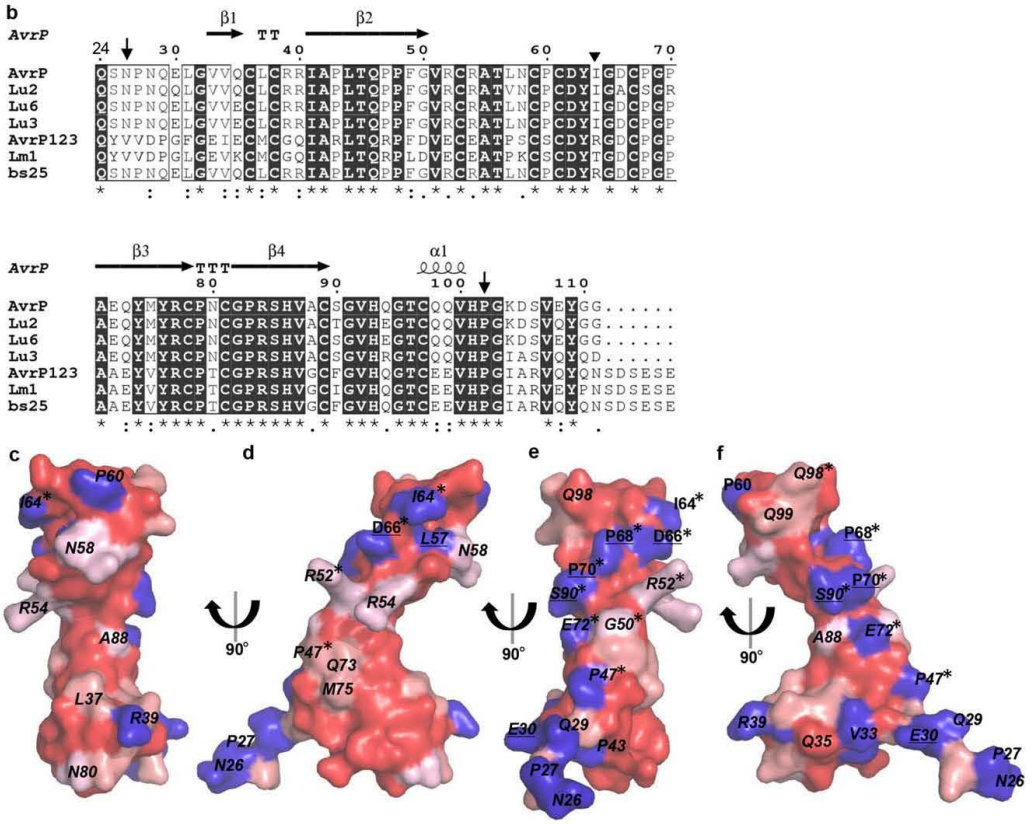

Fig. 5 Polymorphic residues on the surface of AvrP variants. (a) The recognition spectra of AvrP variants by P family resistance proteins (Dodds and Thrall, 2009). The AvrP variants were expressed in flax leaves containing the flax *P* family resistance genes by *Agrobacterium* infiltration. Plants were scored 12 days after infiltration. '+' indicates that cell death was induced, and '–' indicates that no response was induced. (b) Sequence alignment of AvrP variants. The sequences of mature proteins were aligned using Clustal Omega (Sievers *et al.*, 2011). Residue conservation is indicated below the alignment by an asterisk (fully conserved), a colon (strongly similar) and a period (weakly similar), whereas blank means that there is no similarity. The secondary structure elements of AvrP are shown on top of the alignment and the region included in the structure is located between the downward arrows. 'T' corresponds to a β-turn. The inverted triangle indicates the point at which the bs25 sequence changes from AvrP to the AvrP123 sequence. (c–f) Conservation mapping on the surface of the AvrP structure. The degree of conservation, from strong to weak, is indicated by dark to light red. Non-conserved residues are shown in blue. Surface residues that are polymorphic between AvrP and Lu2, and AvrP and AvrP123, are underlined and italicized, respectively. Residues targeted for mutation are marked with an asterisk.

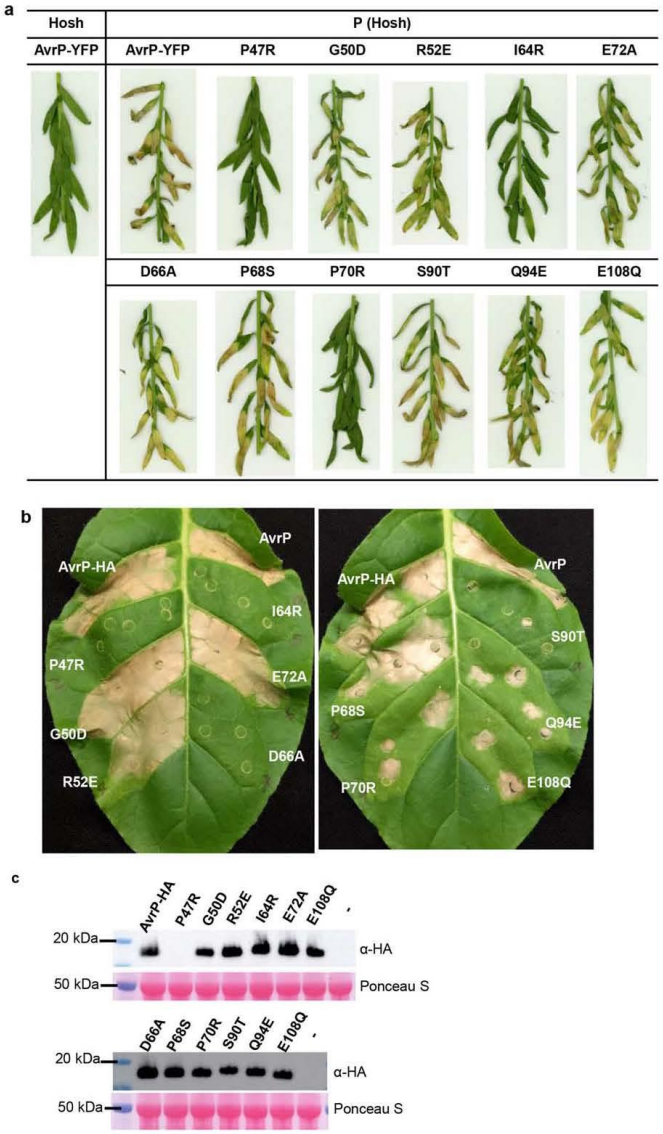

Fig. 6 Mutational analysis of AvrP residues. (a) Cell death assay of yellow fluorescent protein (YFP)-tagged AvrP or AvrP mutants transiently expressed in flax lines with [P (Hosh)] or without (Hosh) the *P* gene. (b) Transgenic tobacco leaf containing the *P* resistance gene from flax was infiltrated with *Agrobacterium* cultures containing plasmids expressing AvrP, or haemagglutinin (HA)-tagged AvrP (AvrP-HA), and corresponding HA-tagged mutants. (c) Protein extracts from (b) and non-infiltrated (–) leaf tissue were size fractionated by gel electrophoresis and analysed by immunoblotting with anti-HA antibodies. Samples were taken at 2 days post-infiltration (dpi). The bottom panel shows Ponceau S staining of Rubisco on the blotted nitrocellulose membrane to indicate relative protein loading. The western blot shows representative images from two independent experiments.

et al., 2010; Dodds *et al.*, 2006), with polymorphic surface residues of AvrL567 and AvrM determining recognition specificity (Ravensdale *et al.*, 2012; Ve *et al.*, 2013; Wang *et al.*, 2007). The highly specific pattern of recognition of AvrP123 variants by the cognate R proteins is consistent with a direct recognition model (Dodds and Thrall, 2009). We tested for direct interaction of AvrP and AvrP123 with P and P2 using Y2H assays, but did not observe any positive interactions (Fig. 7a and S8a, see Supporting

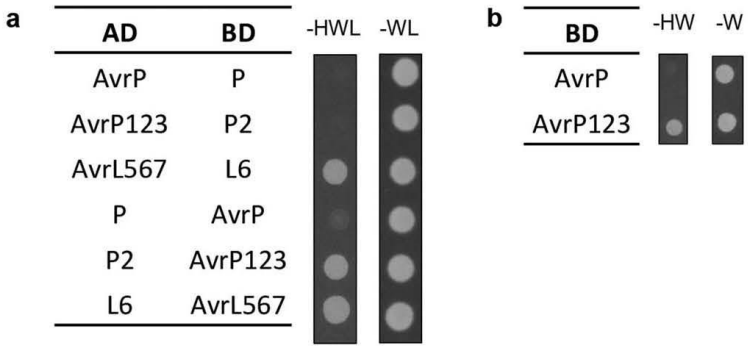

Fig. 7 AvrP123 shows transcriptional activation in yeast. (a) AvrP/AvrP123 and P/P2 interaction assays in yeast. Avr and R gene constructs were fused to either a GAL4 activation domain (AD) or a binding domain (BD) in vectors that enable yeast transformants to grow in minimal medium lacking tryptophan and leucine (–WL), respectively. As a result of the interaction between AD and BD fusion proteins, the *HIS3* reporter gene is activated, enabling the yeast to grow in medium lacking histidine, tryptophan and leucine (–HWL). L6 and AvrL567 constructs were used as positive controls. (b) BD-AvrP123 construct activates yeast growth in the absence of AD constructs in medium lacking histidine and tryptophan (–HW).

Information). Stable protein expression was detected in yeast (Figs S6c and S8c). However, we did note that AvrP123 fused to the GAL4 DNA-binding domain (BD) led to the autoactivation of the reporter gene, even without the activation domain (AD) fusion partners (Figs 7b and S8b). Interaction was also not detected using co-immunoprecipitation *in planta* under the conditions tested (Fig. S8d).

DISCUSSION

We report the crystal structure of the flax rust effector protein AvrP, revealing a novel elongated Zn-binding protein with an unusual Zn-binding topology. The Zn-binding region of AvrP shows limited similarities to DNA-binding and chromatin-associated proteins. Localization studies show that AvrP and AvrP123 fused to the CTR fluorescence tag have a nucleo-cytosolic localization, with an enhanced nuclear accumulation relative to CTR. The structure of AvrP shows that polymorphic residues in the AvrP family that influence R protein specificity map to the surface of the structure. Analysis of the surface conservation amongst AvrP variants, combined with mutational studies, reveals a variable surface that may play a role in specific recognition by the P family of R proteins.

AvrP is a Cys-rich effector protein that binds to Zn ions

Distinct structures of fungal and oomycete effectors have been reported previously. Most structures of the oomycete RXLR effectors that have been published to date comprise a disordered RXLR uptake region and a three-α-helix fold effector domain, termed the WY domain (Boutemy *et al.*, 2011; Win *et al.*, 2012; Yaeno *et al.*, 2011). Despite divergent sequences, the WY domains maintain a conserved structural fold across different oomycete species (Win *et al.*, 2012). Similar to the oomycete RXLR effectors, sequence-divergent effectors identified from the rice blast fungus *Magnaporthe oryzae* contain a common six-stranded β-sandwich structure related to the structure of the wheat pathogen *Pyrenophora tritici-repentis* effector ToxB (de Guillen *et al.*, 2015). These observations suggest that, despite very different sequences amongst fungal and oomycete effectors, structure-based homology searches will contribute significantly to our understanding of effector functions.

Two other *M. lini* effector structures have been reported: AvrL567 (Wang *et al.*, 2007) and AvrM (Ve *et al.*, 2013). Both structures show very low similarity with other known structures, giving no clues to their biological functions. The structure of AvrP is unrelated to either of these effector proteins and, although the entire AvrP structure has no structural homologues, the Zn1-binding region of AvrP shares similarities with Zn-finger proteins. The Zn-binding residues are strictly conserved amongst AvrP variants, suggesting that they probably maintain similar overall structures. A distant homologue of AvrP123, Mlp 124530, has been identified in *Melampsora larici-populina* (poplar leaf rust) (Duplessis *et al.*, 2011; Hacquard *et al.*, 2012). Mlp 124530 has low sequence identity with the AvrP variants (~25%). However, all 12 residues that are involved in Zn-ion binding in AvrP are conserved in Mlp 124530, suggesting that it may have a similar structure to AvrP and that the binding of Zn ions may be a common feature in the AvrP-like effector family. This family can be represented by the $C\text{-}X_{1-2}\text{-}C\text{-}X_{13-14}\text{-}C\text{-}X_5\text{-}C\text{-}X\text{-}C\text{-}X_{5-7}\text{-}C\text{-}X_{10}\text{-}C\text{-}X_6\text{-}C\text{-}X_3\text{-}H\text{-}X_7\text{-}H$ motif, a novel form of Zn-binding motif that can be used for the future identification of AvrP-like effector candidates.

Cys-rich proteins are over-represented amongst fungal effectors and, in most cases, it is expected that these Cys residues form disulfide bonds (Bozkurt *et al.*, 2012; Stergiopoulos and de Wit, 2009), which may enhance protein stability, especially as they are secreted in the protease-rich apoplastic space (van den Burg *et al.*, 2003). Disruption of disulfide bonds can result in the loss of pathogenic function (van den Burg *et al.*, 2003; van den Hooven *et al.*, 2001; Kooman-Gersmann *et al.*, 1997). We show here that the Cys residues in AvrP instead bind to Zn ions. Similar to disulfides, Zn binding may be important for protein stability and may promote correct protein folding. Accordingly, in this study, we showed that mutations of the Zn-binding motifs in AvrP reduce protein accumulation and disrupt effector-triggered cell death *in planta*. Although an expanded family of Zn-finger proteins has been identified in the search for fungal effector candidates (Duplessis *et al.*, 2011; Guyon *et al.*, 2014), no molecular details of Zn binding have been revealed previously.

Enriched nuclear localization of AvrP suggests a nuclear function

The structure of AvrP shows some structural similarities to several Zn-finger proteins, many of which are transcription factors that bind nucleic acids or histones and affect gene expression. Microscopic analysis of CTR-tagged AvrP indicated that it shows enhanced accumulation in the host nucleus compared with the CTR protein when expressed in plant cells. These two properties suggest that AvrP might function inside the nucleus, possibly as a regulator of host cell transcription. However, we observed no significant nucleic acid-binding activity for AvrP or AvrP123. AvrP showed weak ssRNA-binding activity at a high protein concentration, but AvrP123 did not, suggesting that this property may not be biologically significant, assuming that these two proteins share a common pathogenicity mechanism. The ssRNA-binding activity of AvrP may result from the positively charged surface of AvrP. Structural similarities with nucleic acid-binding proteins have been identified for several fungal effectors; however, as found for AvrP, the follow-up biochemical assays did not support a nucleic acid-binding function (Blondeau *et al.*, 2015; Pedersen *et al.*, 2012; Wang *et al.*, 2007). It is possible that nucleic acid-binding domains were used as a structural template for effector diversification during evolution of the pathogen, leading to diverse effector functions (Pedersen *et al.*, 2012).

There are a number of effectors secreted by bacteria that have been shown to influence host gene transcription. For example, the bacterial transcription activator-like (TAL) effector proteins, which contain a nuclear localization signal (NLS) and an acidic transcriptional activation domain (AD), hijack host gene transcription by binding directly to DNA in the host (Zhang *et al.*, 2015). However, AvrP does not have an identifiable NLS. The C-terminal regions of AvrP variants share some similatities with AD domains, which contain an excess of negatively charged (D and E) residues and are structurally disordered (Ptashne and Gann, 1997). In our Y2H assays, BD-fused AvrP123 strongly activated the *HIS3* reporter gene (upstream of GAL4) in the absence of the AD fusion (Fig. 7b), suggesting that AvrP123 can directly influence transcriptional activation in yeast. Further investigation is required to test whether AvrP variants can act as transcriptional regulators in flax, possibly through interaction with host-derived nuclear proteins, and whether nuclear localization is required to trigger R protein-specific defence.

Mutational analysis of AvrP suggests that surface residues control recognition specificity by the P resistance protein

We show that polymorphic residues are located on the surface of the AvrP structure and that non-conserved residues are enriched on one side of the structure. Different cell death activities were observed in flax and tobacco for several AvrP mutants, which may represent differences in protein stability in the two expression systems. The P70R mutant, which was stably expressed in tobacco but not in flax, showed a weak cell death activity in tobacco, but this activity was abolished in flax. The P47R mutant, however, which lost cell death activity in both systems, showed lower protein accumulation in *N. benthamiana* compared with the wild-type protein and no expression in tobacco. Collectively, several point mutations of non-conserved residues in the variable surface of AvrP reduced AvrP-triggered cell death in P-containing flax lines and transgenic tobacco. Amongst these, residues 66, 68, 70 and 90 differ between AvrP and the Lu2 protein, which is not recognized by P. Mutations of these residues in AvrP to Lu2 residues reduced cell death caused by P recognition in tobacco (Figs 6b and S7). When expressed in P-containing flax, mutation of D66 also suppressed cell death, although such suppression was not evident for the P68 and S90 mutants (Fig. 6a). Although residues I64 and E72 are conserved between AvrP and Lu2, mutation of I64 abolished AvrP-triggered necrosis, suggesting that this residue is involved in the recognition of AvrP by P. In AvrP123, I64 and E72 residues are replaced by arginine and alanine, respectively (Fig. 5b). The changes in side-chain charge at these positions may prevent recognition between AvrP123 and P. Mutations of the C-terminal polymorphic residue Q94 and E108 also affect P recognition, even though they are not part of the variable surface. We lack structural information for the C-terminal nine residues of AvrP, including E108. Nevertheless, it is possible that these residues may affect P recognition and the function of adjacent residues, such as Q94.

Like the structures of the AvrL567 and AvrM flax rust effectors, the structure of AvrP revealed a novel protein fold with limited structural similarity to proteins of known function. Although we speculate that AvrP is targeted to the host nucleus during infection, the role of AvrP in pathogen virulence remains unknown.

The coordination of Zn ions by AvrP appears to be important for correct folding of the protein, and therefore for recognition by the P resistance protein. Although a direct interaction between AvrP and P could not be demonstrated here, non-conserved residues clustered on a surface patch of AvrP appear to be involved in specific recognition by P.

EXPERIMENTAL PROCEDURES

Vectors and gene constructs

For transient expression in tobacco, the cDNAs of the AvrP and AvrP123 proteins (Catanzariti *et al.*, 2006), lacking the predicted signal peptides, were cloned into the pL and/or pLH vector, which contain an HA epitope sequence, using ligation-independent cloning (LIC) (Eschenfeldt *et al.*, 2009; Stols *et al.*, 2002). For transient expression in flax and Y2H assays, the same gene fragments were cloned into pAM-PATpro35S:GWY-YFPv (Bernoux *et al.*, 2008) and Gateway-compatible Y2H vectors (Bernoux *et al.*, 2011), respectively, using Gateway cloning. AvrP mutations were introduced into these constructs using the Phusion site-directed mutagenesis kit (Thermo Fisher Scientific, http://www.thermofisher.com/, Waltham, Massachusetts, USA) and primers containing the corresponding mutation. To express proteins in *N. benthamiana* for fluorescence microscopy, gene splicing by polymerase chain reaction (PCR)-driven overlap extension was used to generate constructs containing the AvrP and AvrP123 coding sequences, lacking the predicted signal peptide and stop codon, fused to CTR with an in-frame linker encoding GPGP. The PCR products were cloned as *SpeI-PvuI* fragments into the binary vector pCAMBIA3301 between NOS promoter and terminator sequences (De Block *et al.*, 1984; Horsch *et al.*, 1984). The CTR gene sequence was cloned as an *XbaI-PvuI* fragment into the same vector to generate a CTR-only expression construct. The oligonucleotides used in this study are summarized in Table S3 (see Supporting Information).

Plant material

A transgenic W38 tobacco (*N. tabacum*) line containing the *P* resistance gene was made by transformation with the P2/P-RVX construct (Dodds *et al.*, 2001). The flax (*L. usitatissimum*) lines Hoshangabad, Bison, Koto (containing *P*), Akmolinsk (*P1*), Abyssinian (*P2*) and Leona (*P3*), and the Bison backcross derivatives containing these resistance genes, have been described previously (Islam and Mayo, 1990; Lawrence *et al.*, 1981a). A line containing the *P* resistance gene in Hoshangabad, P (Hosh), was generated by three generations of backcrossing.

Structure determination

AvrP was expressed, purified and crystallized as described by Zhang *et al.* (2017). Data were collected at the Australian Synchrotron MX1 beamline (Cowieson *et al.*, 2015) using Blu-Ice software (McPhillips *et al.*, 2002). The diffraction data were used to a resolution of 2.52 Å and the structure was solved using the MAD technique. The structure was refined to final R_{work} and R_{free} values of 22% and 26%, respectively. The AvrP structure and data used to derive the structure have been deposited with the Protein Data Bank (www.pdb.org.) with PDB ID 5VJJ. Details are described in Methods S1 (see Supporting Information) and Table S1.

Transient *in planta* expression assays

Agrobacterium cultures containing the corresponding vectors were grown overnight at 28 °C in lysogeny broth (LB; 10 g/L tryptone, 5 g/L yeast extract and 10 g/L NaCl) medium with appropriate antibiotic selections. The cells were pelleted and resuspended in infiltration mix (10 mM $MgCl_2$, 200 μM acetosyringone) to an optical density at 600 nm (OD_{600}) of 0.5 or 1.0, followed by incubation at room temperature for 2 h. Cultures were infiltrated into leaves of 4-week-old tobacco or flax with a 1-mL syringe. The infiltrated tobacco plants were incubated in growth chambers at 24 °C with 200 μmol/m^2/s light intensity and an 8-h light and 16-h dark cycle. The flax plants were kept in a glasshouse at 24 °C with natural light and day/night cycle.

Confocal microscopy

Constructs were introduced into *N. benthamiana* leaves via agroinfiltration. Samples were collected at 2 days post-infiltration (dpi) and viewed on a Zeiss (Oberkochen, Germany) LSM 780 confocal microscope using an LD C-Apochromat 40×/1.1 W Korr M27 water immersion objective, with an excitation wavelength of 514 nm and a collection window of 520–600 nm for citrine and 637–759 nm for chlorophyll autofluorescence. Both fluorescence and transmitted light images were collected using the following settings: size, 212 × 212 μm^2; 2048 × 2048 pixels; scan time, 30 s. Fluorescent images of cell nuclei were brought to just below saturation to enable comparison between samples. Cytosolic and nuclear fluorescence intensity values were measured using ImageJ (Schneider *et al.*, 2012) in the Fiji package (Schindelin *et al.*, 2012). Average fluorescence intensities were calculated from 30 cells. Cytosolic samples were taken from regions of the cytosol that were perpendicular to the plane of imaging and free of chloroplasts. Nuclear samples were taken from a central plane avoiding the nucleolus. The experiment was repeated three times. *P* values were calculated using Student's *t*-test. The results were tabulated and graphed in Microsoft Excel.

ACKNOWLEDGEMENTS

This research was supported by Australian Research Council (ARC) Discovery Projects DP120100685, DP130104098 and DP160102244. XZ was a recipient of an ANZ Trustees PhD Scholarship for Medical Research in Queensland. BK is a National Health and Medical Research Council (NHMRC) Principal Research Fellow (1003325 and 1110971). MB was a recipient of an ARC Discovery Early Career Research Award (DE130101292). We acknowledge the use of the University of Queensland Remote Operation Crystallization and X-ray Diffraction Facility (UQ ROCX), and the assistance of Karl Byriel and Gordon King. X-Ray diffraction data collection was undertaken on MX beamlines at the Australian Synchrotron. We thank Kim Newell for providing technical assistance.

REFERENCES

Adams-Cioaba, M.A., Li, Z., Tempel, W., Guo, Y., Bian, C., Li, Y., Lam, R. and Min, J. (2012) Crystal structures of the Tudor domains of human PHF20 reveal novel structural variations on the Royal Family of proteins. *FEBS Lett.* **586**, 859–865.

Anderson, C., Khan, M.A., Catanzariti, A.M., Jack, C.A., Nemri, A., Lawrence, G.J., Upadhyaya, N.M., Hardham, A.R., Ellis, J.G., Dodds, P.N. and Jones, D.A. (2016) Genome analysis and avirulence gene cloning using a high-density RADseq linkage map of the flax rust fungus, *Melampsora lini*. *BMC Genomics*, **17**, 667.

Barrett, L.G., Thrall, P.H., Dodds, P.N., van der Merwe, M., Linde, C.C., Lawrence, G.J. and Burdon, J.J. (2009) Diversity and evolution of effector loci in natural populations of the plant pathogen *Melampsora lini*. *Mol. Biol. Evol.* **26**, 2499–2513.

Bernoux, M., Timmers, T., Jauneau, A., Briere, C., de Wit, P.J.G.M., Marco, Y. and Deslandes, L. (2008) RD19, an *Arabidopsis* cysteine protease required for RRS1-R-mediated resistance, is relocalized to the nucleus by the *Ralstonia solanacearum* PopP2 effector. *Plant Cell*, **20**, 2252–2264.

Bernoux, M., Ve, T., Williams, S., Warren, C., Hatters, D., Valkov, E., Zhang, X., Ellis, J.G., Kobe, B. and Dodds, P.N. (2011) Structural and functional analysis of a plant resistance protein TIR domain reveals interfaces for self-association, signaling, and autoregulation. *Cell Host Microbe*, **9**, 200–211.

Blondeau, K., Blaise, F., Graille, M., Kale, S.D., Linglin, J., Ollivier, B., Labarde, A., Lazar, N., Daverdin, G., Balesdent, M.H. and Choi, D.H. (2015) Crystal structure of the effector AvrLm4–7 of *Leptosphaeria maculans* reveals insights into its translocation into plant cells and recognition by resistance proteins. *Plant J.* **83**, 610–624.

Bonardi, V., Cherkis, K., Nishimura, M.T. and Dangl, J.L. (2012) A new eye on NLR proteins: focused on clarity or diffused by complexity? *Curr. Opin. Immunol.* **24**, 41–50.

Boutemy, L.S., King, S.R.F., Win, J., Hughes, R.K., Clarke, T.A., Blumenschein, T.M.A., Kamoun, S. and Banfield, M.J. (2011) Structures of *Phytophthora* RXLR effector proteins: a conserved but adaptable fold underpins functional diversity. *J. Biol. Chem.* **286**, 35 834–35 842.

Bozkurt, T.O., Schornack, S., Banfield, M.J. and Kamoun, S. (2012) Oomycetes, effectors, and all that jazz. *Curr. Opin. Plant Biol.* **15**, 483–492.

van den Burg, H.A., Westerink, N., Francoijs, K.J., Roth, R., Woestenenk, E., Boeren, S., de Wit, P.J., Joosten, M.H. and Vervoort, J. (2003) Natural disulfide bond-disrupted mutants of AVR4 of the tomato pathogen *Cladosporium fulvum* are sensitive to proteolysis, circumvent *Cf-4*-mediated resistance, but retain their chitin binding ability. *J. Biol. Chem.* **278**, 27 340–27 346.

Catanzariti, A.M., Dodds, P.N., Lawrence, G.J., Ayliffe, M.A. and Ellis, J.G. (2006) Haustorially expressed secreted proteins from flax rust are highly enriched for avirulence elicitors. *Plant Cell*, **18**, 243–256.

Catanzariti, A.M., Dodds, P.N., Ve, T., Kobe, B., Ellis, J.G. and Staskawicz, B.J. (2010) The AvrM effector from flax rust has a structured C-terminal domain and interacts directly with the M resistance protein. *Mol. Plant–Microbe Interact.* **23**, 49–57.

Cowieson, N.P., Aragao, D., Clift, M., Ericsson, D.J., Gee, C., Harrop, S.J., Mudie, N., Panjikar, S., Price, J.R., Riboldi-Tunnicliffe, A. and Williamson, R. (2015) MX1: a bending-magnet crystallography beamline serving both chemical and macromolecular crystallography communities at the Australian Synchrotron. *J Synchrotron Radiat.* **22**, 187–190.

De Block, M., Herrera-Estrella, L., Van Montagu, M., Schell, J. and Zambryski, P. (1984) Expression of foreign genes in regenerated plants and in their progeny. *EMBO J.* **3**, 1681–1689.

Djamei, A., Schipper, K., Rabe, F., Ghosh, A., Vincon, V., Kahnt, J., Osorio, S., Tohge, T., Fernie, A.R., Feussner, I. and Feussner, K. (2011) Metabolic priming by a secreted fungal effector. *Nature*, **478**, 395–398.

Dodds, P. and Thrall, P. (2009) Recognition events and host–pathogen co-evolution in gene-for-gene resistance to flax rust. *Funct. Plant Biol.* **36**, 395–408.

Dodds, P.N. and Rathjen, J.P. (2010) Plant immunity: towards an integrated view of plant–pathogen interactions. *Nat. Rev. Genet.* **11**, 539–548.

Dodds, P.N., Lawrence, G.J. and Ellis, J.G. (2001) Six amino acid changes confined to the leucine-rich repeat beta-strand/beta-turn motif determine the difference between the P and P2 rust resistance specificities in flax. *Plant Cell*, **13**, 163–178.

Dodds, P.N., Lawrence, G.J., Catanzariti, A.M., Ayliffe, M.A. and Ellis, J.G. (2004) The *Melampsora lini* AvrL567 avirulence genes are expressed in haustoria and their products are recognized inside plant cells. *Plant Cell*, **16**, 755–768.

Dodds, P.N., Lawrence, G.J., Catanzariti, A.M., Teh, T., Wang, C.I., Ayliffe, M.A., Kobe, B. and Ellis, J.G. (2006) Direct protein interaction underlies gene-for-gene specificity and coevolution of the flax resistance genes and flax rust avirulence genes. *Proc. Natl. Acad. Sci. USA*, **103**, 8888–8893.

Duplessis, S., Cuomo, C.A., Lin, Y.C., Aerts, A., Tisserant, E., Veneault-Fourrey, C., Joly, D.L., Hacquard, S., Amselem, J., Cantarel, B.L. and Chiu, R. (2011) Obligate biotrophy features unraveled by the genomic analysis of rust fungi. *Proc. Natl. Acad. Sci. USA*, **108**, 9166–9171.

Eschenfeldt, W.H., Lucy, S., Millard, C.S., Joachimiak, A. and Mark, I.D. (2009) A family of LIC vectors for high-throughput cloning and purification of proteins. *Methods Mol. Biol.* **498**, 105–115.

Feng, Y., Yao, H. and Wang, J. (2010) Crystal structure of the crenarchaeal conserved chromatin protein Cren7 and double-stranded DNA complex. *Protein Sci.* **19**, 1253–1257.

Flor, H.H. (1956) The complementary genic systems in flax and flax rust. *Adv. Genet.* **8**, 29–54.

Grishin, N.V. (2001) Treble clef finger – a functionally diverse zinc-binding structural motif. *Nucleic Acids Res.* **29**, 1703–1714.

de Guillen, K., Ortiz-Vallejo, D., Gracy, J., Fournier, E., Kroj, T. and Padilla, A. (2015) Structure analysis uncovers a highly diverse but structurally conserved effector family in phytopathogenic fungi. *PLoS Pathog.* **11**, e1005228.

Guyon, K., Balague, C., Roby, D. and Raffaele, S. (2014) Secretome analysis reveals effector candidates associated with broad host range necrotrophy in the fungal plant pathogen *Sclerotinia sclerotiorum*. *BMC Genomics*, **15**, 336.

Hacquard, S., Joly, D.L., Lin, Y.C., Tisserant, E., Feau, N., Delaruelle, C., Legué, V., Kohler, A., Tanguay, P., Petre, B. and Frey, P. (2012) A comprehensive analysis of genes encoding small secreted proteins identifies candidate effectors in *Melampsora larici-populina* (poplar leaf rust). *Mol. Plant–Microbe Interact.* **25**, 279–293.

Holm, L. and Rosenstrom, P. (2010) Dali server: conservation mapping in 3D. *Nucleic Acids Res.* **38**, W545–W549.

van den Hooven, H.W., van den Burg, H.A., Vossen, P., Boeren, S., de Wit, P.J.G.M. and Vervoort, J. (2001) Disulfide bond structure of the AVR9 elicitor of the fungal tomato pathogen *Cladosporium fulvum*: evidence for a cystine knot. *Biochemistry*, **40**, 3458–3466.

Horsch, R.B., Fraley, R.T., Rogers, S.G., Sanders, P.R., Lloyd, A. and Hoffmann, N. (1984) Inheritance of functional foreign genes in plants. *Science*, **223**, 496–498.

Islam, M.R. and Mayo, G.M.E. (1990) A compendium on host genes in flax conferring resistance to flax rust. *Plant Breed.* **104**, 89–100.

Jones, J.D.G. and Dangl, J.L. (2006) The plant immune system. *Nature*, **444**, 323–329.

Kooman-Gersmann, M., Vogelsang, R., Hoogendijk, E.C.M. and De Wit, P.J.G.M. (1997) Assignment of amino acid residues of the AVR9 peptide of *Cladosporium fulvum* that determine elicitor activity. *Mol. Plant–Microbe Interact.* **10**, 821–829.

Lawrence, G.J., Mayo, G.M.E. and Shepherd, K.W. (1981a) Interactions between genes controlling pathogenicity in the flax rust fungus. *Phytopathology*, **71**, 12–19.

Lawrence, G.J., Shepherd, K.W. and Mayo, G.M.E. (1981b) Fine-structure of genes controlling pathogenicity in flax rust, *Melampsora-lini*. *Heredity*, **46**, 297–313.

McLellan, H., Boevink, P.C., Armstrong, M.R., Pritchard, L., Gomez, S., Morales, J., Whisson, S.C., Beynon, J.L. and Birch, P.R. (2013) An RxLR effector from *Phytophthora infestans* prevents re-localisation of two plant NAC transcription factors from the endoplasmic reticulum to the nucleus. *PLoS Pathog.* **9**, e1003670.

McPhillips, T.M., McPhillips, S.E., Chiu, H.J., Cohen, A.E., Deacon, A.M., Ellis, P.J., Garman, E., Gonzalez, A., Sauter, N.K., Phizackerley, R.P. and Soltis, S.M. (2002) Blu-Ice and the distributed control system: software for data acquisition and instrument control at macromolecular crystallography beamlines. *J. Synchrotron Radiat.* **9**, 401–406.

Mishra, A.K., Gangwani, L., Davis, R.J. and Lambright, D.G. (2007) Structural insights into the interaction of the evolutionarily conserved ZPR1 domain tandem with eukaryotic EF1A, receptors, and SMN complexes. *Proc. Natl. Acad. Sci. USA*, **104**, 13 930–13 935.

Okmen, B. and Doehlemann, G. (2014) Inside plant: biotrophic strategies to modulate host immunity and metabolism. *Curr. Opin. Plant Biol.* **20**, 19–25.

Oliveira-Garcia, E. and Valent, B. (2015) How eukaryotic filamentous pathogens evade plant recognition. *Curr. Opin. Microbiol.* **26**, 92–101.

Pedersen, C., Ver Loren van Themaat, E., McGuffin, L.J., Abbott, J.C., Burgis, T.A., Barton, G., Bindschedler, L.V., Lu, X., Maekawa, T., Weßling, R. and Cramer, R. (2012) Structure and evolution of barley powdery mildew effector candidates. *BMC Genomics*, **13**, 694.

Ptashne, M. and Gann, A. (1997) Transcriptional activation by recruitment. *Nature*, **386**, 569–577.

Qiao, Y., Shi, J., Zhai, Y., Hou, Y. and Ma, W. (2015) *Phytophthora* effector targets a novel component of small RNA pathway in plants to promote infection. *Proc. Natl. Acad. Sci. USA*, **112**, 5850–5855.

Rafiqi, M., Gan, P.H., Ravensdale, M., Lawrence, G.J., Ellis, J.G., Jones, D.A., Hardham, A.R. and Dodds, P.N. (2010) Internalization of flax rust avirulence proteins into flax and tobacco cells can occur in the absence of the pathogen. *Plant Cell*, **22**, 2017–2032.

Rafiqi, M., Ellis, J.G., Ludowici, V.A., Hardham, A.R. and Dodds, P.N. (2012) Challenges and progress towards understanding the role of effectors in plant–fungal interactions. *Curr. Opin. Plant Biol.* **15**, 477–482.

Ramirez-Garces, D., Camborde, L., Pel, M.J., Jauneau, A., Martinez, Y., Neant, I., Leclerc, C., Moreau, M., Dumas, B. and Gaulin, E. (2016) CRN13 candidate effectors from plant and animal eukaryotic pathogens are DNA-binding proteins which trigger host DNA damage response. *New Phytol.* **210**, 602–617.

Ravensdale, M., Nemri, A., Thrall, P.H., Ellis, J.G. and Dodds, P.N. (2011) Co-evolutionary interactions between host resistance and pathogen effector genes in flax rust disease. *Mol. Plant Pathol.* **12**, 93–102.

Ravensdale, M., Bernoux, M., Ve, T., Kobe, B., Thrall, P.H., Ellis, J.G. and Dodds, P.N. (2012) Intramolecular interaction influences binding of the flax L5 and L6 resistance proteins to their AvrL567 ligands. *PLoS Pathog.* **8**, e1003004.

Redkar, A., Hoser, R., Schilling, L., Zechmann, B., Krzymowska, M., Walbot, V. and Doehlemann, G. (2015) A secreted effector protein of *Ustilago maydis* guides maize leaf cells to form tumors. *Plant Cell*, **27**, 1332–1351.

Schindelin, J., Arganda-Carreras, I., Frise, E., Kaynig, V., Longair, M., Pietzsch, T., Preibisch, S., Rueden, C., Saalfeld, S., Schmid, B. and Tinevez, J.Y. (2012) Fiji: an open-source platform for biological-image analysis. *Nat Methods*, **9**, 676–682.

Schneider, C.A., Rasband, W.S. and Eliceiri, K.W. (2012) NIH image to ImageJ: 25 years of image analysis. *Nat. Methods*, **9**, 671–675.

Schornack, S., van Damme, M., Bozkurt, T.O., Cano, L.M., Smoker, M., Thines, M., Gaulin, E., Kamoun, S. and Huitema, E. (2010) Ancient class of translocated oomycete effectors targets the host nucleus. *Proc. Natl. Acad. Sci. USA*, **107**, 17 421–17 426.

Sievers, F., Wilm, A., Dineen, D., Gibson, T.J., Karplus, K., Li, W., Lopez, R., McWilliam, H., Remmert, M., Söding, J. and Thompson, J.D. (2011) Fast, scalable generation of high-quality protein multiple sequence alignments using Clustal Omega. *Mol. Syst. Biol.* **7**, 539.

Stam, R., Howden, A.J.M., Delgado-Cerezo, M., Amaro, T.M.M.M., Motion, G.B., Pham, J. and Huitema, E. (2013a) Characterization of cell death inducing *Phytophthora capsici* CRN effectors suggests diverse activities in the host nucleus. *Front Plant Sci.* **4**, 387.

Stam, R., Jupe, J., Howden, A.J.M., Morris, J.A., Boevink, P.C., Hedley, P.E. and Huitema, E. (2013b) Identification and characterisation of CRN effectors in *Phytophthora capsici* shows modularity and functional diversity. *PLoS One*, **8**, e59517.

Stergiopoulos, I. and de Wit, P.J.G.M. (2009) Fungal effector proteins. *Annu. Rev. Phytopathol.* **47**, 233–263.

Stols, L., Gu, M., Dieckman, L., Raffen, R., Collart, F.R. and Donnelly, M.I. (2002) A new vector for high-throughput, ligation-independent cloning encoding a tobacco etch virus protease cleavage site. *Protein Expr. Purif.* **25**, 8–15.

Vargas, W.A., Sanz-Martin, J.M., Rech, G.E., Armijos-Jaramillo, V.D., Rivera, L.P., Echeverria, M.M., Díaz-Mínguez, J.M., Thon, M.R. and Sukno, S.A. (2016) A fungal effector with host nuclear localization and DNA-binding properties is required for maize anthracnose development. *Mol. Plant–Microbe Interact.* **29**, 83–95.

Ve, T., Williams, S.J., Catanzariti, A.M., Rafiqi, M., Rahman, M., Ellis, J.G., Hardham, A.R., Jones, D.A., Anderson, P.A., Dodds, P.N. and Kobe, B. (2013) Structures of the flax-rust effector AvrM reveal insights into the molecular basis of plant-cell entry and effector-triggered immunity. *Proc. Natl. Acad. Sci. USA*, **110**, 17 594–17 599.

Wang, B., Jones, D.N., Kaine, B.P. and Weiss, M.A. (1998) High-resolution structure of an archaeal zinc ribbon defines a general architectural motif in eukaryotic RNA polymerases. *Structure*, **6**, 555–569.

Wang, C.I., Guncar, G., Forwood, J.K., Teh, T., Catanzariti, A.M., Lawrence, G.J., Loughlin, F.E., Mackay, J.P., Schirra, H.J., Anderson, P.A. and Ellis, J.G. (2007) Crystal structures of flax rust avirulence proteins AvrL567-A and -D reveal details of the structural basis for flax disease resistance specificity. *Plant Cell*, **19**, 2898–2912.

Wang, R.W. and Brattain, M.G. (2007) The maximal size of protein to diffuse through the nuclear pore is larger than 60 kDa. *FEBS Lett.* **581**, 3164–3170.

Win, J., Krasileva, K.V., Kamoun, S., Shirasu, K., Staskawicz, B.J. and Banfield, M.J. (2012) Sequence divergent RXLR effectors share a structural fold conserved across plant pathogenic oomycete species. *PLoS Pathog.* **8**, e1002400.

Yaeno, T., Li, H., Chaparro-Garcia, A., Schornack, S., Koshiba, S., Watanabe, S., Kigawa, T., Kamoun, S. and Shirasu, K. (2011) Phosphatidylinositol monophosphate-binding interface in the oomycete RXLR effector AVR3a is required for its stability in host cells to modulate plant immunity. *Proc. Natl. Acad. Sci. USA*, **108**, 14 682–14 687.

Yao, M., Ohsawa, A., Kikukawa, S., Tanaka, I. and Kimura, M. (2003) Crystal structure of hyperthermophilic archaeal initiation factor 5A: a homologue of eukaryotic initiation factor 5A (eIF-5A). *J. Biochem.* **133**, 75–81.

Zhang, J., Yin, Z. and White, F. (2015) TAL effectors and the executor R genes. *Front Plant Sci.* **6**, 641.

Zhang, X., Nguyen, N., Breen, S., Outram, M.A., Dodds, P.N., Kobe, B., Solomon, P.S. and Williams, S.J. (2017) Production of small cysteine-rich effector proteins in *Escherichia coli* for structural and functional studies. *Mol. Plant Pathol.* **18**, 141–151.

SUPPORTING INFORMATION

Additional Supporting Information may be found in the online version of this article at the publisher's website:

Fig. S1 Protein solution property and protein–lipid binding assays.

Fig. S2 The cross-brace zinc-binding topology.

Fig. S3 Electrophoretic mobility shift assay (EMSA) for nucleic acid binding using the Pentaprobe approach.

Fig. S4 Cell death assay of AvrP and AvrP123 citrine (CTR) fusions.

Fig. S5 Specific recognition of AvrP variants by P family resistance proteins.

Fig. S6 Immunoblotting of AvrP and P.

Fig. S7 Cell death scoring of AvrP mutants.

Fig. S8 Test for interaction of AvrP and AvrP123 with P and P2.

Table S1 X-Ray data collection, structure solution and refinement statistics.

Table S2 Ratios of average fluorescence intensity in the nucleus and the cytosol (Av Nuc:Cyt) for AvrP-CTR, AvrP123-CTR and citrine (CTR).

Table S3 Oligonucleotides used in cloning.

Methods S1 Supplemental experimental procedures.

References S1 Supplemental references.